IMPERIAL COLLEGE OF SCIENCE, TECHNOLOGY
AND MEDICINE

University of London

EXPERIMENTALLY-DERIVED STRUCTURAL MODELS FOR USE IN FURTHER DYNAMIC ANALYSIS

by

Maria Lúcia Machado Duarte

A thesis submitted for the degree of Doctor of Philosophy of the
University of London and for the Diploma of Imperial College

Dynamics Section
Department of Mechanical Engineering
Imperial College of Science, Technology and Medicine
London, SW7 2BX

April 1996

To Gray and my parents

ABSTRACT

The research summarised in this thesis deals with the use of experimentally-derived structural models in further dynamic analysis. Limitations are present in such models and these are investigated here: namely, the number of modes and coordinates included. The main concern, however, is with the study of high-frequency residual terms (i.e. the effects of modes whose natural frequencies lie outside the measured or analysed frequency range). Existing formulations for residuals are presented, together with new ones developed by the author. The aim is to use the calculated values (based on a purely experimental approach) in further dynamic analyses. As it is impractical to study all the applications affected by the models' limitations, only coupling analysis was chosen to be studied in detail. In this application, both FRF coupling and Component Mode Synthesis (CMS) techniques are examined. The importance of including rotational degrees-of-freedom (RDOFs) is also discussed, although this is considered of secondary importance in this work. Nevertheless, important guidelines are given into which the finite-difference approximation (the formulation adopted to derive such coordinates) should be used with each of the above techniques.

As demonstrated, the use of experimentally-derived models may be required by the coupling formulations either to minimise measurement problems or due to the input data format used. In the former category are FRF coupling formulations, while CMS formulations belongs to the latter. An improved CMS formulation was developed for the case when only experimental data are available. It is based on the same formulation normally used when using analytical data. However, no need exists anymore to have the mass matrix of the sub-structures. The new approach is called IECMS and provides much better coupled predictions than the existing standard CMS formulations from experimental data.

Several trends for the residual terms are investigated. Among the trends, a relationship was discovered between the high-frequency residual terms and the mass of the system: the smaller the mass at a particular coordinate, the stronger its residual effect. New high-frequency residual terms' formulations were developed. To mention just a few, one can quote the high-frequency pseudo-mode approximation, the mass-residual approach and the experimental residual terms' formulation in series form. Each one has its own advantages and drawbacks, as explained.

Parameters were devised to assess the quality of the measured and/or predicted FRFs considering all curves in one go. They are, basically, a quick way of comparing two sets of data. Finally, an experimental example is shown to validate the theories presented.

ACKNOWLEDGEMENT

I would like to thank my supervisor, Prof. D. J. Ewins, for his help and guidance during the development of this work. I also thank Mr. D. A. Robb and Dr. M. Imregun for their advice and discussions. Special thanks go to the other members of staff that I have bothered so much during these years, mainly, Ms. Val Davenport, Miss Liz Hearn, Ms. Lisa Kateley, Mr. Paul Woodward and Mr. John Miller.

I had the pleasure to meet a lot of people during this long period of my research. Some of them shared the busy room 564 with me, some were in the neighbouring rooms and some were even from other sections or departments. I think is inappropriate to name just a few here since all of them contributed to this work in some way: either by helping me with their knowledge, by giving me support during the darkest periods of the work or by just being there. There is only one name I would like to mention and that is Dr. Ali Nobari. He gave me great encouragement during the first years of my research, providing me with a lot of discussions and ideas. I am extremely thankful to him.

I gratefully acknowledge the financial support of CNPq (Conselho Nacional de Desenvolvimento Cientffico e Tecnológico).

I also would like to express my deepest gratitude and thanks to the person that helped me the most during all these years; Gray Farias Moita. Without his support, I would have found it very hard to cope with the difficult period towards the end of this work. Finally, my most sincere thanks are reserved for my parents; their moral support and encouragement were extremely appreciated.

NOMENCLATURE

$_rA$	modal constant mode r
A_{ii}^{pm}	pseudo-modal constant
$[Am]$	defined by equation (3.12a)
$_rB$	constant term contribution of other modes than mode r
b	numerator index of FRF in polynomial form
$[Bm]$	defined by equation (3.12b)
$[Cm]$	defined by equation (3.12c)
d	denominator index of FRF in polynomial form
$[D]$, d	hysteretic (or structural) damping matrix / damping value
e	calibration error
e_1, e_2	distance between applied force and neutral axis
$FL(\omega)$	frequency level curve
$FIF(\omega)$	frequency indicator function curve
$[G]$	constrained flexibility matrix
$[H]$, $[H(\omega)]$	generic FRF matrix
$[I]$	identity matrix
I_p	Inertia of the block plus transducers
i	imaginary value
$IFI(\omega)$	inverse frequency indicator
$[K]$, k	stiffness matrix / stiffness value
$[Kc]$	coupled system high-frequency static residual matrix
$[K_e]$	elastic stiffness matrix
$[Km]$	modal stiffness matrix
$[M]$, m	mass matrix / mass value
m	mass of the block plus transducers
M	moment
$[M_{bl}]$	mass matrix of block
$[Mm]$	modal mass matrix
$[R]$	high-frequency static residual matrix
$[R(\omega)]$	high-frequency residual matrix
$[R1]$	first-order dynamic residual matrix
$[R2]$	second-order dynamic residual matrix
S	spacing between accelerometers
$[T]$	transformation matrix
$[T_1]$	transformation matrix containing the response position information
$[T_2]$	transformation matrix containing the force position information
$[Z]$	impedance matrix
$\{f\}$, f	force vector / coordinate
$\{p\}$, P	modal (or principal) response vector / coordinate
$\{q\}$, 4	constrained modal response vector / coordinate
t	time
$\{x\}$, x	physical response vector / coordinate
Y	translational coordinate
$[\alpha]$, $[\alpha(\omega)]$	receptance matrix
$[\beta]$	constraint matrix
$[\phi]$, $\{\phi\}$	mode shape matrix / vector
$[\eta_r]$, η_r	hysteretic damping matrix (diagonal) / value mode r
$[\lambda_r]$, λ_r	damped natural frequency matrix (diagonal) / value mode r; (rad/s)
λ_{hp}^2	high-frequency pseudo-eigenvalue

λ^2_{HF}	high-frequency pseudo-mass mode
λ^2_{pm}	pseudo-natural frequency
θ	rotational coordinate
$[\omega_r]$, ω_r	undamped natural frequency matrix (diagonal) / value mode r; (rad/s)

Superscripts:

-1	inverse of a matrix
T	transpose of a matrix
c	coupling coordinates
s	slave coordinates
	augmented improved matrices (chapter 2)
r	remaining modes (chapter 3, section 3.4)
r	rigid-body modes (chapter 4)
e	elastic modes
l	low-frequency modes
h	high-frequency modes
c	correct ("complete in modal sense") FRF curves
R	regenerated FRF curves
S	static compensated FRF curves
D	dynamic compensated FRF curves
*D*2	second-order dynamic compensated FRF curves
M	modified residual terms

Subscripts:

A	first sub-system of coupled analysis
B	second sub-system of coupled analysis
C	coupled system
A, B or C	accelerometers position
P	point were rotational information is required
i, j	generic coordinate indexes
r	mode number
l	low-frequency modes
h	high-frequency modes
pu	frequency point used for the static residual terms calculation
pu_h	frequency point used for the dynamic residual terms calculation
pu_{h2}	frequency point used for the second-order dynamic residual terms calculation
LF	low-frequency residual
HF	high-frequency residual
0	static residual
S	series form residual
*k*1 to ***kk***	frequency points used
hf	frequency point inside the frequency range of interest
est	estimated
meas	measured
1f	first-order forwards finite-difference approximation
1b	first-order backwards finite-difference approximation
2f	second-order forwards finite-difference approximation
2c	second-order central finite-difference approximation
2b	second-order backwards finite-difference approximation
trans	translational quantities
rot	rotational quantities

Dimensions:

N	Total number of coordinates of the system
n	measured number of coordinates of the system
m	measured number of modes of the system
k	number of frequency points
m l	lowest mode in the frequency range of interest
m2	highest mode in the frequency range of interest
mau	number of modes used for sub-system A
mbu	number of modes used for sub-system B
NA	number of coordinates of sub-system A
NB	number of coordinates of sub-system B
NCC	number of coupling coordinates

Abbreviations:

EMA	Experimental Modal Analysis
FEM	Finite Element Method
DOF(s)	Degree(s)-of-Freedom
FRF(s)	Frequency Response Function(s)
SDM	Structural Dynamic Modification
SCA	Structural Coupling Analysis
CMS	Component Mode Synthesis
IECMS	Improved Experimental Component Mode Synthesis
RHS	Right Hand Side
LHS	Left Hand Side
MAC	Modal Assurance Criteria
dB	decibel
FFT	Fast Fourier Transform

Symbols:

[ ]	matrix
I }	vector
II II	norm
I I	absolute value
6	physical matrix addition

TABLE OF CONTENTS

APPENDICES

LIST OF FIGURES

CHAPTER 1: INTRODUCTION

CHAPTER 2: FRF COUPLING METHOD

CHAPTER 3: COMPONENT MODE SYNTHESIS (CMS) USING EXPERIMENTAL DATA

CHAPTER 4: THE RESIDUAL PROBLEM (MODAL INCOMPLETENESS)

CHAPTER 5: THE SPATIAL INCOMPLETENESS PROBLEM

CHAPTER 6: EXPERIMENTAL CASE STUDY

LIST OF TABLES

CHAPTER 2: FRF COUPLING METHOD

CHAPTER 3: COMPONENT MODE SYNTHESIS (CMS) USING EXPERIMENTAL DATA

CHAPTER 4: THE RESIDUAL PROBLEM (MODAL INCOMPLETENESS)

CHAPTER 5: THE SPATIAL INCOMPLETENESS PROBLEM

CHAPTER 6: EXPERIMENTAL CASE STUDY

CHAPTER 1: INTRODUCTION

1.1. PREAMBLE

The main concern of structural dynamic analysis is to evaluate the natural modes of vibration and the levels of response which a particular structure experiences under certain conditions. To that end, several techniques have been developed over the years and are currently in use. The two most commonly used are Experimental Modal Analysis (EMA) and the Finite Element Method (FEM). Attention is given in this thesis to EMA, where an experimentally-derived model of a structure is sought for use in further dynamic analysis.

FEM provides the basis for a direct analysis of complex engineering structures. However, it is generally accepted that EMA provides a more realistic description of the dynamic behaviour of the structure under investigation. This results from a series of assumptions made in the former approach, which are not present in the latter. Despite that, FEM is normally used as a primary tool to assist in determining the minimum requirements for a modal test (or EMA), which are often difficult to establish. When FEM is used as a primary method of analysis, a validation of the model thus obtained must usually be performed on the basis of EMA results. This subject (called modal updating) has been the emphasis of several researches recently and will not be addressed in detail in this work.

There are three types of model available in order to describe a structure's dynamic behaviour and these are: spatial, ***modal*** and ***response*** models [41]. As **long as they represent the full dynamic description of the structure,** they are interchangeable. Very often, one is left with only an incomplete description and further dynamic analysis has to be performed from this limited information. In this case, some means of compensating for the missing information may have to be provided. Let us assume for the time being that the full description is available. Figure 1.1 shows the interrelation of the various models mentioned above when performing the analysis from a theoretical basis. Figure 1.2 shows the same when starting from an experimental base. It is straightforward to say that experimentally-derived models follow the latter course.

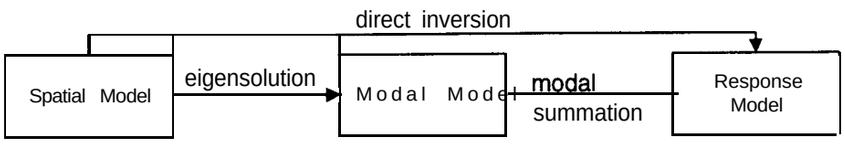

Figure 1.1 - Interrelation between the various types of models in a theoretical route

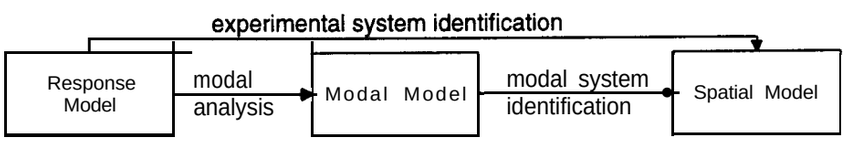

Figure 1.2 - Interrelation between the various types of models in an experimental route

Due to advances in data acquisition and computing capabilities in recent years, it is possible to test and to analyse much more complex structures, than was possible only a few years ago. However, it may be necessary to consider a complex structure in smaller components. The requirement for that can be either due to the size of the structure (smaller components are easier to test) or due to the need of different companies to analyse different parts of it. Each part (or sub-component) is analysed separately and the individual results or models are then combined in order to predict the dynamic behaviour of the complete, assembled, structure. This process is called structural coupling and it is the main application used here. There are several structural coupling analysis formulations available and they can be based on any of the models mentioned above. Section 1.4 gives an introduction into this topic, although only response and modal coupling will be used throughout the thesis. Despite the fact that coupling analysis is an easier way of analysing complex structures, some significant problems are often faced during such a process. Care has to be taken to try to minimise these problems, and that is the main interest of the research summarised here.

1.2. REASONS FOR OBTAINING AN EXPERIMENTALLY-DERIVED MODEL OF A STRUCTURE

The major reason why one wants to obtain an experimentally-derived model of a structure under investigation was already mentioned in the previous section: that is, EMA is considered to produce more accurate results than FEM. Before going further, one has to remember that the experimentally-derived model needed here is to be used in further dynamic analysis (and structural coupling analysis was chosen in this thesis to illustrate this feature). One could ask, then, why the measured data could not be used straight away? And why an experimentally-derived model has to be derived from them?

First of all, not all the applications are developed for use with response models (the ones directly obtained from experimental tests - see Figure 1.2). Also, although measured data have the advantage of including all the information regarding the structure's dynamic behaviour, there are often some inconsistencies in the data set due to measurement errors and noise. These are prone to cause numerical problems in further applications and are better avoided. Experimentally-derived models overcome such inconsistencies. However, they have a disadvantage in that, while removing the noise and calculating a more consistent data set, the information about the modes outside the measured frequency range is lost as well. Nevertheless, for the measured FRF curves, this information can be recovered'. Therefore, among the choices, one is better off using experimentally-derived models and augment them with the missing information.

1.3. LIMITATIONS OF EXPERIMENTALLY - DERIVED MODELS

One of the limitations of the experimentally-derived models was just mentioned: namely, the lack of information about all the modes the structure possesses. This problem is mainly imposed by the need to limit the frequency range measured. So, by modal analysis extraction techniques, it is only possible to obtain the modes within this measured frequency range, despite the fact that the information about all the modes is present in the raw data. Solving this problem is the major concern in this thesis. Another limitation is related to the number of coordinates included in the model. It is important to stress, however, that these limitations are relative. They only present a real problem if one wants to use this model in further analysis. In such cases, catastrophic consequences in the results can happen if due care is not taken to account for their effect.

Therefore, in summary, the limitations of the experimentally-derived models are:

- Modal incompleteness (the so-called residual problem)
- Coordinate incompleteness

When one is performing an experimental modal test, it is common practice to measure only one column (or row) of the full FRF matrix (response model). From this data set, it is possible to derive the modal model of the structure using conventional modal parameter extraction techniques. Ideally, all natural frequencies and mode shapes should be obtained and, from that (using modal summation), it should be possible to regenerate any element in the full FRF matrix. Figure 1.3 represents this ideal route.

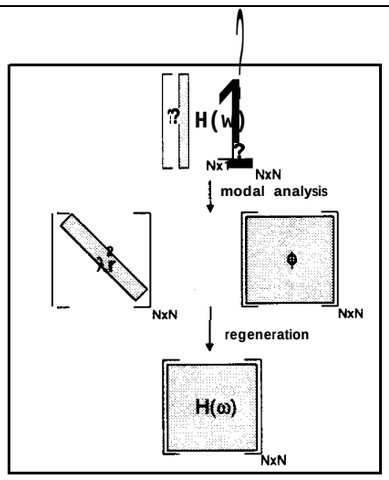

Figure 1.3 - Ideal (theoretical) route

However, the reality is normally far from this ideal situation. Very often, many coordinates simply cannot be measured and time prohibits the measurement of all accessible DOFs. Furthermore, only a finite number of modes can be obtained because measurements can only be made over a finite frequency range. Therefore, the resulting modal model will only possess information related to the measured coordinates and for the modes included within the measured frequency range. It is incapable of providing information about modes outside this range or about unmeasured coordinates. When the FRF regeneration is performed in this case, additional information about the missing modes has to be included in order to obtain the correct properties. For an experimental route, it is possible to calculate this information for the measured FRFs only. None of the other residual terms can be evaluated directly. Therefore, when regenerating the FRFs, only the measured ones can be regenerated correctly. So, if a structural coupling analysis requires information about any DOFs other than those in the measured column, they have to be measured additionally. Such a situation is almost inevitable, since one column can provide correct FRF information for only one coupling DOF. In order to obtain information about the missing coordinates, these have either to be measured or, sometimes, estimated using interpolation functions. Figure 1.4 shows this more realistic experimental route, where no compensation for the missing coordinates was included. Experimentally-derived models are based on the diagram presented there.

It is normally possible to start the measurements from 0 Hz. In such cases, only the information regarding the rigid-body modes has to be included for the low-frequency range. This can normally be done by analysis. Therefore, when one refers to the lack of modes, high-frequency out-of-range modes are the ones of interest. Those are the concern of this work.

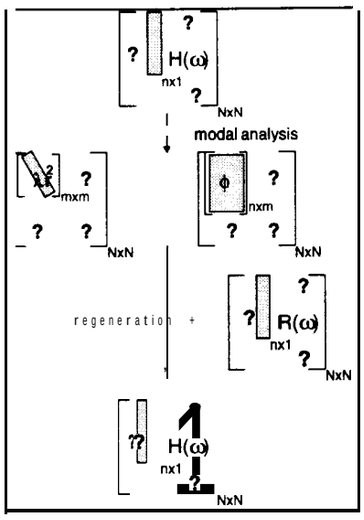

Figure 1.4 - Experimental route

1.4. STRUCTURAL DYNAMIC ANALYSIS

1.4.1. INTRODUCTION

The major part of this thesis deals with the modal incompleteness problem when performing a vibration analysis by an experimental route and when further use of the model is required. Any application involving response levels will be affected by the omission of out-of-range (residual) modes (see chapter 4). As it is practically impossible to study all the applications affected, some of them were chosen to be studied in more detail, namely: FRF coupling and component mode synthesis (CMS). Also affecting these applications is the spatial incompleteness problem (chapter 5), although this is considered of lesser importance in this thesis. The selected applications are part of the so-called structural dynamic analysis methods that are the subject of this section. Here, a brief introduction of structural dynamic analysis is presented. Emphasis is given to the coupled structure analysis part of it, where the above applications lay.

Often, the structural dynamic analyst comes to the situation where he/she wants to know what will be the consequences of making a specific modification to a structure in respect of the dynamic behaviour of that structure. Structural dynamic modification is the topic which deals with that. The referred modification can be either a single modification or a result of two or more structures being coupled together. Although the analysis of the entire structure would be a solution by itself, it can be quite expensive if the size of the problem (number of coordinates) is big; mainly when some of the results are already available. In such cases, an analysis using such results will be more appropriate.

Structural dynamic analysis is a very important tool in vibration problems to try to avoid undesirable frequencies in some structures. As well as avoiding these frequencies, it can also be important to know the particular position of some anti-resonance frequencies in order to achieve the best possible design of the structure.

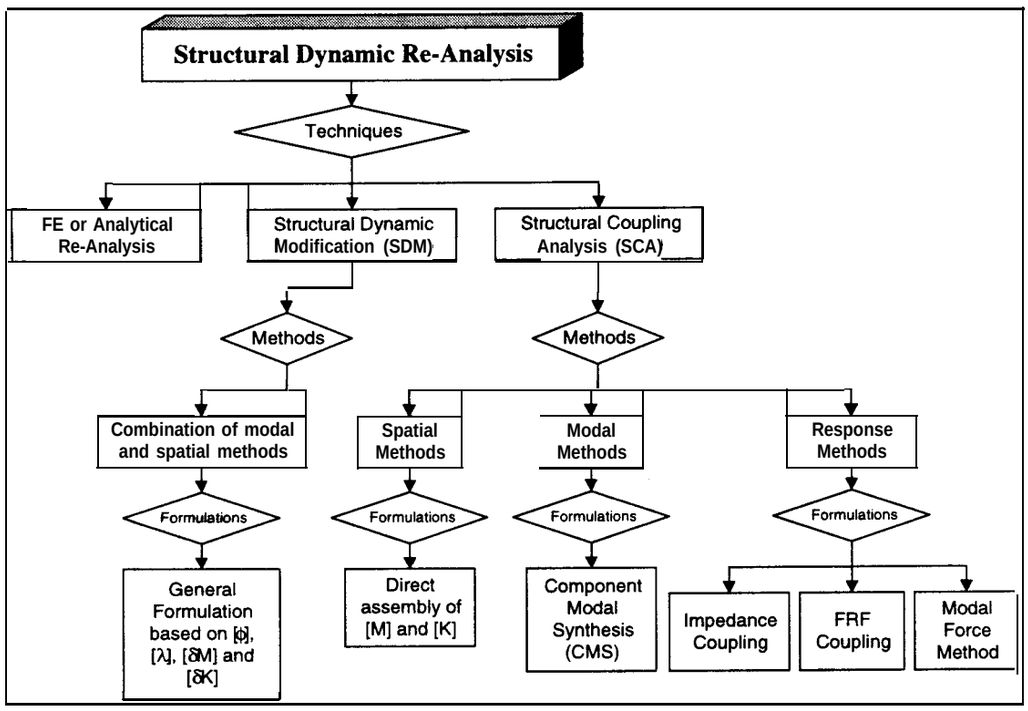

Figure 1.5 - Flow-Chart representing the structural dynamic analysis process.

Figure 1.5 shows a flow-chart representing the entire range of the structural dynamic analysis process. It can be divided into three major techniques: direct analysis, structural dynamic modifications (SDM) and structural coupling analysis (SCA). We are not going to be concerned with the first technique, since an assumption is made that some of the data are already available. Instead, we shall concentrate our attention on the SDM and the SCA techniques. The difference between these is basically the information available to perform the analysis and the size of the modification required. While the former is based on a prior knowledge of the mass and stiffness modifications at a small number of coordinates, the latter is based on substructures' information (therefore, normally involving a bigger number of coordinates). In other words, the SDM corresponds to changes to the existing models (i.e. same number of DOFs), while the SCA adds further components (i.e., normally, more DOFs). To divide a structure into substructures can be necessary sometimes due to a complex geometry or due to the need for different companies to analyse different sub-components of it, as already mentioned.

Several formulations are available to give the analyst a method for predicting the dynamics of the entire modified structure, and these are also shown in Figure 1.5. Some of the formulations are based purely on experimental data, some on purely analytical results and others use a combination of the two. Although the formulations presented here could also be used with analytical results, only those that could be used with experimental data will be discussed further. Attention was concentrated during the research on structural coupling analysis (SCA) and only this will be covered fully. For the reader who wishes to review the SDM technique, reference can be made to [6, 14, 107, 113], just to give some examples. Next, the SCA is explained in more detail.

1.4.2. STRUCTURAL COUPLING ANALYSIS (SCA)

As the applications chosen relate to structural coupling analysis, a detailed flow-chart of the SCA techniques available is presented in Figure 1.6. Although the author is concerned with the experimental route, both theoretical and experimental SCA routes are shown for completeness. From the techniques available, only ***CMS*** and ***FRF coupling*** will be analysed in detail. However, impedance coupling will also be addressed to show the limitations in this formulation and the reason why it was not used.

In Figure 1.6, it is also possible to see the inter-relations between the available dynamic models of the structure. If a complete description of the structure's dynamic behaviour is available (i.e. both in terms of the number of modes and the number of coordinates) any of the mentioned coupling formulations produces the same prediction results. If not, a compensation for the missing terms has to be incorporated into the formulation in order to improve the predictions obtained. These problems will be addressed later on and a comparison between the predictions using each of the different approaches will be performed.

A major advantage of using coupling techniques is the ability to reduce the order of the final set of equations to be solved. Although the reduction is not compulsory, it saves time and money when an analysis is made of the dynamic response of coupled system (as each sub-system normally has a large number of DOFs). Each technique approaches with this reduction task from a different angle and this is the major difference between the different classes of coupling. ***Modal coupling*** reduces the coupled set of equations by using a reduced number of ***modes*** for each sub-system, while retaining all the coordinates; although the latter feature is not necessarily required. The reason why all coordinates are retained is only due to the fact that the modal model is already obtained for all measured coordinates. ***Response coupling,*** on the other

hand, benefits from a reduction in the number of ***coordinates*** included, while retaining the effect of all the modes. ***Spatial coupling*** also performs the reduction in the number of coordinates included. These can be accomplished by using condensation schemes such as Guyan reduction [53] or others [44, 58]. These schemes are based on a transformation matrix relating the remaining DOFs (known in the literature as slave or secondary coordinates) to the retained DOFs (known as master or primary coordinates). The retained DOFs are normally specified by the user, although it is of paramount importance that they include all the coupling coordinates for each sub-system.

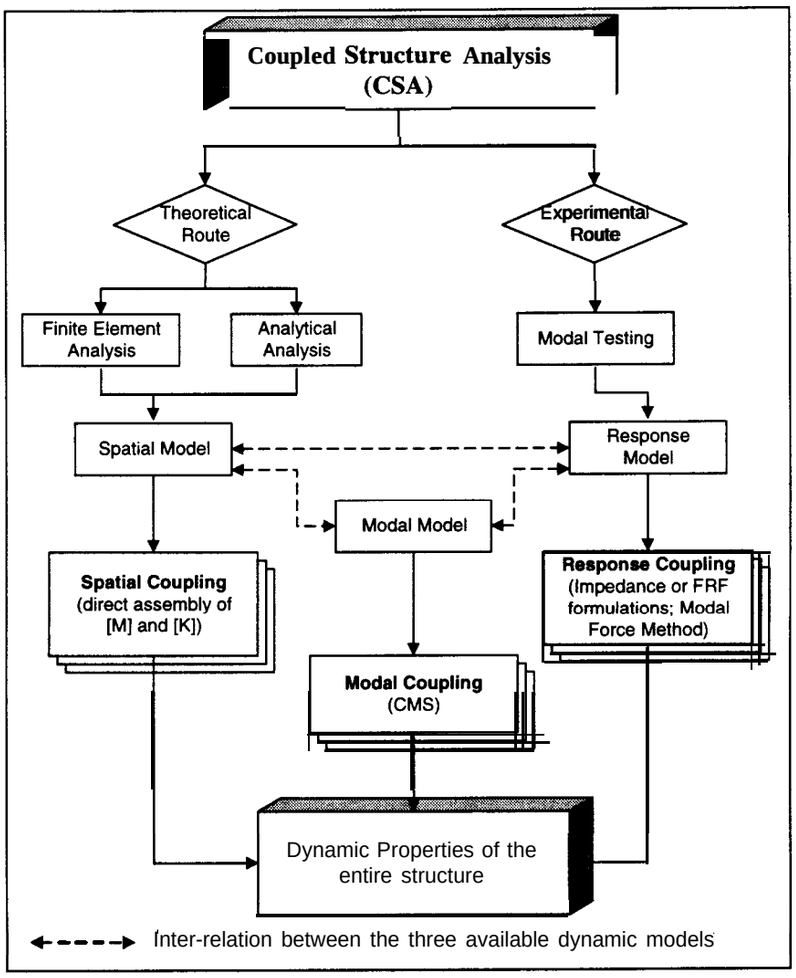

Figure 1.6 - Flow-Chart of the Structural Coupling Analysis (SCA) process.

Some of the formulations available require information about both coupling and slave coordinates, while some only require information about coupling coordinates (if no slave information is of interest). In the former group, one can mention spatial-based approaches, while modal-based and response-based approaches are part of the latter group. ***Coupling***

coordinates (sometimes called junction coordinates) are those where the sub-systems are going to be connected to each other. ***Slave coordinates*** (sometimes called interior coordinates) are the additional coordinates which are not directly related to the coupling but are either necessary for the formulation or of later interest (see Figure 1.7).

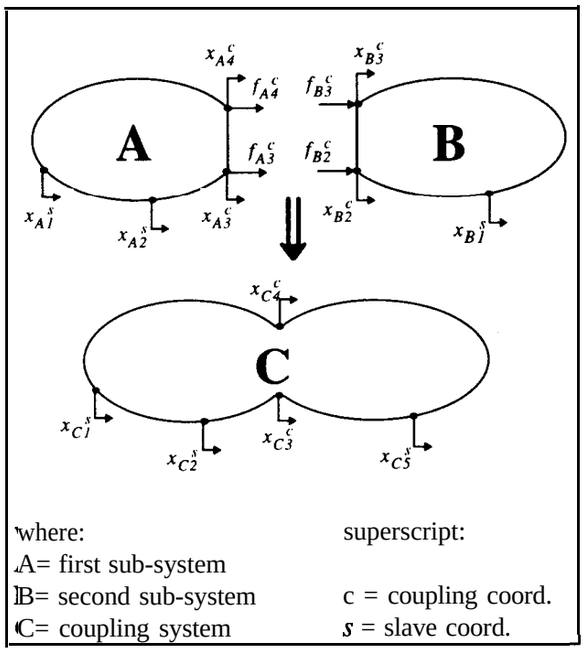

Figure 1.7 - Schematic drawing of a coupling process.

It does not matter which formulation is considered, all are based on the principles of ***compatibility of the displacements*** and ***equilibrium of the forces*** at the coupling coordinates. In order to understand what this means, consider Figure 1.7 again. It shows a schematic drawing of two sub-systems joined together at a certain number of coordinates to form a coupled system. When sub-system **A** is coupled to sub-system **B** to form the coupled system C, the following equations have to be true:

Compatibility:

$$\{x_C^c\} = \{x_A^c\} = \{x_B^c\} \tag{1.1}$$

Equilibrium:

$$\{f_C^c\} = \{f_A^c\} + \{f_B^c\} = \{0\} \tag{1.2}$$

Superscript c is used in the above equations to stress that they only apply to the coupling coordinates. Writing these equations in expanded form for the example shown in Figure 1.7, one obtains respectively:

$$x_{A4}^c = x_{B3}^c = x_{C4}^c \quad \text{and} \quad x_{A3}^c = x_{B2}^c = x_{C3}^c$$

$$f_{A4}^c + f_{B3}^c = f_{C4}^c \quad \text{and} \quad f_{A3}^c + f_{B2}^c = f_{C3}^c$$

Each formulation shown in Figure 1.6 employs equations (1.1) and (1.2) in a slightly different way in order to obtain a dynamic analysis of the coupled system. In chapters 2 and 3, the theory for each of the chosen applications is presented.

1.5. THESIS OBJECTIVES AND OUTLINE

The research presented in this thesis is mainly concerned with the use of experimentally-derived models in structural coupling analysis. To that end, in order to investigate the limitations of this type of model (i.e. number of modes and coordinates included), FRF coupling and Component Mode Synthesis (CMS) were used.

As mentioned in section 1.3, only one column of the full FRF matrix is normally measured in experimental tests. However, coupling analysis usually involves additional coordinates to the ones related to this measured column. In order to obtain the correct experimentally-derived models for these coordinates, they have also to be measured. When the number of coupling coordinates is large, this is a time-consuming process. Therefore, the research's primary objective was to devise a way of compensating for the residual terms' influence at the unmeasured FRFs, such that they could be used in coupling analysis in order to minimise the error caused when they are not included. This task proved to be more intractable than initially thought, and it can only be achieved satisfactory with a knowledge of either the physical matrices of the system or after a pre-test of the structure over a certain frequency range of interest. A correct residual matrix, which is the one containing the effects of the modes outside the range of interest, is difficult to obtain in a different way. A rank-deficient estimate of the residual matrix could be employed [34]. However, this matrix will not correct for the residual effects properly. When performing coupling analysis, one wants the best estimate possible of the coupled structure's behaviour (not just an improvement over the predictions without residual compensation). Therefore, although this primary objective could not be met fully, several improvements were made in the way residual terms are current calculated to be used in coupling analysis.

The specific objectives of the research described in this thesis are as follows:

1. to provide a comprehensive review of FRF coupling and CMS techniques available from experimental data;

2. to compare the above coupling formulations and to specify the benefits of using one or another;
3. to investigate the influence of including/excluding compensation for residual terms at slave and coupling DOFs and to provide some guidelines when they have to be included;
4. to provide an in-depth assessment of the existing residual compensation techniques and to formulate some new improved approaches;
5. to investigate the influence of including/excluding rotational DOFs at the coupling coordinates during a coupling analysis;
6. to work with the formulations used to derive rotational DOFs and provide some guidelines as to which derivation scheme should be used with each of the coupling techniques chosen;
7. to improve the currently-used CMS formulation based on purely experimental results; and
8. to devise a means for comparing the frequency predictions calculated by FRF coupling formulations (where both resonance and anti-resonance are considered) without the need of comparing each pair of curves individually.

The above objectives are distributed throughout the thesis, which is organised in the following way. Before explaining each experimentally-derived models' limitation in more detail and trying to solve them, it is important to understand first each of the applications chosen to be studied. Chapters 2 and 3 deals with these issues. The former chapter presents the theory for FRF coupling, while the latter presents the theory for CMS coupling. The advantages and drawbacks of using each of these coupling techniques are addressed in the respective chapters. However, although the problems faced by each of the applications are pointed out, no attempt is made to try to solve them yet. This will be done in later chapters. Examples are shown to stress the effects which each type of incompleteness has upon the coupled predictions and some guidelines are given to when and where they have to be included.

Once the coupled system predictions are made, it is important to have a parameter or parameters to assess the quality of these predictions. Equally important is the ability to assess the quality of the measurements. A solution for these points is also presented in chapter 2, where a brief review of existing formulations to assess these qualities is given. Most existing methods are based on modal parameters, but it is much more important to be able to predict the quality of the response predictions (as this is a much more complete prediction). Consequently, parameters were developed in this work to do that and although their primary aim is to assess

the quality of the natural frequencies, one of them gives an indication of discrepancies at the anti-resonance frequencies as well. When used with FRF coupling predictions, they save time in extracting the modal parameters or comparing two FRF curves at a time. If no major discrepancies are spotted through these parameters, a more complete comparison can be performed.

Since the work covers a wide range of inter-related subjects, instead of including a literature survey here at the beginning, the author decided that it was appropriate to include that in each chapter. Therefore, each chapter will contain its own summary of previous work.

Chapter 4 is the core of the thesis. It refers to the residual problem (or, in other words, the modal incompleteness problem). First, a definition of the problem is given. Although emphasis is given to the high-frequency residual terms, some insights into low-frequency residual terms are also presented. Trends found for the high-frequency residual terms' effects follow the definitions. Then, the formulations used in order to obtain these terms are presented. Despite the fact that the emphasis of the work is based on an experimentally-derived route, both the experimentally- and theoretically-derived residual formulations are shown, for completeness. A very interesting approach is presented in this chapter relating the high-frequency residual terms with the mass of the structure. This approach is completely different from those normally available in modal analysis which associate the high-frequency residual terms with the stiffness properties of the structure. However, the latter is the correct procedure and, in order to bring the mass-residual approach back to stiffness units, an extra parameter has to be incorporated into the formulation (i.e. a high-frequency pseudo-mass mode). A formulation is proposed to find the best value for the high-frequency pseudo-mass mode. On the same basis, i.e. the use of the mass matrix of the system, an improvement to the static residual is proposed. The static residual approach is the one normally used in experimentally-based CMS formulations. By improving the residual compensation, a better coupling prediction can be obtained using that technique. The referred improvement is already available from FE-derived models but, due to the need for the mass matrix of the sub-structures, was not previously applicable to experimentally-derived models. A formulation is developed to circumvent the necessity for knowledge of the mass matrix. The only information necessary is that already required to calculate the static residual terms.

The spatial incompleteness problem is dealt with in chapter 5. Although this was not the main concern of the research, it is included since it is also a limitation on the use of the experimentally-derived models in the chosen applications. The various existing techniques used

to derive or measure rotational degrees-of-freedom are reviewed and the importance of such coordinates in coupling predictions is stressed. It was discovered that each specific coupling technique worked better with a specific rotational derivation and this fact is explained in detail. Several results are presented for the rotational technique chosen to be used for the experimental validation of the coupling test cases.

Chapter 6 presents a validation of the formulations proposed on the previous chapters using a real case study. First, the test structures are described. This is followed by the experimental set-up, where some possible experimental problems are addressed. Then, the translational measurements are explained and the use of the above-developed comparison parameters is made to assess the quality of the measurements. The importance of the transducer positions is addressed next, as these can have the same sort of effect as the lack of residual modes. Following that, the modal parameters and residual terms' formulations are explained and validated. The derivation of rotational quantities follows. Finally, the results of using the measured data in the coupling analysis chosen are presented, where the various residual compensations (existing and developed) are employed, as well as the rotational DOFs derivation.

Chapter 7 presents the main conclusions derived in the previous chapters. First, the requirements for a correct coupling prediction are given, highlighting the important points about what affects the chosen coupling formulations. Then, the consequences of leaving out modes and coordinates in the coupling process are stressed. This is followed by the residual compensation formulations' appraisal and guidelines, which are presented before the trends observed for the residual terms. Following that, the conclusions related to the rotational DOFs derivation are shown again, with some guidelines given for their use. Then, the conclusions concerning the comparison parameters are addressed, with the conclusions about the importance of the transducer's position shown next. As the final point, and as is customary in a work of this nature, suggestions are made for future work.

CHAPTER 2: FRF COUPLING METHOD

2.1. INTRODUCTION

In this chapter, the FRF formulation for coupled structure dynamic analysis is introduced. The one of particular concern here involves coupling between two sub-structures at a time. Using the FRF properties of these sub-structures, it is possible to predict the corresponding FRF information of the coupled structure. If more them two sub-structures are involved, the coupling process can be performed in a sequential way. The principle behind a FRF coupling process is to reduce the number of coordinates included, while retaining all the modes for each sub-system. By doing that, a reduction in the final set of equations to be solved is accomplished. Care has to be taken to include all the modes and all the necessary coordinates (i.e. at least all the coupling DOFs) in order to get the correct coupled predictions and this is what is going to be investigated in this chapter. Although these problems are mentioned, no attempt is made at this stage to solve them yet. This will be accomplished in the following chapters.

Any general FRF coupling formulation can handle information about both coupling and slave DOFs. However, the latter are only included if one wants to obtain information about such coordinates after the coupling process has been performed. Basically, what differs in the various formulations is the number of coupled systems which can be included, the number of inversions performed during the calculations and the number of coordinates involved in such inversions. A brief introduction about this is given in the following section. After that, the general theory of the FRF coupling formulation is presented. Since the general formulation is not the most efficient one, an improved FRF coupling formulation is shown next. Then, the advantages and drawbacks of using this type of coupling technique are given, followed by the requirements for a correct FRF coupling prediction. In order to see how good the predictions from FRF coupling formulations are, one has to compare two FRF curves at a time. Time can be saved at an earlier stage by checking the natural frequency predictions of the coupled system. Two formulations are proposed in this chapter to assess the quality of both the experimentally-derived FRF models and their further predictions. The first one is called "Frequency Level" (FL) and the second is called "Frequency Indicator Function" (FIF) (or its

inverse "Inverse Frequency Indicator" (IFI)). Both are based on a matrix (or vector) of FRFs. Advantages of the new methods compared with existing ones are addressed. Finally, to conclude, some examples are shown and conclusions are drawn.

2.2. SUMMARY OF PREVIOUS WORK

2.2.1. FRF COUPLING METHOD

FRF coupling is a well-known technique that has been used in vibration analysis for over three decades. It is sometimes referred to as "impedance" or "receptance coupling". Although some earlier works have been reported through an analogy between electrical circuits and vibrating systems (see paper by Duncan [35]), FRF coupling can be regarded to have started with the work of Bishop and Johnson in 1960 [10]. They formulated a way of calculating the dynamic predictions of multi-beam assemblies from an "exact" formulation of the response model of each individual beam. Due to the simplicity of their formulation, it was limited to theoretically-derived models. As practical structures became more and more complex, the need arose to derive the impedance matrices straight from measurements instead of purely from theoretical data. However, the hardware and software available to measure and analyse the dynamic behaviour of structures at the early stages was not very accurate and had many limitations. These limitations motivated a lot of research into that area and, as a result, it became possible to measure much more data, with much more accuracy than before. Consequently, FRF coupling formulations were investigated again.

A criticism on ***some*** of the available FRF coupling techniques can be found in the work of Ren and Beards [97]. According to them, FRF coupling methods should be evaluated based on the following four criteria: (1) accuracy, (2) efficiency, (3) simplicity and (4) generality. By accuracy, they mean the sensitivity of the formulations to computational errors (e.g., rounding off errors). The author would add to this criterion, the sensitivity of the formulations to problems with the measured data. By efficiency, they take two factors into consideration: (i) computational memory and (ii) user time. By simplicity, they regard the fact that the computational code should be simple to allow all kinds of problem to be solved. By generality, both (i) physical and (ii) mathematical generality should be examined. According to them, for a method to be physically general, basically three cases should be allowed: (a) grounding of coordinates, (b) coupling of coordinates on the same structure and (c) coupling of several structures simultaneously. For a method to be mathematically general, it should not be restricted by singularities in the matrices used. They suggest that some weighting factors

should be imposed in each of the above criteria, where higher weights should be applied to the mathematical and physical generality.

The first formulation of FRF coupling found in the literature after the work of Bishop and Johnson is based on the impedance concept. Therefore, it is going to be addressed here as the **impedance coupling formulation.** Considering this formulation to be the basis for the development of more advanced formulas, it is presented in the next section. In essence, it involves a summation of inverse FRF matrices (i.e. impedance matrices), where the number of terms in the summation is related to the number of structures being coupled. In order to obtain the FRF predictions of the coupled structure, the previous result has to be inverted as well. The order of the FRF matrices used is determined by the number of coordinates involved in the coupling process and not by the number of degrees of freedom of either component. As the former is normally less than the latter, the expected reduction in the set of equations to be solved is consequently obtained. Early references of this kind of formulation include the publications in 1968 by Heer and Lutes [56] and Lutes and Heer [79]. After that, one can mention the works of Ewins and his followers, from 1969. Among such references are the papers by Ewins and Sainsbury [37], Ewins and Gleeson [38], Ewins, Silva and Maleci [39] and the report by Ewins [43]. This technique was even included in a text book by Ewins [41].

The requirements and problems of the impedance coupling formulation are addressed in details in two of the works by Ewins [42, 43]. The requirements are also analysed thoroughly in a report by Skingle [106]. In a paper by Stassis and Whittaker [117], special attention is given to the experimental problems that can affect this formulation. Among one of the very important requirements is the inclusion of rotational DOFs. Actually, this is a requirement for any FRF coupling formulations, apart from the one proposed by Larsson [72]. He proposes a new formulation based on constraints to eliminate the need for the rotational DOFs. Basically, he uses the same principle that has been suggested in the derivation of rotation from translation measurements (see chapter 5). He also tries to quantify the possible source of errors. A shortcoming of his proposal is that an initial idea of the displacement close to the interface is necessary. Only beams and plates were used in his work, since the displacements for those are known. Therefore, his formulation does not satisfy criteria 2(ii), 3 and 4(i). The need for rotational coordinates is stressed in reference [46] and in several other papers. Some solutions to the problem of their acquisition are given in references [37] and [38], for example.

Although the impedance coupling formulation could be used for multiple coupling between structures (therefore, satisfying criterion 4(i)), in reference [39] it is suggested to use the

formula in a sequential way. An explanation for that is the possibility of eliminating some coordinates that are no longer of interest, thus reducing the size of the matrices to be handled. Coordinate selection is also very important. As mentioned in reference [37], no unimportant coordinate should be included in the coupling process, as errors on those can jeopardise the accuracy of the predictions (criterion 1). A similar argument can be made to ensure the elimination of linearly dependent coordinate pairs. This subject is addressed later in this section. Despite criterion 4(i) being achieved, the impedance coupling formulation fails in some of the others. First of all, since the inversions are performed on full size matrices and (at least) three of these are required, this formulation can be computationally very expensive (criterion 2(i)). Besides, the sub-structure matrices tend to become ill-conditioned around their resonance frequencies; the same happening around the resonances of the coupled structure. Hence, criterion 4(ii) is not satisfied. The ill-conditioning problem becomes more pronounced when the measured data are contaminated by noise or there are some inconsistencies in the measured FRFs (such as, shifts on the natural frequencies and damping factors). So, criterion 1 is also violated when this happens. Occasionally, spurious peaks can be found in the predicted FRFs, and these are caused mainly by numerical problems. These peaks may be difficult to distinguish from true resonance peaks. Such problems are pointed out in the works by Skingle [107], Urgueira [127] or in references [37, 42, 43, 97]; to mention just a few. It is quoted in the work by Imregun, Robb and Ewins [65] or in reference [41] that, the more damped the structure is, the less sensitive to the mentioned problems the predictions are going to be. In order to minimise the noise problems or the inconsistencies in the measured data, some papers have suggested the use of smoothed FRFs generated from modal parameters [42, 65]. Attention has to be taken to account for the effect of all the modes in this process, so as to avoid the introduction of additional errors [43, 106, 127]. As mentioned in references [38, 39, 43], the smoothing of FRF curves (even without using a consistent data set) has the advantage of reducing the volume of the input data.

An improvement on computational efficiency of the impedance coupling formulation above was achieved with the formulation proposed by Brassard and Massoud [12]. This was realised by reducing the order of the matrices to be inverted. Those matrices are now related to coupling DOFs only, which are normally much fewer than the total number of coordinates involved in the coupling process. Their formulation can be regarded as an intermediate step between the formulation above and the one used throughout this thesis. Although it is computationally more efficient than the impedance coupling formulation (criterion 2(i)), it is no longer physically general (criterion 4(ii)). In the way it was developed, only two sub-structures can be coupled at

a time. Such a limitation is not severe, since this procedure was recommended in [39]. All the other shortcomings of the impedance coupling formulation still apply to their formulation. Despite the fact that only coupling DOFs are involved in the inversions, for some of the coupling predictions, up to three different matrix inversions are still required. This is due to the partitioned nature of their formulation. Actually, if only coupling coordinates are involved, their formulation becomes the same as the impedance coupling one. Consequently, the coupling formulation was developed even further.

The biggest improvement of all was obtained in the work by Jetmundsen, Bielawa and Flannelly [67]. Their formulation managed to reduce the number of inversions required from three to one, while retaining only coupling DOFs in the matrix inversion. It is the most efficient formula in terms of computational requirements (criterion 2(i)) and also satisfies the physical generality criterion 4(i). This formula was chosen to be used in the thesis and it is presented in section 2.3.2. It is going to be called here **improved FRF coupling formulation.** Because only one inversion is necessary, and that is related to the summation of sub-structure FRF matrices at the coupling coordinates, the problems around the resonances of each sub-structure are minimised. Therefore, this formula is mathematically more general (criterion 4(ii)). Inconsistencies in the measured data can still cause numerical difficulties, but using smoothed FRFs tends to remedy such problems. They start the development of the formulation by coupling two sub-structures at a time and, later, extend to the case where several sub-structures are coupled simultaneously. As a result, their formulation allows either sequential or simultaneous coupling of several sub-structures.

In the work by Leuridan et al. [75], the ill-conditioning problem normally present in FRF coupling formulations was tackled using a different approach, which is an SVD based reduction technique. Both spatial and frequency domains are reduced using the SVD approach, where all redundant information is eliminated in a linear least-squares sense. Linearly dependent coordinates are regarded to be redundant information. The threshold on the SVD algorithm has to be carefully chosen in order to retain all the necessary data. Their FRF coupling formulation, although starting as the one proposed in reference [12], was developed further becoming very similar to the one in reference [67]. The SVD approach is performed on the latter one.

None of the formulations proposed so far, however, can cope with the case when several coordinates located on the same structure are coupled together. In reference [43], only some special cases of that, involving a single coupling between coordinates on the same structure,

were derived. The formulation proposed by Ren and Beards in reference [97] was developed to circumvent this limitation, at the same time keeping the advantages of the improved FRF coupling formulation [67], and is called the GRC (General Receptance Coupling) method. The improved FRF coupling formulation is, actually, a special case of the GRC method. Some variations of the method were proposed in the paper, where the one of most interest is the multi-step two-coordinate coupling (MTC). It is very simple to program and can be applied in a systematic way to couple all the required coordinates in a two coordinate basis. Besides, a parameter (a) was developed in this method to detect linearly dependent coordinate pairs based on the coordinates involved. Linearly dependent coordinate pairs are likely to occur if the coordinates involved are situated in a relatively rigid region of the structure [97,127]. The elimination of these linearly dependent coordinates is vital for correct predictions of the FRFs of the coupled system. Reference [97] presents a through investigation into this matter. As mentioned there, although the SVD approach suggested by Leuridan [75] or the QR algorithm suggested by Urgueira [127] could also be used to detect linearly dependent coordinates, both approaches have their shortcomings. These shortcomings, together with the ease of the MTC parameter, make the use of the latter more attractive. However, the a parameter has a shortcoming as well. It can be very large at the anti-resonance frequencies of the FRFs involved, even when the coordinate pairs are linearly independent. This fact can jeopardise the quality of the predictions if wrong use of the parameter is made. To avoid that, they suggest the use of the MTC method in two steps.

There is a class of coupling technique being developed since 1988, by Tsuei and his followers, called Modal Force Method (MFM) which follows the same principle of FRF coupling method. The difference between the two is that the latter requires the inversion of the FRF matrices which is not necessary in the former. Since inversion is one of the shortcomings of the FRF coupling method, the MFM should be more efficient. Another difference between the methods is that the output of the MFM is obtained as modal parameters, not as FRF curves. Only coupling DOFs are involved in the modal force matrix used in the MFM, and that makes this formulation similar to the improved FRF coupling formulation in its input. Since the input data are the same, the MFM also suffers from some of the problems involved in the FRF coupling formulations (i.e. noise on the measured data, for example). Among the papers involving this technique are the ones by Tsuei and Yee [123], Tsuei, Yee and Lin [124], Lin, Yee, Gu and Tsuei [76] and Chen, Yee, Wang and Tsuei [23]. This technique is compared with Leuridan's and impedance coupling formulations in a paper by Hu, Ju and Tsuei [61]. A similar comparison study is performed in reference [23], which also presents a modified modal force

technique using a Unified Matrix Polynomial Approach (UMPA). The MFM is very good and quick to predict the natural frequencies of the coupled system. However, as the output is a set of modal parameters, when the FRFs are regenerated using such a data set, the quality of the responses may not be good enough. This problem will be addressed in more detail in chapter 3, since the same limitation happens there. The MFM will not be used in this thesis. Nevertheless, the author decided to quote it here considering the fact that it is an intermediate method between the FRF coupling and CMS chosen to be used.

The main interest of the research summarised here is not the coupling technique itself, but the quality of the data used in it. Further, the inclusion of the effect of all the modes is the primary aim. Therefore, the improved FRF coupling formulation will be used throughout the thesis, despite the fact that the MTC method is an improvement over it. The author had already developed an FRF coupling program based on the improved FRF coupling formulation, when the MTC method was published. Since the research was not concerned with the coupling within the same structure, there was no real justification to change the program to the MTC method.

2.2.2. FRF COMPARISON PARAMETERS

In order to obtain a correct dynamic prediction of a coupled structure, an accurate experimentally-derived model of the sub-structures has to be obtained first. For that, the whole experimental test and modal analysis extraction procedures have to be carefully monitored to guarantee the quality of the data. There are several techniques to compare the quality of the extracted modal parameters, although there is no technique to compare the quality of the residual terms. The modal parameters' comparison techniques can be employed to compare two sets of experimental data, two sets of analytical data or a mixture of the two. Among such techniques are the frequency and mode-shape comparison plots, the Modal Scale Factor (MSF), the Modal Assurance Criterion (MAC), the Coordinate Modal Assurance Criterion (COMAC), etc. These and other modal comparison techniques are explained in detail in references [41] and [66]. However, comparing just the quality of the modal parameters does not guarantee the quality of the FRFs. So, more important than comparing the modal predictions, the quality of the response predictions should be checked for a more complete assessment.

No widely accepted technique has yet been developed to give a single value to compare two sets of FRF curves. Only one paper discussing the subject in detail has been found [129], although in this paper the interest was a comparison of transient responses and not FRF curves

directly. The paper presents several formulations to compare two response histories, where different error and inequality parameters are given. A similar parameter to the RSS (Root-Sum-Square) quoted in the above reference is used in [96] and that is called the NRD (Normalised Response Difference). The difference between these two parameters is the curve used in the denominator of the equations. When any of the parameters cited in these two references are used for the comparison of FRF curves, they can only give an indication of which set of curves is better than the other. They are unable to establish a single number to represent a good correlation. Moreover, all the above parameters are single term comparison parameters.

So, when FRF coupling is used to predict the dynamic characteristics of coupled system, in order to assess the quality of the predictions, either modal analysis has to be performed or each pair of curves have to be compared individually. Either process takes some time to be accomplished and a preliminary check would be very useful in order to detect any major discrepancy. Some collective parameters have been developed before, although mainly for the identification of modes. Nevertheless, they could be employed as comparison parameters as well by overlapping two sets of results so that some natural frequency discrepancies can be detected. Among such parameters are the Mode Indicator Function (MIF) [130], the multivariate MIF (MMIF) [130], the Complex Mode Indicator Function (CMIF) [34] or the Composite Response Criterion [41]. However, discrepancies at anti-resonances cannot be diagnosed using these parameters and this was the reason that motivated the author to develop the FIF (or IFI) parameter. Residual terms only affect the anti-resonance region of FRF curves and an indication about discrepancies there (before and after a coupling process is performed) is valuable. This new parameter is presented in section 2.4.

2.3. FRF COUPLING FORMULATIONS

2.3.1. THEORY

Before going further, one has to understand the definitions of ***mobility*** and ***impedance,*** as those are the main concepts used in this chapter. Mobility is a generic term used to represent any form of response/force (i.e. receptance, mobility or accelerance). It is also referred to as Frequency Response Function (FRF). The generic term used to represent the inverse ratio force/response is called impedance (i.e. dynamic stiffness, mechanical impedance or apparent mass) [41]. When the force is applied and the response is measured at the same coordinate, a point measurement is obtained. When the coordinates are different, a transfer measurement is obtained. Both mobility and impedance values are coordinate dependent.

In order to simplify the notation during the derivation of the formulation, the receptance FRF will be assumed at the beginning, although mobility or accelerance are equally valid. Receptance is defined as the ratio of the displacement to the force applied for a specific pair of coordinates (ij). It can be represented for a particular frequency point ω (where the terms are complex to accommodate both amplitude and phase information) as follows:

$$\alpha_{ij}(\omega) = \frac{x_i \cdot e^{i\omega t}}{f_j \cdot e^{i\omega t}} \tag{2.1}$$

When the above expression is evaluated over a certain number of frequency points (ω_1 to ω_k), an FRF curve is obtained. When it is evaluated over a certain number of coordinate pairs, an FRF matrix is obtained. The combination of these two (i.e. FRF matrix over a certain frequency range) gives the FRF values needed for the FRF coupling calculations.

To help understand the derivation, the same coupling system given in chapter 1 (Figure 1.7) will be used here as an example. Writing equation (2.1) in matrix form for each of the sub-systems involved in the coupling process there, and assuming that each receptance matrix is non-singular (i.e. that possesses an inverse), yields:

$$\{f_A\} = [\alpha_A(\omega)]^{-1}\{x_A\} \tag{2.2}$$

$$\{f_B\} = [\alpha_B(\omega)]^{-1}\{x_B\} \tag{2.3}$$

$$\{f_C\} = [\alpha_C(\omega)]^{-1}\{x_C\} \tag{2.4}$$

For convenience, from now on, the receptance's frequency dependency is dropped from the expressions. By introducing the equilibrium condition represented by equation (1.2), given in chapter 1, the above equations can be grouped as follows:

$$\{f_C\} = \{f_A\} \oplus \{f_B\} \;\therefore\; [\alpha_C]^{-1}\{x_C\} = [\alpha_A]^{-1}\{x_A\} \oplus [\alpha_B]^{-1}\{x_B\} \tag{2.5}$$

The symbol $\oplus$ is used to represent the addition relative to the physical nature of the coupling. This concept will be clarified later. First, one can simplify the RHS of equation (2.5) further by using the compatibility equation (1.1), also given in chapter 1, i.e.:

$$\{x_C\} = \{x_A\} = \{x_B\} \quad \therefore \quad [\alpha_C]^{-1}\{x_C\} = \left([\alpha_A]^{-1} \oplus [\alpha_B]^{-1}\right)\{x_C\} \tag{2.6}$$

Both sides of equation (2.6) are expressed in terms of the displacement of the coupled system. Therefore, this term can be cancelled out from the equation, leading to:

$$[\alpha_C]^{-1} = [\alpha_A]^{-1} \oplus [\alpha_B]^{-1} \tag{2.7}$$

Equation (2.7) can be expressed in terms of impedance matrices. In such a case, the following equation is obtained:

$$[Z_C] = [Z_A] \oplus [Z_B] \tag{2.8}$$

The problem of using impedance matrices is that, although equation (2.8) is a simpler formula, such matrices are more difficult to obtain directly from experiments. Besides, the relationship between mobility and impedance matrices is only valid if all coordinates are available in the former matrix. When a reduced coordinate set is used, although the mobility matrix stays the same, the impedance matrix will differ for each coordinate set used. This can be understood by recalling the concepts of mobility and impedance functions [41]:

$$\alpha_{ij}(\omega) = \left(\frac{x_i}{f_j}\right)_{f_m=0;\, m=1,N;\neq j} \qquad Z_{ij}(\omega) = \left(\frac{f_i}{x_j}\right)_{x_m=0;\, m=1,N;\neq j} \tag{2.9}$$

It is clear from equations (2.9) that, although it is perfectly feasible to obtain the mobility curve experimentally (by exciting only one coordinate while all the other coordinates are force free), it is much more complicated to obtain the ***impedance*** curve. This requires all coordinates apart from one to be grounded. Therefore, if an extra term has to be included in the impedance matrix, all the other terms have to be re-measured. This constraint does not apply to the mobility matrix. There, only the extra term has to be measured. This explains why FRF coupling formulations were chosen instead of impedance coupling ones.

From now on, a more generic notation for the mobility matrices will be used (where H represents any type of FRF). So, equation (2.7) can be re-written using the generic notation as follows:

$$[H_C]^{-1} = [H_A]^{-1} \oplus [H_B]^{-1} \tag{2.10}$$

If the inverse of equation (2.10) is calculated, the FRF predictions for the coupled system can be obtained as defined below:

$$[H_C] = \left([H_A]^{-1} \oplus [H_B]^{-1}\right)^{-1} \tag{2.11}$$

Equation (2.11) is the impedance coupling formulation referred to in the previous section. It has several shortcomings as mentioned. First of all, it requires three full matrix inversions, what can be very expensive computationally depending on the number of DOFs involved. Another shortcoming can be the condition number of the matrices to be inverted. Despite the fact that the frequency dependency was dropped from this equation for simplification, this fact

has to be brought to attention again. Numerical problems are bound to happen at any frequency value close to the natural frequencies of either sub-system or the final coupled system. In such cases, the respective matrices to be inverted tend to become singular because the response will be mainly dominated by a single mode. The ill-conditioning problem is even more pronounced when there are measurement errors involved (i.e. noise or inconsistencies in the measured data).

At this point, one needs to have a clear understanding of what the referred matrix addition is (represented by the symbol $\oplus$). It basically means that only coupling coordinates are going to be added. The other coordinates, although present, are not directly involved in the addition process. Figure 2.1 represents the matrix addition expressed by equation (2.10) for the particular example used here (Figure 1.7). It should be noticed that the coupling coordinates were rearranged such that the coupling coordinates of ***A are*** coupled with the corresponding coupling coordinates of ***B.*** Moreover, each sub-system matrix was partitioned according to slave (s) and coupling (c) coordinates.

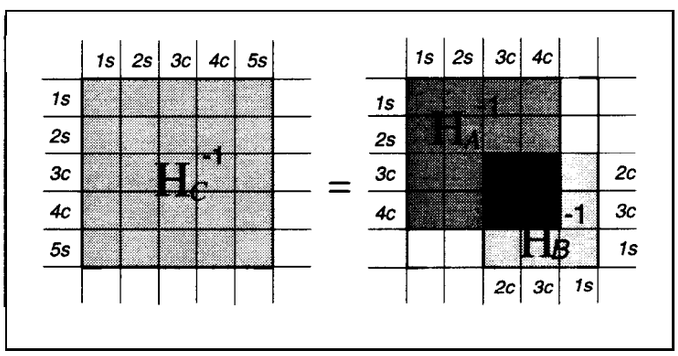

Figure 2.1 - Schematic representation of the matrix "addition"

The shaded areas on the RHS of this figure are actually the necessary information in order to obtain the coupled system predictions (represented by the shaded area on the LHS of the figure). There are some blank areas there which contain no information. The blank areas have to be substituted by zero value matrices or vectors to allow the improved formulation (following next) to be developed. What will determine this dimension for each sub-system matrix is the number of slave coordinates the other sub-system has. Therefore, the matrix addition represented in Figure 2.1 can be expressed in matrix form as:

$$[H_C]^{-1} = \begin{bmatrix} \begin{bmatrix} [H_A^{ss}] & [H_A^{sc}] \\ [H_A^{cs}] & [H_A^{cc}] \end{bmatrix}^{-1} & \begin{bmatrix} [0] \\ [0] \end{bmatrix} \\ \begin{bmatrix} [0] & [0] \end{bmatrix} & [0] \end{bmatrix} + \begin{bmatrix} [0] & \begin{bmatrix} [0] & [0] \end{bmatrix} \\ \begin{bmatrix} [0] \\ [0] \end{bmatrix} & \begin{bmatrix} [H_B^{cc}] & [H_B^{cs}] \\ [H_B^{sc}] & [H_B^{ss}] \end{bmatrix}^{-1} \end{bmatrix} \tag{2.12}$$

2.3.2. IMPROVED FRF COUPLING

In the previous section, some of the shortcomings of the impedance coupling formulations were highlighted. They are related to (i) the number and (ii) the size of matrix inversions and (iii) numerical problems on these mathematical operations. Such problems are circumvented or minimised by the formulation developed by Jetmundsen, Bielawa and Flannelly [67] which is presented next. The first step towards a more improved FRF coupling formulation is to reduce the number of matrix inversions required. Equation (2.12) can be re-written without loss of generality as follows:

$$[H_C]^{-1} = \begin{bmatrix} \begin{bmatrix} H_A^{ss} \end{bmatrix} & \begin{bmatrix} H_A^{sc} \end{bmatrix} \\ \begin{bmatrix} H_A^{cs} \end{bmatrix} & \begin{bmatrix} H_A^{cc} \end{bmatrix} \\ [0] & [0] \end{bmatrix}^{-1} \begin{bmatrix} [0] \\ [0] \\ [I] \end{bmatrix} + \begin{bmatrix} [I] & [0] & [0] \\ [0] & \begin{bmatrix} H_B^{cc} \end{bmatrix} & \begin{bmatrix} H_B^{cs} \end{bmatrix} \\ [0] & \begin{bmatrix} H_B^{sc} \end{bmatrix} & \begin{bmatrix} H_B^{ss} \end{bmatrix} \end{bmatrix}^{-1} - \begin{bmatrix} [I] & [0] & [0] \\ [0] & [0] & [0] \\ [0] & [0] & [I] \end{bmatrix} \quad (2.13)$$

By using identity sub-matrices instead of zero sub-matrices at the diagonal, is possible to take the inverse operation to the outside of each sub-system matrix. So, equation (2.13) can be redefined as[1]:

$$[H_C]^{-1} = \begin{bmatrix} H_A^{ss} & H_A^{sc} & 0 \\ H_A^{cs} & H_A^{cc} & 0 \\ 0 & 0 & I \end{bmatrix}^{-1} + \begin{bmatrix} I & 0 & 0 \\ 0 & H_B^{cc} & H_B^{cs} \\ 0 & H_B^{sc} & H_B^{ss} \end{bmatrix}^{-1} - \begin{bmatrix} I & 0 & 0 \\ 0 & 0 & 0 \\ 0 & 0 & I \end{bmatrix} \quad (2.14)$$

or using a simplified notation[2]:

$$[H_C]^{-1} = [H'_A]^{-1} + [H'_B]^{-1} - [I'] \quad (2.14a)$$

After correct pre- and post-multiplications, equation (2.14a) becomes (see Appendix A):

$$[H_C]^{-1} = [H'_A]^{-1}([H'_B] + [H'_A] - [H'_A][I'][H'_B])[H'_B]^{-1} \quad (2.15)$$

Finally, the coupled system FRF predictions can be obtained by inverting the above equation as follows:

$$[H_C] = [H'_B]([H'_B] + [H'_A] - [H'_A][I'][H'_B])^{-1}[H'_A] \quad (2.16)$$

Therefore, the desired reduction in the number of inversions was achieved by equation (2.16) when compared with equation (2.11). However, this was not the only improvement accomplished. The inversion is performed now after a combination of mathematical operations

[1] The matrix symbol for the partitioned matrices was abandoned for clarity in equation (2.14)
[2] The symbol prime' is used to represent the augmented improved matrices of equation(2.14)

involving the sub-system FRF matrices and not at the individual matrices. Consequently, the numerical problems previously faced close to the resonance frequencies of each sub-system are minimised. They are more likely in this case when the frequency values are close to the resonance frequencies of the coupled system, although not necessary restricted there.

From the enumerated shortcomings of the impedance coupling formulation given at the beginning of this section, just one remains, (iii). Despite the fact that only one inversion is necessary, the size of the matrix to be inverted is still the same as the one in equation (2.11). That is the total number of coordinates wanted for the coupled system. As a result of that, equation (2.16) was developed further to yield the following equation (see Appendix A):

$$[H_C]=\begin{bmatrix} H_A^{ss} & H_A^{sc} & 0 \\ H_A^{cs} & H_A^{cc} & 0 \\ 0 & 0 & H_B^{ss} \end{bmatrix}-\begin{bmatrix} H_A^{sc} \\ H_A^{cc} \\ -H_B^{sc} \end{bmatrix}\left[H_A^{cc}+H_B^{cc}\right]^{-1}\begin{bmatrix} H_A^{cs} & H_A^{cc} & -H_B^{cs} \end{bmatrix} \qquad (2.17)$$

It can be seen in equation (2.17) that the inversion this time is related to the coupling coordinates only (which are normally much fewer than the total number of coordinates wanted for the coupled system). Therefore, numerical problems tend to be reduced even more. As the number of inversions is kept to one, a considerable gain in computational speed has consequently been obtained. Equation (2.17) represents the improved FRF coupling formulation proposed in [67] and is the formulation used throughout this thesis. It is at the same time general (i.e. including both slave and coupling DOFs) and the most efficient.

However, if only coupling coordinates are of interest, there is no need to use equation (2.17). This equation can be simplified to:

$$[H_C]=\left[H_A^{cc}\right]-\left[H_A^{cc}\right]\left(\left[H_A^{cc}\right]+\left[H_B^{cc}\right]\right)^{-1}\left[H_A^{cc}\right] \qquad (2.18)$$

or by means of matrix inversion properties [89], the following equation can be obtained from equation (2.11), which is even simpler than the one above:

$$[H_C]=\left[H_B^{cc}\right]\left(\left[H_B^{cc}\right]+\left[H_A^{cc}\right]\right)^{-1}\left[H_A^{cc}\right] \qquad (2.19)$$

2.3.3. FRF COUPLING METHOD: ADVANTAGES AND DRAWBACKS

The advantages and drawbacks of the FRF coupling method can be evaluated regardless of the formulation used. The major advantage of FRF coupling when compared with other types of coupling methods is due to the format of its final results. These are already FRF curves (i.e.

response model) and, therefore, contain much more information than any other type of model. Besides, since the input data are also FRF curves, it could be derived straight from experiments. Actually, this was the reason why the method was developed in the first place.

However, there are some problems associated with the use of raw experimental data. Despite the fact that some insight into that has been already given in the first section of this chapter, these problems will be addressed in more detail in the next section. The major drawback of the method is the amount of data involved in the calculations. Although dropped from the derivation, all FRF coupling formulas are frequency dependent, i.e. they have to be evaluated over a certain number of frequency points. As a consequence, all FRFs have to be measured with the same frequency increment and include at least a common frequency range. So, only this common range can be used during the calculations and the predicted FRFs are, thus, limited to that range. There is also an inevitable need for matrix inversion operation in order to find the coupled FRF predictions. Although some formulations are better than others in that sense, none of them manage to get rid of the inversion altogether. Inversion is one of the most expensive mathematical calculations in computational terms and the fact that it has to be performed at each frequency point of interest presents a real drawback to the method.

2.3.4. REQUIREMENTS FOR CORRECT FRF COUPLING PREDICTIONS

There are several requirements one should try to fulfil when using the FRF coupling method to obtain the coupled predictions of assembled structures. The closer they are followed, the better the predictions are going to be compared with the correct answers. These requirements are listed below:

1. all FRFs should be noise-free;
2. a consistent data set should be used;
3. all important coordinates should be included for each sub-system;
4. all modes (or their effect) should be included in each FRF used;

Violation in any one of these 4 requirements causes the predictions to be in error. The amount of error introduced by each one is different and sometimes difficult to quantify. Although they are numbered, no more importance should be given to one or another.

The FRFs used in the FRF coupling method can be obtained from different sources. Among the most common, one can quote FE-derived FRFs, analytically-derived FRFs or the ones of most interest here, experimentally-derived FRFs. Each one has its own advantages and shortcomings and these are addressed next. They are also shown in Figure 2.2 for a better visualisation.

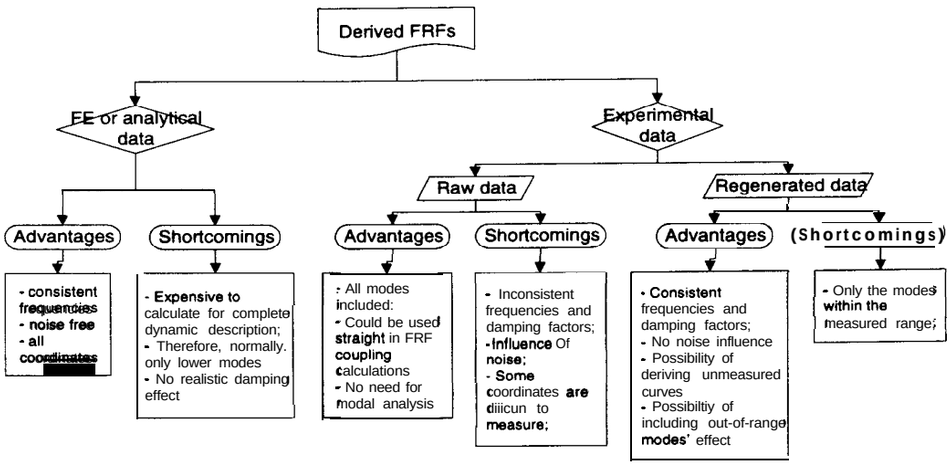

Figure 2.2 - Diagram of advantages and shortcomings of derived FRF curves

The FRFs obtained from FE or analytical models have the advantage of possessing consistent frequencies (requirement 2). They are also, noise free (requirement 1). Both requirements prevent numerical instabilities during the calculations. Moreover, any FRF of interest can be calculated without too much problem (requirement 3); including those involving rotational DOFs (the most troublesome coordinate to measure in a dynamic test, as explained in chapter 5).

However, such curves are expensive to calculate for the complete dynamic description (requirement 4). They can be derived using either spatial or modal models. When the FRFs are calculated using spatial models, this involves the inversion of normally big matrices (damping is usually ignored in FE analysis). As mentioned, inversions are expensive computationally, and for large size models become prohibitive. A condensation scheme could be performed prior the inversion, but the condensation itself has to be carefully performed to avoid the introduction of other errors. Reference [58], although not showing the formulations, presents a good criticism of the advantages and drawbacks of the most commonly-used reduction methods. The most popular for example, called static or Guyan reduction [53], preserves the stiffness properties of the structure at the expense of its dynamic properties. A dynamic condensation could be employed [44] to improve the quality of the former; however, approximations are still imposed. The modal model on the other hand, is also expensive to obtain when all the modes of the structure are required. For each DOF, there is one mode associated. Consequently, for larger systems, the number of modes to be extracted using eigensolver algorithms is also large. Besides, the results are often inaccurate for the high-frequency values". Therefore, when using the modal model to generate FRFs, it is very likely that only the lower modes of vibration are going to be included in these curves. A reliable

[3] due to computational problems

model containing all the modes is only possible when working with systems such as mass-spring-(damper), for which a small number of coordinates are normally involved (and, therefore, modes). Although it is not a real requirement for FRF coupling methods, it has to be remembered that real structures always contain a certain amount of damping (even if the value is small). A representative model, therefore, should be able to include such effects in a realist manner. Analytically or FE-derived FRFs do not normally meet such conditions.

The direct use of experimental FRFs (i.e. raw data) would be a strong advantage of the FRF coupling formulation as it would cut the costs considerably due to the elimination of the modal analysis stage. Besides, experimental data contain the contributions of all the modes present in the structure (requirement 4) and, therefore, can overcome the problem mentioned in the previous paragraph. Moreover, damping is always incorporated in the measured FRFs. However, raw data introduces other problems such as inconsistencies in the frequencies obtained due to experimental errors (requirement 2) and addition of noise (requirement 1). Furthermore, some FRFs can be difficult to measure, such as those involving rotational DOFs or in inaccessible positions (requirement 3).

The problems with raw data can be overcome by use of experimentally-derived models. A consistent modal data set is obtained when using modal analysis extraction techniques, i.e. all natural frequencies and damping factors become the same. Inconsistencies are likely to happen due to mass loading effects of accelerometers or shakers, for example, or due to modal extraction errors and these problems should be avoided. Therefore, before obtaining a consistent modal set, a careful examination into the causes of that kind of inconsistency should be made so as to avoid averaging errors. After a consistent modal set is derived, the FRFs can be synthesised from these modal data in order to get rid of the noise inherent in the experimental process (requirement 1), at the same time as getting a consistent FRF set (requirement 2). Unfortunately, the information about the modes outside the measured frequency range is lost in this case. Their effects, although included in the raw data, cannot be included in the modal data set due to the need of limiting the measured frequency range. So, again the same problem of incompleteness present in FE or analytical-derived FRFs arises. However, since both correct and derived FRF curves are obtained, their effect can be put back, as will be shown in chapter 4 (requirement 4). The problem with inaccessible or rotational coordinates can sometimes be circumvented by using interpolation functions (requirement 3).

From all requirements listed, 3 and 4 should be analysed into more detail. Their influence should be investigated separately for coupling and slave DOFs, as their effect on each one of

these coordinates is different. When a reduced set of coordinates is used in the FRF coupling method, depending on which coordinates are eliminated, the consequences can be severe or not (requirement 3). If the eliminated DOF is a slave one, the only implication is that one is going to be unable to predict the coupled behaviour at that particular DOF. However, if a coupling DOF is eliminated, this means that the boundary conditions of the structure are changed. In other words, some of the dynamic behaviour of one sub-structure is unable to be passed to the other sub-structure. Normally, the eliminated coupling DOFs are related to rotational DOFs, the reason been that these coordinates are difficult to measure. The only situation when a coupling DOF should be eliminated is for the case when the coordinates are located in a very rigid region. This would result in linear dependency of FRF curves [97,127] and, consequently, wrong FRF coupled predictions. This last point is not of interest here.

The inclusion of all modes (or their effect) on the FRF curves involved in the coupling process (requirement 4) also has different effects for coupling and slave DOFs. It is going to be shown in the examples section next that all modes should be included at the coupling FRFs if a correct prediction of natural frequencies and damping factors is sought. The lack of modes in slave FRFs will have no effect in such predictions. This fact can be anticipated by looking at the FRF coupling formulations (equations (2.17) and (2.18)). The slave FRFs play a secondary role in the formulations. They need to be included only when information about the dynamic behaviour at such coordinates is of interest. Therefore, it is expected that information concerning these coordinates should not affect the predictions. The lack of modes at these coordinates will only affect the anti-resonances.

To conclude, it does not matter how the FRFs are obtained, the best alternative is to have a consistent and noise-free model (which consequently has only the lower modes' effect). Then, compensation for the out-of-range modes should be included. Moreover, experimentally-derived FRFs should be used whenever possible, since they provide a more realistic description of the dynamic behaviour of the structure under investigation. Furthermore, all coupling coordinates should be included.

2.3.5. EXAMPLES

Experimentally-derived models are the main interest of the thesis. However, in order to have more control over each of the above requirements, in this section they are going to be examined using simulated data and one at a time. A more complex analysis using real data can be found in chapter 6 which deals with an experimental test case.

Requirements 1 and 2 are not the real concern of the thesis. Nevertheless, since their solution leads to the violation of requirement 4, they are included first to justify the basis for this research (i.e. why the residual problem has to be resolved). The consequences of including/excluding coordinates (requirement 3) are also studied, where the emphasis is on rotational DOFs. Although both residual and coordinate problems are inspected, no attempt is made to solve them yet. This is left open until chapters 4 and 5.

The leading coupling study in this section involves two mass-and-spring systems coupled together. The first one (sub-system **A)** consists of a 9 DOF mass-and-spring system and is shown in Figure 2.3. It is coupled in two coordinates to the 4 DOF mass-and-spring system of Figure 2.4 (sub-system **B), so** as to produce the 11 DOF coupled system of Figure 2.5 (system **CSYS1**). A 1% modal damping was added to all the modes to simulate a more realistic case. Five coordinates are of interest for sub-system **A;** namely coordinates 1, 3, 5, 7 and 9, whereas for sub-system **B,** all coordinates are. The coupling is performed such that coordinates 1A and 5A are coupled to coordinates 3B and 1B, respectively.

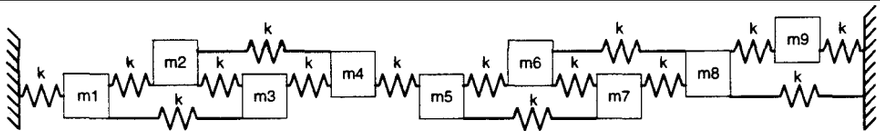

sub-system A

where: ml = m4 = m7 = 0.5 Kg
m2 = m5 = m9 = 1.5 Kg
m3 = m6 = m8 = 1.0 Kg
k = $1x10^6$ N/m
η = 0.01

Figure 2.3 - 9 DOF mass-and-spring system

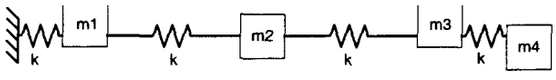

sub-system B

where: ml = 1.O Kg; m2 = 2.0 Kg; m3 = 3.0 Kg; m4 = 4.0 Kg
k = $1x10^6$ N/m
η = 0.01

Figure 2.4 - 4 DOF mass-and-spring system

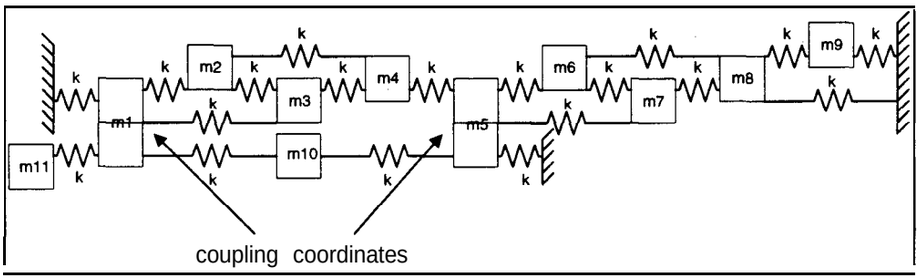

Figure 2.5 - Coupled system CSYS1

Several test cases were performed for coupled system **CSYS1**. Initially, the coupling process was accomplished using error-free FRF curves for both sub-systems, in order to compare the correct predictions with those involving violation in each one of the requirements. The formulation used is the one expressed by equation (2.17). Figure 2.6 shows both modulus and phase of coupling coordinates **FRFs** for sub-systems **A** and **B,** respectively. Only coupling coordinates are included to avoid overcrowding. Some of the FRF predictions using these error-free curves are presented in Figure 2.7.

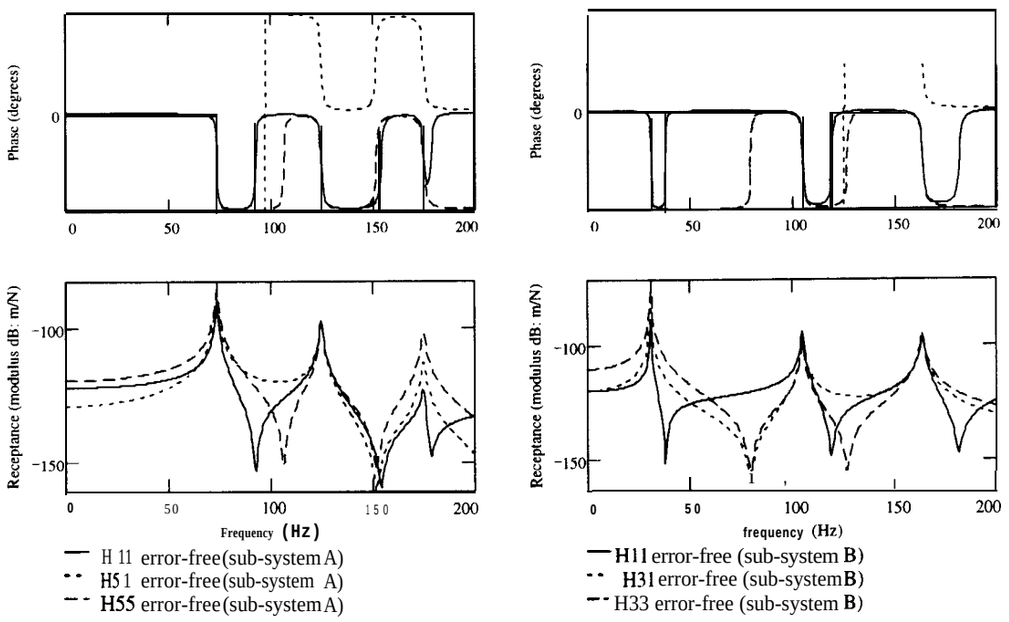

Figure 2.6 - FRF curves at coupling coordinates for sub-systems A and B (error-free curves)

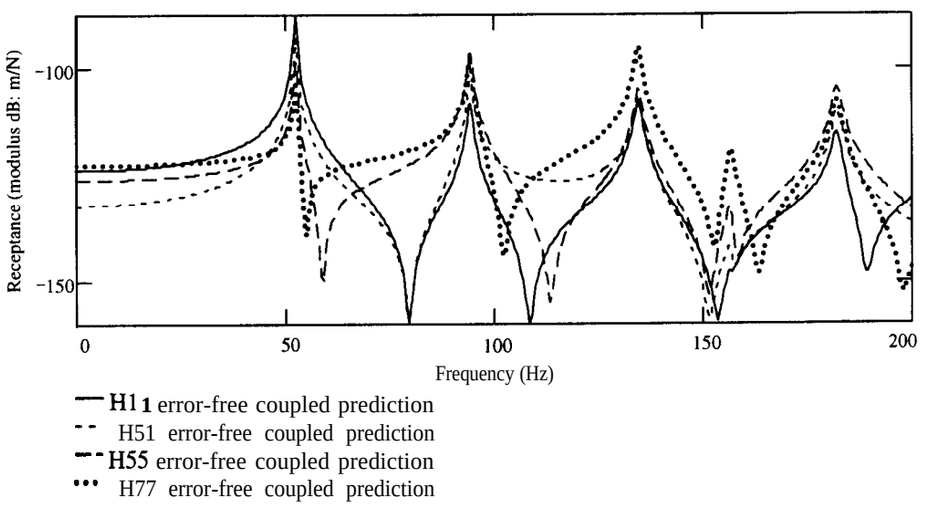

Then, 5% noise was artificially added in all sub-systems FRFs and the coupling was performed again using these data. To allow a better comparison with the previous case, the same FRF curves for each sub-system and the coupled system are plotted here for this new case (Figures 2.8 and 2.9, respectively). The amount of noise added is quite common in real experimental cases. Comparing Figure 2.6 with Figure 2.8, no discrepancies can be noticed. However, when the polluted FRF curves were used in the coupling process, the coupled FRF predictions became extremely noisy (Figure 2.9). This problem was even stronger near some resonances of the sub-systems, where the worst case was around 163.5 Hz. This region corresponds to the 3rd resonance frequency of sub-system **B** and is also very close to the 4th resonance of the coupled system. The coupling performed using this same amount of noise, but in a less damped system (0.1% damping was used), produced a much noisier FRF prediction, confirming the conclusions in references [41] and [65]. Such cases will not be shown here. So, for a normally expected amount of noise, the algorithm does not handle it very well. The problem cannot be associated with errors during the inversion process, since this was checked against an identity matrix and no discrepancies were found. Consequently, noise should be definitely avoided in FRF coupling calculations.

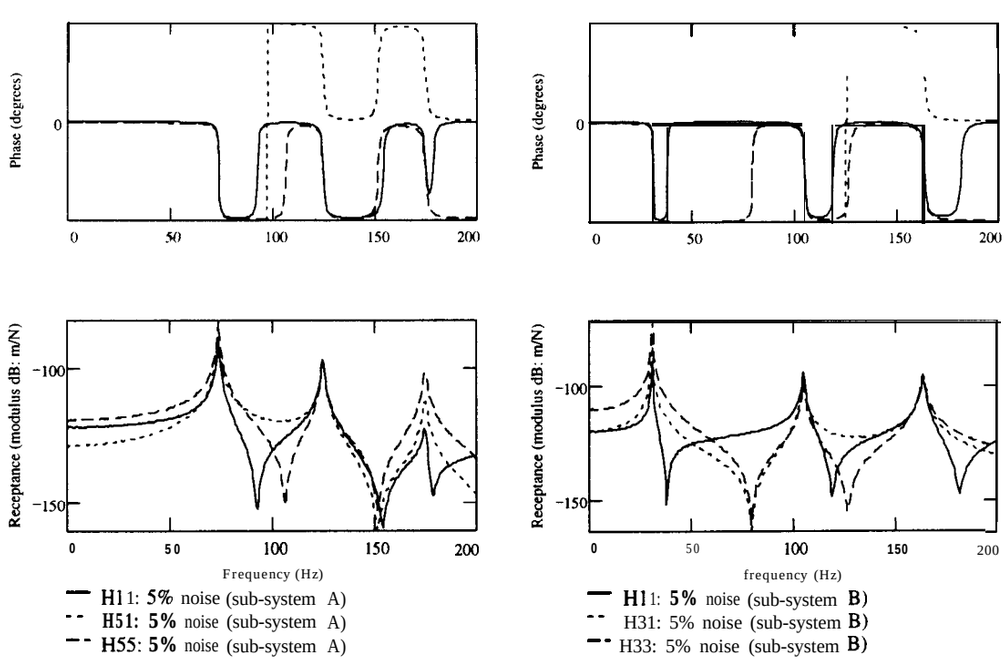

Figure 2.8 - FRF curves at coupling coordinates for sub-systems A and B (5% noise added)

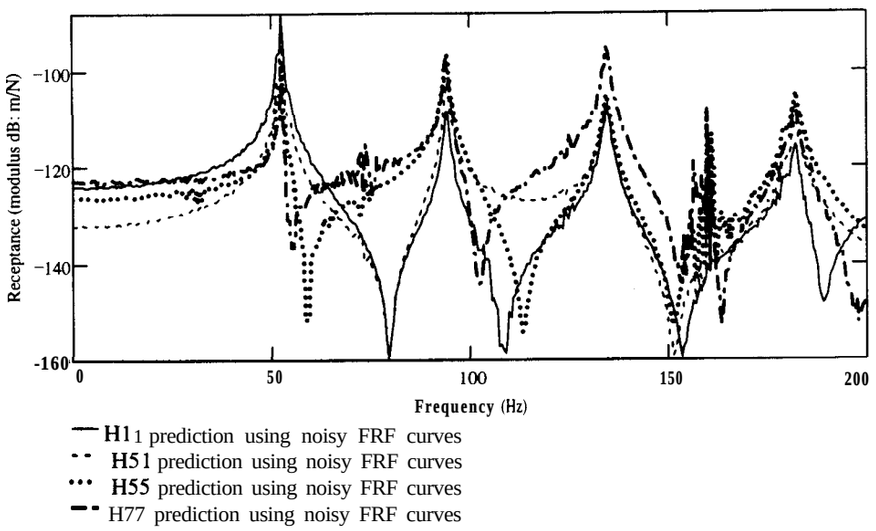

Figure 2.9 - Coupled FRF predictions for system CSYS1 (using 5% noisy FRF curves)

The next test case involves some inconsistencies in the natural frequencies of each sub-system. No other error was added. Normally, the causes for such inconsistencies (as explained in the previous section) do not affect all the modes in the same way. However, for the same measurement column (or row), they normally do. Therefore, such situation was simulated by choosing the amount of error completely at random for each column of the FRF matrix. Tables 2.1 and 2.2 show the percent errors added for sub-systems A and B, respectively. The bold FRFs in each table correspond to coupling coordinates FRFs and are, consequently, the ones involved in the inversion calculation. It should be emphasised that only the lower triangular terms were used, since, in general, the FRF matrix is symmetric for linear systems.

Table 2.1 - Errors added to the natural frequencies of each column of the "measured" FRF matrix used in the coupling process for sub-system A

1 st freq. (2% error)	1st freq. (1% error)	no error	2nd freq. (3% error)	3rd freq. (1% error)
H_{11}				
H_{31}	H_{33}			
"51	H_{53}	**H_{55}**		
'471	"73	H_{75}	H_{77}	
H_{91}	H_{93}	H_{95}	H_{97}	H_{99}

Table 2.2 - Errors added to the natural frequencies of each column of the "measured" FRF matrix used in the coupling process for sub-system B

1st freq. (1% error)	1st freq. (1.5% error)	no error	2nd freq. (0.5% error)
H_{11}			
H_{21}	H_{22}		
H_{31}	H_{32}	**H_{33}**	
H_{41}	H_{42}	H_{43}	H_{44}

This time, no sub-system FRF curves are considered individually. Instead, one FRF curve for each sub-system is plotted, together with the coupled FRF predictions, to highlight the positions where wrong predictions occurred. They happen around sub-system's resonances and vertical lines are also shown to emphasise that. Figures 2.10 and 2.11 show some FRF predictions for the correct case and the case using these inconsistent FRF data (including the sub-system curves above).

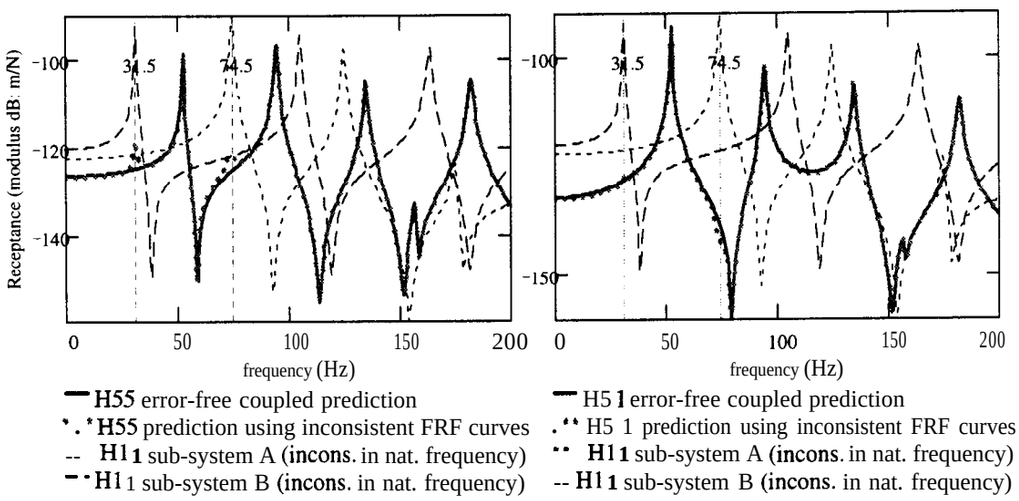

Figure 2.10 - Coupled FRF predictions at coupling coordinates for system CSYS1 (using inconsistent FRF curves)

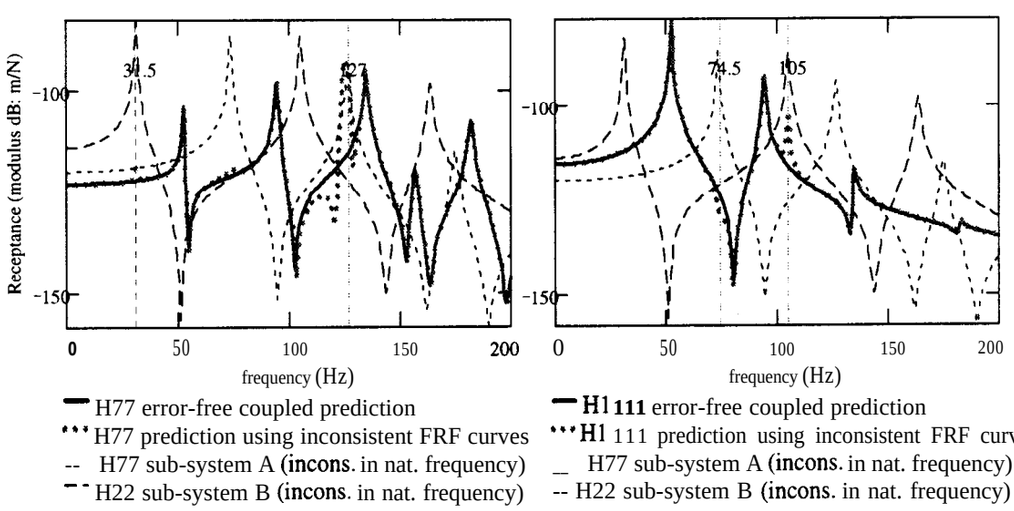

Figure 2.11 - Coupled FRF predictions at slave coordinates for system CSYS1 (using inconsistent FRF curves)

It should be noticed that the significance of such inconsistencies is different for each FRF prediction. The errors associated with coupling coordinate FRFs tend to be spread to all FRF predictions. However, the ones associated with slave coordinates are only present there normally. The effects of natural frequency inconsistencies are usually less serious than noise effects. Nevertheless, spurious peaks may happen around resonances of the sub-system as a consequence of the former and these may be difficult to separate from true peaks. Therefore, inconsistencies should also be avoided.

The final test case for this coupled system was performed including/excluding out-of-range modes at slave and/or coupling DOFs for each sub-system. Several case studies were tried using the above combination and these are summarised in Table 2.3. There, "included" means using the correct FRF curves, whereas "excluded" means using regenerated FRF curves without compensation for the out-of-range modes.

Table 2.3 - Out-of-range modes chart for the FRFs used in the coupling process

Case Study	*coupling DOF*		*slave DOF*	
	system A	system B	system A	system B
M1	included	included	included	included
M2	included	included	excluded	excluded
M3	excluded	excluded	excluded	excluded

Three different curves are plotted for each case study of Table 2.3. These are a point measurement for a coupling DOF (Figure 2.12), a point measurement for a slave DOF (Figure 2.13) and a transfer measurement between a coupling and a slave DOFs (Figure 2.14). For the former figure, as long as the correct FRF curves are used at the coupling DOFs (cases Ml and M2), the correct coupled predictions are obtained, regardless of the curves used for the slave DOFs. This remark was included in the previous section, by analysing equations (2.17) and (2.18). When only regenerated curves are used (case M3 of Table 2.3), it does not matter which coupled prediction one is talking about (all three figures), all exhibit incorrect resonant frequency predictions, as well as wrong response predictions. For this particular example, even the number of modes predicted using these incomplete curves is wrong (4 instead of 5). Leaving out modes only at slave DOFs (case M2), although producing correct frequency predictions, does not produce correct response predictions for some FRFs. Incorrect response predictions are stronger at point measurements (Figure 2.13) than at transfer measurement (Figure 2.14). One remark has to be made here, however. The effects of out-of-range modes are coordinate-dependent and their influence in the coupled predictions is difficult to quantify. It is also linked to the position where the coupling is performed.

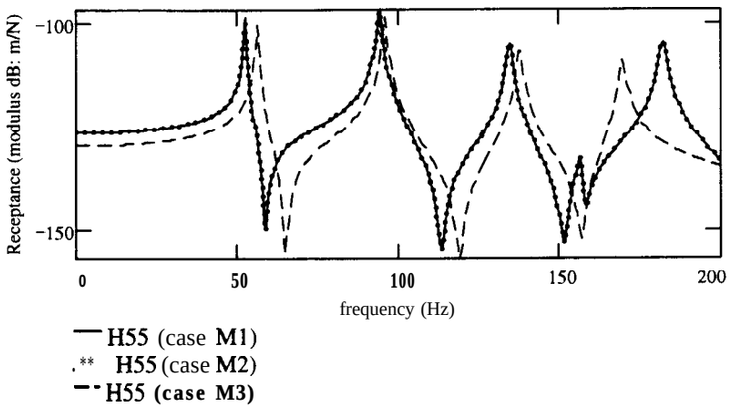

Figure 2.12 - Coupled FRF predictions for system CSYSl at point measurement $H_{5,5}$ (coupling DOF)

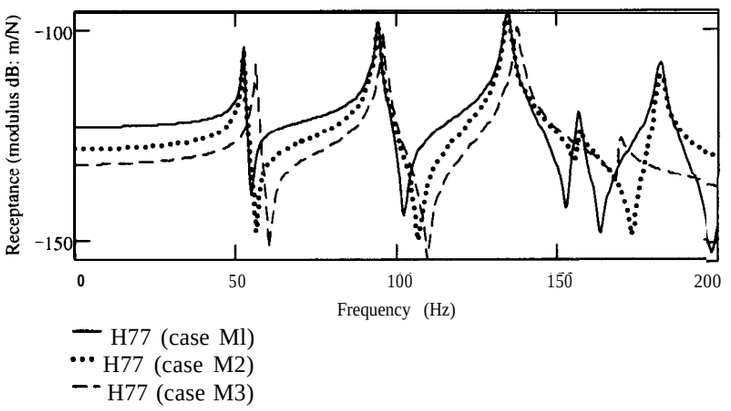

Figure 2.13 - Coupled FRF predictions for system CSYSl at point measurement $H_{7,7}$ (slave DOF)

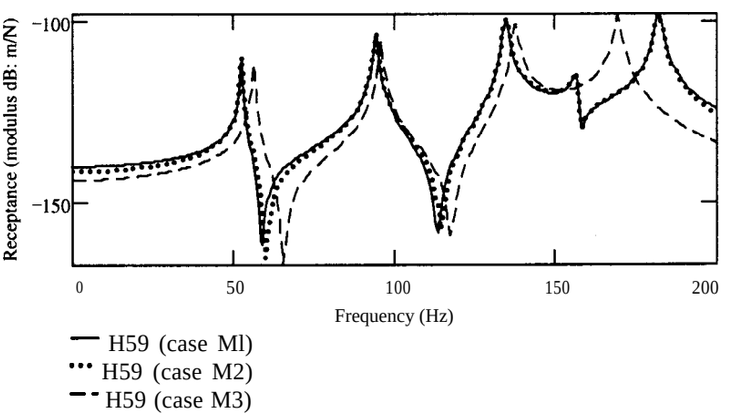

Figure 2.14 - Coupled FRF predictions for system CSYS1 at transfer measurement $H_{5,9}$ (slave/coupling DOF)

The last coupling study investigated in this section uses a structure called "1203A". It consists of 3 plates connected together (referred here as the main frame), plus 2 identical struts. It was analysed using ANSYS software (version 5.0), using shell elements for the plates and 3D beam elements for the struts. Such elements include 6 DOFs/node. The FE mesh for the coupled structure is shown in Figure 2.15. The coupling is assumed to be between the struts and the main frame at the coordinates shown in this figure. Only coupling coordinates are considered of interest for both sub-structures, and that involves a total of 300 FRF curves (already taking into consideration the symmetry of FRF matrix). The main frame was discretised using 116 nodes (i.e. 696 coordinates), while 13 nodes were used for each strut (78 coordinates).

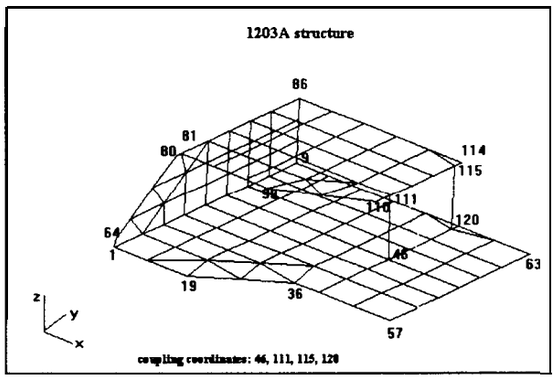

Figure 2.15 - 1203A structure (FE mesh used)

Despite the size of the spatial matrices, the correct FRF curves needed for the coupling process were obtained by direct inversion. No reduction in the number of coordinates was imposed to avoid introduction of errors. Also, no damping was assumed. The regenerated FRF curves were calculated using exclusively the modal parameters found within the specified frequency range of interest (from 0 to 800 Hz). That means no compensation for the out-of-range modes was included. In that range, the main frame has 21 modes (6 rigid-body and 15 flexible), while the struts have only the rigid-body modes (i.e. 6 modes). The modal incompleteness was confined in this study to the main frame. The inclusion/exclusion of rotational DOFs is the primary focus of the results reported here, where the inclusion/exclusion of out-of-range modes is secondary. Some test cases were analysed using the above combinations and they are summarised in Table 2.4.

Table 2.4 - Coordinates and modes chart for the 1203A coupling studies

Case Study	*Main Frame*	*Struts*
R1	all correct FRFs	all correct FRFs
R2	all correct FRFs, except θz related	all correct FRFs, except θz related
R3	all regenerated FRFs	all correct FRFs
R4	only correct translational FRFs	only correct translational FRFs

The only reason why case study R2 was included is to show that, for this particular structure, one of the coupling coordinates was not important; namely, θz (rotation in plane). This fact can be explained by examining the spatial matrices for the sub-systems. This DOF is completely uncoupled from the others and therefore does not affect the results. Its inclusion only allows predictions at such coordinates. Figures 2.16 and 2.17 present the $H_{115z,115z}$ coupled predictions for the case studies of Table 2.4. All the modes are seen in the correct curve (case R1), apart from two of them. Their position is highlighted by two vertical lines in these figures. Analysing the curves in Figure 2.16, it can be noticed that the lack of modes (case R3) overestimates the frequency predictions. The lack of rotational FRFs (case R4), on the other hand, underestimates the frequency predictions (Figure 2.17). Despite the results for the former being slightly better than for the latter, this is not a general rule and cannot be extended to other coupling studies. Besides, the modes are affected differently for the same type of incompleteness.

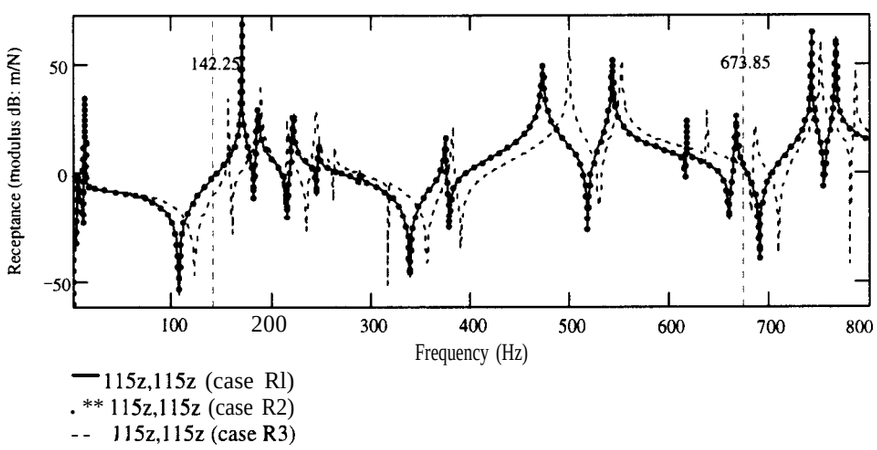

Figure 2.16 - Coupled FRF predictions for 1203A structure (cases R1 to R3 of Table 2.4)

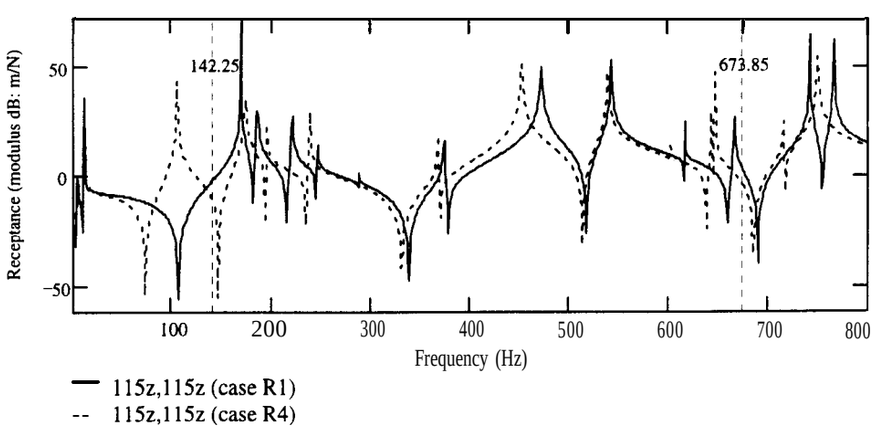

Figure 2.17 - Coupled FRF predictions for 1203A structure (cases R1 and R4 of Table 2.4)

2.4. PARAMETERS TO COMPARE THE QUALITY OF THE FRF CURVES

2.4.1. FL (FREQUENCY LEVEL) CURVE

In order to evaluate the quality of the FRF coupling predictions, FRF comparison parameters were developed. The first one, called "frequency level (FL)", is based on the fact that natural frequencies are global parameters of a structure and, therefore, have the same values regardless of the FRF under consideration. It was created to highlight the levels of the FRFs at the natural frequencies when all the FRF curves are taken into consideration. One of the most straightforward ways of analysing mathematically the size of a matrix (or vector) is through its norm [89], where the Frobenius or 2-norm is defined as:

$$\left\| [A] \right\|_F = \sqrt{\sum_i \sum_j a_{ij}^2} \tag{2.1}$$

So, if the norm is taken of an FRF matrix (or vector) at each frequency point in the range of interest, the frequency level (FL) function sought can be obtained as formulated below:

$$FL(\omega) = \left\| [H(\omega)] \right\|_F \tag{2.2}$$

A plot of the above function will take the same form as an FRF curve and should be plotted in a dB scale for a better visualisation. As no individual curve can have a value bigger than the one calculated, a fairly good indication of the modal energy level can be obtained using this plot. However, since the norm of a matrix is an absolute value, the sign of each FRF is lost in the calculation and no anti-resonance pattern is generally seen. Therefore, only the resonance contents can be checked against the correct values, not the anti-resonances. Any FRF that presents resonance values other than the correct ones will show a peak at that frequency which will be transmitted to the FL curve. One point that should be taken into consideration is when the individual FRFs involved in the calculation have very different levels. When this happens, meaningless results can be obtained. To remedy such problems, partitions of the FRF matrix have to be considered instead.

The main objective of developing the FL curve was to provide a quick way of comparing the quality of the frequency predictions obtained when using FRF coupling formulations. It could also be used for a quick check of measured FRF curves and this point will be demonstrated in chapter 6. Any one of these assessments would require either a modal analysis of the results, or a comparison of the FRFs on a one-by-one basis. By using the FL curve, all FRF curves are compared in one go, although not all the information can be extracted from that (e.g. the anti-resonances). However, if the predictions are required only at the resonance level, it would be

enough. It could equally be used to compare the quality of experimentally-derived models, prior to a coupling process. Nevertheless, since experimentally-derived models are obtained from already-calculated modal parameters, and residual terms only affect anti-resonances, this parameter is not of much use on its own in this case. The whole picture can be obtained with the help of the formulation given next.

2.4.2. FIF (FREQUENCY INDICATOR FUNCTION) OR IF1 (INVERSE FREQUENCY INDICATOR)

Depending on the level of prediction one is interested in (i.e. FRF comparison), it may also be important to have at least a rough estimate of the quality of the anti-resonance regions. This estimate is also valuable in assessing the quality of the experimentally-derived models before the coupling process is performed, as mentioned in the previous section. Anti-resonances are more difficult regions, since they are local parameters (i.e. they vary for each pair of excitation and response in consideration). If the resonance frequencies are correct but the anti-resonances are not, it is very likely that the same results are obtained when comparing correct with predicted FRF curves using the FL function, equation (2.2), unless the anti-resonance discrepancies are very big. This can be understood by the fact that virtually no emphasis is given to the anti-resonances when the above norm is calculated considering the FRFs at each frequency as linear values. Looking at what is done when one wants to check the anti-resonances of an FRF curve, one can extrapolate the above concept to be more sensitive to anti-resonance discrepancies as well. In order to give more or less the same importance to resonances and to anti-resonances, a logarithmic (or dB) scale is normally used. So, the second parameter developed will also be calculated using a dB scale. It is called "Frequency Indicator Function (FIF)" and can be defined as follows:

$$FIF(\omega) = \frac{1}{\left\| \left[20 \cdot \log\left(|H(\omega)| \right) \right] \right\|_F} = \frac{1}{\left\| \left[\mathrm{dB}\left(H(\omega) \right) \right] \right\|_F} \tag{2.3}$$

The reason why the inverse has to be used in equation (2.3) is that, sometimes, minima and maxima will have their positions interchanged[4]. The maxima should correspond to the resonances, whereas the minima should correspond to the anti-resonances effects. When this is not the case, the inverse of the FIF curve has to be considered. This new curve will be called here "Inverse Frequency Indicator (IFI)" and is formulated as:

$$IFI(\omega) = \frac{1}{FIF(\omega)} = \left\| \left[\mathrm{dB}\left(H(\omega) \right) \right] \right\|_F \tag{2.4}$$

[4] For a better explanation about that, go to page 217.

The choice between one type of function or another (i.e. FIF or IFI) should be based on the FL plot, since it tells exactly where the resonances are. Both functions also present the same form as an FRF curve, but now include both resonance and anti-resonance information. Due to the local characteristic of the anti-resonances, though, the anti-resonance pattern may be of very awkward shape. Moreover, they may appear as very small peaks instead of valleys (as will be shown in chapter 6). The importance of the above comparison curves relies on the fact that the same predictions should produce the same FIF or IFI shapes. The problems mentioned with the FL parameter for the case when the levels of the FRFs are very different also apply to the FIF (or IFI) parameter and this fact should be borne in mind when using it.

Since the above formulations are very simple, they can easily be incorporated into any FRF coupling program, hardly increasing its computation time. Then, before the actual predicted FRF curves are compared with the correct ones, a comparison should be performed between the predicted and correct FIF or IFI curves first in order to give an indication about how good the predictions are. If both natural frequencies and anti-resonances are acceptable, it is very likely that the individual curves are good predictions and a more detailed comparison can be performed then. The FIF (or IFI) curves should also be compared before the coupling process is actually performed, i.e. at the experimentally-derived curves. They are equally useful in comparing measured and theoretical FRF curves collectively, as will be illustrated in chapter 6.

2.4.3. EXAMPLE

An example will be shown here to stress the usefulness of the FL and FIF comparison curves in FRF coupling predictions. A truss structure is used for that purpose, since several interesting results were obtained for it. It was analysed using ANSYS, with all bars discretised with 2D spar elements. This element has only two DOFs, namely, translations at x and y. The bars were considered to be solid and made of aluminium alloy. The horizontal bars have diameter 5 mm and the vertical bars, 3 mm. Figure 2.18 shows a sketch of the truss, indicating the other necessary dimensions (in mm) and node numbers. It is considered to be perfectly clamped at nodes 1 and 4.

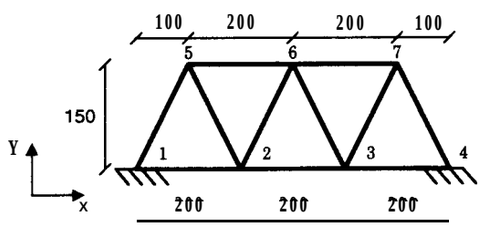

Figure 2.18 - Truss structure used in the FRF coupling analysis

The frequency range of interest specified for each sub-system was from 0 to 4500 Hz (that comprising 5 elastic modes). Because of the boundary conditions imposed, the maximum number of modes available is 10. From the full eigensolution, three different FRFs were generated, varying between them the number of modes included in the regenerated curves. For the first case, all modes were included and, so, those are the correct FRF curves. For the second case, only the modes within the frequency range of interest were included (i.e. 5 modes). For the third case, the FRFs were regenerated including 9 modes out of the 10 available. This means that only 1 residual mode was left out of the regeneration. As the only difference between the FRFs used in the FRF coupling process is the number of out-of-range modes excluded, only those are presented in Table 2.5.

Table 2.5 - Out-of-range modes of the truss structure (frequency in Hz).

	m6	m7	ma	m9	m10
freq.	4527.76	5042.62	6004.98	8739.77	10411.2
η	0.01	0.01	0.01	0.01	0.01
1x	0	0	0	0	0
1y	0	0	0	0	0
2x	0.46806	1.90461	0.58900	3.96112	0.04866
2Y	1.25368	-1.90311	0.53754	-0.04105	0.37449
3x	-0.46806	1.90461	-0.58900	-3.96112	0.04866
3Y	1.25368	1.90311	0.53754	-0.04105	-0.37449
4x	0	0	0	0	0
4Y	0	0	0	0	0
5x	-0.25994	-0.26067	4.42967	-1.10414	3.92276
5y	-4.59337	3.26838	0.13024	0.61644	-0.07321
6x	-2.3e-15	-0.66900	-1.8e-15	-2.0e-15	-4.53295
6y	1.59456	-7.1e-16	-0.51865	-0.65584	8.9e-17
7x	0.25894	-0.26067	-4.42967	1.10414	3.92276
7y	-4.59337	-3.26838	0.13024	0.61644	0.07321

The coupled structure consisted of the truss structure of Figure 2.18, coupled to a replica of itself, upside down. Figure 2.19 shows that assembly, with the new node numbers.

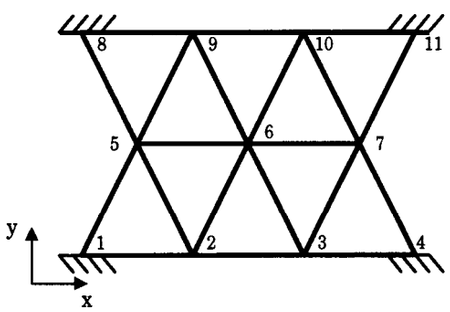

Figure 2.19 - Coupled truss structure

Although the same truss is used to assemble the coupled structure, in order to make the coupling process easier to follow, they are labelled differently. The original truss is considered as

truss A, the upside-down truss as truss B and the coupled structure as truss C. Three different coupling cases were tried, using the three available sets of FRF data above; as summarised in Table 2.6.

Table 2.6 - FRF coupling test cases

truss C	truss A	truss B
case 1	correct FRFs (all modes)	correct FRFs (all modes)
case 2	regen. FRFs (5 modes)	regen. FRFs (5 modes)
case 3	regen. FRFs (9 modes)	regen. FRFs (9 modes)

Only coupling coordinates were of interest here (i.e. 6 coordinates) and those are represented by a shaded box in Table 2.5. Due to the symmetry of the FRF matrix, only half of the FRFs have to be analysed; this means a total of 21 curves. However, the number of FRFs for this particular example can be reduced even further by noticing that, because of the symmetry of the structure, the FRFs relating x to y DOFs are zero. Moreover, FRFs for nodes 5 and 7 are identical and only one of them has to be defined. Therefore, from the initial 21 FRFs, only 8 FRFs have to be compared in the end. This number is still quite big if a one-by-one comparison is to be performed. In practice, such a degree of symmetry in the structure to reduce the number of FRFs to be compared will not always be the case (as is the case for the symmetry in the FRF matrix). This is a typical situation when the FL and FIF parameters are very useful.

Table 2.7 shows the 8 FRFs that have to be compared in order to evaluate the quality of the FRF coupling predictions. The numbers show which FRFs are identical. When they are not, a new number is used for labelling until 8 FRFs are given. The (0) represents the FRFs that, due to the symmetry in the coupled structure, have zero value. The blanks represent the FRFs that do not need to be compared due to the symmetry in the FRF matrix.

Table 2.7 - FRFs which have to be compared in order to evaluate the quality of the predictions

	5x	5y	6x	6y	7x	7y
5x	1					
5y	0	4				
6x	2	0	7			
6y	0	5	0	8		
7x	3	0	2	0	1	
7y	0	6	0	5	0	4

There are 7 modes within the specified frequency range of interest for the coupled system and those can be seen on the FL curve for the correct coupled predictions (case 1 of Table 2.6). Figure 2.20 shows the FL curves between cases 1 and 2 and between cases 1 and 3 of this table. By comparing the FL curves for the former, it is clearly seen that case 2 only managed to predict correctly the second natural frequency. The latter results, on the other hand, produced a

much better frequency prediction. From the 7 modes that should be predicted, 4 are correct (i.e. modes 1, 2, 4 and 6) and those can be seen by the agreement between the levels of the FL curves. However, 3 of them are wrongly predicted. In order to avoid confusion around the 5th mode, two vertical lines are plotted there; one for the correct frequency (case 1) and another for the coupled prediction frequency (case 3). This is to highlight that not only the level, but also the frequency itself, is not the same.

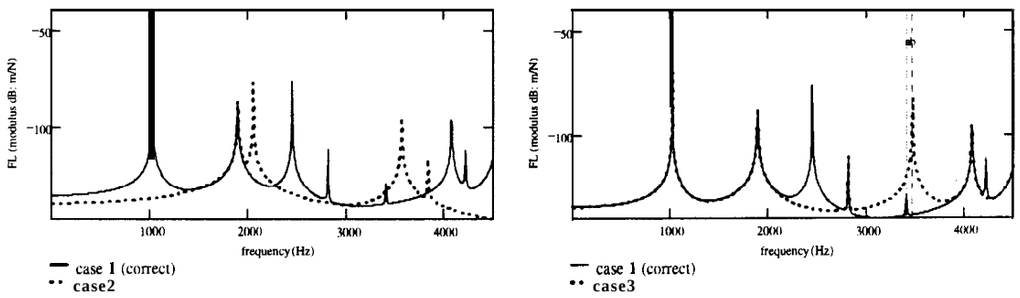

Figure 2.20 - FL curves for cases 1 and 2 and cases 1 and 3 of Table 2.6

As mentioned in section 2.4.1, the FL curves do not normally present any anti-resonance pattern and, for the above case, are very smooth. Nevertheless, they gave a very good indication of the frequency predictions obtained using both cases 2 and 3 of Table 2.6; although they did not necessarily show the discrepancies around the anti-resonance frequencies.

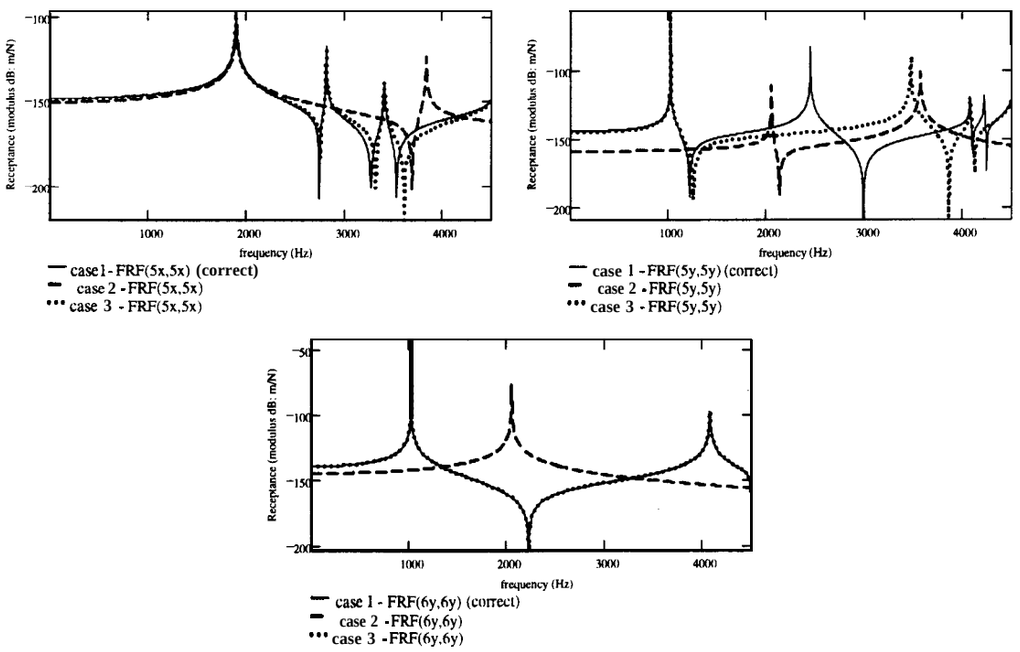

The above comments can be confirmed looking at Figure 2.21, which presents three particular FRFs (i.e. 5x/5x, 5y/5y and 6y/6y) for the three cases of Table 2.6. Those FRFs were chosen as they cover all the 7 modes of the full structure and, on average, give a good indication about the quality of the FRF coupling predictions. Similar results were obtained for the other curves. As shown in this figure, some of the FRF curves predicted for case 3 are completely correct (as it is the case for $H_{6y,6y}$); some of them are completely wrong (as it is the case for $H_{5y,5y}$) and some of them, although with the correct frequency predictions, did not have the correct anti-resonance predictions ($H_{5x,5x}$). When comparing the predictions in a one-by-one basis, if not all curves were compared, the problems could have not been noticed.

Only the problems with the natural frequency predictions could be spotted by the FL curves. Since the levels of the two FL curves (for cases 1 and 3) around the first two modes are the same, one might think that there were no problems there at the anti-resonance level for case 3. This is not the case. Therefore, the FIF curves are plotted to stress that this parameter, besides evidencing the natural frequency predictions, manages to give an indication about the anti-resonance predictions as well. Those curves are presented in Figure 2.22. Although the FIF curves look rather awkward, they manage to do a very good job for the purpose they were developed. Both resonance and anti-resonance discrepancies are seen through a comparison of these curves. The discrepancy at the anti-resonance between the first and the second modes of case 3, for example, that was not seen on Figure 2.20, is clearly seen now in Figure 2.22. Where the level of the reference FIF curve is equal to the level of the comparison FIF curve, it was noticed that the original curves are actually the same.

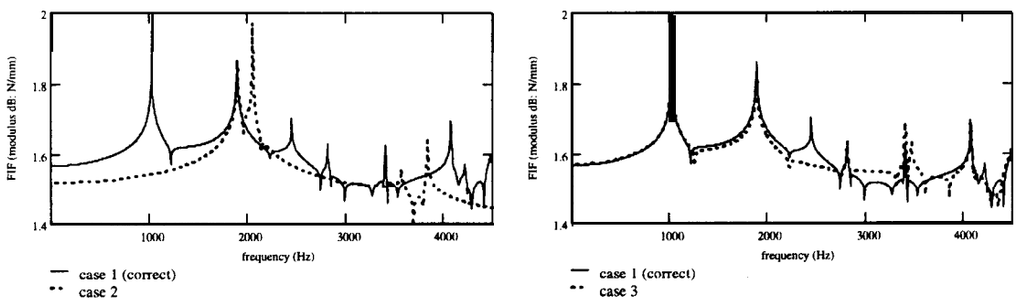

Figure 2.22 - FIF curves for cases 1 and 2 and cases 1 and 3 of Table 2.6

Such problems pointed out by the FIF curve at the prediction level could have been anticipated if the same parameter was evaluated at the sub-structures FRFs before the coupling was performed. This fact will not be shown here, though.

2.5. CONCLUSIONS OF THE CHAPTER

From what has been presented in this chapter, some conclusions can be drawn. All the following requirements should be followed in order to obtain the correct coupled predictions: (1) noise-free data; (2) consistent modal data sets; (3) inclusion of all modes (or their effects) and (4) inclusion of all important coordinates (particularly those related to RDOFs). The consequences of violating one or other of these are different and difficult to quantify.

Whenever possible, experimental data should be used in FRF coupling calculations since they are the most realistic descriptions of the structure's behaviour. However, raw experimental data should be avoided because of measurement noise and inconsistency problems and the use of experimentally-derived models is recommended. The latter should be complete both in terms of number of modes and number of coordinates included.

The consequence of leaving out modes in the coupling process is coordinate-dependent, both in the coupling sense and in the predictions sense. By "coupling sense", one means the positions where the coupling is performed. By "predictions sense", on the other hand, one means the consequences at slave and coupling coordinates. In order to obtain the correct natural frequency predictions for a coupled system, the out-of-range modes of the sub-structures have to be included in all coupling FRFs. Their inclusion in slave FRFs is only necessary if the level of response in such coordinates is of interest. The influence of leaving out coordinates is also coordinate-dependent. All coupling coordinates need to be included for a correct coupled prediction. Nevertheless, when the coordinates are linearly dependent, they have to be eliminated. Slave coordinates are only necessary in a coupling process if predictions at these coordinates are required.

Modal incompleteness tends to overestimate the frequency predictions. On the other hand, spatial incompleteness tends to underestimate them. The combination of the two does not have a clear pattern.

The FL and the FIF (or IFI) comparison curves developed in this chapter are collective parameters, therefore, they save time in extracting the modal parameters or comparing two FRF curves at a time when used with FRF coupling predictions. While the FL is capable of detecting natural frequency discrepancies, the FIF (or IFI) goes beyond and detects discrepancies at the anti-resonance levels as well. Nevertheless, because of the need to stress the anti-resonances, the natural frequencies' discrepancies may not be seen very clearly in the latter. Therefore, for a complete picture of the comparison, both of these curves should be analysed together.

CHAPTER 3: COMPONENT MODE SYNTHESIS (CMS) USING EXPERIMENTAL DATA

3.1. INTRODUCTION

In the preceding chapter, the response coupling method called FRF coupling was presented. There, the problems faced when using raw FRF data were addressed and the use of regenerated FRF curves was recommended to solve some of them. These curves are obtained using a modal summation formulation based on a consistent modal data set. Since a modal model has to be obtained, it seems natural to think about a coupling technique that uses this model directly, without the need of regenerating FRF curves. Component Mode Synthesis (CMS) does exactly that and is the subject of this chapter.

The chapter starts with a summary of previous work. Then, the general idea behind the CMS formulation is presented, followed by each specific formulation. All the formulations introduced can be used with free-interface normal modes, which are the ones obtained from experimental modal analysis and of primary concern here. Initially, the CMS formulation does not include any residual terms compensation (i.e. Hintz's approach). As will be demonstrated, the predictions obtained in such a case are normally inaccurate unless an extremely large number of modes is used. Therefore, formulations were investigated to eliminate such a need and, at the same time, to improve the accuracy. The solution was to include residual compensation for the high-frequency out-of-range modes. A CMS formulation with first-order residual approximation is analysed first (i.e. MacNeal's approach). This is the most-used CMS formulation for the case when only experimental data are available. However, it does not necessarily yield accurate predictions. In order to introduce an improved formulation developed in this research to ameliorate the previous results, the theoretical CMS formulation with second-order residual approximation is shown next (i.e. Craig-Chang's approach). Then, the developed technique is presented: the so-called IECMS (Improved Experimental Component Mode Synthesis) method. Actually, the formulation is the same for the theoretical second-order residual compensation CMS and for the IECMS; only the residual calculations differ. While the mass matrix of the system is needed for the former, all residual terms are obtained from

experimental data for the latter. The major advantage of the formulations chosen is that they are not dependent on the technique used to obtain the residual terms' compensation. Although residual compensation is the subject of the next chapter, an introduction to that is given here such to clarify the formulations presented. A more thorough investigation on how residual terms are calculated is given in chapter 4. Some examples are shown following the theories to validate the points quoted. Finally, conclusions are drawn.

3.2. SUMMARY OF PREVIOUS WORK

CMS techniques are developed on the same basis as spatial coupling formulations [1271. However, the coupling is performed in modal space, instead of in physical space. This conversion is accomplished by a Ritz-type transformation, relating the physical coordinates to the number of modes kept in the process. The thus-derived modal coordinates are subsequently used in the CMS formulations. The advantage of doing that is a reduction in the size of the problem to be solved. Due to modal truncation inherent in real analysis, the dimension of a system in modal space is normally orders of magnitude smaller than its physical space counterpart. However, as already discussed, modal truncation causes problems and care has to be taken to account for the missing information. Some solutions to that are given in the next chapter.

There are several different CMS formulations and they can be grouped into three different categories: fixed-interface, free-interface or hybrid methods. This classification is based on whether the modes are obtained with the coupling coordinates fixed, free or a combination of the two. Loaded interface methods can be regarded as a variation of free-interface methods. Within each category, different classes of modes can be used to define the required substructures' modal (or generalised) coordinates. These are: normal modes, constraint modes, rigid-body modes and attachment modes [30]. Rigid-body modes are a special case of constraint modes. It is common to use more than one class of mode for a given technique. Their selection is made on grounds of linear independence and completeness, computational costs to generate them, good approximation properties and simplicity, as cited in reference [32].

CMS formulations were initially developed to be used with FE analysis, so as to reduce the size of some problems there. However, a need exists to get the same dynamic predictions from experimentally-derived data and this is the main interest of this chapter. From FE, any class of modes can be easily obtained. From experiments, on the other hand, the only set of modes straightforwardly available are free-interface normal modes and attention will be concentrated

on techniques capable of using those. The reader is reminded that experimentally-based methods are the concern of this work.

Most of the references found in the literature using experimental information, actually employ a combination of analytical and experimental data. Even a conference was held treating "Combined Experimental/Analytical Modeling of Dynamic Structural System". The finding of this conference were summarised in a book published by the American Society of Mechanical Engineers (AMD-Vol. 67), whose introduction stresses some of the difficulties in developing such techniques [83]. Most of the problems quoted there are still present now, 10 years later. Very little attention seems to be given, however, to purely experimental approaches. It is important to stress that an analytical solution is not always possible or practical and a method to be general should allow for the situation when only experimental data are available, at least for part of the system.

CMS has been used in dynamic analysis for quite a long time. This subject has been treated in two text books [30,85] and in a list of review papers [28, 29, 31, 32, 59,120], to mention just a few. It started with the pioneer work of Hurty in 1960 [62], who developed a fixed-interface method for frames and beams using displacement mode functions. Subsequently, he generalised and extended the method to other types of structures in 1965 [63]. In 1968, Craig and Bampton [27] modified Hurty's generalised approach and this version of the fixed-interface method became one of the most popular. Nevertheless, from an experimental point of view, both approaches are extremely cumbersome.

So, free-interface methods were developed which are more suitable for using with experimental data. Early work employing that are the ones by Gladwell [47], Goldman [50] and Hou [59]. The first is based on what is called the branch modes' method and was limited to sub-structures connected in a statically determinate condition. The other two are the basis for more refined techniques and although eliminating the need for constraint modes, did not produce very accurate results when compared with fixed-interface methods.

One of the biggest problems of free-interface methods is to assure completeness of the modal representation within the frequency range of interest. When using normal modes, a large number are needed in order to properly describe the dynamic characteristics of each sub-structure, therefore preventing problems with modal truncation. Two different approaches can be adopted to improve the modal representation, without having to measure such large number of modes. The first one is by using additional information concerning the flexibility effects of the

out-of-range modes (i.e. residual terms). This is the procedure followed closest here, since the residual compensation can be easily extended to other types of coupling techniques (FRF coupling, for example). The most significant references related to that are the works by MacNeal [80], Rubin [99], Craig and Chang [29], Martinez, Miller and Came [84], Urgueira and Ewins [126] and Suarez and Matheu [119]. A brief explanation about each one is given shortly.

The second approach is by applying additional mass at the interface such to bring more modes within the frequency range of interest. The effects of the additional mass are analytically subtracted before the coupling is performed. The works by Benfield and Hruda [7], Goldenberg and Shapiro [49], Coppolino [26], Bertran [8] and Gwinn, Lauffer and Miller [54] fall into such a category, although references [8] and [26] also treat other kinds of method. Despite being a valid experimental approach, this method will not be discussed further, as it may be difficult to establish the size of the additional mass necessary to bring enough modes inside the range of interest. Such choice is very much dependent on the analyst experience. In [54], they state only that this size is normally big and the mass should have both translational and rotational inertia. Urgueira [127] goes slightly beyond this, relating the characteristics of the component tested with the size of the added mass; although not giving any guidelines for that.

All the formulations involving residual terms compensate for their effects through the use of a static residual', which is basically a first-order approximation. Some of them go beyond that, while still retaining the former. However, attachment modes can be used to compensate for the residual terms as well, since the two concepts are the same in practice. Attachment modes are defined as "the static deflection of the component which results when a unit force is exerted in one coordinate of the sub-set of the generalised coordinates, while the remaining coordinates in this sub-set are force-free [30]". For a restrained component, attachment modes are just the columns of the flexibility matrix of the structure. The disadvantage of both compensation methods (i.e. static residual and attachment modes) is that they are not available from an experimental approach. Trying to obtain the flexibility matrix from static tests does not produce good results. Besides, the stiffness matrix is not always available to the analyst. Even so, an equivalent experimental approach for the static residual can be obtained by measuring the necessary FRF curves, as explained briefly here and shown in the following chapter.

MacNeal's formulation [80] was the first one to include residual compensation as such, where a first-order approximation is employed to account for the flexibility effects of the truncated

[1] Refer to chapter 4 for more details about residual compensation techniques

higher modes. It was developed on a purely analytical basis using the static residual concept. However, due to the generality of the boundary conditions for the vibration modes and the possibility of calculating the residual compensation purely from experimental data (as mentioned above), it can be easily extended to the latter case. Actually, due to its simplicity, his formulation is still to date the most widely used CMS in such cases. It is presented in section 3.5.2. Urgueira and Ewins' approach [126] is very similar to the one used by MacNeal, where an intermediate elastic system is used to account for the flexibility of the truncated higher modes. The final formulation in both approaches is the same.

Rubin [99] extended MacNeal's method by using a second-order approximation, where both inertial and damping (dissipative) residual effects are added to the formulation*. So, it produces a better convergence and accuracy than the former. As Rubin's method has the potential to provide accurate results from an experimental point of view, Craig and Chang [29] based their improved approach on that. Their method also employs a second-order approximation to the residual terms and becomes more extensively used than Rubin's method. Nevertheless, neither Rubin nor Craig-Chang's methods can be used with purely experimental data, since the mass matrix is necessary in order to account for the residual inertia effects. A breakthrough was achieved in this thesis where a formulation is proposed to circumvent the need for the mass matrix, at the same time accounting for the inertia effects. The new method is called "Improved Experimental Component Mode Synthesis" (IECMS) and is an extension of Craig-Chang's method. The Craig-Chang and IECMS approaches are presented in sections 3.5.3.(a) and 3.5.3.(b), respectively.

Craig-Chang's method was developed even further by Suarez and Matheu [119]. The effects of higher truncated modes are accounted through the use of a second force derivative method which is performed in three parts. The first two parts are equivalent to Craig-Chang's method. The difference is in the third set, which is derived from the previous two. From the author's point of view, this new formulation is much more complex and not always necessary, since Craig-Chang's method is already quite accurate. The only situation when it will be justifiable is for components having an extremely high modal density in the frequency range of interest. Besides, the size of the problem to be solved becomes larger than the one proposed by Craig and Chang, being increased by the number of coupling coordinates involved. Moreover, their formulation requires the knowledge of the high-frequency modes which are not available. This

[2] The inclusion of damping residual effects is not compulsory.

last point could be resolved by using an extension of the IECMS method proposed in this thesis[3].

The formulation developed by Martinez, Miller and Came [84] was directly related to experimental tests. They also use a second-order approximation for the residual terms, although a different one to those proposed by either Rubin or Craig and Chang. In [84], the residual matrix of each sub-structure is inverted separately, and this is more prone to lead to singularities. For instance, if the number of coupling coordinates is bigger than the number of truncated modes, the residual flexibility matrix will become rank-deficient. All residual approximations used so far, perform the inverse after each sub-structure residual matrix has been added and, so, are much more efficient than the one quoted here.

A different approach was proposed by Klosterman [69], who developed two CMS techniques to be used with experimental tests; one based on free-interface modes and the other on fixed-interface modes. His first formulation required a large number of modes to describe adequately the dynamic characteristics of each sub-structure. So, the second approach was developed. Although he described all the necessary steps from an experimental point of view, his formulation is not straightforward to implement. The derivation of a residual flexibility matrix from experiments was first introduced in his work, despite not being directly incorporated in his CMS formulations.

Another formulation worth mentioning is the one proposed by Hintz [57]. Although he uses constraint or attachment modes[4] in conjunction with a severely truncated normal mode set, his formulation can be impiemented for the case when only free-interface normal modes are available (what is more realistic from experimental tests). The effects of the out-of-range modes are already taken into account when using the former set of modes, but that is not true anymore when using normal modes. Therefore, a sufficient number of modes have to be used in order to obtain a correct coupled prediction. His formulation is simple to implement and is the one used here to show what happens when the set of modes used is not complete and when no residual compensation is employed. This is presented in section 3.4.

Some authors have tried to establish the number of modes which should be retained in CMS formulations to avoid problems with modal truncation. Tolani and Rocke [121], for example, proposed two different criteria to select the modes to be kept. The first one is based on

[3] This extension is shown in chapter 4.
[4] He proved that both constraint and attachment modes are statically complete and therefore, equivalent.

frequency and the other on strain energy. Following their conclusion, the latter is slightly better. Rubin [99], on the other hand, set a target of 1.5 times the highest frequency mode of interest. A similar target was proposed by Hruda [60], where 1.4 times the highest frequency is used. Based on the author's experience, the last two targets may be either too conservative or too small, since the residual modes' influence is coordinate-dependent. However, as a basis, they are useful parameters. Ewins [42] mentions the same conclusion as the author's, for a target of 1.5 or 2 times the upper frequency of interest.

Even though the problems related to the lack of rotational DOFs (i.e. coordinate incompleteness) in CMS formulations are acknowledged in some works [54, 83, 84], very few papers try to tackle the problem. The consequences of ignoring such coordinates are the same as for FRF coupling formulations. Since this problem was covered in details previously, only the references treating this subject for CMS formulations are discussed here. In the paper by Chen and Chemg [24], the experimental estimation of rotations is done by measuring the generalised translational FRF matrix. Then, rotations are derived from those by using a first-order finite-difference method similar to the one proposed by Sattinger [103] and discussed further in chapter 5. In the paper by Llorca, Gerard and Brenot [78], they propose a method to evaluate rotational responses based on Love-Kirchoff theory for thin plates. Spatial derivations are made to obtain the rotational values. Sources of error in estimating rotational DOFs are presented. Like in FRF coupling formulations, rotational and/or translational coordinates are only important if related to coupling DOFs. Missing slave rotational DOFs will only results in being unable to estimate responses there.

Also following the comments for the FRF coupling methods, are the recommendations for the inclusion of residual terms' compensation. In order to obtain the correct frequency predictions for a coupled system, they only have to be included at coupling DOFs. Residual information at slave DOFs is only necessary when these coordinates are of subsequent interest. Then, they are included in the transformation of the coupled system mode-shape matrix from the modal space back to the physical space, as shown later.

Nothing was mentioned so far about damping considerations in the formulations quoted. Damped structures are not of particular interest here. However, if the reader wants to be involved in this aspect, reference can be made to Suarez and Singh [120], which paper includes a very good review of existing CMS formulations for damped structures up to 1992 and proposes a new formulation for nonclassically damped systems. More recently, Wang and

results are normally obtained with real CMS formulations when modal damping ratios are about 70% or less. However, **when this value** is exceeded, they recommended the use of a complex CMS method. Their recommendation was not based on the complexity of the eigenvector matrices, though, and nothing was mentioned about that aspect.

Next, the formulations are presented and that is followed by some examples to illustrate the theory.

3.3. GENERAL FORMULATION

The mass and stiffness matrices of a system are not normally available from experiments. However, in order to make the CMS derivation clear, they are going to be used at the beginning. The same coupled system as that shown in chapter 1 (Figure 1.7) will be adopted here once again, to help understand the derivation. Regardless of the formulation dealt with, the basic idea behind a CMS technique **is** to convert the coupling equations of motion from the physical space, $\boldsymbol{x}$, to the modal (or principal) space, $\boldsymbol{p}$. This is accomplished by a Ritz-type transformation as represented below:

$$\{x\} = [\phi]\{p\} \tag{3.1}$$

The normal modes of each sub-system can be obtained from either experimental modal analysis (the interest here) or from the solution of the following eigenvalue problem:

$$\left[K - \omega^2 M\right]\{x\} = 0 \tag{3.2}$$

The general equation of motion to be solved for each sub-system in physical space can be expressed by:

$$[M]\{\ddot{x}\} + [K]\{x\} = \{f\} \tag{3.3}$$

Then, by substituting equation (3.1) into (3.3) and pre-multiplying by $[\phi]^T$, the equation of motion is transformed from physical to modal coordinates as follows:

$$[\phi]^T [M][\phi]\{\ddot{p}\} + [\phi]^T [K][\phi]\{p\} = [\phi]^T \{f\} \tag{3.4}$$

When the specific orthogonality conditions of the mass-normalised eigenvectors are taken into consideration, the above equation can be simplified to:

$$[I]\{\ddot{p}\} + \left[\lambda^2\right]\{p\} = [\phi]^T \{f\} \tag{3.5}$$

Note that no physical matrices are needed any more in equation (3.5). It also considers the fact that, in order to accommodate damping, the eigenvalues can be complex (i.e. $\lambda_r^2 = \omega_r^2(1+i\eta_r)$), as also can the eigenvectors. From experimental modal analysis, this is a more realistic case, although, generally, the amount of damping is very small. However, for the formulation to work properly, the complexity of the eigenvector matrices has also to be small. For the undamped case, the simplification of the above equation is straightforward. Expanding equation (3.5) to both sub-systems yields:

$$\begin{bmatrix} I_A & 0 \\ 0 & I_B \end{bmatrix} \begin{Bmatrix} \ddot{p}_A \\ \ddot{p}_B \end{Bmatrix} + \begin{bmatrix} \lambda_A^2 & 0 \\ 0 & \lambda_B^2 \end{bmatrix} \begin{Bmatrix} p_A \\ p_B \end{Bmatrix} = \begin{Bmatrix} \phi_A^T f_A \\ \phi_B^T f_B \end{Bmatrix} \tag{3.6}$$

Each sub-system in equation (3.6) is still uncoupled. To couple them compatibility of displacements and equilibrium of forces (equations (1.1) and (1.2)) have to be imposed at the coupling coordinates. How this is accomplished for each formulation is given next.

3.4. CMS WITHOUT RESIDUAL COMPENSATION

When no residual compensation is made, an additional constraint equation has to be introduced in modal space to allow the set of equations to be solved. This constraint is used basically to couple the otherwise uncoupled set of equations represented by equation (3.6). For any set of component normal modes, the CMS formulation produces a redundant set of equations in modal space. Therefore, some constraint equations have to be used to eliminate this redundancy which is caused by the coupling DOFs. The concept applied here is the one proposed by Hintz [57]. For a complete normal modal set (untruncated), his formulation produces the correct coupled predictions.

First, the mode-shape matrix of each sub-system has to be partitioned[5]. To assist the understanding of this partition, the superscripts used were chosen such as to represent the dimensions of each sub-matrix. The first index is related to the rows, while the second to the columns. As in the previous chapters, index *s* stands for slave DOFs and index c for coupling DOFs. Index *r* is explained below. So, the partitioned sub-system mode-shape matrix can be represented as follows:

$$[\phi] = \left[\begin{array}{c|c} \phi^{cc} & \phi^{cr} \\ \hline \phi^{sc} & \phi^{sr} \end{array}\right] \tag{3.7}$$

[5] All partitions shown in this section were actually used in programming the above **CMS** formulation.

The only restriction in equation (3.7) is for the first sub-matrix $[\phi^{cc}]$. Its rows are associated with the coupling coordinates, while its columns have to be chosen such that this matrix is square and **does not become singular.** In other words, at least as many modes as the number of coupling coordinates have to be employed. As far as the dynamic predictions of the coupled system are concerned, any combination of modes used will produce the same coupled results, provided that the referred matrix is non-singular. Sub-matrix $[\phi^{cr}]$ has the same row partition as above, however the columns are now the remaining (r) modes not used in the previous sub-matrix. The last two sub-matrices have the slave coordinates in the rows and the same column partitions as before.

The transformation equation (3.1), in partitioned form, can be represented using equation (3.7) as defined below:

$$\begin{Bmatrix} x^c \\ x^s \end{Bmatrix} = \left[\begin{array}{c|c} \phi^{cc} & \phi^{cr} \\ \hline \phi^{sc} & \phi^{sr} \end{array}\right] \begin{Bmatrix} p^c \\ p^r \end{Bmatrix} \tag{3.8}$$

or considering just the coupling coordinates for each sub-system as follows:

$$\left\{x_A^c\right\} = \begin{bmatrix} \phi_A^{cc} & \phi_A^{cr} \end{bmatrix} \begin{Bmatrix} p_A^c \\ p_A^r \end{Bmatrix} \tag{3.9a}$$

$$\left\{x_B^c\right\} = \begin{bmatrix} \phi_B^{cc} & \phi_B^{cr} \end{bmatrix} \begin{Bmatrix} p_B^c \\ p_B^r \end{Bmatrix} \tag{3.9b}$$

By applying the compatibility equation (1.1) to the above equations, the modal coordinates are constrained. Writing this in expanded form results in:

$$\left[\phi_B^{cc}\right]\left\{p_B^c\right\} + \left[\phi_B^{cr}\right]\left\{p_B^r\right\} = \begin{bmatrix} \phi_A^{cc} & \phi_A^{cr} \end{bmatrix} \begin{Bmatrix} p_A^c \\ p_A^r \end{Bmatrix} \tag{3.10}$$

Equation (3.10) is then developed to create the second necessary transformation in this CMS formulation, which is the constrained equation in modal space, described by:

$$\{p\} = [\beta]\{q\} \tag{3.11}$$

Matrix $[\beta]$ is the constraint matrix. The full format of equation (3.11) is:

$$\begin{Bmatrix} p_A^c \\ p_A^r \\ p_B^c \\ p_B^r \end{Bmatrix} = \left[\begin{array}{ccc} 0 & I & 0 \\ I & 0 & 0 \\ Am & Bm & -\mathbf{C}\,\mathbf{m} \\ 0 & 0 & I \end{array}\right] \left|\begin{array}{c} q_A^r \\ q_{A,B}^c \\ q_B^r \end{array}\right\} \tag{3.12}$$

where:

$$[Am] = \left[\phi_B^{cc}\right]^{-1}\left[\phi_A^{cr}\right] \tag{3.12a}$$

$$[Bm] = \left[\phi_B^{cc}\right]^{-1}\left[\phi_A^{cc}\right] \tag{3.12b}$$

$$[Cm] = \left[\phi_B^{cc}\right]^{-1}\left[\phi_B^{cr}\right] \tag{3.12c}$$

Substituting equation (3.11) into (3.6) and pre-multiplying by $[\beta]^T$ yields to the final set of constrained equations:

$$[\beta]^T\begin{bmatrix} I_A & 0 \\ 0 & I_B \end{bmatrix}[\beta]\begin{Bmatrix} \ddot{q}_A \\ \ddot{q}_B \end{Bmatrix} + [\beta]^T\begin{bmatrix} \lambda_A^2 & 0 \\ 0 & \lambda_B^2 \end{bmatrix}[\beta]\begin{Bmatrix} q_A \\ q_B \end{Bmatrix} = [\beta]^T\begin{Bmatrix} \phi_A^T f_A \\ \phi_B^T f_B \end{Bmatrix} \tag{3.13}$$

The eigensolutions can be found for the coupled system by making the external forces in equation (3.13) equal to zero (that is, $f_A = f_B = 0$), as defined below:

$$[\beta]^T[\beta]\{\ddot{q}\} + [\beta]^T[\lambda^2][\beta]\{q\} = \{0\} \tag{3.14}$$

Equation (3.14) is the one proposed by Hintz. However, it can be developed further by taking **into** consideration the partition of matrix $[\beta]$ and the fact that some of its sub-matrices are 0. This is represented as follows:

$$[Mm]\{\ddot{q}\} + [Km]\{q\} = \{0\} \tag{3.15}$$

where:

$$[Mm] \begin{bmatrix} I + Am^T Am & Am^T Bm & -Am^T Cm \\ Bm^T Am & I + Bm^T Bm & -Bm^T Cm \\ -Cm^T Am & -Cm^T Bm & I + Cm^T Cm \end{bmatrix} \tag{3.15a}$$

$$[Km] = \begin{bmatrix} \lambda_{As}^2 + Am^T\lambda_{Bc}^2 Am & Am^T\lambda_{Bc}^2 Bm & -Am^T\lambda_{Bc}^2 Cm \\ Bm^T\lambda_{Bc}^2 Am & \lambda_{Ac}^2 + Bm^T\lambda_{Bc}^2 Bm & -Bm^T\lambda_{Bc}^2 Cm \\ -Cm^T\lambda_{Bc}^2 Am & -Cm^T\lambda_{Bc}^2 Bm & \lambda_{Br}^2 + Cm^T\lambda_{Bc}^2 Cm \end{bmatrix} \tag{3.15b}$$

The eigenvectors obtained for coupled system C using equation (3.15) are in constrained modal space (ϕ_{qC}). To convert them back to physical space, the previous transformations have to be used again, such that:

$$[\phi_{xC}] = \begin{bmatrix} \phi_A & 0 \\ 0 & \phi_B \end{bmatrix}[\beta][\phi_{qC}] \tag{3.16}$$

Performing the first multiplication in equation (3.16), one can write:

$$[\phi_{xC}] = [\phi_{x\beta}][\phi_{qC}] \tag{3.17}$$

where (see Appendix B):

$$[\phi_{x\beta}] = \begin{bmatrix} \phi_A^{cr} & \phi_A^{cc} & 0 \\ \phi_A^{sr} & \phi_A^{sc} & 0 \\ \phi_A^{cr} & \phi_A^{cc} & 0 \\ \phi_B^{sc} Am & \phi_B^{sc} Bm & -\phi_B^{sc} Cm + \phi_B^{sr} \end{bmatrix} \tag{3.17a}$$

Unless all normal **modes for each sub-system are included in the above formulation, the predictions obtained are** in error. Some formulations to circumvent this problem are presented next.

3.5. CMS WITH RESIDUAL COMPENSATION

3.5.1. REMARKS

In this section, attention is given to CMS formulations developed to eliminate the need for measuring a large number of normal modes, at the same time compensating for the lack of high-frequency modes. Truncation of these modes is inevitable from a practical point of view and compensation for this information has to be incorporated in the formulation to provide better coupled predictions. The use of residual compensation greatly improves the response within the frequency range of interest. It may be even better than extending the measured frequency range, since is difficult to establish by how much this needs to be done. A comment to be made about residual terms is that they are frequency-dependent (as shown in chapter 4). However, the residual matrices required by the CMS approaches cannot be. Considering this fact, some formulations include a first-order approximation to the residual terms and some go beyond that with the intention to improve the accuracy. The formulations' degree of complexity increases as the order of the residual approximation goes up. Therefore, the gain in accuracy has to be weighed against the additional effort required. In general, a second-order approximation already produces a quite good accuracy. The only situation when going beyond that is justifiable is for components having an extremely high modal density in the frequency range of interest and that is rarely the case.

The CMS formulations using first- and second-order approximations to the residual terms are shown in the following sections. The latter is split into two parts: (i) correct derivation and (ii) derivation based purely on experimental results (IECMS). In fact, the CMS formulation for both (i) and (ii) is the same. The only difference is in the way the residual terms are calculated.

compensation, this is done in anticipation in this chapter such to keep the CMS formulations together. By doing that, a comparison between the different formulations is possible and conclusions on which formulation is better can be drawn.

3.5.2. FIRST-ORDER APPROXIMATION

The first free-free CMS formulation including residual compensation was the one proposed by MacNeal [80] in 1971. It contains a first-order approximation to the residual terms and is also called the static residual compensation method. As before, the first step of the formulation is to partition the mode-shape matrix of each sub-system. However, this time this is done according to lower (index ***l***) and higher (index ***h***) modes. The lower modes include all rigid-body modes (if any) and all low-frequency elastic modes. Rigid-body modes are normally obtained by analysis and the elastic modes from experimental modal analysis. The higher modes are the unknown out-of-range ones, generally truncated due to the need to limit the measured frequency range. The partitioned form of equation (3.1) for the above case can be represented as follows:

$$\{x\}=\begin{bmatrix}\phi^{l} & \phi^{h}\end{bmatrix}\begin{Bmatrix}p^{l}\\ p^{h}\end{Bmatrix} \tag{3.18}$$

Then, equation (3.5) can be re-written using this partition as:

$$\begin{bmatrix}\lambda_l^2-\omega^2 I & 0\\ 0 & \lambda_h^2-\omega^2 I\end{bmatrix}\begin{Bmatrix} \\ p^{h}\end{Bmatrix}=\begin{bmatrix} \\ \phi^{h}\end{bmatrix}^{T}\{f\} \tag{3.19}$$

Before going further in the CMS derivation, we shall first concentrate our attention on the lower part of equation (3.19) (which is considered unknown), that is:

$$\left[\lambda_h^2-\omega^2 I\right]\left\{p^{h}\right\}=\left[\phi^{h}\right]^{T}\{f\} \tag{3.20}$$

An assumption is now made that the frequencies of the out-of-range modes (i.e. the ones in the high-frequency set ***h***) are much higher than the last frequency of interest. This is represented as:

$$\lambda_h^2 >> \omega^2 \tag{3.21}$$

When this is the case, an approximation for the response of the high-frequency modes can be made. They can be assumed to respond in a quasi-static manner and the inertia term in equation (3.20) can be ignored. This is the approximation used in MacNeal's formulation. So, considering the mentioned approximation, equation (3.20) simplifies to:

$$\left\{p^{h}\right\}=\left[\lambda_h^2\right]^{-1}\left[\phi^{h}\right]^{T}\{f\} \tag{3.22}$$

Substituting the modal coordinates defined in equation (3.22) into the expanded form of equation (3.18) yields:

$$\{x\} = [\phi^l]\{p^l\} + [\phi^h][\lambda_h^2]^{-1}[\phi^h]^T\{f\} \tag{3.23}$$

The last term in equation (3.23) is the modal summation relative to the out-of-range modes. This is the definition of the static residual matrix, as will be demonstrated in chapter 4, i.e.:

$$[R] = [\phi^h][\lambda_h^2]^{-1}[\phi^h] \tag{3.24}$$

This residual formulation was used by Urgueira and Ewins in reference [126]. However, from the beginning was assumed that the higher modes are unknown. Therefore, equation (3.24) cannot be used directly. This fact does not constitute any problem, as the same value can be obtained using different formulations. Those are presented in chapter 4.

At this point, a return to the CMS derivation is possible. The force vector is assumed to be applied only at coupling coordinates. So, taking this fact into consideration, equation (3.23) can be re-written for the coupling coordinates of each sub-system using equation (3.24), as follows:

$$\{x_A^c\} = [\phi_A^{cl}]\{p_A^l\} + [R_A^{cc}]\{f_A^c\} \tag{3.25a}$$

$$\{x_B^c\} = [\phi_B^{cl}]\{p_B^l\} + [R_B^{cc}]\{f_B^c\} \tag{3.25b}$$

Using the compatibility equation (1.1) in the above equations yields:

$$[\phi_A^{cl}]\{p_A^l\} + [R_A^{cc}]\{f_A^c\} = [\phi_B^{cl}]\{p_B^l\} + [R_B^{cc}]\{f_B^c\} \tag{3.26}$$

Then, applying the equilibrium equation (1.2) and the simplification below:

$$[Kc] = \left([R_A^{cc}] + [R_B^{cc}]\right)^{-1} \tag{3.27}$$

one can write the following equations for sub-systems *A* and B:

$$\{f_A^c\} = [Kc]\left([\phi_B^{cl}]\{p_B^l\} - [\phi_A^{cl}]\{p_A^l\}\right) \tag{3.28a}$$

$$\{f_B^c\} = [Kc]\left([\phi_A^{cl}]\{p_A^l\} - [\phi_B^{cl}]\{p_B^l\}\right) \tag{3.28b}$$

Substituting equations (3.28a) and (3.28b) into (3.5) and writing the coupled equation of motion in matrix form, yields:

$$\begin{bmatrix} I_A & 0 \\ 0 & I_B \end{bmatrix}\begin{Bmatrix} \ddot{p}_A^l \\ \ddot{p}_B^l \end{Bmatrix} + \begin{bmatrix} \lambda_{Al}^2 + \phi_A^{clT} Kc\, \phi_A^{cl} & -\phi_A^{clT} Kc\, \phi_B^{cl} \\ -\phi_B^{clT} Kc\, \phi_A^{cl} & \lambda_{Bl}^2 + \phi_B^{clT} Kc\, \phi_B^{cl} \end{bmatrix}\begin{Bmatrix} p_A^l \\ p_B^l \end{Bmatrix} = \begin{Bmatrix} 0 \\ 0 \end{Bmatrix} \tag{3.29}$$

This is the CMS formulation proposed by MacNeal and later also by Urgueira. To solve for the coupled system, the eigensolutions of equation (3.29) have to be found. This formulation has one shortcoming that should be addressed. Although extremely unlikely in practice, an inadequacy may happen when analysing mass-and-spring systems. If the total number of modes used is bigger than the total number of coordinates of the coupled system (i.e. mau+mbu > NA+NB-NCC), the set of equations to be solved in (3.29) becomes redundant. They can be solved but as many as the number of redundant modes used will be either negative or several orders of magnitude bigger than the correct coupled frequency predictions. They can be ignored (since to spot them is easy), or an additional set of constraint equations can be introduced to eliminate the redundancy. Following the latter option, the author tried to use the constraint matrix [β] (equation (3.12)) into equation (3.29). However, using that is the same as eliminating the residual compensation matrix [Kc] (equations (3.27)) in the above formula. This is proved in detail in Appendix C. As no other constraint could be found, the former option seems more viable.

The eigenvectors from equation (3.29) can be transformed to physical space as follows:

$$[\phi_{xC}] = \begin{bmatrix} \phi_A & 0 \\ 0 & \phi_B \end{bmatrix} [T] [\phi_{pC}] \tag{3.30}$$

Matrix [*T*] is a transformation matrix of correction terms related to the residual terms' compensation. The first multiplication on the RHS above can be represented as:

$$[\phi_{xC}] = [\phi_{xAB}] [\phi_{pC}] \tag{3.31}$$

where (see Appendix D):

$$[\phi_{xAB}] = \begin{bmatrix} \phi_A^{sl} - R_A^{sc} Kc \phi_A^{cl} & R_A^{sc} Kc \phi_B^{cl} \\ \phi_A^{cl} - R_A^{cc} Kc \phi_A^{cl} & R_A^{cc} Kc \phi_B^{cl} \\ R_B^{cc} Kc \phi_A^{cl} & \phi_B^{cl} - R_B^{cc} Kc \phi_B^{cl} \\ R_B^{sc} Kc \phi_A^{cl} & \phi_B^{sl} - R_B^{sc} Kc \phi_B^{cl} \end{bmatrix} \tag{3.32}$$

The above is the correct uncoupled mode-shape matrix in physical space for the sub-systems. However, when no residual compensation is assumed at the slave DOFs, this mode-shape matrix can be simplified to:

$$[\phi_{xAB}] = \begin{bmatrix} \phi_A^{sl} & 0 \\ \phi_A^{cl} - R_A^{cc} Kc \phi_A^{cl} & R_A^{cc} Kc \phi_B^{cl} \\ R_B^{cc} Kc \phi_A^{cl} & \phi_B^{cl} - R_B^{cc} Kc \phi_B^{cl} \\ 0 & \phi_B^{sl} \end{bmatrix} \tag{3.33}$$

Residual compensation at the slave DOFs is only necessary for obtaining the correct mode-shape matrix in physical space at those coordinates. To calculate the natural frequencies of the coupled system, they have no influence at all. So, to reduce the time in measuring and calculating the necessary residual terms only the required slave DOFs should be considered.

After performing the multiplication in equation (3.31), the two middle partitioned rows (relative to the coupling DOFs) will be the same due to the compatibility equation. The mode-shape matrix in modal space $[\phi_{pC}]$ is not constrained and this is the reason why the values are repeated. Therefore, one set of them can be eliminated.

3.5.3. SECOND-ORDER APPROXIMATION

3.5.3.(a) CORRECT FORMULATION

In the previous section, a first-order approximation for equation (3.20) was used in the derivation of equation (3.22), that is:

$$\left[\lambda_h^2 - \omega^2 I\right]^{-1} = \left[\lambda_h^2\right]^{-1} \tag{3.34}$$

This result is valid as long as equation (3.21) is satisfied. For components having a high modal density in the frequency range of interest, this may not be possible. In order to validate this equation in this case, a very large number of modes would be necessary. There is a way of circumventing this problem and that is by using a second-order approximation for the LHS of equation (3.34). A MacLaurin series can be used to expand the LHS of this equation as follows:

$$\left[\lambda_h^2 - \omega^2 I\right]^{-1} = \left[\lambda_h^2\right]^{-1} + \omega^2\left[\lambda_h^2\right]^{-2} + \omega^4\left[\lambda_h^2\right]^{-3} + \cdots \tag{3.35}$$

This expansion is true provided that ω^2 is smaller than the elements of λ_h^2 [1 10]. As a second-order approximation is sought, only the first two terms of the RHS of equation (3.35) are needed. Then, re-writing equation (3.22) in terms of the second-order approximation, yields:

$$\{p^h\} = \left(\left[\lambda_h^2\right]^{-1} + \omega^2\left[\lambda_h^2\right]^{-2}\right)\left[\phi^h\right]^T \{f\} \tag{3.36}$$

Substituting the modal coordinates expressed now by equation (3.36) into the expanded form of equation (3.18), after the correct manipulation, leads to:

$$\{x\} = \left[\phi^l\right]\{p^l\} + [R]\{f\} + \omega^2[R1]\{f\} \tag{3.37}$$

In equation (3.37), matrix [R] is defined by equation (3.24) (or any of its derivations shown in chapter 4) and matrix $[R1]$ is expressed as below:

$$[R1] = [\phi^h][\lambda_h^2]^{-2}[\phi^h]^T \tag{3.38}$$

Matrix $[R1]$ can be considered to be a dynamic contribution to the neglected high-frequency modes. It accounts for the inertia effects ignored in the first-order approximation. As it happened with matrix $[R]$, equation (3.38) cannot be evaluated directly (since the high-frequency modes are assumed to be unknown). Therefore, other formulations have to be employed to circumvent this problem[6]. For instance, it can be derived using the static residual matrix [R] already calculated and the mass matrix, as follows:

$$[R1] = [R]^T[M][R] \tag{3.39}$$

By substituting equation (3.24) into (3.39), it can be proved that the latter is actually equivalent to equation (3.38). Equation (3.39) is very easy to obtain from an FE point of view. Nevertheless, it is not from experiments, since the mass matrix is not available in such a case. As mentioned in the introduction of this chapter, a breakthrough was achieved in this thesis, where a formulation to circumvent the need for the mass matrix was developed. This is presented in the following section. Before going on to that, however, the CMS formulation using this second-order approximation to the truncated high-frequency modes needs to be derived. This is done following the same steps of the first-order approximation, as demonstrated below.

Equation (3.37) can be written for each sub-system when only the coupling coordinates are considered as:

$$\{x_A^c\} = [\phi_A^{cl}]\{p_A^l\} + ([R_A^{cc}] + \omega^2[R1_A^{cc}])\{f_A^c\} \tag{3.40a}$$

$$\{x_B^c\} = [\phi_B^{cl}]\{p_B^l\} + ([R_B^{cc}] + \omega^2[R1_B^{cc}])\{f_B^c\} \tag{3.40b}$$

Applying the compatibility equation (1.1) to the physical coupling coordinates above, one can write:

$$[\phi_A^{cl}]\{p_A^l\} + ([R_A^{cc}] + \omega^2[R1_A^{cc}])\{f_A^c\} = [\phi_B^{cl}]\{p_B^l\} + ([R_B^{cc}] + \omega^2[R1_B^{cc}])\{f_B^c\} \tag{3.41}$$

Then, the equilibrium equation (1.2) is introduced in equation (3.41), what results after some manipulation in[7]:

$$[\phi_A^{cl}]\{p_A^l\} - [\phi_B^{cl}]\{p_B^l\} = \left[([R_A^{cc}] + [R_B^{cc}]) + \omega^2([R1_A^{cc}] + [R1_B^{cc}])\right]\{f_B\} \tag{3.42}$$

---

[6] Some formulations for that are given in chapter 4.

[7] Only the equation for sub-system ***B*** will be derived here, as the extrapolation to sub-system *A* is straightforward.

R-e-multiplying equation (3.42) by (3.27) and re-arranging yields:

$$\{f_B\} = \left([I_B] + \omega^2 [Kc]\left([R1_A^{cc}] + [R1_B^{cc}]\right)\right)^{-1} [Kc]\left([\phi_A^{cl}]\{p_A^l\} - [\phi_B^{cl}]\{p_B^l\}\right) \quad (3.43)$$

The above matrix inversion can be approximated by the first two terms of its MacLaurin series expansion [1 10]:

$$\{f_B\} = \left([Kc] - \omega^2 [Kc]\left([R1_A^{cc}] + [R1_B^{cc}]\right)[Kc]\right)\left([\phi_A^{cl}]\{p_A^l\} - [\phi_B^{cl}]\{p_B^l\}\right) \quad (3.44)$$

The following simplification is used above, so as to result in equation (3.46):

$$[Mc] = [Kc]\left([R1_A^{cc}] + [R1_B^{cc}]\right)[Kc] \quad (3.45)$$

$$\{f_B\} = [Kc][\phi_A^{cl}]\{p_A^l\} - [Kc][\phi_B^{cl}]\{p_B^l\} - \omega^2[Mc][\phi_A^{cl}]\{p_A^l\} + \omega^2[Mc][\phi_B^{cl}]\{p_B^l\} \quad (3.46)$$

Substituting equation (3.46) into (3.5), the following equation can be writen after some simplifications:

$$\begin{aligned} &\left([I_B] + [\phi_B^{cl}]^T [Mc][\phi_B^{cl}]\right)\{\ddot{p}_B^l\} + \left(-[\phi_B^{cl}]^T [Mc][\phi_A^{cl}]\right)\{\ddot{p}_A^l\} \cdots \\ &\cdots + \left([\lambda_{Bl}^2] + [\phi_B^{cl}]^T [Kc][\phi_B^{cl}]\right)\{p_B^l\} + \left(-[\phi_B^{cl}]^T [Kc][\phi_A^{cl}]\right)\{p_A^l\} = \{0\} \end{aligned} \quad (3.47)$$

A similar equation is obtained when considering $\{f_A\}$, although it is not shown here. Expressing both equations in matrix form yields:

$$\begin{bmatrix} I_A + \phi_A^{clT} Mc \phi_A^{cl} & -\phi_A^{clT} Mc \phi_B^{cl} \\ -\phi_B^{clT} Mc \phi_A^{cl} & I_B + \phi_B^{clT} Mc \phi_B^{cl} \end{bmatrix} \begin{Bmatrix} \ddot{p}_A^l \\ \ddot{p}_B^l \end{Bmatrix} + \begin{bmatrix} \lambda_{Al}^2 + \phi_A^{clT} Kc \phi_A^{cl} & -\phi_A^{clT} Kc \phi_B^{cl} \\ -\phi_B^{clT} Kc \phi_A^{cl} & \lambda_{Bl}^2 + \phi_B^{clT} Kc \phi_B^{cl} \end{bmatrix} \begin{Bmatrix} p_A^l \\ p_B^l \end{Bmatrix} = \begin{Bmatrix} 0 \\ 0 \end{Bmatrix} \quad (3.48)$$

Equation (3.48) is the one proposed by Craig and Chang [29] and the one used for the IECMS formulation presented next. Actually, the only difference between the formulation presented here and the following is the way in which matrix [Mc] is calculated. The IECMS calculates all the necessary residual compensations using only experimentally-derived data.

To convert the mode-shape matrix obtained from equation (3.48) to physical space, equations (3.31) and (3.32) can be used, despite the second-order approximation for the residual terms. Matrix [R1] is normally very small relative to [R] and its influence in the mode-shape matrix is virtually negligible.

3.5.3.(b) IECMS FORMULATION

As mentioned in the previous section, in order to obtain the second-order residual compensation to the high-frequency modes, the mass matrices of the sub-systems have to be available. From

an experimental point of view, this is not possible and, consequently, only the first-order approximation is normally employed (i.e. MacNeal's approach). The formulation derived in this section will resolve this problem.

Comparing the formulations for the static and dynamic residual terms (equations (3.24) and (3.38) respectively), it can be seen that the difference between them is actually the power of the middle matrix (i.e. the diagonal natural frequency matrix). When each term of the static residual matrix is divided by a constant high-frequency pseudo-eigenvalue, this would approximate the effect of the power missing in equation (3.38) and a good approximation for the dynamic residual matrix can be obtained. The problem is to know which value to use for the high-frequency pseudo-eigenvalue. An automatic way of evaluating that will be presented later.

The residual matrices required by the IECMS approach cannot be frequency-dependent. Therefore, both the static and the dynamic residual matrices have to be calculated at a single frequency point. From experimental data, any particular term of the static residual matrix can be calculated by subtracting the correct (measured) FRF matrix from the regenerated curve calculated using the modal parameters within the low frequency range of interest. It is important in this case that the regenerated curves include also the contribution of the rigid-body modes. The residual curve can be represented by:

$$R_{ij}(\omega) = H_{ij}^{C}(\omega) - H_{ij}^{R}(\omega) \tag{3.49}$$

When all terms are needed, the above equation can be written in matrix form as:

$$\left[R(\omega)\right] = \left[H^{C}(\omega)\right] - \left[\phi^{l}\right]\left[\left(\lambda_{l}^{2} - \omega^{2}\right)\right]^{-1}\left[\phi^{l}\right]^{T} \tag{3.50}$$

As the required residual value wanted is a static approximation to the higher modes, equation (3.49) or (3.50) has to be calculated at $\omega = 0$ or at a value close to that. From now on, the latter formula will be assumed. When this matrix is added to the regenerated FRF matrix, a static residual compensated FRF matrix is obtained. Using notation *pu* to indicate the frequency point where the static residual terms were calculated, the above static residual compensated FRF matrix can be defined as:

$$\left[H^{S}(\omega)\right] = \left[\phi^{l}\right]\left[\left(\lambda_{l}^{2} - \omega^{2}\right)\right]^{-1}\left[\phi^{l}\right]^{T} + \left[R(\omega_{pu})\right] \tag{3.51}$$

However, when equation (3.21) is not satisfied, the FRFs calculated using equation (3.51) will still be in error, although the error will be mainly at frequency values close to the upper end of the frequency range of interest. Following the same sort of approximation as the one expressed

by equation (3.37), the correct FRF curves can be approximated by adding extra terms in the series at **different** frequency points as follows:

$$\left[H^C(\omega)\right] \approx \left[H^R(\omega)\right] + \left[R(\omega_{pu})\right] + \omega^2\left[R1(\omega_{pu_h})\right] + \cdots \tag{3.52}$$

The first two terms in equation **(3.52)** are actually the LHS terms of equation (3.51). The approach developed above can be understood from the fact that, considering the static residual terms to be the error between the correct and the regenerated curves, the dynamic residual terms can be considered to be the error between the correct and the static residual compensated FRF curves and so on. In order to calculate each extra term correctly, they have to be evaluated after the previous compensated curve has been calculated. A different frequency point has to be used since, at the same frequency point, no error exists. The error here is only caused by the fact that the residual compensation will not be frequency-dependent as it should be (see equation (3.49) or (3.50)). Therefore, following the explanation above, each element of the above matrix $[R1]$ (the last term of the RHS of equation (3.52)), can be evaluated from the experimental results using:

$$R1_{ij}\left(\omega_{pu_h}\right) = \frac{H_{ij}^C\left(\omega_{pu_h}\right) - H_{ij}^S\left(\omega_{pu_h}\right)}{\left(\omega_{pu_h}\right)^2} \tag{3.53}$$

This is actually the value of the dynamic residual compensation matrix needed for the IECMS formulation. As seen, equation (3.53) is evaluated at a frequency point pu_h whose choice is of vital importance to the quality of the derived matrix $[R1]$ and, consequently, of the coupled predictions. Some indications are given next on how to choose this point. As mentioned at the beginning of this section, matrix $[R1]$ can be also evaluated using the following expression:

$$R1_{ij}\left(\omega_{pu_h}\right) = \frac{R_{ij}\left(\omega_{pu}\right)}{\left(\lambda_{hp}^2\right)_{ij}} \tag{3.54}$$

The high-frequency pseudo-eigenvalue (λ_{hp}^2) needed in equation (3.54) can be evaluated now very easily. Since the correct value of the dynamic residual compensation is expressed by equation (3.53), the high-frequency values needed in equation (3.54) can be calculated by interchanging their positions in the former equation, as:

$$\left(\lambda_{hp}^2\right)_{ij} = \frac{R_{ij}\left(\omega_{pu}\right)}{R1_{ij}\left(\omega_{pu_h}\right)} \tag{3.55}$$

The values obtained through equation (3.55) are the ones used to monitor the choice of the frequency point pu_h. Therefore, in fact, equation (3.54) should be the one used in the IECMS formulation. Since matrix $[R1]$ is used to approximate the second-order effect of the high-frequency residual modes, each pseudo-frequency value calculated by equation (3.55), should be above the last frequency of interest for that particular sub-system. This sometimes is not true, mainly when pu_h is chosen close to the upper end of the frequency range of interest. However, choosing pu_h very close to the beginning of the frequency range of interest may produce a high-frequency pseudo-eigenvalue so high that almost no improvement is obtained when compared with the first-order approximation, although this is not necessarily true. When the high-frequency pseudo-eigenvalue lies within the frequency range of interest, it tends to' lower the natural frequency predictions compared with the correct ones. The best choice of this point will be case-dependent. However, a good suggestion is to use 10% of the maximum frequency of interest, as shown later.

At this point, all the necessary residual term compensation for the IECMS were derived and so, they can be used in equation (3.48) to calculate the required coupled predictions. To obtain the physical mode-shape matrix for the coupled system, equations (3.31) and (3.32) are employed.

3.6. EXAMPLES

In order to evaluate the quality of the predictions obtained when using one CMS formulation or another, a series of examples is used. First of all, it has to be observed that the final number of modes produced by each CMS formulation is different. The CMS formulations including residual compensation return the sum of the modes used for each sub-system. On the other hand, the CMS formulation without residual compensation returns the same number as before minus the number of coupling coordinates. This fact should be taken into consideration when analysing the results.

The first example here uses coupled system **CSYS1** shown in chapter 2 (Figure 2.5). This is done with the intention to allow a comparison between CMS and FRF coupling predictions. Therefore, when plotting the FRF curves, the same frequency range is used, even though more modes may be obtained from the CMS coupling process. CMS has an advantage over FRF coupling in that, since modal data are used, no problems with noise are present and the FRF curves obtained are really smooth. However, when the total number of modes produced is not enough to account for the flexibility of the coupled system, some residual problems may still occur around anti-resonance regions, as will be demonstrated here.

The first set of results shown for coupled system **CSYSI** is for the case when only the modes within the frequency range of interest (i.e. from 0 to 200 Hz) are used for each sub-system. This implies using 3 modes for sub-system A and 3 modes for sub-system B, as seen in Figure 2.6 (chapter 2) for example. Since the coupling process involves 2 coordinates, following the comments above, the maximum number of modes which can be obtained with the CMS formulation without residual compensation is 4 (3+3-2). For the CMS formulations with residual compensation, 6 modes are produced. In fact, the coupled system has only 5 modes within the frequency range of interest. The extra mode obtained from the CMS with residual compensation would be used to try to account for the flexibility effects of the coupled system.

Table 3.1 - Notation used for the different CMS approaches

Hurty	no residual compensation
MacNeal	first-order residual compensation
Craig-Chang	second-order correct residual compensation
IECMS	second-order experimental residual compensation

To make the references to each CMS formulation easier, Table 3.1 shows the notation used in this section for each one. Craig-Chang's approach, although not purely experimental (the mass matrix is required), is included to allow a comparison of results with the new experimentally-derived approach proposed in this thesis (IECMS). Table 3.2 shows the predicted natural frequencies for this coupled system when using the formulations listed in Table 3.1. The modes within the frequency range of interest are highlighted in bold. The first line of results corresponds to the correct frequency values, calculated using the physical matrices of the coupled system. A percentage error between the correct and predicted values is presented underneath each frequency prediction, to enable an assessment of which formulation yields better results.

Table 3.2 - Frequency predictions (Hz) for coupled system CSYSI when using the different CMS formulations

case	formulation	**m1**	**m2**	**m3**	**m4**	**m5**	m6
	Correct	52.412	94.274	134.689	156.615	182.104	222.18
1	Hurty	56.181	95.917	137.724	169.455	x	x
	error (%)	-7.19	-1.74	-2.25	-8.2	x	x
2	MacNeal	52.469	94.454	135.412	163.68	206.355	262.813
	error (%)	-0.11	-0.19	-0.54	-4.51	-13.32	-18.29
3	Craig-Chang	52.412	94.275	134.692	156.706	182.285	222.965
	error (%)	0	0	0	-0.06	-0.1	-0.35
4	IECMS	52.412	94.273	134.686	156.643	182.201	222.853
	error (%)	0	0	0	-0.02	-0.05	-0.3

Some comments can be made about the results in Table 3.2. It can be noticed that the higher the order of the residual compensation, the better the results are. This improvement is achieved from the lower to the higher modes. Moreover, between the IECMS and Craig-Chang's

approach, the former is slightly better, although both lead to errors of less than 0.4% (0.1% within the frequency range of interest). This fact stresses the potential of the new approach. As pointed out before, Hurty's approach missed one mode of the coupled system altogether. Also, because of the approximation adopted in MacNeal's approach (that is, static approximation), the lower modes are correct; the error increasing with the mode number.

The IECMS approach was calculated by setting pu_h for each sub-system (equation (3.53)) to the value which would correspond to 10% the maximum frequency of interest as suggested before (i.e. 20 Hz). Since the FRFs were discretized using 801 frequency points (or in other words, with 0.5 Hz frequency increment) that means using pu_h=8 1. The frequency point pu used for the static residual compensation (equation (3.50)) was set to pu=1 (i.e. 0 Hz). The high-frequency values produced by equation (3.55) using these frequency points are shown in Table 3.3. All the values are above the maximum frequency of interest, what indicates a good choice for frequency point pu_h (as can be confirmed by the results in Table 3.2).

Table 3.3 - High-frequency values (Hz) from IECMS for system A and B ($freq_{pu}$= 0 Hz and $freq_{pu_h}$= 10% freq. max. = 20 Hz)

coord. A	1	5	coord. B	3	1
1	396.329	212.747	3	245.127	245.127
5	212.747	267.009	1	245.127	245.127

However, natural frequency comparison is not the only means of assessing the quality of the formulations. Mode-shapes and response predictions should also be compared to give a more complete description. Figures 3.1 to 3.3 show some point FRF predictions using the different CMS formulations for coupling coordinate 5 (i.e. $H_{5,5}$). A coupling DOF was chosen at the beginning, since residual compensation at slave DOFs has no influence. So, only the formulation itself would be assessed. The curves in these figures were obtained using all calculated modes for the above case.

Figure 3.1 presents the predictions using Hurty's approach. As seen, the whole FRF curve is in error (i.e. both natural frequencies and response levels). This result can be compared with the one obtained for the FRF coupling method when no residual compensation was included there (i.e. case M3 - Figure 2.12). The predictions from both methods are the same. When the first-order approximation to the residual terms is included (Figure 3.2), an improvement over the previous prediction is clearly perceived, mainly at the lower frequency range. However, within the range of interest, only 4 modes are found. The predictions obtained by Craig-Chang and IECMS approaches are plotted together in Figure 3.3 to show that they led to the same response predictions. Although the natural frequency contents of the curves are correct, an error is seen

around the anti-resonances. This fact highlights the problems which may arise when the total number of modes for the coupled system is not enough to account correctly for the flexibility effects. Comparing all three figures, it should be emphasised that each residual compensation improved the previous one from the lower modes upwards.

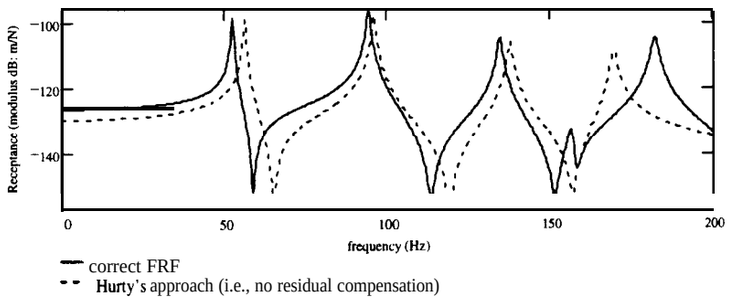

Figure 3.1 - $H_{5,5}$: Only modes within frequency range for each sub-system (i.e. 3A+3B), Hurty's approach (CSYSI)

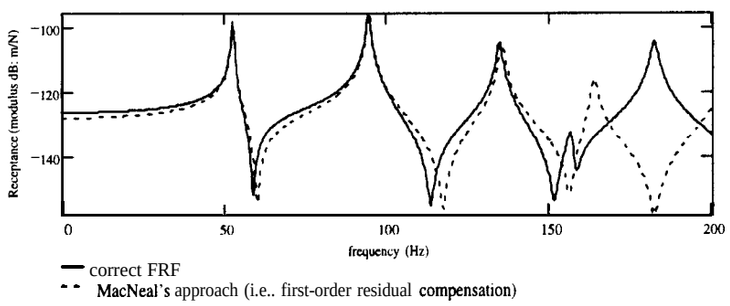

Figure 3.2 - $H_{5,5}$: Only modes within frequency range for each sub-system (i.e. 3A+3B), MacNeal's approach (CSYSI)

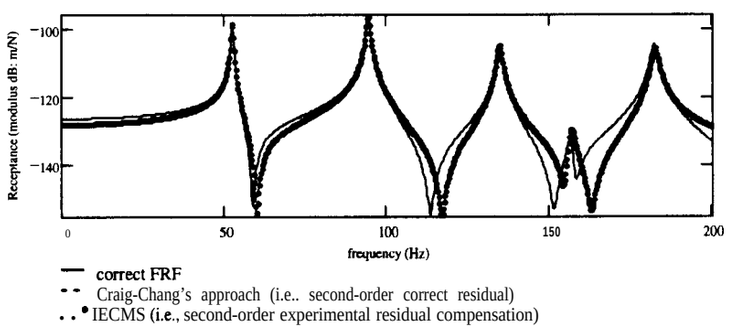

Figure 3.3 - $H_{5,5}$: Only modes within frequency range for each sub-system (i.e. 3A+3B), Craig-Chang's and IECMS approaches (CSYSI)

Returning to the sufficiency of number of modes, Figures 3.4 and 3.5 are presented. One extra mode was added to the calculations which produced the FRF curves there (i.e. the final number of modes for the coupled system is 7, instead of 6, as previously). Apart from showing the need

for having enough modes, these results also show the different effects residual terms have on the predictions. Figure 3.4 used 4 modes for sub-system **A** and 3 modes for sub-system **B,** while Figure 3.5 used 3 modes for sub-system **A** and 4 modes for sub-system **B** (i.e. no out-of-range mode left for **B).** Since it was proved that Craig-Chang and IECMS lead to the same results, only the latter is plotted here. For both cases above, the IECMS approach yielded to the correct frequency and response predictions. However, Hurty and MacNeal's approach produced different predictions when the extra mode was added at the different sub-systems. When residual terms are only affecting sub-system **A** (Figure 3.5), the results are much better than when residual affects both sub-systems (Figure 3.4). Another comment is worth mentioning about Hurty's approach. The inclusion of more modes in the formulation improves the coupled modes not in a specific pattern. For instance, in this example, the second mode was normally better predicted than the first.

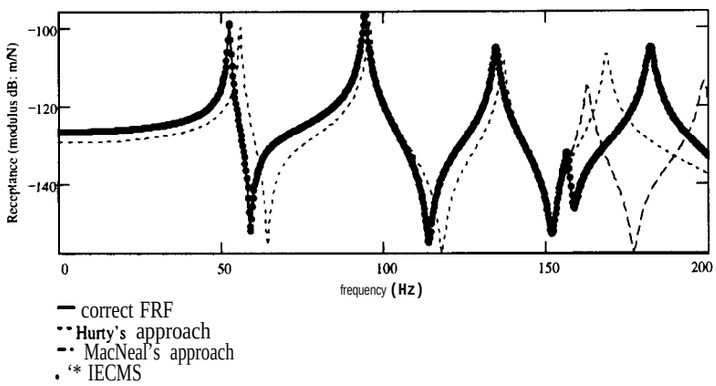

Figure 3.4 - $H_{5,5}$: Modes within frequency range plus one for sub-system A and only modes within frequency range for sub-system B (i.e. 4A+3B) (CSYSI)

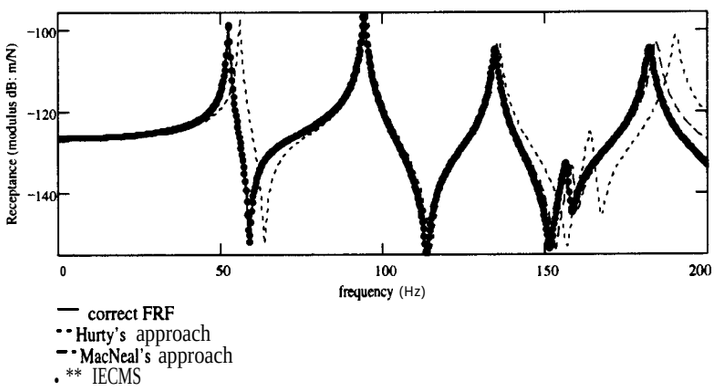

Figure 3.5 - $H_{5,5}$: Only modes within frequency range for sub-system A and modes within frequency range plus one for sub-system B (i.e. 3A+4B) (CSYSI)

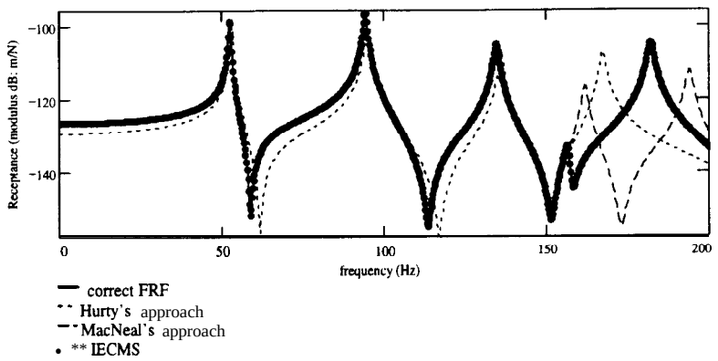

Figure 3.6 - $H_{5,5}$: All modes minus one for each sub-system (i.e. 8A+3B) (CSYS1)

In Figure 3.6, another set of plots is provided to stress the fact that the predictions may still not be good enough, even when only one mode is omitted from the formulation for each sub-system. For the coupled system under examination, both Hurty and MacNeal's approaches still did not manage to produce results as good as the ones presented in Figure 3.5. Residual compensation tends to be much better than extending the number or modes included, as seen here.

As demonstrated, Hurty's approach in general does not yield very accurate results unless an extremely high number of modes is used. Therefore, from now on, it will not be considered any more. Having compared the natural frequency and response predictions, it is time to compare the mode-shapes. This is done with the intention of checking how different they would be when residual compensation is included or excluded at the slave DOFs (i.e. equations (3.32) and (3.33), respectively). The mode-shape comparison is performed here using the MAC concept [2]. Only the MacNeal and IECMS approaches will be assessed, as the latter produced the same results as Craig-Chang's approach. The number of modes used in the MAC formula for the correct coupled system mode-shapes was limited to 6 (i.e. the same number of modes found through the CMS formulations). The MAC values for the above cases are shown in Tables 3.4 and 3.5, respectively. The difference between the values with and without residual compensation is not very strong, and would justify the use of the simplified formula (3.33) in this case. As it is going to be shown in the next example, this is not a general rule.

Table 3.4 - MAC between MacNeal (MN) x correct mode-shape values with and without residual compensation at slave DOFs - CSYS1

$$\begin{bmatrix} 100 & 17 & 0 & 3 & 1 & 4 \\ 17 & 100 & 2 & 5 & 3 & 2 \\ 0 & 2 & 100 & 0 & 0 & 13 \\ 2 & 4 & 1 & 87 & 10 & 2 \\ 5 & 11 & 1 & 24 & 77 & 0 \\ 1 & 0 & 19 & 0 & 13 & 92 \end{bmatrix}$$

with MN x correct

$$\begin{bmatrix} 100 & 17 & 0 & 3 & 1 & 4 \\ 17 & 100 & 2 & 4 & 2 & 2 \\ 0 & 2 & 99 & 0 & 0 & 11 \\ 2 & 3 & 1 & 80 & 16 & 3 \\ 6 & 12 & 0 & 14 & 83 & 0 \\ 0 & 0 & 11 & 0 & 8 & 89 \end{bmatrix}$$

without MN x correct

Table 3.5 - MAC between IECMS x correct mode-shape values with and without residual compensation at slave DOFs - CSYS1

100	17	0	3	1	4
17	100	2	5	3	2
0	2	100	0	0	14
3	6	0	100	0	1
2	3	0	0	100	3
4	3	13	1	2	98

with IECMS x correct

100	17	0	3	1	4
17	100	2	4	2	2
0	2	100	0	0	11
4	5	0	98	1	3
1	3	0	1	97	1
3	2	5	3	0	88

without IECMS x correct

The following example uses a different mass-and-spring system to point out that it is not always possible to ignore the residual compensation at slave DOFs when these coordinates are of interest. The system used, called **ESYSI,** is sketched in Figure 3.7. The slave DOFs for the individual systems are related only to sub-system **D** and are confined to two coordinates. The frequency range of interest considered for each sub-system was the same, extending from 0 to **4.50** Hz. Over that range, there are **2** modes for sub-system C (1 rigid-body and 1 elastic) and **4** modes for sub-system **D. So,** for the CMS formulations including residual compensation (the ones considered from now on), a total of 6 modes can be obtained for the coupled system. Actually, by coincidence, this is the total number of modes the coupled system has. The FRFs were acquired with a frequency increment of 0.5625 Hz, giving a total of 801 frequency points.

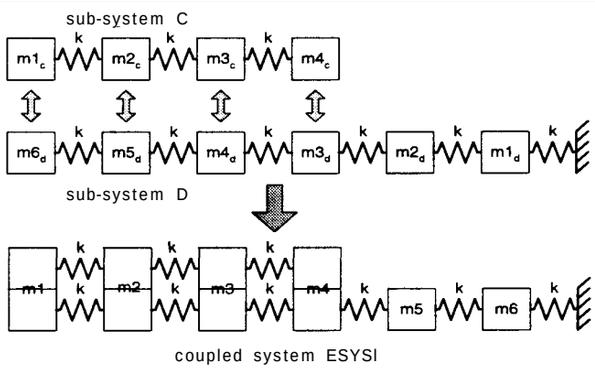

where: ml, = 1 Kg; $m2_c$ = 2 Kg; $m3_c$ = 3 Kg; $m4_c$ = 4 Kg
$m1_d$ = 1 Kg; $m2_d$ = 2 Kg; $m3_d$ = 3 Kg; $m4_d$ = 4 Kg; $m5_d$ = 5 Kg; $m6_d$ = 6 Kg
k = 1x10" N/m
η = 0.01

Figure 3.7 - Sub-systems C and D and coupled system ESYSI (second CMS study)

Table 3.6 presents the natural frequency predictions for coupled system **ESYSI** when using the different CMS formulations with residual compensation. MacNeal's approach for this case yielded very poor results, the last two modes having an extremely high error. Craig-Chang's formulation led to an error-free frequency prediction, while the IECMS had very little error (less or equal 0.25%, which is quite a good prediction). The IECMS approach was calculated again using a value of pu_h which would correspond to 10% of the maximum frequency of interest (i.e. pu_h=81 or 45 Hz). The frequency point pu used for the static residual compensation

(equation (3.50)) was set this time to pu=2 (i.e. 0.5625 Hz), as for the sub-system C, the FRF curves are singular at the first frequency point (i.e. 0 Hz). The high-frequency values produced by equation (3.55) using these frequency points are shown in Table 3.7. The great majority of the values are above the maximum frequency of interest; the ones within this range are highlighted. In any case, the values within the range of interest are all higher the last frequency for both sub-systems, shown in Table 3.8. From the results in Table 3.6, one can see that the choice of the frequency point pu_h was quite good.

Table 3.6 - Frequency predictions (Hz) for coupled system ESYS1 when using the different CMS formulations

case	mode number	m1	m2	m3	m4	m5	m6
	Correct	50.43	209.5	361.4	443.23	505.43	775.48
1	MacNeal	50.44	210.33	402.99	509.31	1.31E+3	7.72E+4
	error (%)	0.01	0.4	11.51	14.91	159.44	9860.02
2	Craig-Chang	50.43	209.5	361.4	443.23	505.43	775.48
	error (%)	0	0	0	0	0	0
3	IECMS	50.43	209.49	361.09	442.71	504.17	774.26
	error (%)	0	0	0.09	0.12	0.25	0.16

Table 3.7 - High-frequency values (Hz) from IECMS for system C and D ($freq_{pu}$= 0.5625 Hz and $freq_{pu}$ = 10% freq. max. = 45 Hz)

C (10%)	1	2	3	4	D (10%)	6	5	4	3
1	532.638	800.945	431.829	451.958	6	523.515	523.518	523.531	523.58
2	800.945	658.318	548.799	508.25	5	523.518	523.527	523.557	523.674
3	431.829	548.799	469.94	465.908	4	523.531	523.557	523.647	523.999
4	451.958	508.25	465.908	464.277	3	523.58	523.674	523.999	525.271

Table 3.6 - Natural frequencies (Hz) for each sub-system within the frequency range of interest (i.e. O-450 Hz):

mode number	1	2	3	4
system C	0	262.665	x	x
system D	56.562	196.693	319.127	417.492

The next comparison before the response predictions will be for the mode-shapes. Tables 3.9 and 3.10 show the MAC values for MacNeal and IECMS approaches, respectively, for the case when residual compensation is included or excluded at the slave DOFs. Comparing these cases, it is observed that the slave residual compensation this time plays a very important role in the mode-shape predictions. The quality of the correlation quickly drops as the mode number increases. This is better seen when the FRF curves for the slave DOFs are plotted.

Table 3.9 - MAC between MacNeal (MN) x correct mode-shape values with and without residual compensation at slave DOFs - ESYS1

100	2	3	4	1	0
2	100	12	15	4	1
4	10	99	35	12	4
3	12	21	92	1	6
3	11	15	53	78	3
0	1	5	12	7	99

with MN x correct

100	2	4	5	1	0
2	100	13	16	5	1
3	8	100	29	10	3
2	7	12	83	0	3
0	0	4	4	69	0
1	2	7	1	65	0

without MN x correct

Table 3.10 - MAC between IECMS x correct mode-shape values with and without residual compensation at slave DOFs - ESYS1

$$\begin{bmatrix} 100 & 2 & 3 & 4 & 1 & 0 \\ 2 & 100 & 11 & 14 & 4 & 1 \\ 3 & 11 & 100 & 30 & 9 & 4 \\ 4 & 14 & 30 & 100 & 13 & 8 \\ 1 & 4 & 9 & 12 & 100 & 4 \\ 0 & 1 & 4 & 8 & 4 & 100 \end{bmatrix}$$

with IECMS x correct

$$\begin{bmatrix} 100 & 2 & 4 & 5 & 1 & 0 \\ 2 & 100 & 12 & 15 & 5 & 1 \\ 3 & 10 & 100 & 27 & 8 & 3 \\ 2 & 6 & 13 & 94 & 6 & 4 \\ 1 & 3 & 6 & 8 & 57 & 1 \\ 1 & 1 & 5 & 47 & 43 & 0 \end{bmatrix}$$

without IECMS x correct

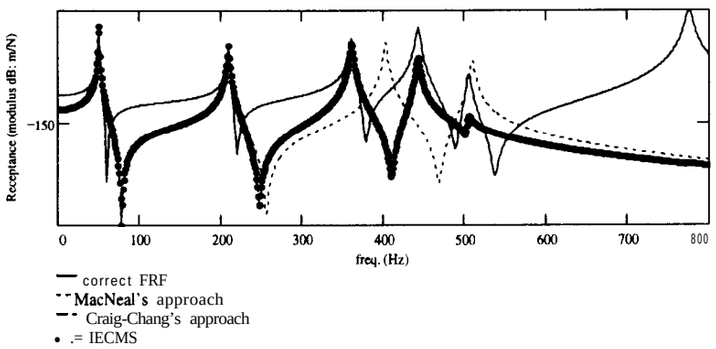

— correct FRF
- - MacNeal's approach
— · — Craig-Chang's approach
• . = IECMS

Figure 3.8 - $H_{6,6}$: Only modes within frequency range for each sub-system (i.e. 2A+4B), no residual compensation at slave DOFs (ESYS1)

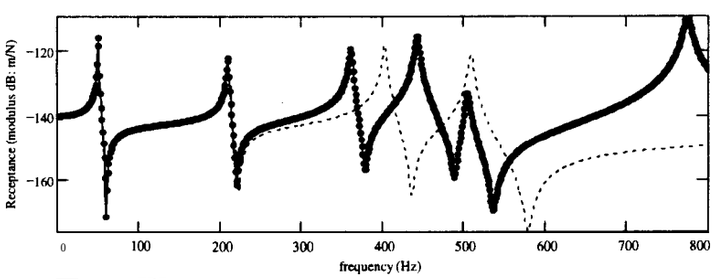

— correct FRF
- - MacNeal's approach
— · — Craig-Chang's approach
• ** IECMS

Figure 3.9 - $H_{6,6}$: Only modes within frequency range for each sub-system (i.e. 2A+4B), with residual compensation at slave DOFs (ESYS1)

Figures 3.8 and 3.9 show a point FRF for slave coordinate 6. Although the natural frequency predictions from Craig-Chang and IECMS are quite good, the response predictions for this FRF are only correct when such approaches include residual compensation at slave DOFs.

Coupled system ESYS1 will also be used to show the importance of pu_h choice. Three different cases were tried, apart from the one shown above. They were 0.5%, 5% and 50% the maximum frequency of interest, i.e. $freq_{pu_h}$ = 2.25 Hz, $freq_{pu_h}$ = 22.5 Hz, $freq_{pu_h}$ = 225 Hz, respectively. The frequency point used for the static residual compensation was still the same (i.e. $freq_{pu}$ = 0.5625 Hz). The frequency predictions obtained using the above choices are presented in Table 3.11.

When a frequency point very close to the beginning was chosen (i.e. 0.5% maximum frequency), the frequency predictions were still a bit overestimated, meaning that the correct residual compensation was not yet achieved. For 5% the maximum frequency of interest, the results were almost correct, being actually better than the previously 10% choice. For 50%, the predictions became a bit underestimated. The high-frequency values calculated to monitor the choice of frequency point pu_h are shown in Table 3.12. There, the darker the shading, the further inside the frequency range of interest is the calculated high-frequency value.

Table 3.11 - Frequency predictions (Hz) for coupled system ESYS1 when using IECMS formulation with different frequency points pu_h

mode number	m1	m2	m3	m4	m5	m6
Correct	50.43	209.5	361.4	443.23	505.43	775.48
pu_h=0.5%	50.43	209.56	363.68	447.91	517.28	811.63
error (%)	0	-0.03	-0.63	-1.04	-2.29	-4.45
pu_h=5%	50.43	209.5	361.35	443.15	505.22	775.49
error (%)	0	0	0.02	0.02	0.04	0
pu_h=50%	50.43	209.23	351.27	424.11	475.72	742.23
error (%)	0	0.13	2.89	4.51	6.25	4.48

Table 3.12 - High-frequency values (Hz) from IECMS for system C and D ($freq_{pu}$= 0.5625 Hz and $freq_{pu_h}$ = OS%, 5% and 50% max. freq. interest)

C (0.5%)	1	2	3	4	D (0.5%)	6	5	4	3
1	552.25	827.37	448.181	468.986	6	542.631	542.634	542.647	542.697
2	827.37	681.499	568.902	527.103	5	542.634	542.643	542.674	542.795
3	448.181	568.902	487.562	483.398	4	542.647	542.674	542.767	543.131
4	468.986	527.103	483.398	481.713	3	542.697	542.795	543.131	544.444
c (5%)	1	2	3	4	D (5%)	6	5	4	3
1	534.357	801.294	433.551	453.698	6	525.087	525.09	525.103	525.151
2	801.294	659.672	550.495	509.991	5	525.09	525.099	525.129	525.246
3	433.551	550.495	471.688	467.655	4	525.103	525.129	525.219	525.572
4	453.698	509.991	467.655	466.023	3	525.151	525.246	525.572	526.843
C (50%)	1	2	3	4	D (50%)	6	5	4	3
1	477.785	808.043	376.784	398.005	6	474.791	474.794	474.806	474.854
2	808.043	618.225	494.82	452.558	5	474.794	474.803	474.832	474.948
3	376.784	494.82	413.996	410.008	4	474.806	474.832	474.921	475.269
4	398.005	452.558	410.008	408.398	3	474.854	474.948	475.269	476.523

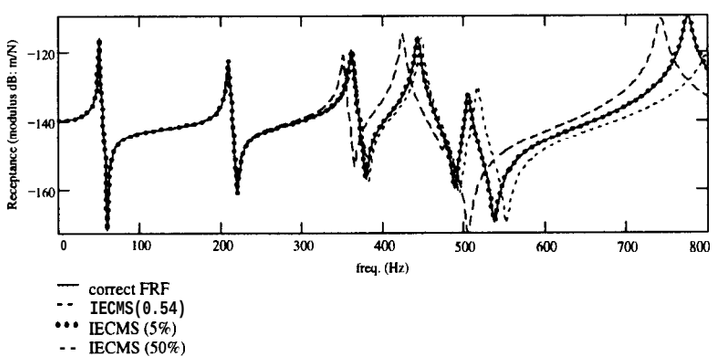

Figure 3.10 - $H_{6,6}$: Only modes within frequency range for each sub-system (i.e. 2A+4B), with residual compensation at slave DOFs (ESYS1) - IECMS predictions

The predictions shown in Table 3.11 are plotted in Figure 3.10 for the same FRF investigated before. The results obtained using 5% completely overlap the correct curve. The others follow the comments made for the referred table.

No example will be shown here for the case when rotational DOFs are not included in the formulation. The problems caused by their lack are the same as for the FRF coupling method and will be demonstrated again for the experimental results **in chapter 6.**

3.7. CONCLUSIONS OF THE CHAPTER

In this chapter, the CMS formulations which can be used with experimentally-derived data were presented. When no residual compensation is included (i.e. Hurty's approach), the coupled structure predictions obtained are not very good. A very large number of modes would have to be used to improve that. Residual compensation is then used to eliminate this need.

The first-order approximation to the residual terms generally yields good estimate around the lower end of the frequency range of interest due to its static approximation nature. When the modal density is high, more terms would have to be employed in the residual approximation to bring the higher modes' frequencies closer to their correct values. However, the higher the order of the approximation, the more complex the formulation would be. It was demonstrated here that, generally, an adequate prediction is obtained by using a second-order approximation.

The second-order approximation formulation available so far would require knowledge of the mass matrices of the sub-system and these are not readily available from experiments. The formulation developed in this chapter circumvents such a need, at the same time yielding a very accurate prediction compared with the correct formulation using the mass matrix. It is based on the same static residual matrix already needed for the first-order formulation and a high-frequency pseudo-eigenvalue. An automatic way of calculating this pseudo-eigenvalue was established and it is used to monitor the point where the second-order approximation matrix $[R1]$ is calculated.

CHAPTER 4: THE RESIDUAL PROBLEM (MODAL INCOMPLETENESS)

4.1. INTRODUCTION

In the previous two chapters, one of the many applications affected by residual terms was introduced, namely: structural coupling analysis (SCA). There, response- and modal-based coupling formulations were presented. Solutions to the residual problem were briefly addressed in the latter chapter to clarify some of the formulations exposed and here the residual problem will be addressed again, now explained in detail. It constitutes the core of this research.

This chapter treats the residual problem, sometimes also referred to as "modal incompleteness" or "modal truncation". Several trends found for the residual terms are noted, with special attention given to a new one relating the high-frequency residual terms with the mass of the system. The subject is addressed starting from either analytical, experimental or a combined approach, as modal truncation affects both FE and EMA derived models. Formulations for each case are presented, where emphasis is given to solve the high-frequency residual problem, and reasons for that are explained. Basically, three new formulations from the ones found in the literature are introduced here: (a) the mass-residual approach; (b) the experimental residual terms in series form and (c) the high-frequency pseudo-mode approach. Comparisons of the predictions using each are performed by means of simple examples.

FE and EMA methods have to limit the number of modes included in the analysis due to practical reasons. To obtain all modes the structure possesses is a somewhat costly and almost impossible process. The FEM normally requires a large number of coordinates in order to correctly predict the structure's dynamic behaviour. Corresponding to each coordinate there is a mode, and so, solving for the full eigensolution is an expensive and often inaccurate procedure for the high-frequency modes. Referring to EMA, the problem is mainly imposed by the need to limit the measured frequency range and consequently, it is only possible to obtain the modes within that range. A real structure possesses an infinite number of modes and so, even if the structure is tested over a wider frequency range than that of interest, many more modes are still

Next, a review is made of some of the existing work treating the residual problem. This is followed by a definition of the problem, its general formulation and interpretation. Then, some trends in the residual terms are shown and the high-frequency residual terms' formulations introduced. Finally, some examples are presented to clarify the theory and the main conclusions **derived.**

4.2. SUMMARY OF PREVIOUS WORK

The residual compensation techniques found in the literature are normally linked to a particular application where modal truncation has to be minimised. Very few works treated the residual compensation by itself. This is explained by the fact that **residual terms are only important if further use is to he made of the data.** Any application involving level of response may be influenced by that. Apart from the above application (SCA), one can also quote: eigenvalue sensitivity, forced response, structural dynamic modification (SDM), model identification and model updating, to mention just a few. In any of these applications, modal truncation (when not properly accounted for) can have serious consequences on the calculations performed, depending on how strong the out-of-range modes' effects are within the range of interest.

It is difficult to cover all applications and so, the solutions here will try to cover mainly those ones relevant to SCA (the application chosen throughout this work). Despite that, since modal truncation was extensively studied and it is quite well understood for SDM, their most important references will be quoted as well. Some conclusions can be extended to SCA. Ram and Braun, for instance, have published a series of papers showing how to predict the interval containing the natural frequencies of the modified structure for the case of modal truncation. Among their list of publications, it is worth mentioning references [14] and [94], inside which, their other references can be found. Unfortunately, their approach to calculate the lower and upper bounds for the natural frequencies is not applicable to SCA formulations and no other bounds could be derived from that. In the paper by Braun [13], the above and some other cases of modal truncation are treated, where both the analysis and the design problem are tackled. It is basically a summary of all relevant work published by him and his co-workers. Elliot and Mitchell [36] showed that, in SDM, the modified modal vector is a weighted linear sum of the original modal vector. So, modal truncation may affect almost any mode in a modification process. As a result, the model must include not only a sufficient number of modes, but also the ***correct modes*** for the ***type*** and ***locution*** of the modifications. These conclusions were also quoted by Brinkman [17] or Avitable and O'Callahan [6] and are equally valid to SCA predictions. In these last references, residual influence is related to the location and type of

coupling performed. In the paper by Deel and Luk [33], various errors that can be present in the modal model are analysed, where special attention is paid to modal truncation errors. As stated by Ulm [125], estimating the amount of error caused by modal truncation is difficult, as the flexibilities represented by different modes have different levels of importance. Gleeson [48] visualised the high-frequency residuals as springs attached to each spatial coordinate. This definition was extended to SDM later by Sohaney and Bonnecase [114]. They interpreted the high-frequency residual effects as a spring in series with the stiffness modification and the low-frequency residual effects as a mass in series with the mass modification.

Nothing has been mentioned yet about how the residual terms can be compensated for. The first residual compensation technique found in the literature, and still the most popular one, is the so-called "static residual approach". Only high-frequency residual terms are compensated using this method so the low-frequency modal set has to be complete. Static residuals have been used in vibration analysis since the early 70's after the pioneering work of MacNeal [SO], who applied it to CMS (as reviewed in chapter 3). Some other techniques are also improved using the same concept. The inertia effects of the higher modes are ignored altogether there. Originally, it was an FE-based approach, where the stiffness and the low-frequency modal parameters are needed. The residual is, then, evaluated at 0 Hz, as shown later. Craig's book [30] and the paper by Wang and Kirkhope [128] show an extension of MacNeal's approach for the case when the structure is considered to be unrestrained (as the stiffness matrix becomes singular in this case and cannot be inverted). Static residual terms may also be calculated from the modal summation of the out-of-range modes [26, 84, 126]. Although no singularity happens in this case, such a situation is not very realistic, since these modes are assumed to be unknown.

In 1972, Klosterman [69] showed how to circumvent the need for the stiffness matrix in the static residual approximation and to obtain this parameter from a purely experimental approach. His formulation is also evaluated at a constant frequency value (although not at 0 Hz) by subtracting from the total measured response the contribution related to the calculated low modal frequency parameters. He stated that the best accuracy would be achieved at a frequency near anti-resonances in the modal response. He also showed that better representation was obtained by using only the modes within the range of interest plus the above residual compensation than by using a larger number of modes. As before, only high-frequency residual terms were considered (i.e. no low-frequency residuals were present).

As briefly addressed in chapter 3, the static residual approximation fails to provide a good dynamic representation over the entire frequency range for systems with a high modal density.

So, Rubin [99] improved this dynamic representation by including a second-order residual compensation. This same compensation was later used by Craig and Chang [28], Martinez et al. [84] and others. The accuracy of the high-frequency residual compensation can be improved even further by including higher terms in the approximation. This is done in a series form similar to that originally proposed by Leung [74]. Camarda et al. [21], Maldonado and Singh [81], Suarez and Matheu [119], Suarez and Singh [120], all used such a concept in their applications. Smith and Hutton [111] also proposed a residual compensation approach based on a series form. It requires calculation of the residual terms at a single frequency point plus the mass matrix of the system. They suggest that a good convergence for the series is obtained when using any point corresponding to a value lower than one half of the first out-of-range natural frequency. All the above references require the knowledge of the physical parameter matrices (apart from [120] that uses left-eigenvectors). This constitutes a shortcoming of the methods from an experimental point of view. The formulation proposed in this thesis to circumvent this requirement allows the approaches presented in the above references to be used. Although left-eigenvectors can now be experimentally derived using the formulation shown in [13], the previous formulations are simpler.

One of the most important works treating the experimental residual terms' compensation and the one most extensively referred to is that by Lamontia [71]. Using a similar procedure to the one proposed by Klosterman, he showed that both low- and high-frequency residual terms can be calculated, one at a time, by subtracting from the test data the response corresponding to the measured modal parameters. A least-squares curve-fitting procedure locates precisely the position of the residual line which is then added over the entire frequency range. Only one term of the low- and/or high-frequency residual matrix can be obtained at a time using such method. If more terms are needed, they have to be calculated individually. This approach was also used by Sohaney and Bonnecase [114] and by Okubo and Matsuzaki [92]. In the latter paper, a method is proposed to correct the residual terms calculated above, since the measured FRFs are normally contaminated by noise which should be eliminated. They state that the low-frequency modal matrix is orthogonal to a vector of residual parameters. When checking this formula for a mass-and-spring system, it was discovered that only for the case when all mass elements have a constant value it proved to be true. So, as this is not the case from experiments, their approach is of no practical use. Smith and Peng [112] also referred to difficulties in correctly estimating the residual flexibility parameters as proposed by Lamontia, since all the errors of the curve-fit modes add to the error in this estimation. They noted that, where there are many overlapping modes, the errors are amplified by resonance effects. Moreover, test errors have a systematic

tendency to increase the estimate of residual flexibility. One of the most problematic aspects of residual estimation according to them is that there are few checks which can be performed.

In the paper by Allemang and Brown [3], they say that residual terms are limited to frequency response function models, as the inclusion in the time domain is more difficult. Residual modes, although of no physical significance, are required to account for the strong dynamic influences of outside modes. As discussed by Gleeson [48], Ewins [40] and Goyder [51], from an experimental point of view, one of the biggest problems with residual terms is that they cannot be derived. Consequently, **no unmeasured FRFs' residual can be obtained from measured FRF information.** Goyder demonstrated that some errors around anti-resonances occur when regenerating unmeasured FRFs from the modal data. In order to compensate for the residual effects, he used a curve-fitting procedure including the contribution of the out-of-range modes. Some other authors also used curve-fitting approaches (as will be addressed later) and the same limitation applies. Recently, Doebling [34] proposed a method for calculating a rank-deficient estimate of the **unmeasured** partition of the high-frequency residual matrix based on the measured data. He used this approach successfully in the measurement of structural flexibility matrices. However, such a method cannot be extrapolated to SCA techniques, as the quality of the results will be jeopardised by the approximation.

Since residuals cannot be derived, Ewins [42] suggested two ways of compensating for the out-of-range modes experimentally: (1) by measuring all necessary FRF curves in the range of interest or (2) by measuring the selected FRF data over a much wider range than that of interest. Brillhart et al. [15] added to this list the mass loaded approach (although they actually calculated their residual terms as proposed by Lamontia). The mass loaded approach was used in the paper by Gwinn et al. [54], for example. However, it will not be considered here, as it may be difficult to establish the size of the additional mass necessary to bring enough modes inside the range of interest (as discussed in more detail in chapter 3).

Several different methods are available to calculate the residual compensation when using (1); some already referred and others to be referred later. When using (2), the problem would be to establish by how much the measured frequency range has to be extended to correct compensate for the residual effects. In trying to solve (2), several authors have suggested either the number of additional modes that should be included or the upper frequency limits to be measured. References [33] and [71], for example, recommended the inclusion of two or three more modes in the measured frequency range. Such guidelines are argued in [36]. In [99] and [60], an upper frequency limit of 1.5 and 1.4 times the maximum frequency in the range of interest is

recommended, respectively. These limits are disbelieved in [42], where a limit of 1.5 or 2 is regarded as maybe too conservative or still inadequate. Such limits were based purely on intuition. So, lately, Imamovic [64] developed a technique called "FOREST" to calculate an upper frequency value below which all modes should be included. It has a mathematical basis to it and is based on the fact that, away from the range of interest, the effects of the outside modes tend to decrease within this range. It requires all modes from the frequency range in which the FRFs need to be accurately regenerated, plus the regenerated FRFs calculated using such modes. The user specifies the accuracy with which the FRFs are needed. It was originally developed to be used in FE analysis and rotational effects were ignored. This technique is not considered further, as the upper frequency limit is in general very high to be measured accurately using normal experimental techniques. This fact is even stronger when rotational coordinates are of interest, as is the case in this work. However, from an FE standpoint, it is very useful in the sense that FRFs can be regenerated accurately from modal summation formulae instead of direct inversion of the dynamic stiffness matrix. To obtain more modes from an FE model will be computationally cheaper than inverting a big matrix.

In reference [17] it is suggested that one extra mode below and one above the frequency range of interest should be included by means of a global curve-fitting algorithm [16]. Several other papers also compensate for the residual effects by using curve-fitting procedures. Chung and Lee [25], Ahmed [1], Kochersberger and Mitchell [70] and Randall et al. [95], all used a different curve-fitting approach. In reference [25], the residual is compensated as a fictitious mode beyond the frequency range of interest. The modal parameters are then obtained by an iterative SDOF curve-fitting. A list of papers where curve-fitting procedures are used for compensating the errors due to higher or lower modal truncation is presented there. Chung and Lee indicate that the assumption of constant residual terms may not be valid for the whole frequency range. Accordingly, they developed a frequency-dependent modal parameter residual estimation method. Also using a fictitious mode is the approach to calculate the residual terms using an extra mode at an arbitrary frequency lower/higher than the frequency range of interest. Such procedure was used by Gleeson [48], Silva and Femandes [105] or Urgueira [127]. It is even implemented in the commercial software MODENT [86]. As pointed out in [48] and [127], there is no mode-shape associated to the fictitious residual mode. A different and much simpler fictitious mode approach to compensate for the high-frequency residual terms is proposed in this thesis (high-frequency pseudo-mode formulation).

There are some trends in the residual terms as mentioned in [40], [51] or in the work of Skingle [107] and they are shown later in this chapter. For example, residual terms for point FRFs tend

to be bigger than for transfer FRFs, with the difference becoming larger as the physical separation of the points on the structure increases. In [40], it is mentioned that it was not yet clear what determines the importance of the out-of-range modes. Grafe [52] has shown which parameters govern each frequency region. An extrapolation from his work allows the above point to be answered.

4.3. DEFINITION

The definition of residual terms was already mentioned in the previous section. "Residual" is a general term used to describe the effects of the modes that, although existing in the structure, cannot be analysed or measured due to the practical need of limiting the frequency range of interest. They are divided into two categories and are known in the literature as [1]:

- low-frequency residual terms ("inertia restraint" or "residual mass");
- high-frequency residual terms ("residual flexibility" or "residual stiffness").

The inertia restraint is used to describe both rigid-body modes (when the structure is considered unrestrained) and low-frequency flexible modes below the minimum frequency of interest (low-frequency modes). The residual flexibility describes only the effects of the modes that lie above the maximum frequency of interest (high-frequency modes). The best way of understanding residual terms is by analysing the FRF formula. This is done in the following section, where the general residual formulation is derived and explained in details.

Both residual terms can be important. However, it is normally possible to start the analysis of a structure from 0 (zero) Hz and, in this case, no low-frequency residual terms are necessary. Only unrestrained structures are an exception to this rule. There, low-frequency residual terms are present and are associated with the rigid-body modes. These can be calculated analytically and when they are added to the regenerated curves, the correct FRFs are recovered (if no high-frequency residuals are present). Therefore, high-frequency residual terms represent the major problem and this is the reason why only these terms were focused on the research.

4.4. GENERAL FORMULATION AND INTERPRETATION

To start the derivation of residual terms, the FRF formula for the case when all the modes of the structure are available (i.e. complete information) is considered initially. Using the modal

[1] Actually, the first name is the one used throughout this thesis and the ones within brackets are the names used in the literature.

model, the FRF curve for response point (i) and excitation point (j) can be calculated in receptance form, as follows:

$$H_{ij}(\omega) = \sum_{r=1}^{N} \frac{{}_rA_{ij}}{\omega_r^2 - \omega^2 + i\omega_r^2\eta_r} \tag{4.1}$$

where:

$${}_rA_{ij} = \phi_{ir}\phi_{jr} \tag{4.2}$$

However, in a modal test, a limited frequency range is measured. Moreover, it is standard practice to measure only one column (or row) of the whole FRF matrix. From these data, only the modes within this measured range can be calculated. In order to accommodate the modes outside the range of measurement (i.e. to consider all the modes of the structure), equation (4.1) can be divided in the following way:

$$H_{ij}(\omega) = -\frac{{}_{LF}R_{ij}}{\omega^2} + \sum_{r=m1}^{m2} \frac{\phi_{ir}\phi_{jr}}{\omega_r^2 - \omega^2 + i\omega_r^2\eta_r} + {}_{HF}R_{ij} \tag{4.3}$$

where:

$$-\frac{{}_{LF}R_{ij}}{\omega^2} = \sum_{r=1}^{m1-1} \frac{\phi_{ir}\phi_{jr}}{\omega_r^2 - \omega^2 + i\omega_r^2\eta_r} \qquad \text{for } \omega > \omega_r \tag{4.3a}$$

$${}_{HF}R_{ij} = \sum_{r=m2+1}^{N} \frac{\phi_{ir}\phi_{jr}}{\omega_r^2 - \omega^2 + i\omega_r^2\eta_r} \qquad \text{for } \omega < \omega_r \tag{4.3b}$$

The values expressed by equations (4.3a) and (4.3b) are the low- and high-frequency residual terms, respectively. They are dependent on the frequency range of interest chosen. Therefore, the narrower this range, the more modes are included in the series represented by the above equations. Consequently, the bigger will be the value of the residual terms. Exceptions can occur for transfer FRFs (see section 4.5.2). The middle term in equation (4.3) represents the actual frequency range of interest. Parameters ml and m2 are the lowest and highest modes in this range, respectively. Since the out-of-range modes are unknown for real structures, residual terms cannot be calculated using the explicit formulation above and usually an approximation is considered. In the following sections, this and some other formulations available or developed by the author for that are going to be introduced for the high-frequency residual terms.

An important point to stress at this stage is that the residual terms are **local** parameters. This means, apart from the fact that they are dependent on the frequency range of interest, that they *are* also dependent on the particular response and excitation points in question. This is because of the mode-shape contribution for each term of the series represented by equations (4.3a) and (4.3b). As each FRF is made up of a summation of all the modes the structure possesses and not

all the modes can be found for real cases, it is not possible to calculate the whole FRF matrix from the knowledge of only one row or column [40]. This is due to the fact that residual terms cannot be derived (as quoted in section 4.2) in the same way that modal constants can. This statement can be interpreted analysing the following equations. Although the relationship below is valid:

$$ {}_rA_{ij} = {}_rA_{ii}\,{}_rA_{jj} \tag{4.4} $$

one cannot say the same for FRFs (see Appendix E)[2]:

$$ H_{ij}^2 = H_{ii}\,H_{jj} \tag{4.5} $$

because[3]:

$$ R_{ij}^2 \neq R_{ii}\,R_{jj} \tag{4.6} $$

Equation (4.5) is only true when all the modes are available, that is, no residual information is left out. It would also be true considering just the regenerated portion of the FRF (i.e. the modes within the frequency range of interest), since the in-range information follows the modal constant relationship.

As illustrated next, residual terms have specific characteristics within the frequency range of interest. To aid the explanation, an SDOF system is considered at first. The modulus of the FRF curve for this case can be calculated as follows:

$$ |H(\omega)| = \frac{1}{m\sqrt{\left(\omega_r^2 - \omega^2\right)^2 + \left(\eta_r\omega_r^2\right)^2}} \tag{4.7} $$

At high frequencies, i.e. $\omega >> \omega_r$, equation (4.7) becomes:

$$ |H(\omega)| = \frac{1}{m\omega^2} \tag{4.8} $$

At low frequencies, i.e. $\omega << \omega_r$, it becomes:

$$ |H(\omega)| = \frac{1}{m\omega_r^2\sqrt{1+\eta_r}} \tag{4.9} $$

As the damping coefficient (η_r) is usually small in real cases, the term under the square root above can be ignored. Moreover, $\omega_r^2 = k/m$. So, equation (4.9) can be simplified further as:

---

[2] When no superscript is used in the FRF symbol means that the correct FRF curve is considered (i.e. all modes are included).

[3] No subscript was used in this equation, as it is true for both low- and high-frequency residual terms.

$$|H(\omega)| = \frac{1}{k} \tag{4.10}$$

Considering the above equations, one can make an analogy between the SDOF case and a more realistic MDOF case. Analysing equation (4.8) first, it can be clearly seen that the modes below the first frequency of interest are governed by the mass term within that range. Equation (4.10), on the other hand, shows that the modes above the last frequency of interest are governed by the stiffness term within that range. In other words, one can say that the low-frequency residuals have a mass-like behaviour within the frequency range of interest, while the high-frequency residuals have a stiffness-like behaviour [40, 71].

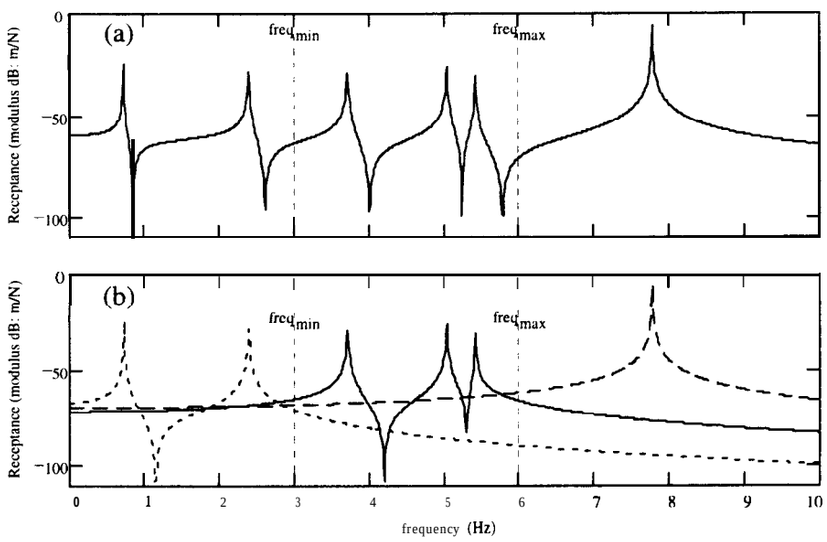

Figure 4.1- (a) Correct FRF (i.e. including all the modes) and (b) FRF curve split into its three frequency ranges (i.e. low-, interest and high-frequency ranges)

Figure 4.1 shows a visualisation of equation (4.3) for a point FRF (relative to a 6 DOF mass-spring system). The total frequency range includes all the modes of the system and is split into three intervals (low-frequency range, frequency range of interest and high-frequency range). These intervals are limited by the two vertical lines, representing, respectively, the lower and upper frequencies for the frequency range of interest. The first part of this figure, (a), shows the complete FRF curve, including all 6 modes. The second part, (b), shows the same FRF curve, but now split into the three main terms of equation (4.3). Each curve is plotted for the total frequency range, however, including only the modes within that specific frequency range. Therefore, analysing each of the frequency ranges, the total response is the effect of the modes within that range plus a contribution of the other modes belonging to the other two ranges. The summation of all the curves shown in (b) will result in the curve shown in (a).

4.5. TRENDS IN THE RESIDUAL TERMS

4.5.1. RESIDUAL EFFECTS AT RESONANCES AND ANTI-RESONANCES

There are some trends in the residual terms that need to be pointed out. At first, their influence at resonances and anti-resonances is investigated. For that, the SDOF assumption is considered. In the vicinity of a resonance, the dynamic behaviour of most structures is dominated by a single mode. In algebra terms, this is equivalent to saying that only one term of the series represented by equation (4.1) contributes to the magnitude of the FRF. This term is associated with the particular mode in question. All other modes (for a small range of frequencies close to the natural frequency) can be considered to be contributing a constant term. Expressing this assumption in algebra notation means that equation (4.1) can be re-written as:

$$H_{ij}(\omega) = \frac{{}_rA_{ij}}{\omega_r^2 - \omega^2 + i\omega_r^2\eta_r} + \sum_{\substack{s=1 \\ s\neq r}}^{N} \frac{{}_sA_{ij}}{\omega_s^2 - \omega^2 + i\omega_s^2\eta_s} \tag{4.11}$$

or, for the small frequency range close to the natural frequency as:

$$H_{ij}(\omega \approx \omega_r) \cong \frac{{}_rA_{ij}}{\omega_r^2 - \omega^2 + i\omega_r^2\eta_r} + {}_rB_{ij} \tag{4.11a}$$

This formula is the basic concept used in some SDOF modal parameter extraction techniques [41]. By definition, the residual terms are the contribution of all the modes outside the frequency range. Therefore, following the above formulation, one can conclude that, close to each natural frequency, the residual term has hardly any effect (as the constant term in equation (4.1 la) is generally small). However, as one starts considering frequency points away from resonance, this term can have some influence. The lower the response levels, the stronger the chances of having residual effects. Consequently, residuals will be most significant close to anti-resonances. To clarify the above statement, each of the three curves plotted in Figure 4.1 is considered again. However, attention is focused on the middle part of the plot (frequency range of interest), which is shown in Figure 4.2.

In Figure 4.2a, the major curve is the regenerated FRF (i.e. the one calculated considering only the modes within the range of interest). The other two curves are expressed by the mass-line contribution of the lower modes (low-frequency residual effect) and the stiffness-line contribution of the higher modes (high-frequency residual effect). The FRF curves are plotted on a dB (logarithmic) scale. When a dB scale is used, if the residual line intercepts the regenerated curve it means that the effect of the outside modes associated with that specific line

are important. The **strength of the residual effect can be assessed by the area between the residual and the regenerated curves.** The bigger the area, the greater is the residual effect. Therefore, looking at the first part of this figure, one can see that the low-frequency residual terms have a smaller overall influence (for that particular FRF) than do the high-frequency residual terms. The former affects only the first anti-resonance, while the latter affects both anti-resonances.

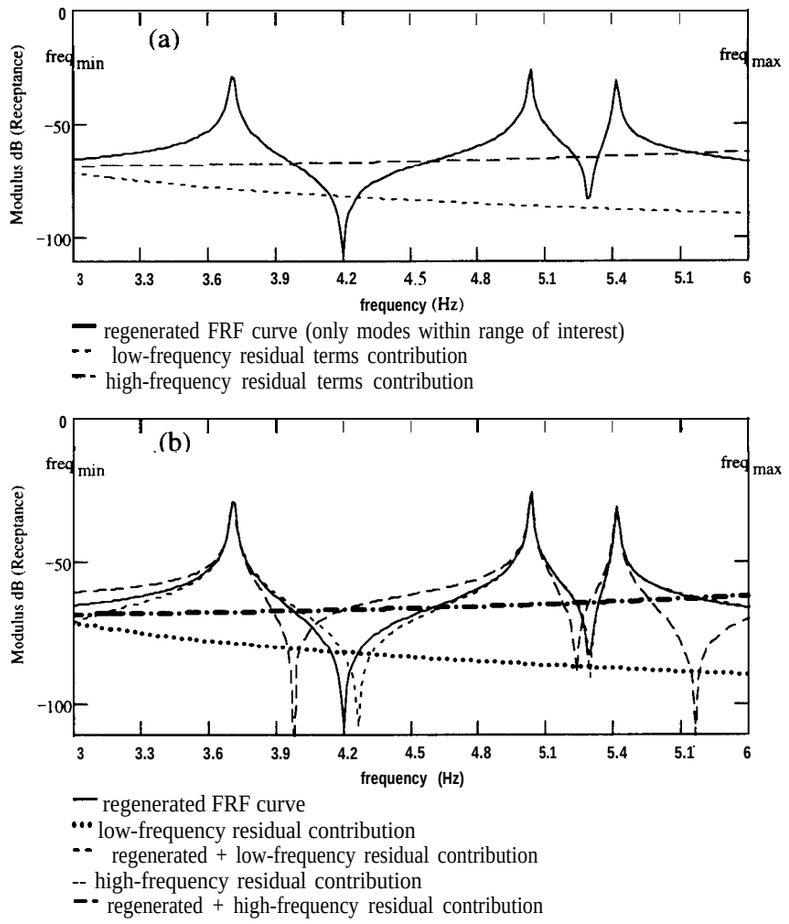

Figure 4.2- (a) FRF curve split into its three frequency ranges (i.e. low, interest and high) plotted for the frequency range of interest; (b) regenerated FRF curve plus the contribution of the residual terms to the regenerated curve.

When residual terms are important, their omission has the effect of shifting the correct position of anti-resonances. Figure 4.2b shows this shift caused by each of the residual terms at a time. Looking carefully at the curves, it can be noticed that the "corrected" position for the anti-resonances is found to be where the residual line intercepts the regenerated curve and the sign of these curves is different. The term "corrected" is written in inverted commas because there are two residual terms affecting the above regenerated curve. Only after one of them has been

added to the regenerated curve can the **correct** position of the anti-resonance be found as explained above. It should also be emphasised that **the resonances are not affected by the lack of residual compensation, only the anti-resonances,** as we wanted to show.

4.5.2. RESIDUAL TERMS FOR POINT AND TRANSFER F'RFs

Another important trend of the residual terms is related to their sizes when comparing point and transfer FRFs. As mentioned in [40, 51, 107], it is normally found that the high-frequency residual terms are smaller for transfer FRFs than for point FRFs. The reason for this can be understood from the following formulae (only the high-frequency residual is considered initially):

$$_{HF}R_{ii} \approx \sum_{r=m2+1}^{N} \frac{\phi_{ii}^2}{\omega_r^2} \qquad _{HF}R_{ij} \approx \sum_{r=m2+1}^{N} \frac{\phi_{ir}\phi_{jr}}{\omega_r^2} \tag{4.12}$$

As the eigenvector elements can vary in sign, the summation in the first formula above will always give a positive value for the point residual term ($_{HF}R_{ii}$), in contrast to what happens with the second formula. There, the summation can have a negative value sometimes, decreasing, consequently, the final value for the transfer residual term ($_{HF}R_{ij}$). However, cases can arise where the eigenvectors used in the calculation of a point residual term are so small that the transfer residual term can have a bigger value. Such a situation will be shown in section 4.7. So, more conclusive than the remark at the beginning of this section, one can say that **the biggest residual term will be for a point FRF, while the smallest will be for a transfer FRF.** Although high-frequency residual terms were used at the beginning, it could be shown that the same comments are equally valid for low-frequency residual terms.

Because of the oscillation in sign for the transfer residual terms, an intriguing fact can happen sometimes. The inclusion of more terms in equation (4.12) can produce smaller values for the residual terms than for the case of fewer terms included. This is an interesting observation, as it is known that decreasing the frequency range of interest (consequently, increasing the number of terms for the residual terms) will produce bigger residual values. This fact will also be shown in section 4.7.

4.5.3. RELATIONSHIP BETWEEN THE MASS OF THE SYSTEM AND HIGH-FREQUENCY RESIDUAL TERMS

Another very interesting trend of the residual terms, although not a straightforward one to see, is the relationship between the mass of the system and the values of the high-frequency residual

terms. It was discovered through some mass-and-spring system studies that **the smaller the mass, the bigger the high-frequency residual effects.** This observation will be demonstrated in section 4.7. The explanation for that was a bit intuitive at the beginning. Later on, analysing the work done by Grafe [52], a more mathematical explanation for that emerged. The author believes that a similar interpretation could be made for the low-frequency residual terms, although they were not investigated in the research. They could probably be linked to the stiffness of the system in an alike fashion.

Coming back to the high-frequency residual terms, an intuitive explanation is given first. The smaller the mass, the bigger the motion of the coordinate associated with it. If one considers that the motion of a structure is represented by its mode-shapes and the mode-shape is the bigger contributor for the residual value, this explains the statement. However, this remark is only valid for point FRFs. For transfer FRFs it will be more complicated to conclude anything. There, the residual terms will involve a combination of mode-shapes (and, consequently, masses) of two particular coordinates.

Grafe, on the other hand, used the fractional polynomial form of an FRF, as presented by Ewins [41], to show distinct patterns between the physical parameters of a system and the excitation frequency ω. The FRF in polynomial form can be expressed as:

$$H_{ij}(\omega) = \frac{b_o + b_1\omega^1 i + b_2\omega^2 + b_3\omega^3 i + \cdots + b_{2(N-1)-1}\omega^{2(N-1)-1} i + b_{2(N-1)}\omega^{2(N-1)}}{d_o + d_1\omega^1 i + d_2\omega^2 + d_3\omega^3 i + \cdots + d_{2N-1}\omega^{2N-1} i + d_{2N}\omega^{2N}} \qquad \textit{(4.13)}$$

The above polynomial form considers both real and imaginary parts, whereas Ewins' form only considers real part (i.e. damping was neglected). Therefore, the indexes of the coefficients are different when comparing the two equations. In equation (4.13), the indexes are the same as the powers of the excitation frequency ω. Coefficients ***b***'s and d's are, actually, provided by expressions involving the mass, damping and stiffness parameters of the system. To understand that relationship, one simple example ignoring damping is given in [41]. Grafe built a table linking these coefficients with the maximum power occurring for each physical parameter. To get that, he solved an analytical 2 DOF mass-and-spring system, similar to the one shown in [41]; however, considering a consistent mass matrix. Later on, he solved for a higher-order system in order to generalise the pattern.

Table 4.1 shows the findings in [52]. The superscripts on the physical parameters denote their maximum power. Blank spaces indicate the absence of that particular parameter. These are organised such that mass is shown first, followed by damping and then the stiffness parameters.

The columns of ω represent the maximum frequency power in the numerator or denominator of equation (4.13). For example, for a 2 DOF system (i.e. N=2), the numerator corresponds to column ω^2, while the denominator corresponds to column ω^4, while for a 3 DOF system, these are respectively ω^4 and ω^6; and so on.

Table 4.1 - Maximum powers of the physical parameters occurring for each coefficient on the numerator/denominator of the FRF in polynomial form

	ω^2	ω^4	ω^6	ω^8	ω^{2N}	ω^{2N-2}	comments
d_o or b_o	(, , k^1)	(, , k^2)	(, , k^3)	(, , k^4)	⋮	⋮	real
d_1 or b_1	(, d^1,)	(, d^1, k^1)	(, d^1, k^2)	(, d^1, k^3)			imag.
d_2 or b_2	(m^1, ,)	(m^1, d^2, k^1)	(m^1, d^2, k^2)	(m^1, d^2, k^3)			real
d_3 or b_3		(m^1, d^1,)	(m^1, d^3, k^1)	(m^1, d^3, k^2)			imag.
d_4 or b_4		(m^2, ,)	(m^2, d^2, k^1)	(m^2, d^4, k^2)			real
d_5 or b_5			(m^2, d^1,)	(m^2, d^3, k^1)			imag.
d_6 or b_6			(m^3, ,)	(m^3, d^2, k^1)			real
d_7 or b_7				(m^3, d^1,)			imag.
d_8 or b_8				(m^4, ,)			real
⋮					⋮	⋮	⋮

Studying this table, it can be noticed that stiffness parameters are dominant in the lower coefficients ($d_o, d_1, \ldots . b_{,,,} b_1$), while mass parameters are dominant in the higher coefficients ($..., d_{2N}, b_{2(N-1)}$). Damping affects neither the last nor the first terms of the polynomials. Its importance increases and subsequently decreases, reaching its maximum power in the middle of the coefficients range. The significance of the stiffness parameters decreases continuously as the coefficients increase. Similarly, the importance of the mass parameters continuously decreases as the coefficients decrease. The power associated with the mass and stiffness parameters is the same for a particular pair of real and imaginary coefficients; the change in power happening for the following pair.

However, the study by Grafe does not say anything relating the magnitudes of the physical parameters with the magnitudes of residual terms. It only states what dominates each frequency region. Besides, the above comments for the importance of the mass and stiffness at the high and low frequency ranges, respectively, were made implicitly in section 4.4. There it was said that the low-frequency out-of-range modes have a mass behaviour within the frequency range of interest, while the high-frequency out-of-range modes have a stiffness behaviour within this range. A further step is necessary in order to conclude something about the size of the mass parameters and the size of the high-frequency residual terms, as stated at the beginning of this section. High-frequency modes (which are responsible for the high-frequency residual terms) are in the high-frequency region and, consequently, are associated with the mass parameters. However, this only says that the two parameters are linked. Nevertheless, considering that the frequency power of the denominator in equation (4.13) is higher than the frequency power of

the numerator, the necessary further step is achieved. The mass power is bigger for higher coefficients. So, the denominator will have a bigger mass contribution. Consequently, the smaller the mass, the bigger the residual effects, as we wanted to demonstrate.

4.5.4. RESIDUAL TERMS FOR TRANSLATIONAL AND ROTATIONAL FRFS

As a final trend for the residual terms, their importance for translational and rotational FRFs is investigated. It was observed, and will be demonstrated in section 4.7, that residual terms are normally much bigger for rotational/rotational FRFs than for translational/translational FRFs. The importance of residual terms for FRFs involving a mixture of translational and rotational coordinates lies somewhere **in between.**

A **similar explanation to the one provided** in the previous section can be used here to clarify this statement. The residual terms are related to the amount of motion allowed in the particular FRF. In the high-frequency region, the rotational motions are bigger than the translational one, thereby explaining the conclusions draw. Ewins [40] described this fact for a beam structure. He quoted that for translational/translational FRFs, modal contributions decrease as the mode number rises. For rotational/rotational FRFs, the modal contributions have the same magnitude for all modes. Therefore, leaving out modes at the latter will have much more effect than at the former, also confirming what was just stated.

4.6. HIGH-FREQUENCY RESIDUAL TERMS FORMULATIONS

4.6.1. INTRODUCTION

From now on, only the high-frequency residual terms will be considered. Therefore, the indexes (*HF* and *LF*) used in the previous sections are dropped for simplification and *R* will denote simply high-frequency residual terms. There are several formulations for calculating the high-frequency residual terms' contribution. For the ones introduced here, reference will be made to whether they can be used in FRF coupling and/or CMS formulations; the main objective. The formulations can be based on a purely experimental approach, on a purely analytical approach or on a mixture of the two. **Although all the experimental approaches can be used starting from analytical data, the contrary is not true. So,** largely due to this comment, experimentally-based approaches will be the target, although all of them will be referred to. Besides, experimentally-derived models are the subject of this thesis. Each of the formulations has its own advantages and shortcomings. The choice of formulation depends to a great deal on the application where it is going to be used and the ease of obtaining the necessary values. There

are some standard procedures to eliminate the residual terms' effect which are widely accepted within the modal analysis community and these are summarised below:

1. measure just one column (or row) of the FRF matrix on a much wider frequency range than that of interest;
2. measure the whole FRF matrix (or at least those FRFs which are going to be needed for future applications) in the frequency range of interest only;
3. obtain a mathematical model of the structure and the modal model within the frequency range of interest.

The first approach is not a residual formulation as such, but a way of eliminating the effects of out-of-range modes without having to resort to residual calculations. Although the least expensive of the three, from an experimental point of view, it is quite troublesome to be implemented accurately. This is linked with the difficulty of establishing in advance by how much one needs to extend the measured frequency range to compensate correctly for the residual effects. The most effective way of establishing that limit so far is the formulation proposed by Imamovic [64]. However, his formulation normally leads to quite a high upper frequency limit, as already mentioned, which is difficult for measurement. Besides, for rotational-related FRFs, this range has to be extended so much that it will be quite a costly and inefficient procedure. Therefore, this approach was not pursued further.

The problem with the second approach is that it is expensive from an experimental point of view (both in terms of measurement and computation effort) when the number of FRFs needed is high. Normally, it involves calculating the residual terms one at a time, unless a least-squares or curve-fitting approach is used. However, it is the most accurate way of compensating for the residual terms and it was the approach followed closest in this thesis.

The third approach is limited for practical reasons (although allowing for all the necessary residual terms to be calculated in one go). In some cases, only the measured results are known to the analyst and from those results it is not yet possible to obtain an accurate and complete mathematical model of the structure. Trying to obtain an FE model of the system may be a very expensive solution, especially for a complicated geometry. The use of coarse FE meshes (therefore, cutting the costs in generating the FE model) may not be appropriate to correctly compensate for the residual effects. A formulation is proposed in this thesis to circumvent the need for the physical matrices of the system, although the requirements will fall into the previous category.

Next, some of the formulations used to calculate the high-frequency residual terms will be introduced, starting from the purely analytical approaches, followed by the combined analytical/experimental ones and finally, the purely experimental approaches. The formulations are developed further and further to reach the objective of obtaining all the necessary residual terms purely from experimentally-derived data, as is sought. A flow chart is given in Figure 4.3 to show the evolution of the formulations.

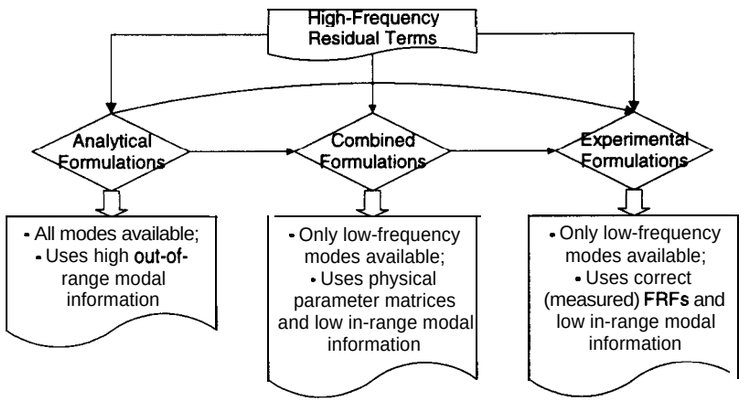

Figure 4.3 • Flow-chart of the high-frequency residual terms formulation

4.6.2. ANALYTICALLY-BASED FORMULATIONS

4.6.2.(a) SINGLE-TERM FREQUENCY-DEPENDENT FORMULATION

Only for analytical systems it is possible to obtain a full dynamic analysis of a structure, i.e. all the eigenvalues and eigenvectors. Then, the high-frequency residual terms can be evaluated using the out-of-range modal information as shown by equation (4.3b). Considering complex natural frequency notation from now on (for generalisation), and the fact that the referred equation is, in reality, frequency-dependent, the required residual term can be expressed as[4]:

$$R_{ij}(\omega) = \sum_{r=m+1}^{N} \frac{\phi_{ir}\phi_{jr}}{\lambda_r^2 - \omega^2} \qquad (4.14)$$

The advantage of the above equation is that it helps to understand more complex formulations. However, each residual term has to be calculated individually. Moreover, it is mainly of theoretical interest, as these modes are not available for systems other than mass-spring-(damper) ones. When analysing other types of system using FE analysis, even if all the modes are solved for, the higher ones will be less accurate than the lower ones, unless the order of the

[4] As only one limit has to be established, parameter m will be used from now on (instead of the previously used m2), to indicate the last mode included in the frequency range of interest.

system is not very high (not the normal case). The residual compensation above can be employed with FRF coupling formulations. However, as CMS formulations do not allow frequency-dependent residual terms, it cannot be used there. This problem will be resolved soon, but before going onto that, a multiple residual formulation will be introduced.

4.6.2.(b) MULTIPLE-TERM FREQUENCY-DEPENDENT FORMULATION

As just quoted, equation (4.14) has to be evaluated for every single residual term needed. This process could be simplified by using the high-frequency modal parameter matrices, as follows:

$$[R(\omega)] = [\phi^h]\left[\left(\lambda_h^2 - \omega^2\right)\right]^{-1}[\phi^h]^T \tag{4.15}$$

The middle matrix above is diagonal. All comments made in the former sub-section apply here as well. The only advantage of this formulation compared with equation (4.14) is that all residual terms can be calculated at once.

4.6.2.(c) ANALYTICAL STATIC RESIDUAL FORMULATION

In order to be able to use the above equations in CMS formulation, they have to be evaluated at a single frequency value. Equation (4.15) will be used here, however, since it allows all terms to be calculated in one go and is, consequently, more efficient. Several authors used the concept of static residual for that [26, 84, 126]. This is nothing more than calculating equation (4.15) at 0 Hz frequency, as introduced in the previous chapter by equation (3.24) and is repeated here:

$$[R_0] = [\phi^h]\left[\lambda_h^2\right]^{-1}[\phi^h]^T \tag{4.16}$$

A subscript 0 (zero) was added in the above residual notation to highlight that this term is a static residual approximation. Apart from being the equation employed in CMS formulations, it can also be used with FRF coupling formulations. However, in both cases, if the modal density is high, it will not be appropriate to compensate for the high-frequency residual terms over the entire frequency range of interest and an improvement is necessary. This is presented next.

4.6.2.(d) ANALYTICAL RESIDUAL MATRIX IN SERIES FORM

For the case, when the modal density is high, the assumption that the inertia effects can be neglected is not valid anymore. In such situations, the residual terms can be calculated using all the terms in the series expressed by equation (3.39, and repeated here:

$$\left[\lambda_h^2 - \omega^2 I\right]^{-1} = \left[\lambda_h^2\right]^{-1} + \omega^2\left[\lambda_h^2\right]^{-2} + \omega^4\left[\lambda_h^2\right]^{-3} + \cdots \tag{4.17}$$

Then, the residual formulation will take the following series form[5] [119]:

$$[R_S(\omega)] = [\phi^h][\lambda_h^2]^{-1}[\phi^h]^T + \omega^2[\phi^h][\lambda_h^2]^{-2}[\phi^h]^T + \omega^4[\phi^h][\lambda_h^2]^{-3}[\phi^h]^T + \cdots \quad (4.18)$$

In general, using just the first two terms in this series already produces a very good approximation to the high-frequency residual terms. Therefore, equation (4.18) could be truncated after that. For the FRF coupling, including more and more terms would not be a problem, as the formulation does not change by that, only the FRFs. However, for the CMS formulations, higher terms mean more complexity in the formulation and, therefore, extra terms are not always justifiable. Considering the series form truncated after the second term and using the notation assumed in the previous chapter, equation (4.18) can be simplified as:

$$[R_S(\omega)] \approx [R_0] + \omega^2[R1_0] \quad (4.19)$$

Subscript 0 (zero) was also introduced in the dynamic residual matrix [R1], to denote a matrix calculated at 0 Hz frequency. The two matrices on the RHS of equation (4.19) are the ones used in the second-order CMS formulations, as shown in chapter 3. It should be emphasised here that, although the high-frequency residual terms' matrix is frequency-dependent, the matrices needed for the CMS formulation are not.

4.6.3. COMBINED FORMULATIONS (ANALYTICALLY/EXPERIMENTALLY-BASED)

4.6.3.(a) FREQUENCY-DEPENDENT FORMULATION

As stated in the preceding section, the high-frequency modes are not normally available. Therefore, the equations presented there are of theoretical interest only. In order to consider more realistic situations, this problem can be circumvented for the high-frequency residual formulation by using the physical parameter matrices of the system and the available low-frequency modes. The mass, stiffness and damping matrices can be obtained from FE (or analytical) analysis, as also can be the low-frequency modal parameters. When this is the case, the formulations given here will lie in the earlier category (i.e. analytically-based formulations). However, the low modal parameters can also be obtained from experimental modal analysis. This is the reason why this section is referred to as "combined formulations" and those are the target. The damping matrix is included here just for completeness as most of the FE packages do not incorporate damping in the solution.

[5] Subscript S is used to denote series form.

Before going further, it has to be remembered that the high-frequency residual terms are the contributions of the modes above the measured frequency range. Therefore, they can be calculated by subtracting from the total response the response relative to the measured frequency range (i.e. the low modes). When both physical and low modal parameter matrices of the structure are available, following the above definition, equation (4.15) can be re-formulated without loss of generality, as:

$$[R(\omega)] = \left([K] - \omega^2[M] + i[D]\right)^{-1} - \left([\phi^l]\left[\lambda_l^2 - \omega^2\right]^{-1}[\phi^l]^T\right) \tag{4.20}$$

Residual terms calculated in this way are very expensive computationally, since the first term on the RHS of equation (4.20) involves the inversion of a normally big matrix (the result of which is called the dynamic flexibility matrix) at every single frequency point. It cannot be used with a CMS formulation as it is frequency-dependent. When it is used with FRF coupling formulation, there is no need anymore for the residual terms if all data are obtained from FE analysis, since the frequency-dependent dynamic flexibility matrix already provides the correct FRF curves. When the modal data are obtained from experimental modal analysis, the residual curves obtained using (4.20) have to be adjusted using least-squares approach. This procedure is necessary because of inconsistencies between the FE model and the experimental model. The same type of procedure is also recommended in section 4.6.4.(e), as will be mentioned.

The only advantage of the above formulation is that all necessary residual terms can be calculated at once. On the other hand, if only a few terms are needed, this advantage becomes a disadvantage in that the first term on the RHS still has to be solved "fully" (or almost fully[6]) in any case. There are some more efficient formulations having this mentioned advantage, without too many disadvantages, and those are introduced in the following sub-sections. Therefore, the above formulation will not be discussed further.

4.6.3.(b) COMBINED STATIC RESIDUAL FORMULATION

One way of making the above formulation more efficient is to calculate the residual matrix at a single frequency value. Initially, the static residual formulation will be considered, extending later to the more general series formulation. Several authors have used the static residual presented in this section, [30, 80, 128]. When no damping is considered (normally the case for FE analysis), equation (4.20) can be re-written for the static residual as:

---

[6] Depending on the algorithm used, only the columns associated to the necessary FRFs need to be included to obtain the matrix inversion, although the other dimension is complete.

$$[R_0] = [K]^{-1} - [\phi^l][\lambda_l^2]^{-1}[\phi^l]^T \tag{4.21}$$

Equation (4.21) has one disadvantage when compared with equation (4.16) and that is for free-free structures. In such cases, the stiffness matrix is singular and therefore cannot be inverted. Also, the second term on the RHS of equation (4.21) is indeterminate at the rigid-body frequencies. Therefore, equation (4.21) cannot be used in this simple form.

The rigid-body mode problem can be solved by considering only the elastic modes for the residual terms. This is supported by the fact that rigid-body modes do not really contribute to the high-frequency residual terms and, consequently, can be eliminated from the formulation. Their significance is confined to the low-frequency residual terms. Therefore, it is important to stress that these modes have to be present in the regenerated FRF curves where the static residual terms are going to be used. Following the above argument, instead of using the flexibility matrix represented by the first term of the RHS of equation (4.21), the concept of elastic flexibility matrix is introduced [30]. Then, the static residual matrix can be calculated assuming a knowledge of the mass, as well as the stiffness and the rigid-body mode-shape matrices of the system, as will be explained next.

First, in order to be able to invert the stiffness matrix, the same number of rigid-body modes present in the structure have to be eliminated from this matrix. Then, the remaining stiffness matrix (referred to here as $[K_e]$) is inverted and the result augmented by zeros at the rigid-body eliminated coordinates. Which coordinates are eliminated in the stiffness matrix is not important, as long as the system is made statically determinate. The constrained flexibility matrix can be expressed for the case when the last rows are eliminated as:

$$[G] = \left[\begin{array}{c|c} K_e^{-1} & 0 \\ \hline 0 & 0 \end{array}\right] \tag{4.22}$$

Assuming a mass-normalised rigid-body mode-shape matrix $[\phi^r]$, a transformation matrix [P] used to filter the effects of these rigid-modes can be introduced as follows:

$$[P] = [I] - [M][\phi^r][\phi^r]^T \tag{4.23}$$

So, using the above equations, one can re-write equation (4.21) for the general case of either restrained or unrestrained structures as:

$$[R_0] = [P]^T[G][P] - [\phi^{el}][\lambda_{el}^2]^{-1}[\phi^{el}]^T \tag{4.24}$$

Subscript l denotes low-frequency, whereas e denotes elastic (or flexible) modes. The first term on the RHS of equation (4.24) is the elastic flexibility matrix mentioned previously. It is easy to see, following the derivation, that for the case of restrained structure, [P] = [I] and [G] = $[K]^{-1}$. Therefore, equations (4.24) and (4.21) are equivalent in this case. This general formula will be considered from now on. All the criticism made for the analytical static residual terms apply here as well, including those made to their use in FRF coupling or CMS formulations.

4.6.3.(c) COMBINED RESIDUAL MATRIX IN SERIES FORM

As for the analytical formulations, residual terms are better represented in series form than by static terms. References [74],[21],[81] and [111] used such an approach. Undamped case will be assumed here again. Basically, one has to get a series expansion for the two terms on the RHS of equation (4.20), in a fashion similar to the one presented for equation (4.18). The first term in (4.20) can be expressed in recursive form (considering the general formulation) as:

$$\left(K-\omega^2 M\right)^{-1}=\left([P]^T[G][P]\right)\sum_{p=0}^{\infty}\left(\omega^2[M][P]^T[G][P]\right) \tag{4.25}$$

The second term can be represented (also considering the general formulation) as:

$$\begin{aligned}&[\phi^{el}]\left[\left(\lambda_{el}^2-\omega^2\right)\right]^{-1}[\phi^{el}]^T=[\phi^{el}][\lambda_{el}^2]^{-1}[\phi^{el}]^T+\omega^2[\phi^{el}][\lambda_{el}^2]^{-2}[\phi^{el}]^T+\cdots\\&+\omega^4[\phi^{el}][\lambda_{el}^2]^{-3}[\phi^{el}]^T+\cdots\end{aligned} \tag{4.26}$$

Substituting equations (4.25) and (4.26) into the RHS of (4.20), and grouping the appropriate terms, yields:

$$\begin{aligned}&[R_S(\omega)]=\left([P]^T[G][P]-[\phi^{el}][\lambda_{el}^2]^{-1}[\phi^{el}]^T\right)+\cdots\\&\cdots\omega^2\left([P]^T[G][P][M][P]^T[G][P]-[\phi^{el}][\lambda_{el}^2]^{-2}[\phi^{el}]^T\right)+\cdots\\&\cdots\omega^4\left([P]^T[G][P]\left([M][P]^T[G][P]\right)^2-[\phi^{el}][\lambda_{el}^2]^{-3}[\phi^{el}]^T\right)+\cdots\end{aligned} \tag{4.27}$$

The first term in this series was shown in the previous section to be the static residual formulation (defined by equation (4.24)). The other terms are the dynamic improvements over that, provided by the inclusion of the inertia terms. However, this is not the simplest formula to calculate the high-frequency residual matrix in series form. One could calculate the static residual matrix first and take advantage of that. Then, equation (4.27) could be re-written as:

$$[R_S(\omega)]=[R_0]+\omega^2[R_0][M][R_0]+\omega^4[R_0][M][R_0][M][R_0]+\cdots \tag{4.28}$$

or, simplifying the notation (in a fashion similar to equation (4.25)), as:

$$[R_S(\omega)] = [R_0]\sum_{p=0}^{\infty}(\omega^2[M][R_0]) \tag{4.29}$$

The easiest way of proving that equation (4.28) is correct is by substituting equation (4.16) into it to obtain, as a result, equation (4.18). This last equation is the equivalent of equation (4.27) for the analytical case. Following the argument made for the analytical formulation, the series can be truncated after the second term, and that results in equation (4.19). However, matrix $[R_0]$ is now defined by equation (4.24), with matrix $[R1_0]$ defined as follows:

$$[R1_0] = [R_0][M][R_0] \tag{4.30}$$

These two matrices are the ones necessary for the second-order CMS formulation. For the first-order formulation, only equation (4.24) is used. Any of the series formulations above can be used with FRF coupling formulations.

4.6.3.(d) MASS-RESIDUAL APPROACH

Looking at equation (4.14) again, it is seen that the residual terms' contribution differs for each FRF curve only for the mode-shapes used in the calculation. This is because mode-shapes are local parameters, while natural frequencies and damping factors are global parameters. That is, the latter are related only to the mode number in question while the former are related to the coordinate numbers involved as well. Based on this observation, it was decided to try a different approach to the high-frequency residual terms. The basic idea behind it was to see what would happen if, instead of calculating the residual terms using all parameters, only the local parameters were included. Before showing that, however, equation (4.14) will be re-defined assuming the high-frequency residual as the difference between the total and the low-frequency response. The new approach was based on that form. Equation (4.14) is expressed for this case as:

$$R_{ij}(\omega) = \sum_{r=1}^{N}\frac{\phi_{ir}\phi_{jr}}{\lambda_r^2-\omega^2} - \sum_{r=1}^{m}\frac{\phi_{ir}\phi_{jr}}{\lambda_r^2-\omega^2} \tag{4.3 1}$$

Assuming only the local parameters, equation (4.3 1) can be written as:

$$R_{ij}^{M} = \sum_{r=1}^{N}\phi_{ir}\phi_{jr} - \sum_{r=1}^{m}\phi_{ir}\phi_{jr} \tag{4.32}$$

or in matrix notation as:

$$[R^M] = [\phi][\phi]^T - [\phi^l][\phi^l]^T \tag{4.33}$$

Superscript M is used to represent the modified residual terms. It should be noticed that the new formulation is no longer a function of frequency. This difference will be solved afterwards. One important point in the formulation is to assume mass-normalised mode-shapes, i.e.:

$$[\phi]^T[M][\phi] = [I] \tag{4.34}$$

When this is the case, the following equation can be derived:

$$[M]^{-1} = [\phi][\phi]^T \tag{4.35}$$

Equation (4.35) represents exactly the first term on the RHS of equation (4.33) although it cannot be used for the second term because it is singular when the number of modes is smaller than the number of coordinates. The maximum rank for this case will be the number of modes available. However, only the first term in equation (4.33) is unknown from a practical point of view and this is when equation (4.35) is used. Substituting equation (4.35) into (4.33), yields:

$$[R^M] = [M]^{-1} - [\phi^l][\phi^l] \tag{4.36}$$

Apart from the basic concept of this new approach, that it does not include global parameters, it is interesting to note the following when one compares equation (4.36) with (4.21): the residual matrix, instead of being related to the stiffness matrix, now becomes related to the mass matrix. This observation appears to contradict the concept of high-frequency residual terms as they have a stiffness-like effect within the frequency range of interest. It is the low-frequency residual terms that have a mass-like effect. However, the results obtained by equation (4.36) are not yet the final results. In order to agree with the correct values, the global parameters have to be included for the new high-frequency residual terms, somehow. What is done follows the same sort of approach as that which will be shown in section 4.6.4.(d). The missing global parameters are included as a chosen, constant, high-frequency pseudo-mass mode[7], evaluated over the entire frequency range of interest. This is when the frequency-dependency of the residual terms is actually taken into account. Furthermore, by doing that, one brings the residual values from the units of l/m to l/k, as they should be. Reformulating either equation (4.33) or (4.36) to include this correction factor, yields:

$$[R^M(\omega)] = \frac{1}{\lambda_{HF}^2 - \omega^2}[R^M] \tag{4.37}$$

[7] The name high-frequency pseudo-mass mode was chosen to differ from the other pseudo-mode values used in the experimentally-based formulations.

Following some case studies, it was concluded that a good estimation for the high-frequency pseudo-mass mode (λ^2_{HF}) would be to take 1.5 to 2 times the value of the last natural frequency in the range of interest. The interesting point about this is that those are exactly the values currently been used to extend the measured range in order to compensate for the residual terms within the range of interest. However, there is a more automatic way of calculating this value, although this requires the correct response for one particular FRF.

In section 4.5.3, it was stated that, the smaller the mass, the bigger the residual effect. Besides, this relationship was only valid for point FRFs. Therefore, in order to find the high-frequency pseudo-mass mode, the best option is to use the FRF related to that coordinate. One can re-write equation (4.37) in its expanded form for this coordinate as:

$$H^C_{ii}(\omega) - H^R_{ii}(\omega) = \frac{\left(M^{-1} - \phi\phi^T\right)_{ii}}{\lambda^2_{HF} - \omega^2} \tag{4.38}$$

So, in order to find the required term, the following equation can be used:

$$\lambda^2_{HF} = \frac{\left(M^{-1} - \phi\phi^T\right)_{ii}}{H^C_{ii\,(\omega=0)} - H^R_{ii\,(\omega=0)}} \tag{4.39}$$

To approximate the value of the static residual term, equation (4.39) was evaluated at 0 Hz. The advantage of this formula, however, compared with the static residual formulation, is that the residual value can be evaluated over the entire frequency range. Therefore, it improves the regenerated FRF curves much more than for the static residual, without the need of using residual series. The choice of the high-frequency pseudo-mass mode is of vital importance for a correct residual compensation and should be carefully examined. Its value should always be above the last frequency in the range of interest to approximate the high-frequency residual terms and this fact should be controlled. When equation (4.39) does not provide such frequency, a different frequency point should be considered, instead of 0 Hz[8].

There are some other advantages the author sees in calculating the residual terms using the new approach. Although this is still limited to the case where a mass matrix is available, this matrix is easier to confirm experimentally to be correct or not (i.e. weighing the structure and checking if the FE model produces the same weight). Besides, the mass matrix is always positive-definite and therefore, possesses an inverse no matter the structure is restrained or not (the only exception is when shell elements are used in the analysis and the elements associated with θz

[8] Why equation (4.39) may fail at 0 Hz is given on page 217.

coordinate are all zero). What is not certain yet, is how good an experimentally-derived mass matrix would be for the above residual compensation, as experimental problems may jeopardise the quality of the approximation. The proposed mass-residual approach could be used for both FRF coupling and CMS formulations, where in the latter case, as before, one single frequency value has to be used.

4.6.4 EXPERIMENTALLY-BASED FORMULATIONS

4.6.4.(a) REMARKS

The combined residual formulations presented previously, while more realistic than the analytical formulations, still have a shortcoming from the experimental point of view: the physical matrices of the system are not available in the latter case. However, if the FRFs are measured, the necessary residual terms can be calculated in exactly the same way as presented there, substituting the correct response expressed by the first term on the RHS of the residual equations by the measured curves. These curves are the complete ones, since the effects of all the modes are present. The second term in these equations can be calculated by obtaining the necessary modal parameters through parameter extraction techniques [41,86]. All experimentally-based formulations are established on this principle. However, they start from different approaches and some are more efficient than others. A flow-chart of these formulations is given in Figure 4.4 to illustrate the possible options.

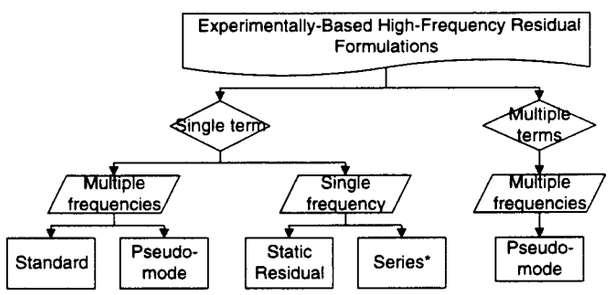

Figure 4.4 - Flow-chart of the experimentally-based residual formulations

4.6.4.(b) STANDARD FREQUENCY-DEPENDENT FORMULATION

The measured FRFs are normally single terms in the matrix. Consequently, the residual formulations obtained from experimental data are generally individual terms as well. If the regenerated curve is subtracted from the complete one, the difference is the contribution of the modes outside the measured range, that is, the residual curve [71]. This statement can be formulated as:

$$R_{ij}(\omega) = H_{ij}^{C}(\omega) - \sum_{r=1}^{m} \frac{\phi_{ir}\phi_{jr}}{\omega_r^2 - \omega^2 + i\omega_r^2\eta_r} \tag{4.40}$$

As the last term of equation (4.40) represents the regenerated FRF curve, the same notation as introduced in chapter 3 (equation (3.49) repeated below) could be used here:

$$R_{ij}(\omega) = H_{ij}^{C}(\omega) - H_{ij}^{R}(\omega) \tag{4.41}$$

The residual curve obtained using either one of the above equations requires a least-squares approach to minimise the noise effects which are normally incorporated in the measurements. Also, by doing that, the best estimation for the residual value is obtained. In the least-squares approach, when solving for the high-frequency residual term, one should consider frequency points close to the upper end of the residual curve for a better estimation. The major advantage of this formulation is that, once the residual term is added to the regenerated curve, the correct curve obtained from this process is smoothed. It is ideal for using with FRF coupling formulations, as it corrects the FRFs over the entire frequency range. However, in this case, the modal parameters used in the regenerated curves have to be consistent (i.e. obtained from a single column (or row) of measured FRFs). Otherwise, numerical problems may occur around the resonances of **the** sub-systems in the coupling process (refer to chapter 2). Using a consistent modal data set, on the other hand, may lead to some difficulties in the least-squares approach. This is caused by some strong peaks around resonance values in the residual curve, as a result of the averaging process to obtain the natural frequencies. From the author's point of view, although this formulation is the most widely used experimentally, the series form proposed in this thesis would be a better option due to the above problems. Going to CMS formulations, equation (4.41) cannot be used for the same reason as previously that this equation is frequency dependent. For that, the following static residual formulation can be applied.

4.6.4.(c) EXPERIMENTAL STATIC RESIDUAL FORMULATION

The experimental static residual terms can be calculated, as before, by considering equation (4.41) estimated at 0 Hz. However, it may be difficult to obtain this term experimentally at that frequency, especially for free-free structures (more common situation). So, what can be done is to compute it not at 0 Hz but at a value close to that limit. Another way would be to calculate it considering the previous formulation and to extrapolate the result of the least-squares approach to 0 Hz. This latter procedure will increase the calculation effort required and the earlier option may be better. The experimental static residual can be defined as:

$$R_{ij}(\omega_{pu}) = H_{ij}^{C}(\omega_{pu}) - H_{ij}^{R}(\omega_{pu}) \tag{4.42}$$

Subscript *pu* was introduced to represent the frequency point where the static residual formulation is evaluated experimentally, since in this case it may be a different point to that at 0 Hz. The high-frequency residual terms become asymptotic to a flat line towards the very low-frequency range and the above argument is justified by that. The same approach could also be used for the analytical or combined static residual formulations. However, there is no problem at 0 Hz frequency there, unless for the combined formulation with rigid-body modes (solved by the use of the elastic flexibility matrix). The above formulation could be employed for both FRF coupling and CMS formulations. In the latter case, the terms have to be assembled in matrix form, although calculated individually.

4.6.4.(d) EXPERIMENTAL RESIDUAL TERMS IN SERIES FORM

As already mentioned several times, an improvement over the static residual formulation is necessary for FRF curves with high modal density. From experiments, neither the high-frequency out-of-range modes nor the mass matrix are available and, therefore, the previous formulations cannot be used. However, there is a way of obtaining that improvement without knowledge of the mass matrix for the system. This approach was introduced in chapter 3 (IECMS formulation) and will be developed further here. Basically, extra terms need to be added to the regenerated FRF curves in order to obtain the correct FRFs. This procedure can be expressed as:

$$H_{ij}^{C}(\omega) = H_{ij}^{R}(\omega) + R_{ij}(\omega_{pu}) + \omega^2 R1_{ij}(\omega_{pu_h}) + \omega^4 R2_{ij}(\omega_{pu_{h2}}) + \cdots \tag{4.43}$$

The residual terms in equation (4.43) are evaluated sequentially by taking the difference between the correct and the previous compensated curve at different frequency points, as explained below. The reason why different frequency points have to be used was explained in the previous chapter and is related to the fact that, at the same frequency point, no residual effect is present. To understand the formulation, equation (4.43) will be re-written grouping each compensated curve using a different name as follows:

$$H_{ij}^{C}(\omega) = \frac{\underbrace{H_{ij}^{R}(\omega) + R_{ij}(\omega_{pu})}_{H_{ij}^{S}(\omega)} + \omega^2 R1_{ij}(\omega_{pu_h}) + \omega^4 R2_{ij}(\omega_{pu_{h2}}) + \cdots}{H_{ij}^{D}(\omega)} \Bigg/ H_{ij}^{D2}(\omega) \tag{4.44}$$

The static residual term is calculated as the difference between the correct and the regenerated FRF curves at a frequency point, *pu*, as expressed by equation (4.42). When this term is added

to the regenerated curve, the first two terms on the RHS of equation (4.43) can be grouped as the static FRF curve, as indicated by H_{ij}^{S} in equation (4.44). The other residual terms are obtained in a similar way as defined below':

$$R1_{ij}\left(\omega_{pu_h}\right) = \frac{H_{ij}^{C}\left(\omega_{pu_h}\right) - H_{ij}^{S}\left(\omega_{pu_h}\right)}{\left(\omega_{pu_h}\right)^2} \tag{4.45a}$$

$$R2_{ij}\left(\omega_{pu_{h2}}\right) = \frac{H_{ij}^{C}\left(\omega_{pu_{h2}}\right) - H_{ij}^{D}\left(\omega_{pu_{h2}}\right)}{\left(\omega_{pu_{h2}}\right)^4} \tag{4.45b}$$

$R1$ and R2 are the first- and second-order dynamic residual terms and this is the reason why when these terms are added to the previous curve, their superscript is represented by a letter D.

However, instead of using equation (4.43), a much simpler formulation can be employed and this is based on a high-frequency pseudo-eigenvalue calculated to monitor the choice of the frequency point used for the first-order dynamic residual term. As highlighted in chapter 3, this point has to be chosen such that the pseudo-eigenvalue is beyond the last frequency of interest. This simplified formulation can be represented as:

$$H_{ij}^{C}(\omega) = H_{ij}^{R}(\omega) + R_{ij}\left(\omega_{pu}\right) + \omega^2 \frac{R_{ij}\left(\omega_{pu}\right)}{\lambda_{hp}^2} + \omega^4 \frac{R_{ij}\left(\omega_{pu}\right)}{\left(\lambda_{hp}^2\right)^2} + \cdots \tag{4.46}$$

The basis for the above formula can be understood by looking at each term of equation (4.18). It can be observed that each residual term there differs from the others by the power of the eigenvalue. Therefore, equation (4.46) has the same background as the mass-residual approach in that the missing high-frequency eigenvalues can be approximated by a constant single high-frequency pseudo-eigenvalue. The same pseudo-eigenvalue can be used for all terms (as shown) since the higher the term, the less influential is the residual effect. Besides, as stated previously, only the first two terms in the residual series would be enough for most practical structures. Then, only one high-frequency pseudo-eigenvalue will be needed anyway. By equating the third term on the RHS of each of equations (4.43) and (4.46), the necessary high-frequency pseudo-eigenvalue can be evaluated as expressed by equation (3.55) and repeated below:

$$\left(\lambda_{hp}^2\right)_{ij} = \frac{R_{ij}\left(\omega_{pu}\right)}{R1_{ij}\left(\omega_{pu_h}\right)} \tag{4.47}$$

The residual compensation described in this section is the ideal one for use in CMS formulations to improve the accuracy when compared with the static residual formulation. It can be equally used in FRF coupling formulations. It is, in a sense, much better and quicker than the standard residual formulation and yields very accurate results. Its only shortcoming is that every required residual term has to be calculated individually.

4.6.4.(e) HIGH-FREQUENCY PSEUDO-MODE FORMULATION

As just noted, the way the residual terms are calculated from experiments requires each residual term to be calculated individually. If the column (or row) of measured FRFs involves a large number of elements, this is a tedious and time-consuming process. The best thing to do in this case is try to find all the terms in one go. This can be done using a sort of least-squares approach, as explained next, where a high-frequency pseudo-mode based on this measured column (or row) is calculated. The major reason why the author tried this approach, however, was not to save time in calculating the column (or row) of residual terms, but it was thought at the beginning that this pseudo-mode approach could be used as well for the unmeasured columns (or rows) of FRFs in order to compensate for the high-frequency residual terms there. Some comments about that will be made at the end of this section.

The principle behind the pseudo-mode idea is to calculate an extra mode (pseudo-mode) to be incorporated in the modal solution. If the contribution of all out-of-range modes is going to be represented by a single pseudo-mode, this contribution can be represented for a certain frequency point ω_k as:

$$H_{ij}^{C}(\omega_k) - H_{ij}^{R}(\omega_k) = \frac{A_{ij}^{pm}}{\left(\lambda_{pm}^2 - \omega_k^2\right)} \tag{4.48}$$

where the modal constant (A_{ii}^{pm}) and the natural frequency (λ_{pm}^2) can be either complex or real to accommodate or to ignore damping. As mentioned in section 4.5.2, it is known that the residual terms are normally bigger for point FRFs than for transfer FRFs. Thus, the modal parameters of the pseudo-mode are going to be found first for the point FRF curve and then they are made constant in order to find the mode-shape of the other points. The formulation can be seen below, step by step. It should be stressed that the regenerated curves include ail the low-frequency modes.

First, one needs to calculate the difference between the correct and the regenerated point FRF curves at a certain number of frequency points, ω_k, chosen to be used in the least-squares calculation:

$$\Delta H_{ii}^{\omega_k} = H_{ii}^{C}(\omega_k) - H_{ii}^{R}(\omega_k) \qquad k=1, 2, \ldots \tag{4.49}$$

Substituting equation (4.49) into (4.48), one obtains for a single frequency point, ω_k:

$$A_{ii}^{pm} = \Delta H_{ii}^{\omega_k}(\lambda_{pm}^2 - \omega_k^2) \tag{4.50}$$

When this difference is calculated for a number of frequency points, ***kl*** to ***kk,*** the natural frequency (λ_{pm}^2) and the modal constant (A_{ii}^{pm}) for this pseudo-mode at the point measurement can be calculated more accurately using a least-squares fit, as follows:

$$\begin{bmatrix} \Delta H_{ii}^{\omega_{k1}} & -1 \\ \Delta H_{ii}^{\omega_{k2}} & -1 \\ \vdots & \vdots \\ \Delta H_{ii}^{\omega_{kk}} & -1 \end{bmatrix}_{kx2} \begin{Bmatrix} \lambda_{pm}^2 \\ A_{ii}^{pm} \end{Bmatrix}_{2x1} = \begin{Bmatrix} \left(\Delta H_{ii}^{\omega_{k1}}\right)\left(\omega_{k1}^2\right) \\ \left(\Delta H_{ii}^{\omega_{k2}}\right)\left(\omega_{k2}^2\right) \\ \vdots \\ \left(\Delta H_{ii}^{\omega_{kk}}\right)\left(\omega_{kk}^2\right) \end{Bmatrix}_{kx1} \tag{4.5 1}$$

where: $A_{ii}^{pm} = \left(\phi_i^{pm}\right)^2$ (4.52)

The pseudo-mode shape amplitude at the measurement point can then be calculated, as shown in equation (4.52), by taking the square-root of the modal constant found through equation (4.51). Using this value, and the value of λ_{pm}^2 found, one can calculate the mode-shape amplitudes of the other points from:

$$\phi_i^{pm}\phi_j^{pm} = A_{ij}^{pm} = \Delta H_{ij}^{\omega_k}\left(\lambda_{pm}^2 - \omega_k^2\right) \tag{4.53}$$

When the same frequency points *kl* to ***kk*** (as above) are used, following equation (4.53), the mode-shape amplitudes of the other points can be calculated using the same sort of least-squares fit from (where superscript ***pm*** was dropped from the equation):

$$\begin{vmatrix} \phi_i & 0 & \cdots & 0 \\ \vdots & \ddots & \vdots & \vdots \\ \phi_i & 0 & \cdots & 0 \\ 0 & \phi_i & \cdots & 0 \\ \vdots & \vdots & \ddots & \vdots \\ 0 & \phi_i & \cdots & 0 \\ \vdots & \vdots & \ddots & \vdots \\ 0 & 0 & \cdots & \phi_i \\ \vdots & \vdots & \ddots & \vdots \\ 0 & 0 & \cdots & \phi_i \end{vmatrix}_{kNxN} \begin{Bmatrix} \phi_i \\ \phi_j \\ \vdots \\ \phi_N \end{Bmatrix}_{Nx1} = \begin{vmatrix} \left(\Delta H_{ii}^{\omega_{k1}}\right)\left(\lambda_{pm}^2 - \omega_{k1}^2\right) \\ \left(\Delta H_{ii}^{\omega_{kk}}\right)\left(\lambda_{pm}^2 - \omega_{kk}^2\right) \\ \left(\Delta H_{ij}^{\omega_{k1}}\right)\left(\lambda_{pm}^2 - \omega_{k1}^2\right) \\ \left(\Delta H_{ij}^{\omega_{kk}}\right)\left(\lambda_{pm}^2 - \omega_{kk}^2\right) \\ \left(\Delta H_{iN}^{\omega_{k1}}\right)\left(\lambda_{pm}^2 - \omega_{k1}^2\right) \\ \left(\Delta H_{iN}^{\omega_{kk}}\right)\left(\lambda_{pm}^2 - \omega_{kk}^2\right) \end{vmatrix}_{kNx1} \tag{4.54}$$

The first vector in equation (4.54) is the pseudo-mode shape of the system and it is included after its measured mode shapes in order to improve the regenerated FRF curves.

Some points can be made about the way the above derivation should be used. Although it is not the real purpose of the technique, when deriving the pseudo-mode shape for the other coordinates in the system (equation (4.54)), one could perfectly use only a certain number of coordinates. Then, the pseudo-mode shape amplitudes at the other coordinates are set to zero. The pseudo-mode shape found in this way will be the best for that particular set of coordinates used.

Another very important point to make is that the choice of the frequency points used in the above pseudo-mode approach is important, as these will affect significantly the quality of the results. It has to be remembered that the pseudo-mode is sought to compensate for the lack of the high-frequency residual terms. The parts of the regenerated curves normally most affected by the lack of residual terms are near anti-resonances. Nevertheless, the high-frequency residual terms are generally not constant within the whole frequency range of interest and their levels are higher towards the end of this range. Consequently, they tend to have higher influence in that region. Therefore, the best choice of points to be used for the high-frequency residual are ones close to the upper frequency of interest. In some of the test cases tried, depending on the choice of the frequency points, the pseudo-mode frequency found was sometimes inside the measured frequency range. This is wrong, as the pseudo-mode is intended to represent the effect of the modes outside the measured frequency range, and so it should never be inside this range. Otherwise, either a spurious peak would occur or the pseudo-mode would coincide with one of the natural frequencies of the system providing, consequently, no residual compensation. Examples of that will be given in section 4.7.

A third important point to make concerns the type of FRF used in the derivation. The formulation, as derived here, used the receptance FRF (i.e. displacement/force [41]). However, any other type could be used, as long as care is taken to account for that. Any type of FRF has to produce the same results. However, the author believes that the easiest one to program is really receptance. From that, the other types of curves can be derived after the pseudo-mode has been found.

The last point to be mentioned is about the quality of the modal parameters calculated within the measured frequency range. These have to be as accurate as possible, so that the only errors in the regenerated FRFs will be the residual effects to be compensated by the given approach.

Although the pseudo-mode approach proved to work quite well in order to compensate for the high-frequency residual terms for the measured FRFs used during the calculation, it is of relatively little use for other columns (i.e. for the unmeasured FRFs). Even if it manages to improve the regenerated FRFs for the unmeasured column, it will not be good enough to bring the curve to what should be the "measured" one.

For this approach to be applied to CMS formulations, equation (4.48) has to be calculated at 0 Hz, although it is not the most efficient formula to use. However, it can be easily employed in FRF coupling, with the same advantage as before in that the FRFs will be compensated over the entire frequency range. Normally, the FRFs involved in the coupling process include more than one column. To keep the consistency in the natural frequencies, the same modal data set has to be used to regenerate the FRFs, as mentioned with the standard experimental approach.

4.6.4.(f) HIGH-FREQUENCY PSEUDO-MODE SINGLE-TERM FORMULATION

The previous formulation was inspired by the approach used in the software MODENT [86] for modal analysis. This approach is used in its SDOF modal parameter extraction techniques. Being used in SDOF formulations, the residual terms are calculated for each FRF separately (therefore the reason for the name "single-term formulation" used here). In [86], both low- and high-frequency residual terms have to be calculated due to the system of equations to be solved, even if all the modes are included in the low-frequency range. This formulation will be explained first and an extrapolation to the case when only high-frequency residual terms are required will be introduced afterwards.

The residual terms are calculated as two extra modal constants to be included in the modal constant table (later to be collated as pseudo-mode shapes). For that, a set of two equations and two unknowns is solved. Each equation is similar to the one shown in equation (4.48), where an additional term relative to the low-frequency residual is added on the RHS. The user specifies the frequency values where he/she wants the residual terms to be calculated and the values for the natural frequencies of the pseudo-modes. The latter have to be values well below and above the frequency range of interest. So, the only unknowns to be solved for are the pseudo modal constants. As the formulation is solved for two frequency points only, it is very sensitive to the choice of these points. The best options are frequency points corresponding to strong anti-resonances of the correct FRFs.

The same formulation expressed in equation (4.48) can be used for the case when only high-frequency residual terms are needed. However, now the natural frequency of the pseudo-mode

is specified by the user, leaving only its modal constant as an unknown (as in the above case). Subscript *hf* is used to stress that the frequency point has to be chosen inside the frequency range of interest, whereas ***HF*** is outside this range. This is represented below:

$$H_{ij}^{C}(\omega_{hf}) - H_{ij}^{R}(\omega_{hf}) = \frac{A_{ij}^{pm}}{\left(\lambda_{HF}^{2} - \omega_{hf}^{2}\right)} \tag{4.55}$$

Once the pseudo modal constants are found, they are incorporated into the mode shape matrix in exactly the same way as the other modal constants (i.e. using equations (4.52) and (4.53)). The comment made previously is even stronger for the above formulation, i.e. the choice of the frequency point *hf* is of vital importance for a correct residual compensation. Therefore, the same suggestion needs to be followed. This formulation is less efficient than the one proposed by the author for the simple reason that it is a single-term formulation and thus very dependent on a single frequency point. All the other remarks made for the author's approach are equally valid here, including its applicability in FRF coupling and CMS formulations.

4.7. EXAMPLES

In this section, some examples are presented to illustrate the comments made about both the trends in the residual terms (section 4.5) and the high-frequency residual terms' formulations (section 4.6). For that, the 9 DOF mass-and-spring system (system A) and the 1203A structure used in chapter 2 will be employed again (Figures 2.3 and 2.15, respectively).

System A is used first and the same frequency range of interest used in the previous chapters is assumed again (i.e. from 0 to 200 Hz). That includes 3 modes, leaving 6 residual modes to be accounted for. In order to compare the residual trends at point and transfer FRFs, a single frequency point has to be investigated. Moreover, all residual terms have to be compared simultaneously at the same frequency. The best option for that is to use the static residual formulations (i.e. at 0 Hz). The one expressed by equation (4.16) was applied here, since all modes are available for this system. Either one of the other static residual formulations (i.e. combined or experimental at 0 Hz) would have produced exactly the same residual values, as no noise was assumed for the correct curves. Figure 4.5 shows the correct residual values in pictorial matrix form for system A, plotted considering the correct sign. It is clear that the diagonal terms are much bigger than the off-diagonal ones. Therefore, the comment made about the relative size of the residual terms at point and transfer FRFs can be confirmed. However, because of the oscillations in sign, it is a bit confusing to see the whole picture on this figure.

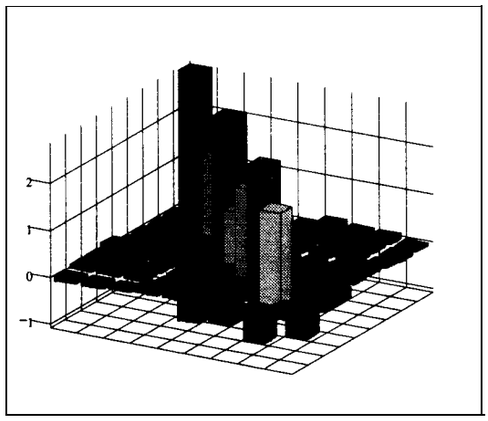

Figure 4.5 - Correct residual values for system A, i.e. considering all 6 out-of-range modes (3D matrix form)

Figure 4.6 shows the same results as before, now plotting the rows of the residual matrix in sequence. The arrows in this figure (and the subsequent one) indicate point FRF residual terms. As mentioned above, it can be seen that the point residual terms are bigger than the transfer ones, in general, although some transfer terms have bigger values than some point terms. This fact was highlighted in section 4.5.2 and can be better observed when all the residual terms are plotted as absolute values (Figure 4.7). There, it was quoted that when the out-of-range eigenvectors associated with a specific coordinate are small, the transfer residual terms may have bigger values than the point ones if the other related eigenvectors for the former are large. Figure 4.8 shows the mode-shape matrix for system A to aid understanding that. In this figure, each block represents a mode and the arrows indicate diagonal terms. Some of the coordinates have their biggest mode-shape contribution after the range of interest.

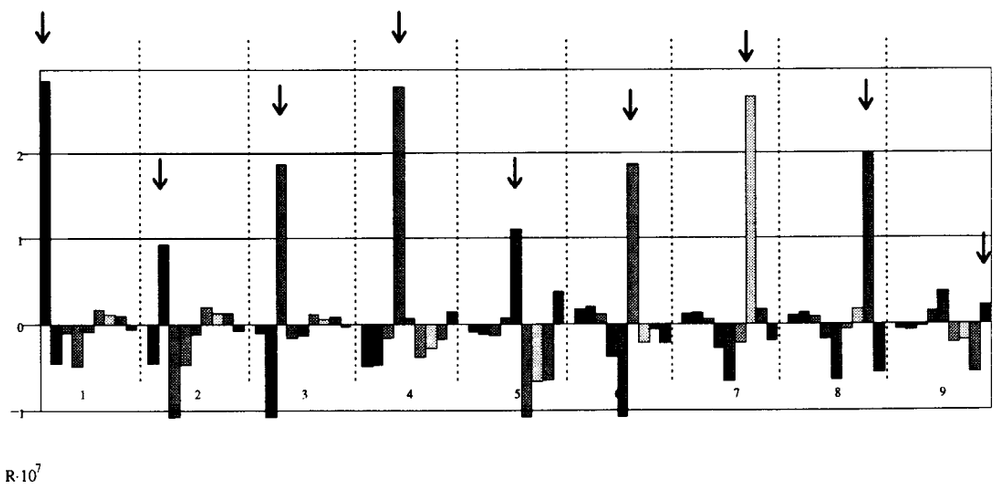

Figure 4.6 - Correct residual values for system A, i.e. considering all 6 out-of-range modes (rows side by side)

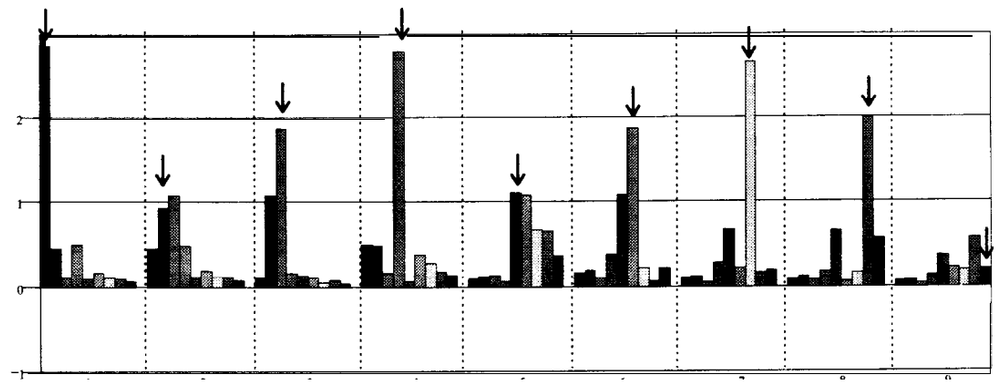

$\overrightarrow{[R]} \cdot 10^7$

Figure 4.7 - Correct absolute residual values for system A, i.e. considering all 6 out-of-range modes (rows side by side)

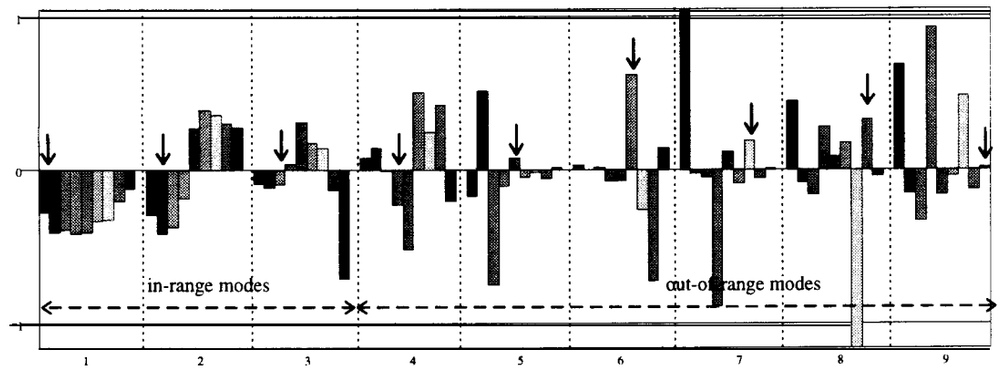

Φ

Figure 4.8 - Mode-shape matrix for system A (modes side by side)

The relationship between the mass of the system and the residual terms can also be seen by analysing the above figures. For this, the mass values associated with each coordinate, and given in Figure 2.3, have to be looked at in conjunction with the residual term matrix (for example, Figure 4.7). The smallest mass values for system **A** (i.e. 0.5 Kg) are linked with coordinates 1, 4 and 7. The biggest mass values (i.e. 1.5 Kg) are linked with coordinates 2, 5 and 9. When the residual values are checked against these mass values, it is observed that the former group of coordinates have the biggest residual values, whereas the latter group have the smallest. This confirms the statement made in section 4.5.3. It has to be stressed here, however, as may have been noticed, that this statement does not say that the same mass values produce the same residual term. The residual value will be affected by the adjacent masses as well and, therefore, the above remark should not be expected.

Before turning to examine another trend, one more point needs to be addressed: the comment made about transfer residual terms and the inclusion of more modes in the series. As mentioned, residual values for transfer FRFs may vary in sign. Therefore, the inclusion of one more mode may worsen the regeneration prediction instead of improving it and a clear example of that is given for $H_{4,8}$ in Figure 4.9. There it can be seen that including 3 or 4 residual modes more in the regenerated FRF produce quite a good approximation to the correct curve, as the residual value for these cases is close to zero. However, if one tries to improve that even more, by including one more mode (i.e. 5 residual modes), the prediction quickly deteriorates and only with the next residual modes also included is a good approximation to the correct FRF obtained (in this case, the correct one). The effect the inclusion of one more residual mode has on the FRF curves is presented in Figures 4.10 and 4.11. This result was split into two figures to allow a better visualisation of the results. It should be observed that there is a shift in the anti-resonance values due to the sign of the residual values.

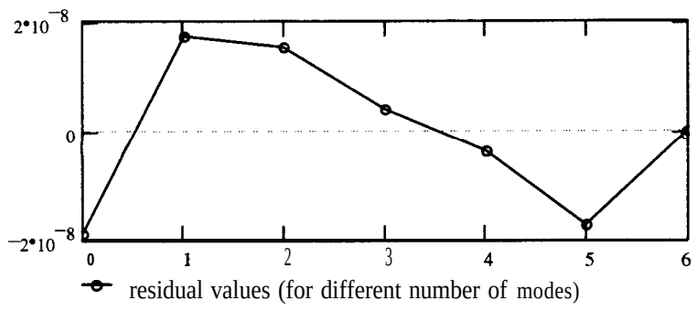

Figure 4.9 - $H_{4,8}$ residual values when including different number of residual modes in the series

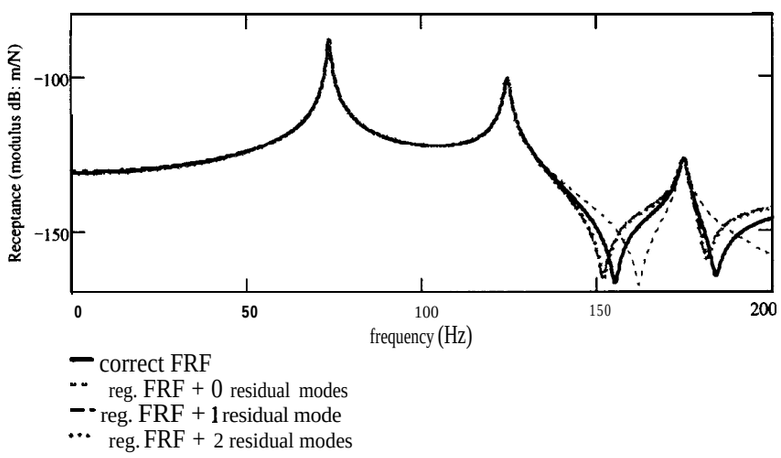

Figure 4.10 - $H_{4,8}$ curves for system A, including different number of residual modes (from 0 to 2)

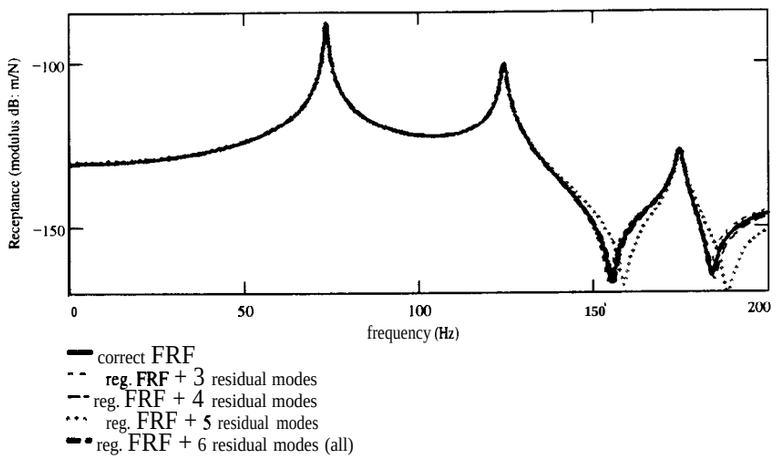

Figure 4.11 - $H_{4,8}$ curves for system A, including different number of residual modes (from 3 to all)

The last trend for the high-frequency residual terms cited in section 4.5 (i.e. their relative significance for translational and rotational FRFs) is investigated using the main frame of the 1203A structure only. This is because, in the frequency range of interest (from 0 to 800 Hz), only rigid-body modes appear for the struts. At the same time as looking at this trend, the approach to compensate for the high-frequency residual terms by extending the number of modes included within the frequency range of interest is analysed. Ninety modes (from 0 to 5142 Hz) were included to regenerate FRFs in a range of interest that contains only 21 modes (6 rigid-body modes + 15 flexible modes). In this case, the frequency range was extended to include over 4 times as many modes as those within the range of interest. In terms of frequency, the extended range means over 6 times the higher frequency limit. To show the trends stated in section 4.5.4, the results are split into three parts": (a) FRFs involving only TDOFs; (b) FRFs involving a mixture of TDOFs and RDOFs and (c) FRFs involving only RDOFs.

For the FRFs in group (a), in general, the residual terms had very little effect within the frequency range of interest and, consequently, the extended frequency range was enough (in the majority of the FRFs) to compensate for that effect (Figure 4.12). For the FRFs in group (b), although not a lot of curves were affected by the residual effects, when the residual terms did have an effect, the extension of the frequency range was enough (in the majority of the FRFs) to compensate for that effect (Figure 4.13). For the FRFs in group (c), many more curves were affected by the residual terms and now, the extension of the frequency range was no longer enough to compensate for the residual effect, although it did improve the FRF predictions when

[10] The notation TDOFs stands for translational DOFs; whereas RDOFs stands for rotational DOFs.

compared with the case with no compensation (Figure 4.14). Therefore, these figures illustrate the fact that extending the measured frequency range may not be a good approach to compensate for the residual effects when RDOFs are involved. This is the major reason why the FOREST technique [64] was not considered further for the present applications. As mentioned in section 4.5.4, and was intended to be demonstrated here, the residual effects for rotational/rotational FRFs were much bigger than those for translational/translational FRFs. The effects for translational/rotational (or rotational/translational FRFs, due to the symmetry) were somewhere in between, as expected.

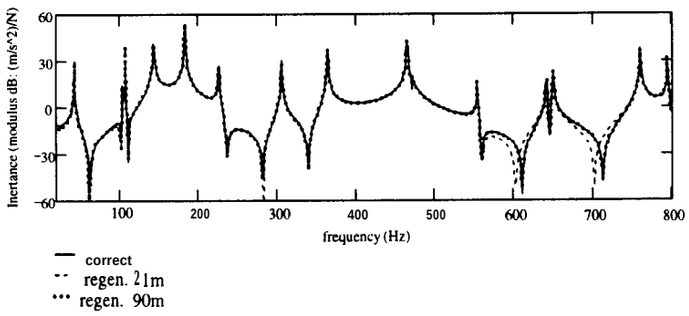

Figure 4.12 - Translational/Translational FRF curves ($H_{115z,115y}$) for the main frame of 1203A structure

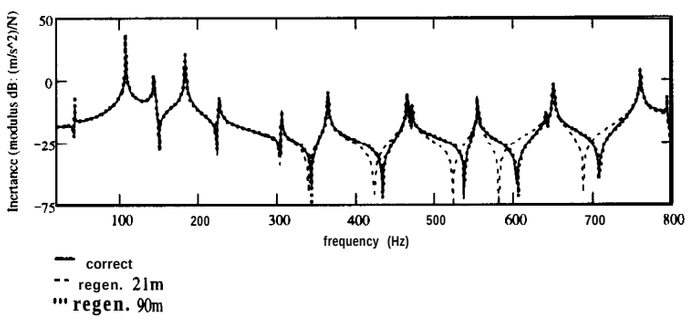

Figure 4.13 - Translational/Rotational FRF curves ($H_{46\theta x,46y}$) for the main frame of 1203A structure

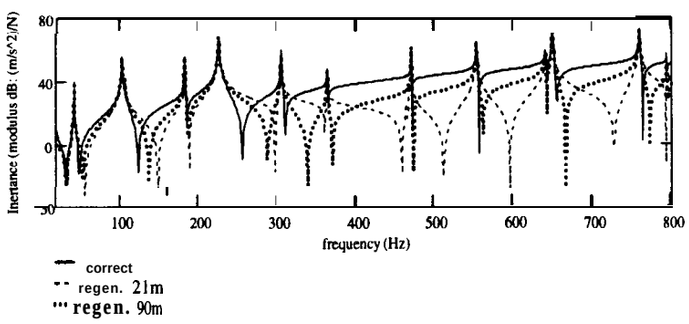

Figure 4.14 - Rotational/Rotational FRF curves ($H_{46\theta z,46\theta z}$) for the main frame of 1203A structure

Taking into consideration what was just demonstrated, other approaches should be analysed in order to compensate for the high-frequency out-of-range modes. Therefore, the formulations presented in section 4.6 are examined. All matching residual formulations introduced for the analytical or combined case should produce the same results. The choice between one or another is based only on the availability of the data. Provided no noise is present in the data, the same results should also be obtained for the experimental formulations. The exception would be for the experimental residual formulation in series form, as it is an approximation to circumvent the need for either the high-frequency out-of-range modes or the mass matrix of the system. However, noise is normally present in the measurements and the quality of the results may be jeopardised by that. The experimentally-based formulations are the ones considered here. Where pertinent, the analytical and combined formulations will be compared with the experimental one. The other formulation which will be analysed is the mass-residual approach, as this is only available for the combined case.

To compare the efficiency of each of the formulations, an FRF curve with strong residual effects should be considered. Moreover, a point FRF is better since, for such curve, there is an anti-resonance between each pair of resonance (transfer FRFs may have a minimum instead). As illustrated in section 4.5.1, anti-resonances (and low values) are more likely to suffer from residual effects. It was decided to use $H_{1,1}$ initially, with no noise incorporated, since this function has the biggest residual value (see Figure 4.6, for example). A more realistic case, with noise and inconsistencies in the modal data will be considered in chapter 6.

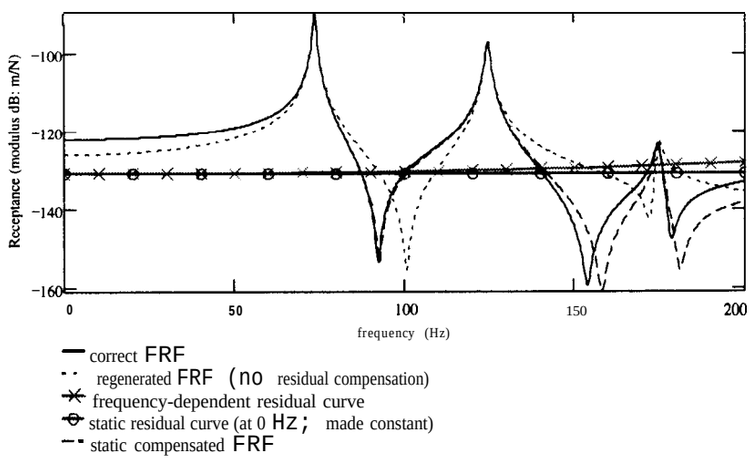

Figure 4.15 - $H_{1,1}$ for system A: correct, regenerated and static compensated FRF curves with correspondent residual curves

Figure 4.15 presents some results for $H_{1,1}$. The correct FRF curve is plotted first, followed by the regenerated curve without any residual compensation. It is clearly noticeable how different the two curves are. The discrepancy is caused by the lack of residual compensation. The frequency-dependent residual curve (calculated using equation (4.40)) is also plotted there to illustrate that. As quoted in section 4.5.1, residual effect causes a shift in the anti-resonances' position. Since no noise is present, no least-squares calculation had to be used to obtain a best estimate of the position of the residual curve. Therefore, where this curve intercepts the regenerated one (and the signs are opposite), should indicate the correct anti-resonance position. The same frequency-dependent residual curve would have been obtained using either the analytical or combined formulations (equations (4.14) or (4.20), respectively).

However, as stated in section 4.6, frequency-dependent residual terms cannot be used with CMS formulations and static residual terms are usually employed. To view the effect the static residual has over the frequency range it is trying to compensate, this term is also plotted in Figure 4.15. It is made constant over the entire frequency range of interest. Towards the upper end of the frequency range of interest, it is noticeable that there is a difference between the frequency-dependent residual curve and the static residual curve. When the static residual curve is added to the regenerated one, the thus-derived statically-compensated curve is obtained. Although the latter is an improvement over the former, the quality of this improvement decreases as the frequency increases. If this FRF curve were to be used with FRF coupling formulations, inaccurate predictions would be obtained towards the upper frequency range as a result.

To solve the problem just mentioned: that is, to improve the regenerated curve over the entire frequency range of interest, the series term expressed by equation (4.44) can be used. By adding extra terms to the regenerated curve the improvement gets better as one goes to higher frequencies. This fact can be clearly seen in Figure 4.16. The results plotted there were obtained by considering $pu = 1$ (i.e. at 0 Hz) and pu_h = 10% of the upper frequency of interest (i.e. at 20 Hz), as recommended in chapter 3. The choice of this last point was checked by equation (4.47), which resulted in a high-frequency value of 396.3 Hz (i.e. almost twice the upper frequency of interest), with damping equal 1%, as initially imposed. In this figure, each subsequent curve represents equation (4.44) truncated after the addition of one extra term. Stopping at the second-order residual compensation, i.e. first-order dynamic residual term (as suggested), succeeded in bringing the regenerated curve quite close to the correct one. However, this is linked with the position of minimum response for this curve and the direction of the improvement just mentioned (from the lower frequencies upwards). If the minimum

response were located more towards the upper frequency of interest, more terms would be necessary. Such a situation can be seen when plotting $H_{7,7}$ instead (Figure 4.17).

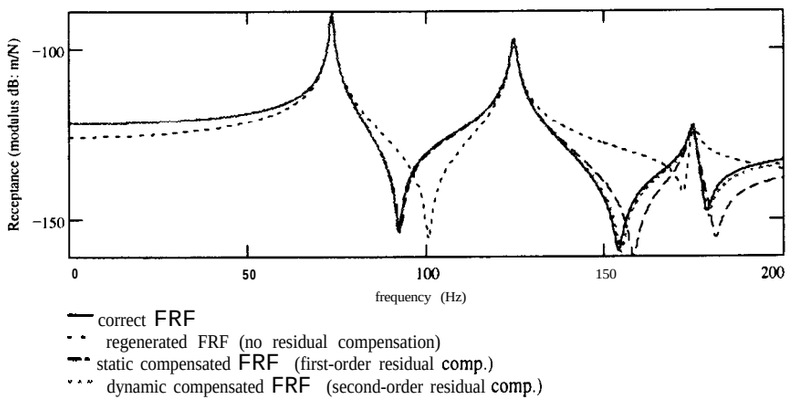

Figure 4.16 - $H_{1,1}$ for system A: correct and residual compensated FRFs in series form (different number of terms)

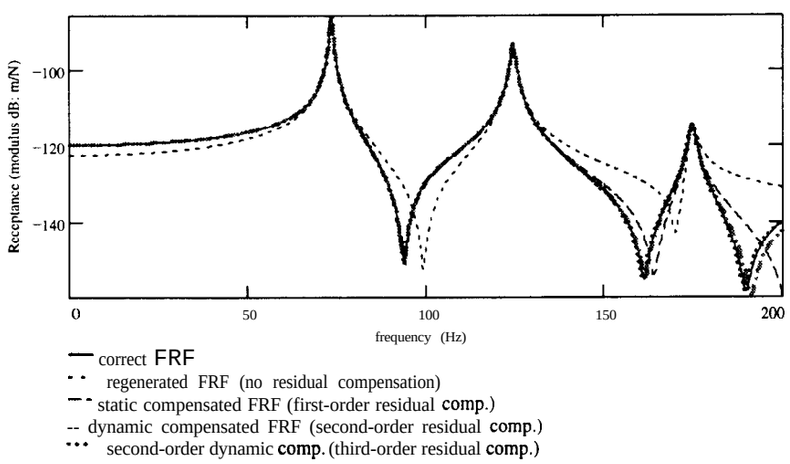

Figure 4.17 - $H_{7,7}$ curves for system A: correct and residual compensated in series form (different number of terms)

In Figure 4.17, one extra term in the residual series was included. However, this last term (the second-order dynamic residual) was calculated considering equation (4.46) instead. The other terms do not change from this equation to (4.44), as the high-frequency pseudo-eigenvalue has to be evaluated using equations (4.45a) and (4.47). By doing that, only two different frequency points need to be used to calculate the necessary residual compensation (i.e. ω_{pu} and ω_{pu_h}), and that simplifies the approach. The same points as before were used for this FRF and that produced a high-frequency value equal to 390.0 Hz (with damping also 1%). This frequency is almost the same as that for $H_{1,1}$, since the residual value for these two curves is not very different. Nevertheless, as the minimum response for this curve is very close to the upper

frequency of interest, this is the reason why more terms were needed in the series. Including one extra term would improve the predictions even more. However, the result obtained so far is already quite good.

The advantage of using a mass-and-spring system is that the "experimental" formulation can be compared with the correct ones (either analytical or combined formulations). Consequently, the quality of the experimental formulation can be assessed. The results obtained using equations (4.18), (4.27) and (4.44) were examined in the light of the FRF curves. The comparison was performed by truncating the series after the second-order residual compensation. Initially, the same frequency points as used previously for the experimental formulation were employed here. The results using all three residual series approaches (i.e. analytical, combined and experimental) are presented in Figure 4.18. It can be noticed that all predictions are effectively the same, despite the fact that one extra term should be included, as illustrated in Figure 4.17.

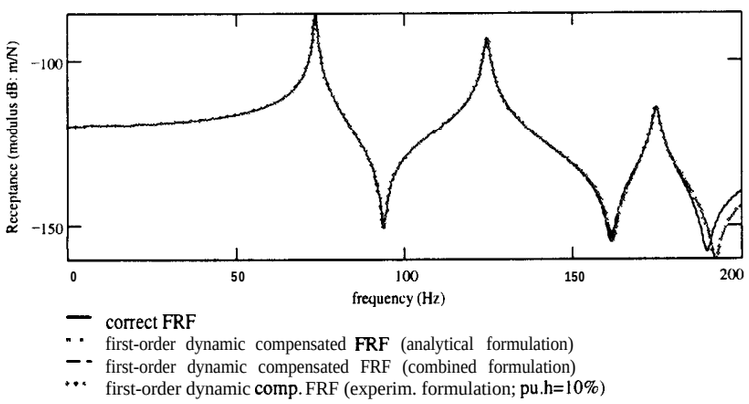

Figure 4.18 - $H_{7,7}$ curves for system A: comparison of the predictions using the second-order residual compensated curves (pu_h = 10% upper frequency = 20 Hz)

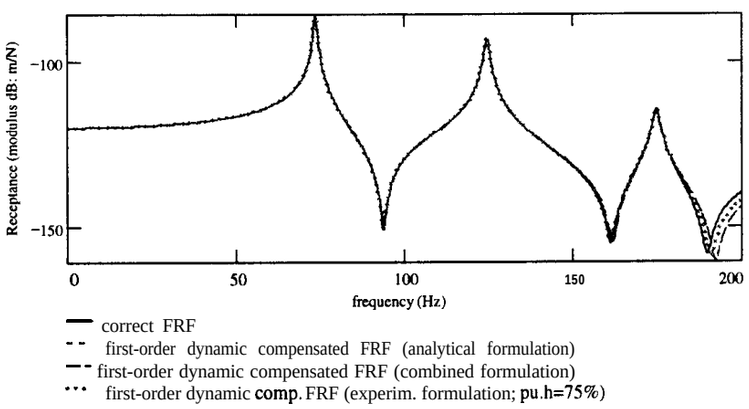

Figure 4.19 - $H_{7,7}$ curves for system A: comparison of the predictions using the second-order residual compensated curves (pu_h = 75% upper frequency = 150 Hz)

The advantage of the experimental formulation is that a different frequency point can be used and a better prediction can be obtained without resorting to a higher residual term. An example of that is shown in Figure 4.19. There, instead of using pu_h corresponding to 10% the upper frequency limit, a 75% that value was used. Controlling such frequency point choice produced a corresponding high-frequency value of 353.61 Hz, with damping equal to 1.24%. The second-order residual compensation produced an improved regenerated FRF as good as that achieved for the third-order residual compensation with a smaller frequency point.

The high-frequency pseudo-mode formulations are addressed next. The general formulation, i.e. that one based on a column of FRF curves, is analysed first. The results presented here were obtained using column 1 of the FRF matrix as the "measured" column. Two different choices of frequency points were assumed to highlight the importance of this choice. In the first choice, the frequency points are evenly spread from 0 to 200 Hz, in 5 Hz increments. In the second one, the initial limit for this interval was made higher; starting now from 150 Hz.

Figure 4.20 shows these predictions, together with the correct and the regenerated FRF curves for $\mathbf{H}_{1,1}$. A spurious peak is seen around 153 Hz (highlighted by a vertical line) for the first choice of frequency points. For the second choice, the compensated FRF (using the pseudo-mode eigenvector) recovered the correct FRF very well. Therefore, even using fewer points in the least-squares calculation, the second choice of points proved to be better. As stated previously, the frequency points should be chosen more towards the upper end of the frequency range of interest and this explains the above results. Comparing Figure 4.20 and Figure 4.16, it is observed that the pseudo-mode approach produced better results than the residual term in series form in this case.

Figure 4.21 presents another set of results, this time for $\mathbf{H}_{4,1}$. This FRF is not the point FRF used to calculate the pseudo-mode eigenvalue (equation (4.51)) and a better evaluation of the approach is possible. The same comments made for the point FRF are valid.

As the last case, an FRF is shown involving coordinates other than the ones for which the high-frequency pseudo-mode was obtained. Figure 4.22 shows such predictions for $\mathbf{H}_{4,4}$. Although the spurious mode is not any more apparent (although it is still present), none of the frequency choices manage to improve the regenerated FRF without residual compensation. Despite other curves are not shown, this trend can be extended generally.

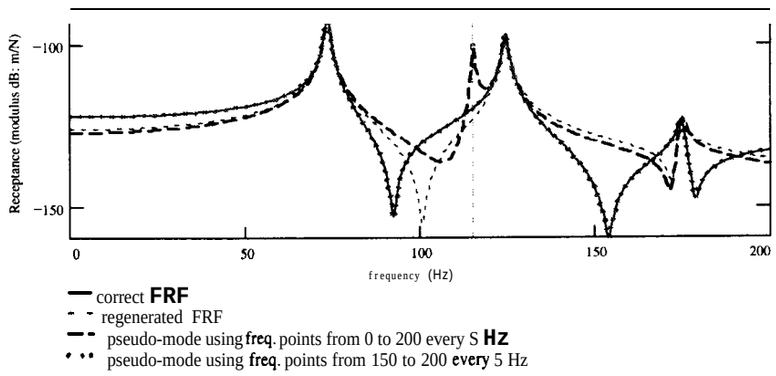

Figure 4.20 - $H_{1,1}$ for system A: pseudo-mode approach using column 1

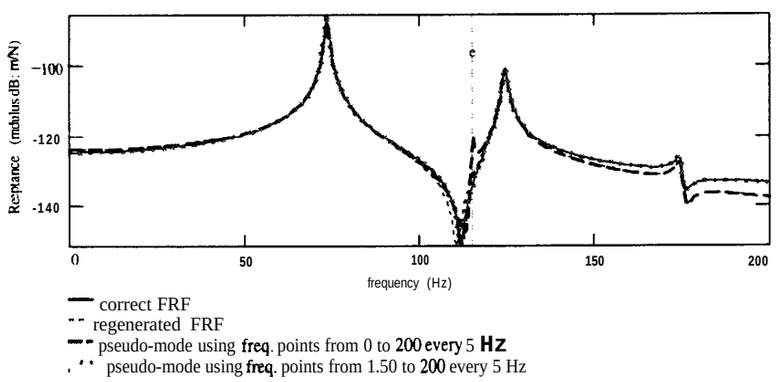

Figure 4.21 - $H_{4,1}$ for system A: pseudo-mode approach using column 1

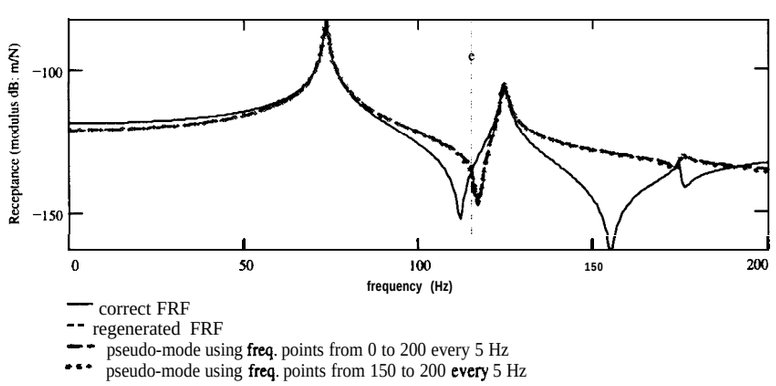

Figure 4.22 - $H_{4,4}$ for system A: pseudo-mode approach using column 1

Figure 4.23 shows the predictions for point $H_{1,1}$ for the case when the single-term pseudo-mode formulation was used. The high-frequency value (λ_{HF}) was adopted to be 1.5 times the upper frequency of interest. Two different frequency points were chosen to evaluate the formulation and those are represented there by pl and p2, respectively. Despite the fact that none of the choices really provides the correct prediction, the second one yielded a better result. Using a

different high-frequency value could have improved that further. The results are shown only to stress that the former approach is better and, at the same time, faster.

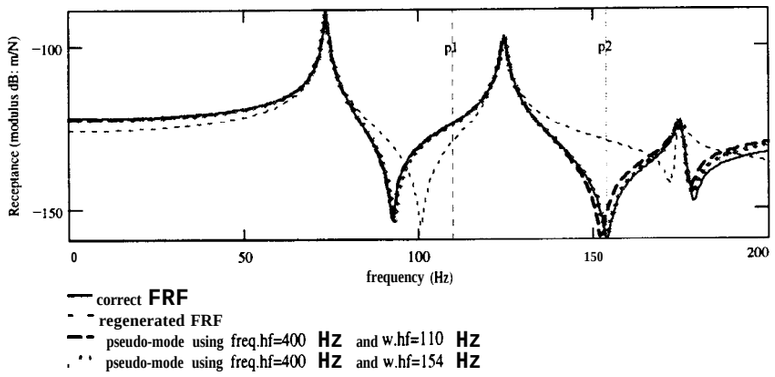

Figure 4.23 - $H_{1,1}$ for system A: single term pseudo-mode approach using different frequency point

The last formulation to be assessed is the mass-residual approach. The residual values obtained using such a formulation are presented in Figure 4.24. These results are in the same format and scale as those in Figure 4.6 to allow a comparison of the predictions using the correct and the mass-approach residual formulations. As the smaller masses are those related to coordinates 1, 4 and 7, it was decided to use coordinate 1 for the approach. Therefore, equation (4.39) was evaluated using $H_{1,1}$. Using this curve produced a high-frequency pseudo-mass value of 402.41 Hz with 1% damping. Comparing the mentioned figures, it is observed that the biggest residual values were very well predicted (those are the important ones). The other values, although not so well predicted, maintained the correct sign, in general.

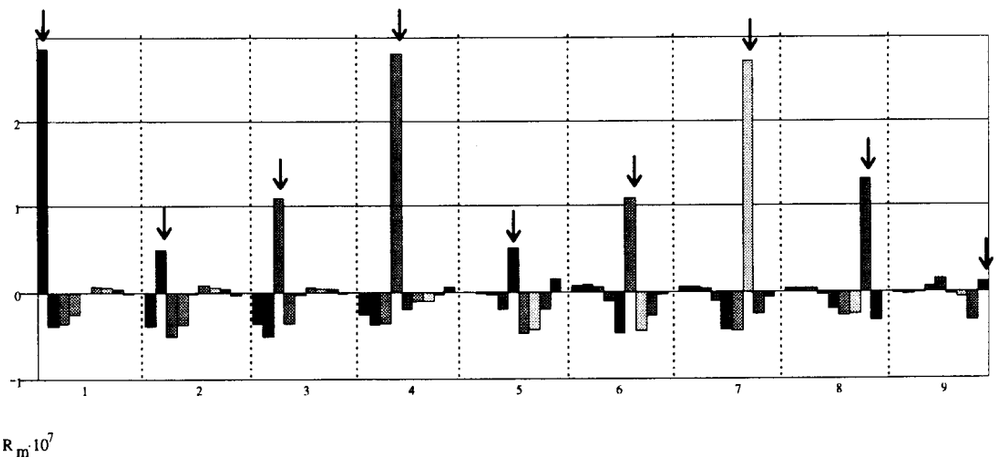

Figure 4.24 - Mass-approach residual values for system A, i.e. considering all 6 out-of-range modes (rows side by side) and calculated for point FRF $H_{1,1}$

Figure 4.25 shows the mass-residual approach predictions alongside the correct ones for $H_{7,7}$. A different FRF than that used for the calculation of the pseudo-mass value is shown to highlight the efficiency of the approach to correct predict the strong-residual FRFs. However, as mentioned, some of the predictions were not very good and a result for that is shown in Figure 4.26. It is worth mentioning that these results are better than those obtained not including any residual compensation at all. This is a general trend observed for other FRFs as well.

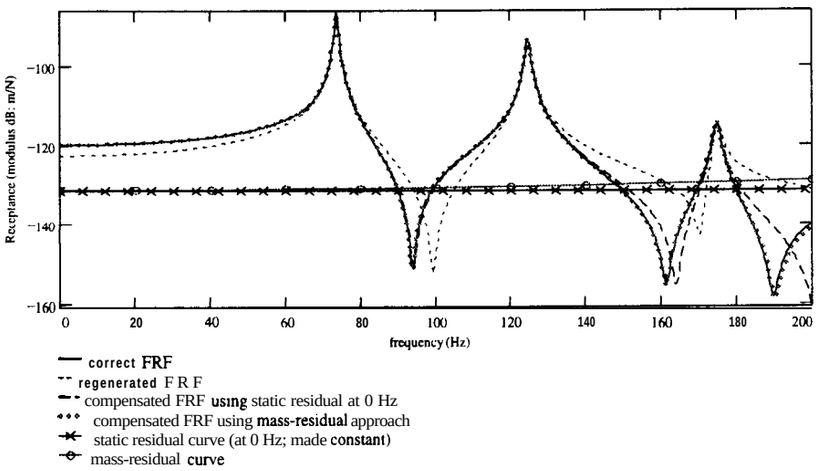

Figure 4.25 - $H_{7,7}$ for system A using static-residual and mass-residual approaches

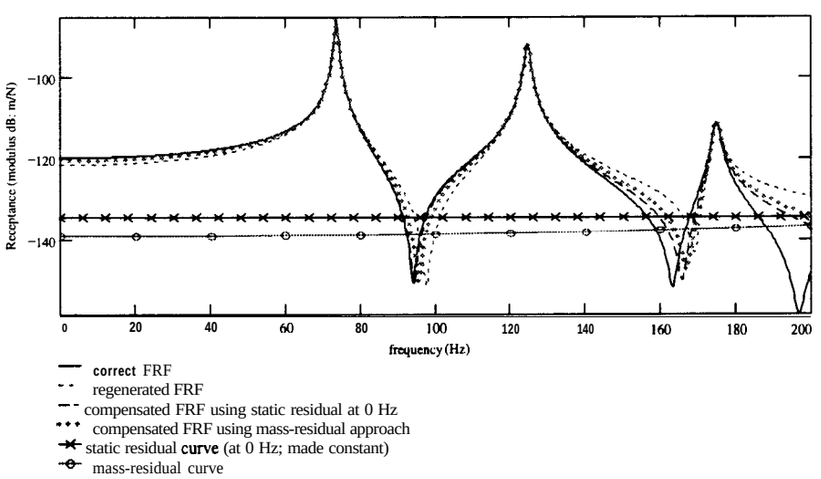

Figure 4.26 - $H_{6,6}$ for system A using static-residual and mass-residual approaches

4.8. CONCLUSIONS OF THE CHAPTER

The experimentally-based high-frequency residual formulations developed in this chapter proved to be a very efficient means of compensating for the lack of high-frequency residual modes. The standard experimentally-based residual formulation may present some difficulties when using a consistent modal data set, and so the residual calculated at individual frequencies

is normally a better approach (either static or series residual terms). Since the static residual formulation may fail to provide a good compensation for the whole frequency range of interest, extra terms in the residual series are recommended. Generally, one extra term in this series is enough (making two terms for the residual compensation). Although these terms are straightforward to calculate from analytical or combined approaches, the lack of the high-frequency modes or the physical parameters' matrices, respectively, prevents their use with experimentally-derived data. The formulation proposed in this chapter circumvents such a need, at the same time providing quite accurate predictions. However, the choice of the frequency points used in the experimental residual series has to be controlled. The only shortcoming of such an approach is that all necessary residual terms have to be calculated individually.

To compensate for the lack of high-frequency modes in all measured FRFs at once, the high-frequency pseudo-mode approximation has been developed. It proved to be quite accurate for the measured column of FRF terms used in the calculations, although it is of little use for the other columns. If compensation is needed for more than one column, the process has to be repeated for each column separately. Nevertheless, it saves time when estimating the residual terms and the results are not so sensitive to the frequency points used as is the case for the single-term pseudo-mode approximation.

The mass-residual approach can be used to estimate unmeasured residual terms, although the need for the mass matrix of the system is still a shortcoming of the formulation from experiments. The author believes this matrix is easier to derive and to confirm experimentally than is the stiffness matrix and such a solution should be pursued. From an analytical approach, the use of this formulation proved to be better than not using any residual compensation at all. For the strong residual terms, it generally proved to be quite accurate.

The high-frequency residual terms are the stiffness-like effects of modes at frequencies much lower than their natural frequencies. Nevertheless, a link was discovered between these terms and the mass of the system: the smaller the mass at a particular coordinate, the bigger the residual effects at that coordinate. This observation helps to choose which FRF should be used in the mass-residual approach or to measure the most important FRFs. The other trends for the high-frequency residual terms are related to their relative unimportance at resonances and importance at anti-resonances; their relative effects comparing point and transfer FRFs, and their importance at translational and rotational DOFs.

CHAPTER 5: THE SPATIAL INCOMPLETENESS PROBLEM

5.1. INTRODUCTION

In this chapter, another major problem affecting coupled structure predictions is addressed; that is, spatial incompleteness. This is viewed from the experimental point of view, where the measurement of rotational DOFs (RDOFs) represents the major obstacle. Although this is not the principal objective of the work summarised here, ways of measuring (or deriving) such coordinates had to be investigated in order to improve the coupled predictions obtained from experimentally-derived models. Beam- and plate-like structures are the most affected by a lack of RDOF data. Existing techniques for obtaining such coordinates are introduced in this chapter. Attention is dedicated to the finite-difference method, as it proved to be the simplest one to use and provided quite accurate predictions (when due care was taken, as explained later). Both FRF- and modal-based finite-difference approaches are analysed. Conclusions are drawn as to which derivation approach should be used with each of the coupling techniques employed in this work and important guidelines are given in that direction. Simple examples are shown at the end to clarify the comments.

A real structure is a continuous system. However, in order to analyse its dynamic behaviour, it is necessary to discretise it into a finite number of elements. This is normally referred to as the mesh of the structure. Each element has a certain number of nodes and related to each node there are normally 6 DOFs. Considering these concepts, two requirements can be made relative to spatial completeness:

1. The mesh has to be fine enough to properly describe the dynamic behaviour of the structure and;
2. All DOFs should be included in the model (i.e. both translational and rotational).

The first requirement has an additional pre-requisite. The mesh has to be kept to the smallest size possible to cut costs when analysing (and/or measuring) the structure. From FE analysis, a good indication about how good a mesh is can be obtained by analysing the structure again using a more refined mesh. If the results are not changed, a good mesh was already achieved.

that the mesh has to be fine enough to describe the mode-shapes of the structure accurately. This is normally given on the basis of a FE pre-test analysis. Therefore, requirement 1 does not present any difficulty to the modal analysis process.

The second requirement is the most problematic and is mainly related to the inclusion of rotational DOFs in the model, since translational ones only are normally considered. It can be achieved without too much problem when using the FEM. However, due to the difficulty in measuring RDOFs, it is seldom achieved from experiments. Therefore, RDOFs for experimentally-derived models are the primary problem related to spatial incompleteness and this is the subject of this chapter.

Next, a summary of existing techniques to obtain RDOFs is provided. Only two of them will be addressed in detail, namely: (1) the block technique and (2) the finite-difference technique. The latter will be considered from both FRF and modal parameters points of view and reasons for using one or the other will be explained. Following that, some examples to validate the observations made for the finite-difference methods are given. Finally, conclusions are drawn.

5.2. SUMMARY OF PREVIOUS WORK

There are several different techniques for measuring or deriving RDOFs and these are presented in Table 5.1 with the respective references sorted by date to show their chronological evolution. Some of the references appear in more than one category, either because they cover more than one technique or because the approach is actually a combination of methods.

The choice of the technique will depend on many points, such as: (1) cost; (2) accuracy; (3) ease of application (or implementation) and (4) further use of the derivations. From the cost point of view, the most expensive approach is the laser technique and, consequently, this is not widely available. Moreover, although the most accurate of all, it is rather difficult to implement. Angular response transducers are also very expensive, besides having a poor accuracy/cost ratio to justify its use. Nevertheless, it is the easiest and only technique that allows a direct measurement of rotational quantities; all others requiring a mathematical manipulation of the data to derive such information. Some of the techniques quoted in this table derive the rotational-related FRF curves directly, while others derive only the rotational mode-shapes. This fact should be borne in mind when using the derived results (point 4 above). The accuracy of the techniques is dependent on many factors. However, in general, one can say that it is related to the noise incorporated in the data. Some other problems may affect the accuracy but those will be technique dependent.

Table 5.1 - RDOFs references according to year and approach

date	Block	Mass Additive	Finite Difference	Estimation	Ang. Transd.	Laser
1969	[109] Smith					
⋮						
1972	[37] Ewins and Sainsbury					
⋮						
1975	[38] Ewins and Gleeson					
1976	[100] Sainsbury					
⋮						
1978	[104] Silva					
1979	[48] Gleeson					
1980	[39] Ewins, Silva & Maleci		[103] Sattinger			
⋮						
1984	[4] ASA Standards [108] Smiley and Brinkman	[132] Yasuda et al.	[4] ASA standards [84] Martinez et al.	[108][1] Smiley and Brinkman		
1985			[24] Chen and Cherng [82] Maleci and Young	[90][2,3] O'Callahan et al.	[77] Licht	
1986		[68] Kanda et al.		[45][4] Furusawa and Tominaga [91][3] O'Callahan et al. [55][2] Haisty and Springer		
1987	[105] Silva and Fernandes			[5][3] Avitable et al.		
⋮						[93] Oliver
1989	[127] Urgueira [107] Skingle		[127] Urgueira	[127][2] Urgueira	[98] Rorrer et al.	[127] Urgueira
1990				[131][2] William and Green		[115] Sriram et al.
1991					[9] Bill and Wicks	[18] Cafeo et al.
1992					[73] Laughlin et al.	[19] Cafeo et al.
1993	[102] Sanderson		[101] Salvini and Sestieri	[87][2] Ng'andu et al. [20][3] Cafeo et al. [101][4] Salvini and Sestieri		[11] Bokelberg et al. [20] Cafeo et al. [122] Trethewey et al.
1994				[78][1] Llorca et al.		[116] Stanbridge and Ewins
1995				[88][2] Ng'andu et al.		
1996		[118] Stebbins et al.		[22][2] Chang et al.	[118] Stebbins et al.	[96] Ratcliffe and Lieven

Estimation methods: [1] Derivative; [2] Fitting functions; [3] Expansion (FE based); [4] Constraint Equations

The block and the mass additive techniques could be grouped into a wider category, since they are based on the same principle that the attached mass behaves as a rigid-body. The extra added mass is analytically subtracted from the process. The basis for the methods is the work of Smith [109]. The theory of the excitation block is fully developed in references [100] and [104], with several different types of blocks for single or twin shakers presented in the former. An engineering use of this technique was demonstrated in [39]. However, there are several problems associated with the use of the block, such as: cross-sensitivity of the accelerometers, mass-loading effects, base strain effects, etc. These are explained in references [48] and [107] and will be covered in detail in section 5.3.2 since they affect the accuracy. It was demonstrated by several authors [e.g. 38, 127] that the functions most susceptible to errors using this

technique are those related to moment excitations. In [102], a different approach to the block technique is given. This reference is split into two parts, the first containing a theoretical study, while the second covers the experimental validation of the theory. The method presented there employs a pair of ordinary exciters operated in phase opposition so as to provide a moment excitation which is combined with measurements of rotational velocity. The two bias errors, namely, errors in the excitation of rotational motion and errors in the measurement of the moment applied to the structure are addressed. Although both errors can be compensated for, the former normally requires a separate measurement. The technique presented in [118] does not allow for the removal of the mass/inertia effects of the rigid body used in the procedure. To perform this removal, Perturbed Boundary Condition (PCB) testing procedure has to be used.

Problems with moment-related FRFs are also present in the finite-difference approach [103, 127]. This technique is based on acquiring a matrix of translational measurements, from which the rotational measurements are derived using either first- [24] or second-order [103] finite-difference formulas. In [103], the backward, central and forward finite-difference formulas are given. The choice between them is dependent on whether the location where rotation is desired is an inside, middle or outside location, or on whether it is on the positive or negative end of the global axis. The spacing between the measurement points is vital for the correct estimation of rotational-related FRFs [103,127] and this parameter has to be carefully controlled. It is suggested in [4] and [103] that some analytically- or experimentally-obtained crude knowledge of mode-shapes is useful in determining such spacing. Reference [84] suggests a similar procedure to the one used in [103]. However, instead of using experimental translational FRFs, translational mode-shapes are used together with residual information so as to eliminate measurement noise. This approach was also used in [127]. The finite-difference technique will be presented in section 5.4, where both FRF- and modal-based approaches will be addressed. The block and the finite-difference techniques (using FRF curves) were published by the Acoustical Society of America (ASA) [4], in 1984.

All estimation methods, like the finite-difference one, are dependent on the spatial description of measured translations. In reality, the finite-difference technique could be regarded as a derivative method. Considering the estimation methods shown in Table 5.1, the use of expansion techniques will not be examined, since they are FE-based and not a purely experimental approach, as is desired here. So, only the other methods will be analysed. The derivative approaches, for instance, proved to be effective for simple structures [108, 78], whereas the fitting functions cover either simple or complicated structures. The latter are divided into two groups: polynomials [90,131] and splines [55, 87, 88] fitted to the

translational data. As quoted in [87], polynomials are ideal for representing relatively uncomplicated relationships. Splines, on the other hand, are more suitable for representing very complex ones. Besides, they are computationally efficient and more stable numerically than polynomials. Guidelines are given in [88] for the use of spline functions for estimating rotational parameters (including the case of noisy data and different boundary conditions). In reference [20] the authors made a comparison between the laser and the polynomial fit techniques, where it is shown that significant errors may arise using the latter approach. Also, in reference [19] they say that the use of cubic splines should only be relied upon for modal constants with high accuracy and virtually noise-free data. The constraint equation method proposed in [101] is actually used to restore the real boundary condition of the structure for the case when the real one is not possible to be implemented in a test. To derive rotational parameters, the finite-difference approach is suggested there. The method proposed in [45] uses constraint equations of a rigid-body motion to derive the RDOFs. In reference [22], Lagrange interpolation is used to approximate the RDOFs. There, 2nd, 3rd and 4th-order interpolation formulas are shown. In reality, the second-order Lagrange interpolation formula is the same as the second-order forward finite-difference formula when applied to the modal parameters.

Some research has been dedicated to angular transducers, so as to improve the quality of direct rotational measurements. The initial transducers were very cost and of poor accuracy [77, 98]. Recently, a load cell capable of measuring three forces and three moment inputs has been proposed but is still at the prototype stage [118]. The uncoupling of the moments and the translational forces is achieved by a calibration matrix rather than by the design of the load cell, and that reduces the complexity of the design, difficulty and cost. Some problems were encountered and another prototype is under construction.

The first use of laser techniques is reported much earlier than the references quoted here. However, at the beginning, they were not directed to rotational parameters' estimation [93]. Reference [115], for example, is one of the many papers explaining the theory of the laser doppler vibrometer (LDV). There, some early references using the LDV can be found. The main advantage of using laser technique is its non-contacting nature. Therefore, it is particularly suitable for lightweight structures or where is not possible to attach accelerometers. There are still several applications for the LDV techniques other than that of measuring RDOFs. In [127], the laser technique was used to scan a line of measurements with the data subsequently fitted using different degrees of polynomial functions to suit the curvature of the mode-shape. The first technique developed to measure rotational parameters directly using such a device was presented initially in [18]. This is capable of measuring one translation and two

rotations simultaneously. This same technique was later presented in more detail in [19], where it was shown that significantly improved definition of mode-shape characteristics could be obtained by integrating translational and rotational modal deflections at each response measurement site. A detailed explanation of the 3 DOF technique was given in [122]. An extension of the above technique was proposed in [11], where all 6 DOFs were measured simultaneously (i.e. 3 translations and 3 rotations). A different laser technique is presented in [116]. There, by using a sinusoidal scanning approach, one rotation and one translation can be obtained. However, if a circular scanning is used instead, two rotations are obtained. The laser technique proposed in [96] fits a plane to the experimental translational data in a least-squares sense. The accuracy of the technique is dependent on the amount of corruption present on these translational data. Although it is capable of determining the rotation/force FRFs, cannot determine the rotation/moment one. An important point to stress about all laser techniques is their sensitivity to the correct set-up of the equipment (which is normally very complicated) and care should be taken when preparing this.

5.3. RDOFS VIA EXCITATION BLOCK TECHNIQUE

5.3.1. INTRODUCTION AND FORMULATION

Although it was not the technique used during this work, the first method for measuring RDOFs to be addressed in detail here is the so-called T-Block technique. Following the conclusions in [37], the single-excitation technique is explained [38], since it requires a simpler set-up than the twin-excitation method which provides the same degree of accuracy. The main design requirement for the block is that it has to be sufficiently rigid over the entire frequency range of interest to behave as a rigid body. By using rigid-body equilibrium equations, the translational measurements are translated to the connection point to obtain the parameters required.

One of the possible configurations for the block is represented schematically in Figure 5.1. Point P is connected to the test structure at the position where the rotation needs to be derived. Force inputs are provided and the respective accelerations measured through the use of two accelerometers. The forces are applied in two individual runs. The number of runs may increase depending on the analyser adopted. For some of the analysers, just two channels are available. Therefore, only one force and one response can be measured at a time. To avoid reciprocity problems when changing the position of the accelerometer in this case, the other accelerometer site should be supplied with either a dummy mass of the same weight and inertia as the accelerometer used or with another accelerometer having the same size.

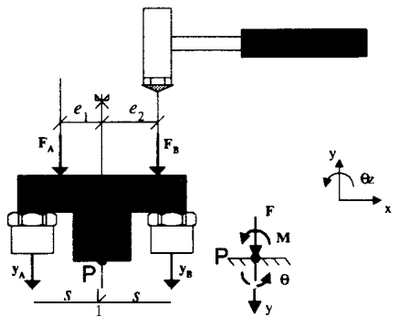

Figure 5.1 - T-Block method for RDOFs measurement

The following equation is used to obtain the rotational FRF data at the attachment point, from the measurement of translational FRFs:

$$[H_{est}] = [T_1][H_{meas}]([T_2] - [M_{bl}][T_1][H_{meas}])^{-1} \tag{5.1}$$

The desired FRF matrix $[H_{est}]$ and the measured FRF matrix $[H_{meas}]$ are, respectively:

$$[H_{est}] = \begin{bmatrix} \ddot{y}_P/F_P & \ddot{y}_P/M_P \\ \ddot{\theta}_P/F_P & \ddot{\theta}_P/M_P \end{bmatrix} = \begin{bmatrix} H_{yy} & H_{y\theta} \\ H_{\theta y} & H_{\theta\theta} \end{bmatrix} \tag{5.2}$$

$$[H_{meas}] = \begin{bmatrix} \ddot{y}_A/F_A & \ddot{y}_A/F_B \\ \ddot{y}_B/F_A & \ddot{y}_B/F_B \end{bmatrix} \tag{5.3}$$

Matrix $[T_1]$ is a transformation matrix containing information relative to the response positions. For the above configuration $[T_1]$ is represented by:

$$[T_1] = \begin{bmatrix} 1/2 & 1/2 \\ 1/2s & -1/2s \end{bmatrix} \tag{5.4}$$

Matrix $[T_2]$ is also a transformation matrix, but this time relative to the position of the forces induced to the block. The elements of matrix $[M_{bl}]$ are the mass and inertia of the block plus transducers, and are used to remove their loading effects on the structure. The referred matrices can be expressed as:

$$[T_2] = \begin{bmatrix} 1 & 1 \\ e_1 & e_2 \end{bmatrix} \text{ and } [M_{bl}] = \begin{bmatrix} m & 0 \\ 0 & I_p \end{bmatrix} \tag{5.5}$$

5.3.2. ADVANTAGES AND DRAWBACKS

The main advantage of the block technique is to provide a way of eliminating the mass-loading effects of the block and transducers mounted on it. Moreover, compared with the 2nd-order

finite-difference technique addressed next, less data have to be measured to derive the necessary quantities and the technique is not very sensitive to the spacing between the transducers. However, there are several problems associated with it, as explained next. Some of these are common to other techniques as well. One of the many problems pertinent to the use of this technique is the need to ensure that the block is attached with sufficient rigidity such that the behaviour of the structure is fully transmitted to the transducers. Base strain effects may have very strong influence in the final results [38].

Another problem is the large physical size and mass of the whole measurement system (i.e. block plus transducers). The system has to accommodate at least two accelerometers and a force gauge, when using an excitation method other than a hammer. Although this effect can be removed during the post-measurement processing (quoted as an advantage above), the accuracy of equation (5.1) depends a great deal on the mobility of the measurement point [107]. If the point is not very mobile, the effects of the measurement system are expected to be small, therefore providing a good accuracy in the final results. However, if it is very mobile, its effects may dominate the response at that point and then the removal of the mass effects may not yield the required predictions very accurately.

The cross-sensitivity of the accelerometers is another feature that may lead to poor results [38, 48, 107]. This sensitivity may be very important when taking the difference of two FRF signals of similar size. This problem is even stronger when the motion in the transverse direction is large. To minimise this effect, it is necessary to use accelerometers with very small cross-sensitivities, usually of less than 1.0%. Also, it is required to align the direction of maximum cross-axis sensitivity of each accelerometer with the direction of minimum transverse motion. However, polar plots of cross axis sensitivity are hardly available and the whole process becomes even more difficult. Apart from accurately matching the accelerometers' position, these devices should also be carefully calibrated.

In general, the two rotational responses are the most difficult to measure accurately (i.e. $\ddot{\theta}/F$ and $\ddot{\theta}/M$), with the latter one being the most problematic and giving the poorest results of all. It depends on the difference between two accelerometers and the above-mentioned problem (of cross-sensitivity) may make the predictions even worse. To improve the quality of these derivations, reference [38] suggests to obtain these mobilities from the measurements of $\ddot{y}/F$ and $\ddot{y}/M$, using modal identification techniques. Then, the direct measurement of rotations is not necessary any longer. The shortcoming of such an approach is that residual terms cannot be derived in the same way and the predictions may be affected by the lack of residual modes.

5.4. RDOFs VIA CLOSELY-SPACED ACCELEROMETERS: THE FINITE-DIFFERENCE TECHNIQUE

5.4.1. INTRODUCTION

The actual technique adopted for the experimental results shown in this thesis was that of "close" accelerometers. This was decided on the basis of simplicity, as the measurement of RDOF was not the main objective of the research. As represented schematically in Figure 5.2, three (or two) accelerometers (according to the finite-difference formula employed) are placed close to each other, in a constant spacing (s). Then, translational measurements are made and finite-difference formulas used to derive the necessary rotational quantities [103, 24]. The grounds for that are the relationship between rotations and translations; the former being the spatial derivatives of the latter. One of the accelerometers is located at the point where rotation needs to be derived (represented here by point P in the figure), and the positions of the other accelerometers are dependent on the finite-difference formula employed and the direction of the global axis. As found with the block technique, the only special consideration here is for the case when the analyser has just two channels. Then, the other accelerometer positions should be supplied with either dummy masses or with accelerometers having the same size to avoid reciprocity problems when performing the measurements around the necessary configuration.

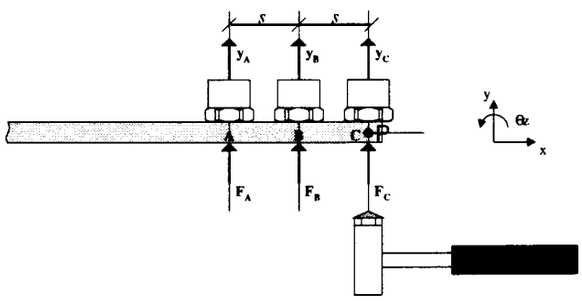

Figure 5.2 - Close-accelerometers method for RDOFs measurement

Next, the first- and second-order finite-difference transformation matrices needed for the estimation of the necessary rotational parameters are introduced.

5.4.2. FINITE-DIFFERENCE TRANSFORMATION MATRICES

5.4.2.(a) FIRST-ORDER APPROXIMATION

The simplest approximation to use and the one requiring least data to be measured is that of the first-order approximation. Only two location sites have to be considered in this case. To

elucidate the formulas, points B and C of Figure 5.2 will be used. The first-order forward- and backward-difference transformation matrices, respectively, are expressed as follows:

$$[T_{1f}] = \begin{bmatrix} 0 & 1 \\ 1/s & -1/s \end{bmatrix} \tag{5.6a}$$

$$[T_{1b}] = \begin{bmatrix} 0 & 1 \\ -1/s & 1/s \end{bmatrix} \tag{5.6b}$$

It should be noticed that only the last rows of these matrices are different (being of opposite sign). Equation (5.6a) would be used if either point P (where rotational parameters are required) coincides with measurement point B (i.e. P = B) and the coordinate system is the one assumed in Figure 5.2, or if P = C and the coordinate system is in the opposite direction. Equation (5.6b), on the other hand, would be used for the configuration represented in Figure 5.2 or if P = B and the coordinate system is in opposite direction as the one represented there. Both transformation matrices are of equivalent accuracy.

5.4.2.(b) SECOND-ORDER APPROXIMATION

The other possible transformation matrices to use are those of second-order approximation. In this case, three location sites are needed, as shown in Figure 5.2. Three different formulas can be employed depending on the accelerometer and coordinate system positions. The second-order forward-, central- and backward-difference transformation matrices are, respectively:

$$[T_{2f}] \quad T_{2f} = \frac{2s}{1} \begin{bmatrix} 1 & 0 & 0 & 2s \\ 1 & 0 & 0 & 3 \\ 1 & 0 & 0 & 1 \end{bmatrix} \tag{5.7a}$$

$$[T_{2c}] \quad T_{2c} = \frac{2s}{1} \begin{bmatrix} -1 & 0 & 0 & 2s \\ 0 & 0 & 0 & 0 \\ 1 & 0 & 0 & 1 \end{bmatrix} \tag{5.7b}$$

$$[T_{2b}] \quad T_{2b} = \frac{2s}{1} \begin{bmatrix} 1 & 0 & 0 & 2s \\ -4 & 0 & 0 & 3 \\ 1 & 0 & 0 & 1 \end{bmatrix} \tag{5.7c}$$

As for the previous case, the forward and backward approximation matrices differ from each other only by the sign of the last row. Equation (5.7a) would be used if either point P = A and the coordinate system is the one assumed in Figure 5.2 or if P = C and the coordinate system is in opposite direction. Equation (5.7c), on the other hand, would be used for the configuration represented in this figure or if P = A and the coordinate system is in the opposite direction to the one represented there. Equation (5.7b) would be used if point P = B and, in this case, the coordinate system has no importance. As for the first-order approximation, all three transformation matrices above are of equivalent accuracy.

5.4.3. FRF-BASED APPROACH

5.4.3.(a) FORMULATION

The original application of the finite-difference approach to derive rotational properties was related to the calculation of FRF curves. Translational FRF curves are measured and, using the transformation matrices introduced in the previous section, the corresponding full set of FRFs (i.e. those related to translational and rotational coordinates) is obtained at a specific point. This is achieved by solving the following equation (where the frequency dependency of the formulation is dropped for simplification):

$$[H_{est}] = \begin{bmatrix} H_{yy} & H_{\theta y}{}^{T} \\ H_{\theta y} & H_{\theta\theta} \end{bmatrix} = [T_?][H_{meas}][T_?]^T \tag{5.8}$$

Subscript ? is used to remind the reader that any of the matrices expressed in equations (5.6) or (5.7) can be used. Therefore, the size of the measured FRF matrix is related to the approximation employed and symmetry should always be considered for this matrix. Developing equation (5.8) for the first-order forward- and backward-difference approximations, respectively (as represented in section 5.4.2.(a)), and considering symmetry, yields:

$$[H_{est}]_{1f} = \begin{bmatrix} H_{CC} & -\frac{1}{s}(H_{CC} - H_{CB}) \\ sym. & \frac{1}{s^2}(H_{CC} - 2H_{CB} + H_{BB}) \end{bmatrix} \tag{5.9a}$$

$$[H_{est}]_{1b} = \begin{bmatrix} H_{CC} & \frac{1}{s}(H_{CC} - H_{CB}) \\ sym. & \frac{1}{s^2}(H_{CC} - 2H_{CB} + H_{BB}) \end{bmatrix} \tag{5.9b}$$

As seen above, the only difference between the derived functions using the mentioned approximations is for the off-diagonal terms which have their signs reversed. A similar result occurs for the second-order backward- and forward-difference approximations, as expressed below. The development of equation (5.8) using the transformation matrices introduced in section 5.4.2.(b), results in:

$$[H_{est}]_{2f} = \begin{bmatrix} H_{CC} & -\frac{1}{2s}(H_{CA} - 4H_{CB} + 3H_{CC}) \\ sym. & \frac{1}{4s^2}(H_{AA} - 8H_{BA} + 6H_{CA} + 16H_{BB} - 24H_{CB} + 9H_{CC}) \end{bmatrix} \tag{5.10a}$$

$$[H_{est}]_{2c} = \begin{bmatrix} H_{BB} & \frac{1}{2s}(H_{CB} - H_{BA}) \\ sym. & \frac{1}{4s^2}(H_{AA} - 2H_{CA} + H_{CC}) \end{bmatrix} \tag{5.10b}$$

$$[H_{est}]_{2b} = \begin{bmatrix} H_{CC} & \frac{1}{2s}(H_{CA} - 4H_{CB} + 3H_{CC}) \\ sym. & \frac{1}{4s^2}(H_{AA} - 8H_{BA} + 6H_{CA} + 16H_{BB} - 24H_{CB} + 9H_{CC}) \end{bmatrix} \quad (5.10c)$$

5.4.3.(b) ADVANTAGES AND DRAWBACKS

The main advantage of the FRF-based finite-difference technique is that, as the name suggests, FRF curves are obtained. In addition, no special apparatus is required; only the transducers normally used in a standard modal testing. Moreover, no special set-up is necessary and the modal test is carried out very much in the normal way. This approach is particularly suitable for using with FRF coupling techniques due to its final format.

Nevertheless, some problems are associated with its use and care has to be taken to minimise their influence. The first problem is to establish the spacing between the accelerometers so as to predict the necessary quantities correctly. This has to achieve a balance between resolution and proper approximation of derivatives over the frequency range of interest. A crude knowledge of the mode-shapes is useful in determining this spacing. The distance s (see Figure 5.2) has a direct relation to the position of anti-resonances, with a shift being caused by increasing or decreasing this parameter. Some examples showing this are given in section 5.5, where a fuller assessment of the consequences is made. Another problem, directly related to the one above, is the order of the approximation used. For a given spacing, the second-order approximation is generally better at estimating the derived FRFs than is the first-order approximation, with $H_{y\theta}$ better predicted than $H_{\theta\theta}$. Nevertheless, the last comment is also valid for the first-order approximation. This fact will also be demonstrated in section 5.5.

The direct use of measured translational FRFs, normally yields unacceptably noisy rotational FRF data. This is a result of subtracting quantities that are very similar. Therefore, relatively small errors in the measured data may result in large errors in the estimated responses. The $H_{y\theta}$ curves are normally less noisy than those for $H_{\theta\theta}$. However, the noise on both these derived curves tends to decrease as the frequency increases. To obtain modal parameters from these derived curves is very difficult at the lower frequency range, as the noise plays an important role in that region. An additional problem is related to inconsistencies in the modal parameter data set. It will be demonstrated in section 5.5 that some anti-resonances may be lost as a result of such inconsistencies. The use of regenerated FRF curves is recommended to solve these problems. However, the regenerated curves have to include the effects of all the modes the structure possesses to avoid the addition of residual problems. Since it has been suggested that the regenerated translational FRFs may be used in this way, it seems natural to extend the

finite-difference approach to the translational modal parameters, so as to regenerate the rotational curves direct from the derived parameters. This is presented in next.

5.4.4. MODAL-BASED APPROACH

5.4.4.(a) FORMULATION

To minimise the noise incorporated into the measured translational FRFs, these curves have to be smoothed before the finite-difference approach is applied. So, if this approach is applied directly at the translational modal parameters, the same results as for the FRF-based approach should be expected. The only problem would be to assure that enough modes are included. The modal parameters are normally obtained from a less extensive modal test, where only one column (or row) of the FRF matrix needs to be measured. As thoroughly discussed previously, only the modes within the measured frequency range can be obtained using such a procedure and the regenerated FRFs have to be augmented by residual terms. In order to use the finite-difference approach to the translational modal parameters and to avoid modal truncation problems, a similar procedure has to be employed to the residual matrix as well. This procedure can be formulated as follows:

$$[H_{est}(\omega)] = [\phi^{l}_{est}][\lambda_l^2 - \omega^2]^{-1}[\phi^{l}_{est}]^T + [T_?][R_{meas}][T_?]^T \tag{5.11}$$

where:

$$[\phi^{l}_{est}] = [T_?][\phi^{l}_{meas}] \tag{5.12}$$

The same formulas expressed in the previous section (i.e. equations (5.9) and (5.10)) would be obtained for the second term on the RHS of equation (5.11). However, the FRF curves used in the former equations are now substituted by the residual curves (or terms). This distinction is made because any form of residual compensation introduced in chapter 4 could be used here, where the comments made there are equally valid here.

5.4.4.(b) ADVANTAGES AND DRAWBACKS

The main advantage of the modal-based finite-difference technique is that noise is eliminated from the measured data and so, consequently, smoothed derived curves are obtained. The same comments as made previously related to the simple set-up and lack of need for additional apparatus are, of course, still valid. It is the ideal technique to use with CMS formulations, as the modal parameters and the residual terms needed are derived straightaway. Nevertheless, it is also good for using with FRF coupling formulations, since the necessary FRFs can be regenerated using the derived parameters and smoothed curves are obtained. In reality, the

modal-based approach is even better than the FRF-based one, as it allows different finite-difference approximations to be used thus yielding better predictions.

The problems mentioned previously in establishing the spacing between the accelerometers and deciding which approximation order to use, are equally present here. However, as stated above, a mixture of approximations is permitted now. It will be illustrated in the next section that the first-order approximation is better for estimating the derived rotational amplitudes, whereas the second-order approximation is more suitable for estimating the derived residual values.

5.5. EXAMPLES

Two beams were tested to validate the techniques shown throughout this thesis and they will be referred to as short and long beams. The coupling between them will be reported later using the FRF coupling and CMS techniques (explained in chapters 2 and 3, respectively) with the results for that shown in chapter 6. However, in order to obtain the correct coupled predictions, it was essential to have rotational-related quantities (either FRFs or modal parameters, depending on the coupling technique employed). Therefore, the results obtained for one of the beams will be shown in this chapter to illustrate the finite-difference technique when that is used for RDOFs derivation'. Residual compensation will also be investigated for that, as their need for the coupling process is essentially related to the necessary coupling coordinates (in this case, involving the RDOFs).

The long beam will be adopted. This was made of mild steel with dimensions 70 x 6.35 x 0.635 cm, as shown in Figure 5.3. Although 6 directions are shown in this figure, only two out-of-plane vibration was considered. These assumptions reduced the total number of DOFs per node from 6 to 2 (respectively, z and θx). The beam was discretised experimentally with 15 nodes, with one extra node used for the rotational derivation (node 16). An FE analysis was also performed for comparison purposes. However, the latter had to be more finely discretised, and a total of 57 nodes were used. The correspondence between the FE and experimental nodes needed for the rotational derivation studies is also shown in Figure 5.3.

The node where rotational parameters are required is at the tip of the beam (node 15 for the experimental mesh and 57 for the FE mesh)[2]. The beam was tested in a "free-free" configuration, suspended with the y axis vertical by soft elastic bands at the hole shown. Node

[1] By RDOF derivation one means both the rotational amplitude derivation and the rotational FRF derivation.

1 could not be located exactly at the end of the beam for the experimental configuration, because of the suspension used, and was located 2.5 cm from the end. For the experimental mesh, apart from the special nodes, all the others are 5 cm apart. For the FE mesh, all nodes are 1.25 cm apart. Considering the coordinate system shown in Figure 5.3 and the position of node 15, the forward finite-difference formula was employed to derive the necessary rotational quantities. The beam was tested at the neutral axis such that no torsional modes were excited. The derived FRFs for the axis system shown in this figure are $H_{z,z}$, $H_{\theta x,z}$, $H_{\theta x,\theta x}$.

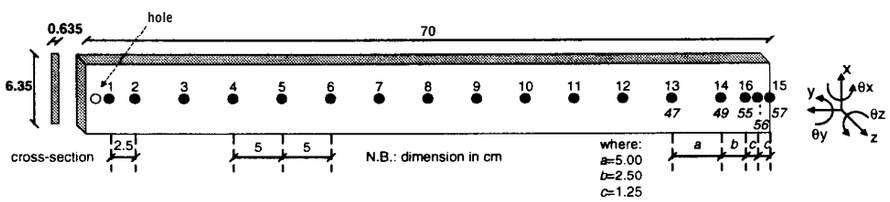

Figure 5.3 - Long beam used for validation purposes

In order to stress some of the points mentioned, the theoretical data is used initially. The reason is that no noise is present in this case. Theoretical data are ideal for assessing the spacing and the order of the finite-difference approximation when estimating the FRF-based rotational quantities. Urgueira [127] compared the quality of the derived FRFs at low- and high-frequency regions, according to these parameters (i.e. spacing and order). However, it is important to obtain a good prediction in both frequency regions. Therefore, the author suggests a different comparison, where the spacing and order would be evaluated at estimating the different derived FRFs instead. There is no point in comparing the quality of $H_{z,z}$ for the theoretical results as, for this case, there is no prediction in that curve. Only the derived rotational ones will be investigated.

Figure 5.4 shows the derived $H_{\theta x,z}$ and $H_{\theta x,\theta x}$ FRF curves for the first- and second-order approximations, considering different spacing in the finite-difference formulas. The spacings used corresponded to 1.79%, 3.57% and 7.14% of the total length of the beam and are represented in Figure 5.3 by c, *b* and a, respectively. One percent damping (η=0.01) was artificially added to the translational FRFs to smooth the peaks and to resemble the measured results more closely. As will be shown later, this damping value was slightly high for the higher modes, although its significance was only on the smoothing of the peaks. It is clearly seen by studying Figure 5.4 that the bigger the spacing, the less accurate will be the predictions in the high-frequency region. Moreover, the second-order approximation produced better results

[2] Node referencesin the subsequent figures will always be related to the experimental mesh.

overall. Comparing all the predictions shown there, a compromise of accuracy can be achieved by considering the second-order approximation with spacing s = 0.025 m (i.e. 3.57% of total length). Urgueira [127] concluded in his work that the second-order approximation with 10% of the total length spacing would be the ideal situation. The value suggested in his work proved to be very high for the structure used here, where spacing s = 0.050 m (i.e. 7.14%) is already quite big for the rotation/moment FRF.

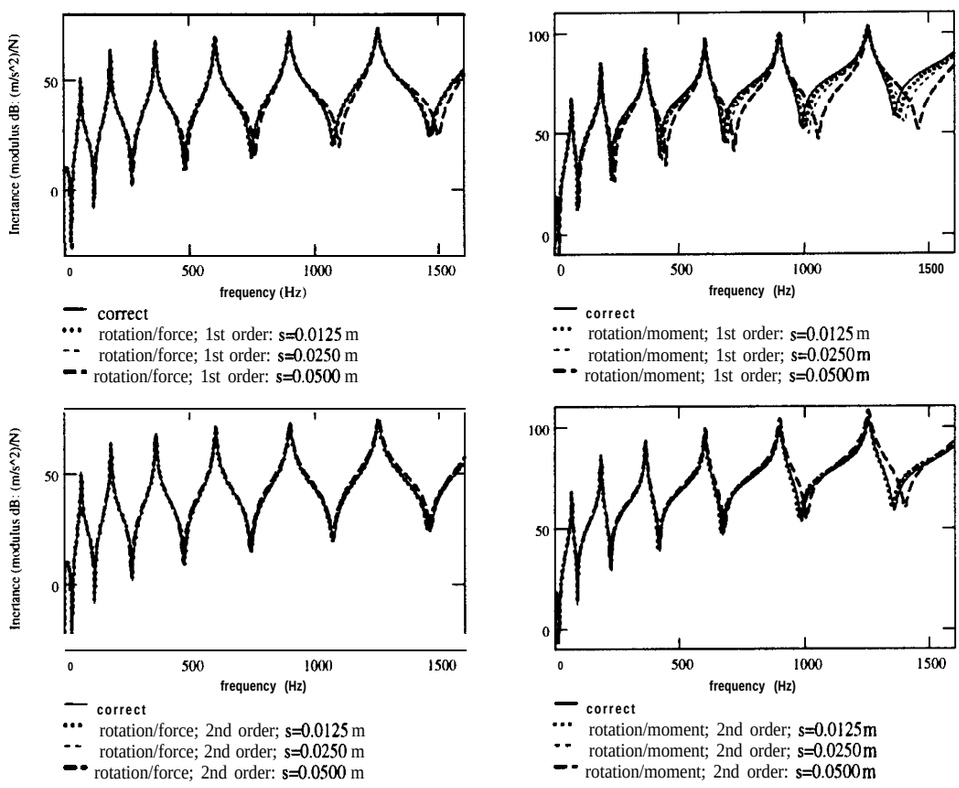

Figure 5.4 - $H_{15\theta x,15z}$ and $H_{15\theta x,15\theta x}$ derived from theoretical translations (different orders and spacing)

Table 5.2 shows a relationship between the order of the approximation and the spacing between accelerometers to obtain the same degree of accuracy for the rotational-related derivations. This table summarises the findings shown in Figure 5.4. For instance, the interpretation of this table says that for a better prediction of $H_{\theta x,z}$, increasing the order of the approximation requires a reduction in the spacing used.

Table 5.2 - Relationship between order of the approximation and spacing for predicting each rotational derived FRF

derived FRF	order	spacing
$H_{\theta x,z}$	↑	↓
$H_{\theta x,\theta x}$	↑	↑

At this point one can analyse the predictions made using experimental FRFs with more confidence. Following the conclusions draw above, s = 0.025 m was adopted for the experimental RDOF derivations used for the coupled structure predictions. Before proceeding however, the first point to be checked is that the translational FRFs used for the RDOF derivations are correct and that this FRF matrix is indeed symmetric. This can be done by performing reciprocity checks. For the majority of linear structures, Maxwell's rule states that the same result should be obtained by either applying a force at coordinate i and measuring the response at coordinate j, or by applying a force at coordinate j and measuring the response at coordinate i. Failure in that rule may indicate changes in the structure under test. These changes may be a result of mass-loading effects of accelerometers and/or force-gauge, shaker-structure iteration, etc., and such problems as these should be avoided. Only two channels could be measured at the time with the analyser employed'. So, to guarantee the quality of the reciprocity check, dummy masses were used at the other accelerometers' locations (as suggested previously). When performing reciprocity checks, nine individual measurements had to be made to derive the necessary rotational quantities using the second-order finite-difference approximation. These could be reduced to six considering the symmetry of the FRF matrix, if no reciprocity check is made.

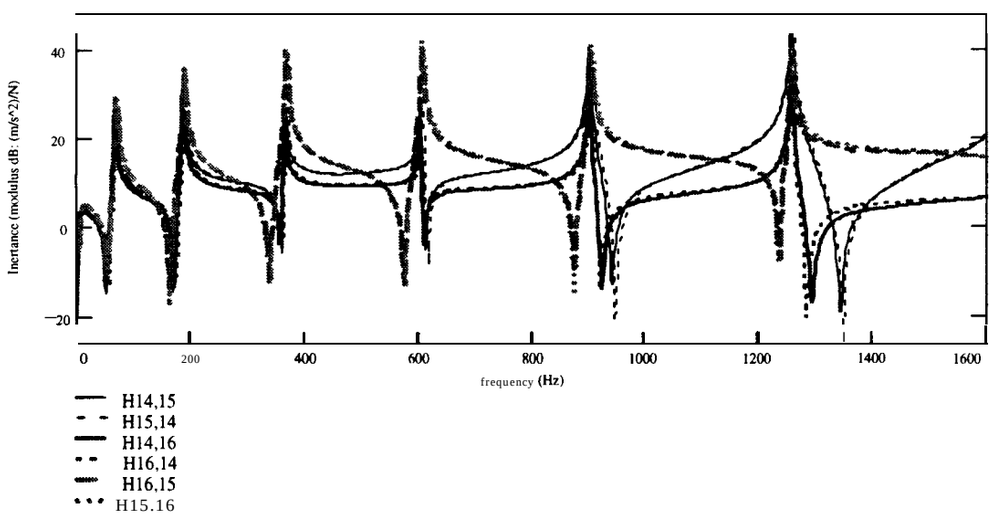

Figure 5.5 - Reciprocity checks for the experimental translational FRFs needed for the rotational derivations, s=0.025 m (z direction)

Figure 5.5 shows the reciprocity check for the translational FRFs needed for the rotational derivations. Apart from a small discrepancy in the last anti-resonance for $H_{14z,16z}$ and $H_{16z,14z}$, all other reciprocity checks were quite good. Following the reciprocity check, the rotational

[3] More information about the experimental set-up and techniques used will be given in chapter 6.

calculations can be performed. For the first-order approximation, two different spacings can be investigated considering the 9 FRFs measured. This is done with the intention of showing the influence of noise when changing the spacing parameter. Two spacing parameters can be considered for the derivation of the rotation/force FRF using the second-order approximation, while only one spacing can be considered for the rotation/moment in this case. A comparison between the measured and the FE-calculated $H_{z,z}$ will be presented for the experimental case to show the quality of the agreement. Although this comparison is shown together with the second-order derivations (Figure 5.9), the curve is not related to the approximation used. The translation/force FRF in any of the approximations corresponds to the FRF curve measured at the point where rotation is required.

Figure 5.6 shows the rotational related predictions using the first-order approximation with two different spacings. The same conclusions as for the theoretical case can be mentioned here, that is, increasing the spacing deteriorates the predictions in the higher frequency range. This problem is worse for the rotation/moment FRF than for the rotation/force FRF. However, there is a feature not easily seen in this figure: the noise in the predictions. To show that more clearly, each of the rotational related FRFs is plotted separately in Figure 5.7. Analysing the results shown there, it should be noticed that noise is normally stronger at the lower frequency range, and it is more pronounced at the rotation/moment FRFs. Increasing the spacing used in the finite-difference formula minimises the noise, although having the side effect of shifting the position of the anti-resonance. Figure 5.8 shows the predictions for the second-order approximation. As seen, $H_{\theta x,z}$ is predicted much better than is $H_{\theta x,\theta x}$. Although noise is very strong in the lower frequency range of the latter FRF, no shift in the anti-resonances is seen in the higher frequency range. As happened with the first-order approximation, increasing the spacing would have the noise effects minimised. However, this would be achieved at the expense of shifting the anti-resonances in the higher frequency region (although this fact is not shown). Figure 5.9 shows the individual FRF predictions for each case considered for the second-order approximation, to highlight these noise effects.

One point not stressed yet is that noise is hardly seen in the translational FRFs used in the calculations. It comes as a consequence of the mathematical manipulation of the data. Comparing the first- and second-order approximations, it is noticed that noise effects are much less strong in the former. So, although the second-order approximation gives better anti-resonance predictions compared with the first-order approximation, the noise effects jeopardise its usefulness. The experimental and FE $H_{z,z}$ curves agree very well with each other.

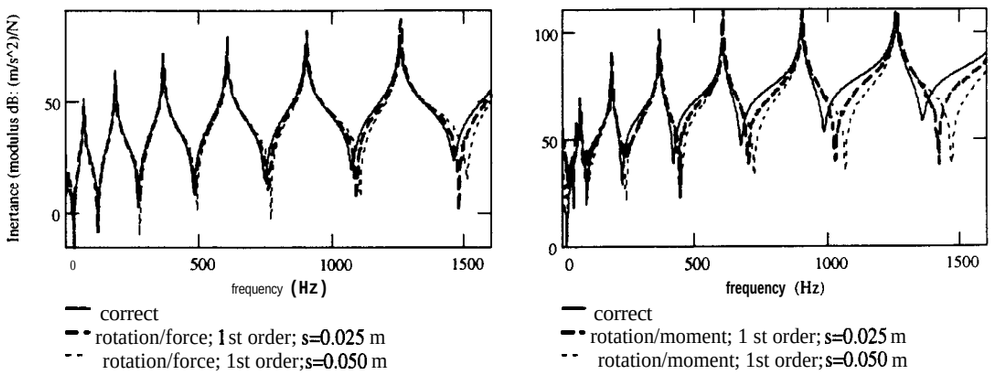

Figure 5.6 - $H_{15\theta x,15z}$ and $H_{15\theta x,15\theta x}$ derived from experimental translations (first-order approximation and different spacings) to show shift in anti-resonances

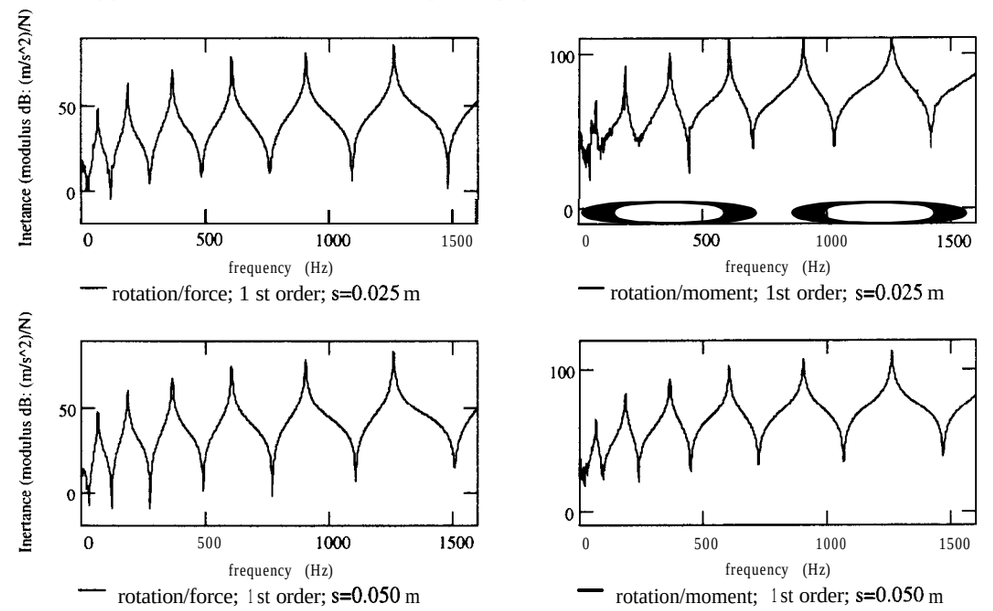

Figure 5.7 - Individual $H_{15\theta x,15z}$ and $H_{15\theta x,15\theta x}$ derived from experimental translations (first-order approximation and different spacings) to highlight noise effects

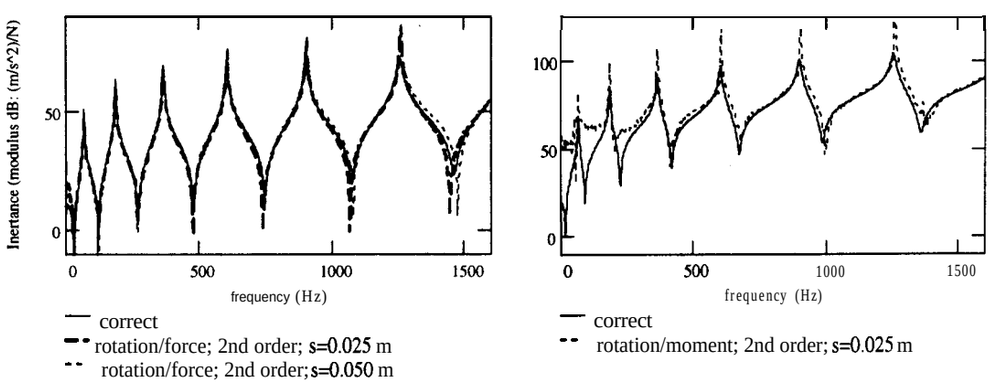

Figure 5.8 - $H_{15\theta x,15z}$ and $H_{15\theta x,15\theta x}$ derived from experimental translations (second-order; different spacings) to show shift in anti-resonances

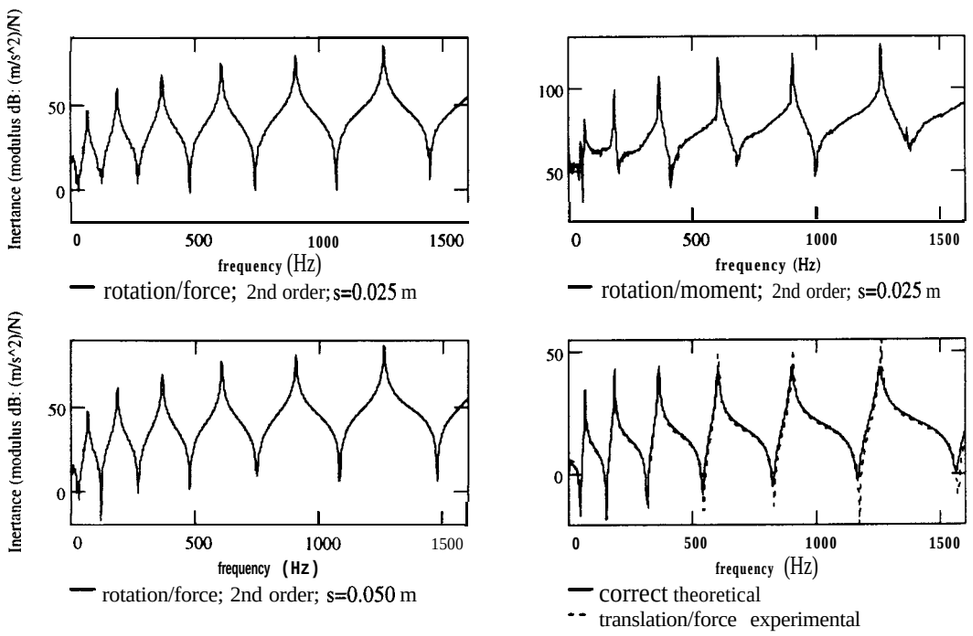

Figure 5.9 - Individual $H_{15\theta x,15z}$ and $H_{15\theta x,15\theta x}$ derived from experimental translations (second-order; different spacings) and theoretical against experimental $H_{15z,15z}$

To minimise the effects of noise, the FRFs had to be smoothed first, as recommended. Several cases will be shown here to highlight the problem of correct residual compensation (Figures 5.10 to 5.14). The results presented are for the second-order finite-difference approximation with spacing s = 0.025 m. Since the theoretical and experimental $H_{z,z}$ curves agreed well with each other, it is assumed that the theoretical data are correct. Therefore, the results presented for the smoothed derived curves will be compared with those. Figure 5.10 shows the rotational-derived FRF curves when using regenerated translational FRFs (i.e. without residual compensation) as input data. The quality of the predictions is very much influenced by the lack of out-of-range modes' information. The last anti-resonance in this case is missed altogether in all the predictions. Figure 5.11 shows the predictions when the input translational FRFs are compensated using a static residual term (equation (4.42), of chapter 4). The predictions are considerably improved when compared with the previous results, although the last anti-resonance is still either not present or with some error on it. Figure 5.12 shows the predictions when using dynamic residual compensation, where the results were improved even further, and Figure 5.13 shows the predictions when using translational FRFs compensated using the pseudo-mode approach introduced in the previous chapter (section 4.6.4.(e)). The difference between this last figure and the following one (Figure 5.14) is that the latter used a consistent eigenvector to obtain the pseudo-mode related to all the columns, while the former used its own eigenvector for each column. These eigenvectors were calculated by measuring three columns

of the FRF matrix and using modal parameter extraction techniques in each of these columns. In this case, slightly different natural frequencies and mode-shapes are calculated for each column as a result of measurement and modal analysis errors. As a consequence, when using these inconsistent input data, the lower frequency anti-resonances lose their shape and look like minima instead. This problem happened, however, only for the $H_{\theta x,z}$ curve. Comparing Figure 5.13 with Figure 5.9, it can be seen that this loss in shape is in reality a smoothed version of the noise data presented in the latter. When the consistent pseudo-mode compensated input data was used, the derived FRFs are very good compared with the theoretical results.

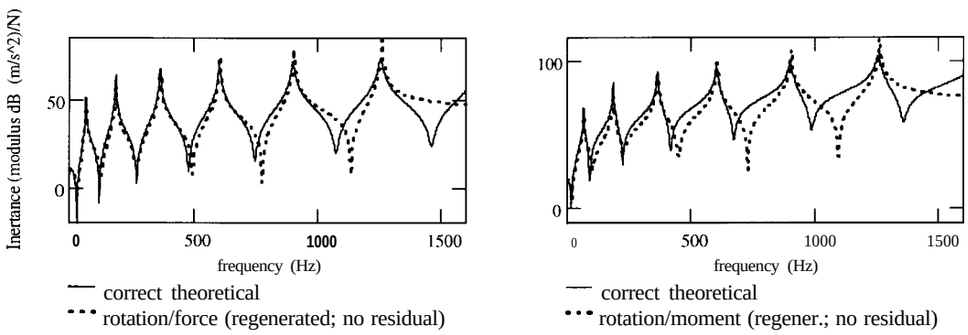

Figure 5.10 - Rotational derived FRFs using regenerated translational FRFs (second-order approximation; s = 0.025 m)

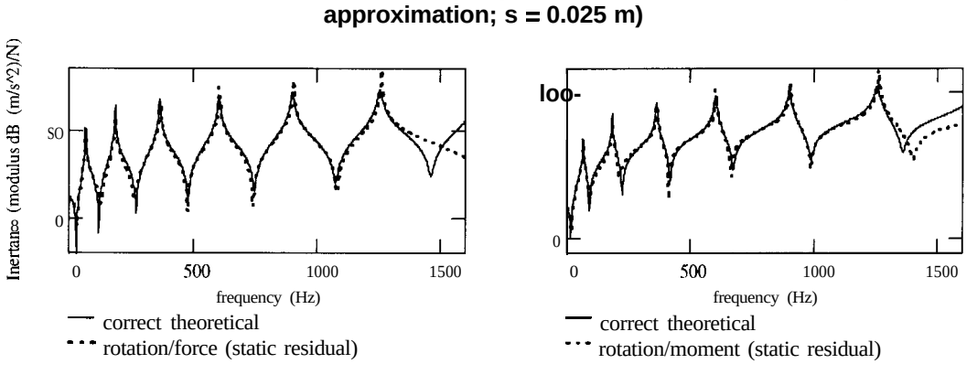

Figure 5.11 - Rotational derived FRFs using static-residual compensated translational FRFs (second-order approximation; s = 0.025 m)

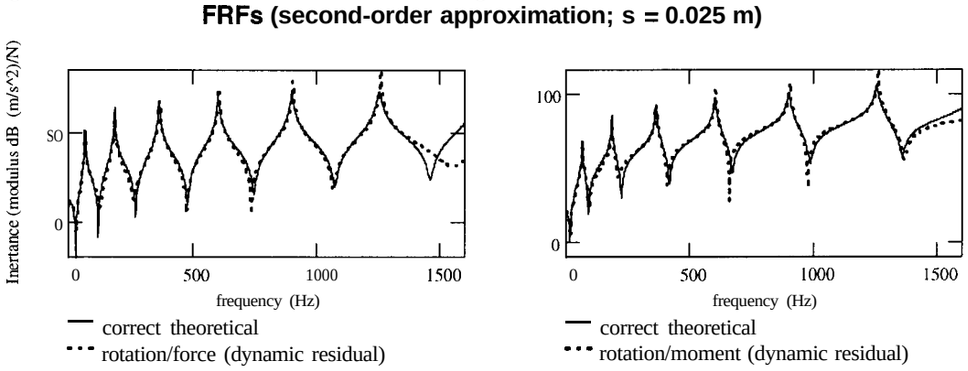

Figure 5.12 - Rotational derived FRFs using dynamic-residual compensated translational FRFs (second-order approximation; s = 0.025 m)

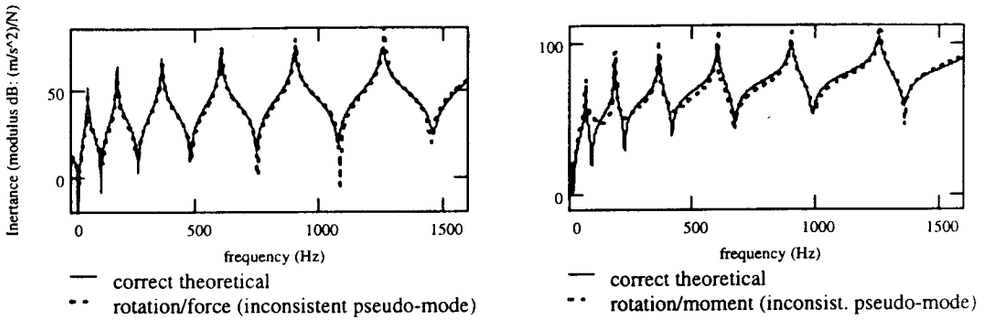

Figure 5.13 - Rotational derived FRFs using inconsistent pseudo-mode compensated translational FRFs (second-order approximation; s = 0.025 m)

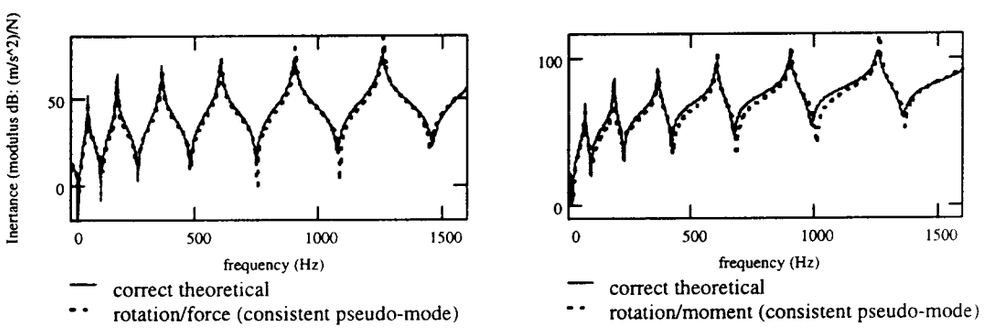

Figure 5.14 - Rotational derived FRFs using consistent pseudo-mode compensated translational FRFs (second-order approximation; s = 0.025 m)

Having shown the rotational FRF predictions obtained from the FRF-based approach, the modal-based approach is investigated next. Most of the results here will be calculated using the theoretical translations. To simplify the presentation of the results, however, no damping is considered this time. This is justified by the fact that only an indication about spacing and order of the approximation to be used are required here and damping will not affect that. The first parameters compared are the derived residual matrices.

Table 5.3 shows the correct theoretical static residual matrix for comparison with the matrices derived using first- and second-order theoretical approximations (different spacings). For each of the derived values, the corresponding error associated with it (when compared with the correct ones) is given. Analysing this table, it can be seen that it does not matter which approximation or spacing is used, the rotation/force residual values are normally predicted better than the rotation/moment residual values. The exception is for the second-order approximation with s = 0.025 m. The smallest error for the rotation/moment residual value was obtained using this combination and since $R_{\theta x,\theta x}$ is the most important quantity (the residual is stronger), the use of second-order approximation with s = 0.025 m is recommended in this case.

Table 5.3 - Theoretical static residual matrix: correct, first- and second-order approximations ($x10^7$)

correct					
0.3749	-19.1482				
-19.1482	1342.9968	1st order		2nd order	
	s=0.0125	0.3749	-18.6924	0.3749	-20.5641
		-18.6924	1079.1917	-20.5641	1539.9664
	error	0%	2.4%	0%	-7.4%
		2.4%	19.6%	-7.4%	-14.7%
	s=0.025	0.3749	-16.8207	0.3749	-22.0056
		-16.8207	796.651	-22.0056	1523.5267
	error	0%	12.2%	0%	-14.9%
		12.2%	40.7%	-14.9%	-13.4%
	s=0.050	0.3749	-11.6359	0.3749	-19.8527
		-11.6359	373.6458	-19.8527	1121.4183
	error	0%	39.2%	0%	-3.7%
		39.2%	72.2%	-3.7%	16.5%

Table 5.4 - Theoretical dynamic residual matrix: correct, first- and second-order approximations ($x10^{15}$)

correct					
0.1985	-8.1514				
-8.1514	345.6268	1st order		2nd order	
	s=0.0125	0.1985	-8.1068	0.1985	-8.4044
		-8.1068	340.7381	-8.4044	371.0851
	error	0%	0.5%	0%	-3.1%
		0.5%	1.4%	-3.1%	-7.4%
	s=0.025	0.1985	-7.8093	0.1985	-9.2603
		-7.8093	312.9477	-9.2603	454.097
	error	0%	4.2%	0%	-13.6%
		4.2%	9.5%	-13.6%	-31.4%
	s=0.050	0.1985	-6.3582	0.1985	-10.5446
		-6.3582	204.2165	-10.5446	567.302
	error	0%	2 22%	0%	-29.4%
		22%	40.9%	-29.4%	-64.1%

Table 5.4 shows the same set of results but now for the dynamic residual matrix. The errors associated with this matrix are much smaller than that obtained for the static residual matrix. However, it has to be stressed that the values of the dynamic residual terms are very small in any case (i.e. to the power of 10^{15}, against the 10' for the static residual terms). Although some of these errors seem to be very large, when they are used in the improvement of the regenerated matrix, due to their small value, they manage to compensate quite well. This fact will be illustrated later. No higher-order residual matrices will be considered, as the modal-based approach is more suitable for deriving the parameters necessary for the CMS technique and only two residual matrices are required without increasing the complexity of the formulations.

The other parameters that have to be compared in a modal-based approach are the rotational-derived mode-shapes. Table 5.5 shows the necessary translational mode-shape values for the different spacings adopted in this study. The values presented are such that both first- and

second-order approximation can be used. The experimental mode-shape values for s = 0.025 m are also given so to compare with the theoretical ones. As the structure was tested in a "free-free" configuration, the first two modes are actually the rigid-body modes. For the experimental mode-shape values, these rigid-body modes were calculated considering the geometry of the structure [127] and were mass-normalised using Gram-Schmidt orthogonalization [89]. Despite the apparent disagreement between theoretical and experimental values, when comparing the FRF curves regenerated using such parameters, the discrepancy is not as strong as it seems. This fact will not be shown here and will be reserved until the comparison is made of the FRF curves regenerated from the derived modal parameters using such translational parameters. The error for the necessary experimental mode-shape values is stronger at node 14, as most of these values have very small amplitudes due to the proximity of modal lines, especially for modes 5 and 6.

Table 5.5 - Translational mode-shapes needed for the first- and second-order approximation (different spacings)

type	spacing	node	m1	m2	m3	m4	m5	m6	m7	m8
theor.	s=0.0125	55	-0.6668	-1.0447	1.0474	0.869	0.7078	0.5548	0.4	606
		56	-0.6668	-1.0854	1.1565	1.0527	0.9636	0.8825	0.8	276
		57	-0.6668	-1.1262	1.2656	1.2367	1.2208	1.2139	1.2	101
theor.	s=0.025	49	-0.6668	-0.9631	0.8298	0.5061	0.2125	-0.0585	-0.3	5112
		55	-0.6668	-1.0447	1.0474	0.869	0.7078	0.5548	0.4	606
		57	-0.6668	-1.1262	1.2656	1.2367	1.2208	1.2139	1.2	101
exp.	s=0.025	14	-0.672	-0.997	0.811	0.45	0.158	-0.11	-0.346	-0.547
		16	-0.672	-1.08	1.025	0.847	0.665	0.513	0.372	0.225
		15	-0.672	-1.164	1.234	1.166	1.154	1.128	1.141	1.133
	error	14	-0.78	-3.52	2.27	11.08	25.65	-88.03	-14.49	-7
		16	-0.78	-3.38	2.14	2.53	6.05	7.53	8.49	13.66
		15	-0.78	-3.36	2.5	5.72	5.47	7.08	5.84	6.37
theor.	s=0.050	47	-0.6668	-0.7999	0.4036	-0.161	-0.5839	-0.8329	-0.8755	-0.7107
		49	-0.6668	-0.9631	0.8298	0.5061	0.2125	-0.0585	-0.3022	-0.5112
		57	-0.6668	-1.1262	1.2656	1.2367	1.2208	1.2139	1.2118	1.2101

Table 5.6 shows both the translational and rotational-derived mode-shape values at node 15. Actually, only the rotational values are derived, as the translational ones are the same as the input ones at this coordinate. Analysing the derived values using theoretical input, it is noticed that using the first-order approximation with the smallest spacing produced the best predictions. Increasing both the order and the spacing deteriorates the predictions as one goes to the higher modes. The second-order with s = 0.0125 m produced more or less the same accuracy as the first-order with s = 0.025 m. As for the experimental results, despite the biggest errors for the measured mode-shapes being related to modes 5 and 6 (as quoted), the derived rotational parameters at these modes did not have the same degree of error. For the experimental results, the first-order approximation produced the best predictions for the lower modes, while the second-order approximation produced the best predictions for the higher ones.

Table 5.6 - Derived mode-shapes at tip node 15

type	approx.	coord.	m1	m2	m3	m4	m5	m6	m7	m8
theor.	correct	z	-0.6668	-1.1262	1.2656	1.2367	1.2208	1.2139	1.2118	1.2101
		θx	0	3.2636	-8.7322	-14.7245	-20.581	-26.5264	-32.5743	-38.676
theor.	1st-order	z	-0.6668	-1.1262	1.2656	1.2367	1.2208	1.2139	1.2118	1.2101
	s=0.0125	θx	0	3.2636	-8.732	-14.723	-20.5751	-26.5096	-32.5355	-38.598
	% error	θx	0	0	0	0	0	0.1	0.1	0.2
theor.	2nd-order	z	-0.6668	-1.1262	1.2656	1.2367	1.2208	1.2139	1.2118	1.2101
	s=0.0125	θx	0	3.2636	-8.734	-14.7375	-20.6295	-26.6562	-32.8581	-39.217
	% error	θx	0	0	0	-0.1	-0.2	-0.5	-0.9	-1.4
theor.	1st-order	z	-0.6668	-1.1262	1.2656	1.2367	1.2208	1.2139	1.2118	1.2101
	s=0.025	θx	0	3.2636	-8.73	-14.7086	-20.5206	-26.3631	-32.2129	-37.978
	% error	θx	0	0	0	0.1	0.3	0.6	1.1	1.8
theor.	2nd-order	z	-0.6668	-1.1262	1.2656	1.2367	1.2208	1.2139	1.2118	1.2101
	s=0.025	θx	0	3.2636	-8.7437	-14.8059	-20.8741	-27.2781	-34.1456	-41.5306
	% error	θx	0	0	-0.1	-0.6	-1.4	-2.8	-4.8	-7.4
exp.	1st-order	z	-0.672	-1.164	1.234	1.166	1.154	1.128	1.141	1.133
	s=0.025	θx	0	3.36	-8.36	-12.76	-19.56	-24.6	-30.76	-36.32
	% error	z	-0.8	-3.4	2.5	5.7	5.5	7.1	5.8	6.4
		θx	0	-3	4.3	13.3	5	7.3	5.6	6.1
exp.	2nd-order	z	-0.672	-1.164	1.234	1.166	1.154	1.128	1.141	1.133
	s=0.025	θx	0	3.38	-8.26	-11.2	-19.2	-24.44	-31.78	-39.04
	% error	z	-0.8	-3.4	2.5	5.7	5.5	7.1	5.8	6.4
		θx	0	-3.6	5.4	23.9	6.7	7.9	2.4	-0.9
theor.	1st-order	z	-0.6668	-1.1262	1.2656	1.2367	1.2208	1.2139	1.2118	1.2101
	s=0.050	θx	0	3.2635	-8.7164	-14.6113	-20.1672	-25.4481	-30.2802	-34.426
	% error	θx	0	0	0.2	0.8	2	4.1	7	11
theor.	2nd-order	z	-0.6668	-1.1262	1.2656	1.2367	1.2208	1.2139	1.2118	1.2101
	s=0.050	θx	0	3.2636	-8.8121	-15.246	-22.2875	-30.4282	-39.6871	-49.643
	% error	θx	0	0	-0.9	-3.5	-8.3	-14.7	-21.8	-28.4

Nevertheless, analysing the derived modal parameters and residual matrices separately does not give an overall view of the quality of the FRF predictions using such parameters. To that end, these parameters will be used in the regeneration of FRF curves and these curves will be compared. Initially, the regenerated curves without any residual compensation will be considered. The experimentally-derived $H_{15z,15\theta x}$ and $H_{15\theta x,15\theta x}$ will be plotted together with the correct and theoretically derived curves, so as to show the effects of the errors. This is presented in Figure 5.15 and Figure 5.16, respectively. As the experimental spacing between accelerometers for the RDOF derivations was considered as s = 0.025 m, only this theoretical case will be shown. Although the correct FRF curve is not plotted in these figures, comparing the curves here with the ones presented in Figure 5.10, it is noticed that the same predictions are obtained. Despite the error associated with the derived experimental mode-shapes, the regenerated FRFs using such data are not very different from the regenerated ones using the correct data. The only major discrepancies are for $H_{15\theta x,15\theta x}$ using second-order approximation, where the errors are much higher. For both derived FRF curves, using the first-order approximation produced a better FRF prediction.

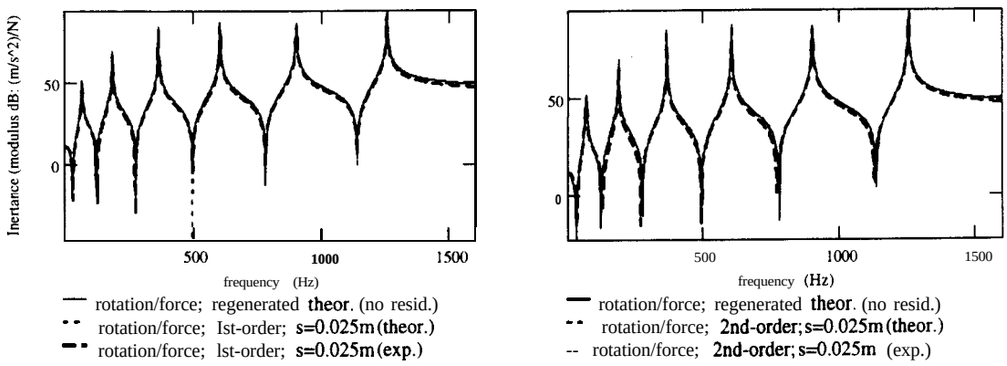

Figure 5.15 - Regenerated $H_{15z,15\theta x}$ (no residual) using modal data presented in Table 5.6

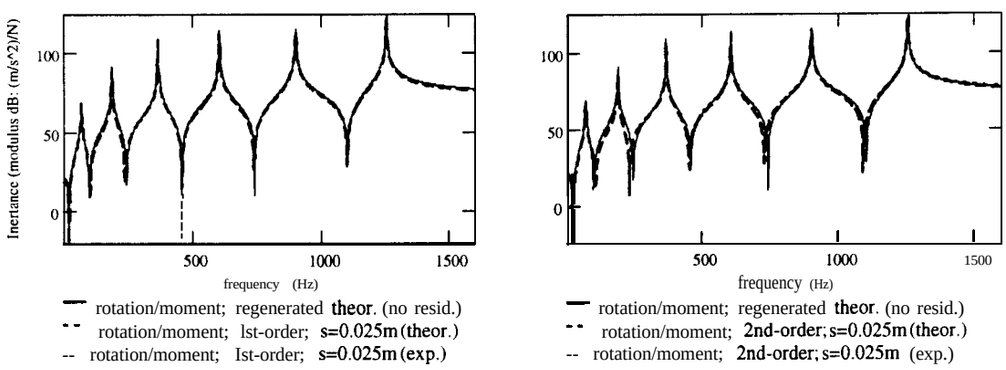

Figure 5.16 - Regenerated $H_{15\theta x,15\theta x}$ (no residual) using modal data presented in Table 5.6

However, the regenerated-derived curves are not yet the correct ones due to the lack of high-frequency residual terms. To improve the quality of these curves, residual terms have to be included. As mentioned previously, only the static and dynamic residual compensation matrices will be investigated here, as the modal-based approach is to be used more with CMS formulations. The results using these compensation matrices for $H_{15z,15\theta x}$ and $H_{15\theta x,15\theta x}$ are shown in Figure 5.17 and Figure 5.18, respectively. There, combinations between approximations used for derived modal parameters and derived residual matrices are presented so as to compare with the correct theoretical results. The first curve in each set is the correct FRF, followed by the regenerated curve compensated by static residual term and finally, the regenerated curve compensated by both static and dynamic residual terms. Some interesting facts happened. The results of the approximations should not be better than the results using the correct residual matrices. Nevertheless, since they are approximations, this is not what happens. For both derived FRF curves, i.e. $H_{15z,15\theta x}$ and $H_{15\theta x,15\theta x}$, the best predictions were obtained using the first-order approximation for the modal parameters and the second-order approximation for the residual matrices. The predictions for this combination are even better than the ones using the correct residual matrices and presented in the first set of curves for each figure.

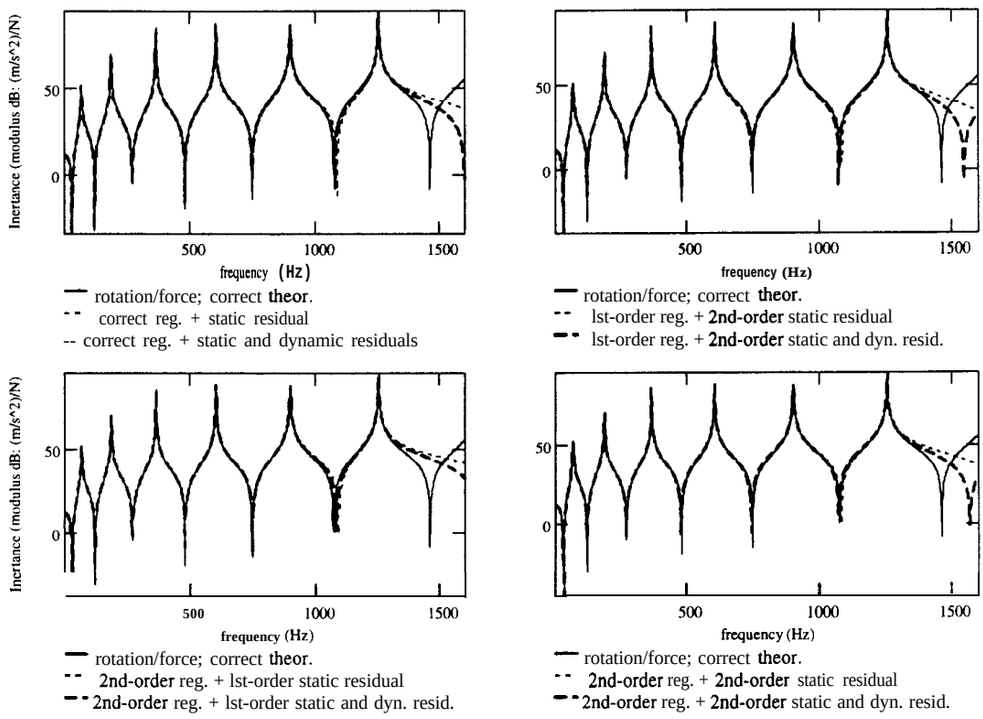

Figure 5.17 - Regenerated $H_{15z,15\theta x}$ using modal data presented in Table 5.6 + residual compensations given by Table 5.3 and Table 5.4

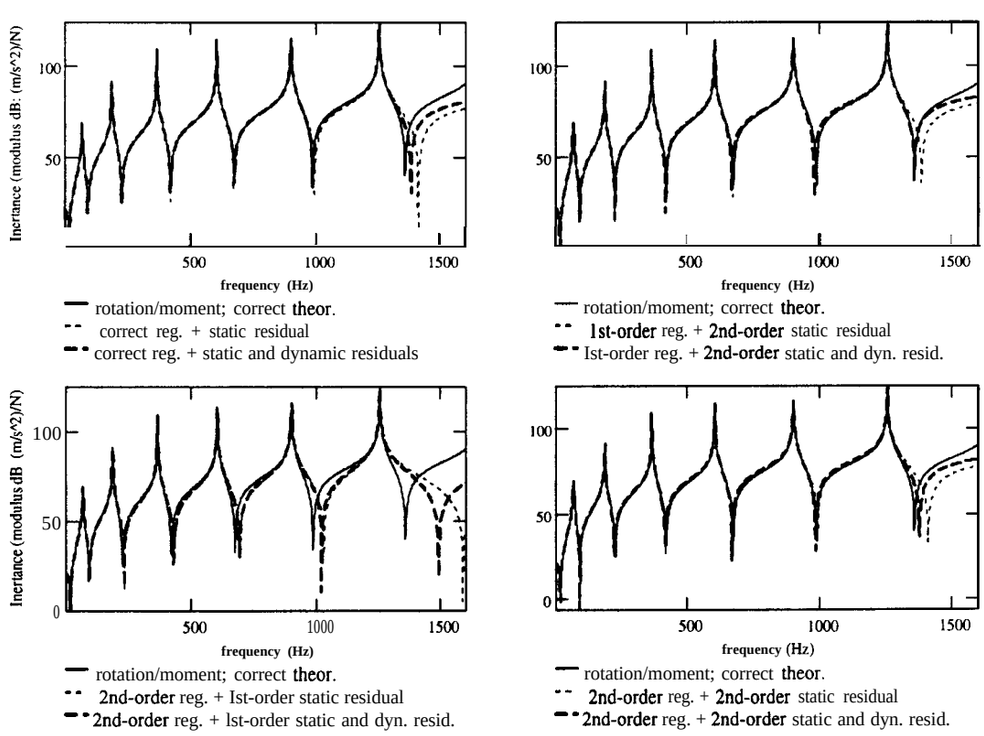

Figure 5.18 - Regenerated $H_{15\theta x,15\theta x}$ using modal data presented in Table 5.6 + residual compensations given by Table 5.3 and Table 5.4

5.6. CONCLUSIONS OF THE CHAPTER

In this chapter, the spatial incompleteness problem associated with the lack of RDOFs in experimentally-derived models was addressed. The finite-difference approach was chosen to be used to derive such parameters due to the simplicity of its implementation, while good accuracy can be obtained. In this approach, noise effects are strongly amplified in the derived curves when using raw FRF data. Therefore, the smoothing of the translational FRFs prior to the calculations is recommended (i.e. the use of experimentally-derived models), where the inclusion of enough modes and the use of a consistent modal data set are important. Any residual compensation can be used to smooth the curves. For the results presented here, the consistent pseudo-mode approximation managed to produce very accurate results.

The quality of the predictions is dependent on the spacing and order used in the approximation and these two points are inter-related. Increasing the approximation order for the rotation/force FRF requires a smaller spacing between the transducers. On the other hand, increasing the order for the rotation/moment FRF requires a larger spacing. The choice of spacing is related to the mode-shapes of the structure in the frequency range of interest. The first-order approximation generally produces better results for the rotation/force FRFs, while the second-order approximation produces better results for the rotation/moment FRFs.

Instead of smoothing the FRFs and deriving the rotational related FRFs from these smoothed curves, modal parameters and residual matrices can be used instead. The advantage of using this latter approach is that a mixture of approximations is possible, resulting in better predictions. In addition, this approach provides the necessary input data for CMS formulations directly. Moreover, consistent modal parameters are used and smoothed FRF curves can be obtained if required. The first-order approximation is better for deriving rotational modal parameters, while the second-order approximation is better for deriving FRFs or residual-related parameters. The spacing between accelerometers remains an issue, with the same previous comment applying here.

CHAPTER 6: EXPERIMENTAL CASE STUDY

6.1. OBJECTIVES

After all the essential theory has been presented, the next step is to validate it using real test data. Such a procedure is necessary since the majority of the validations performed up until now used simulated data instead of real data and did not always represent real-world situations. Of particular concern are the coupling formulations and the techniques for solving some of their problems, specifically, residuals and RDOFs. Despite the use of simple structures in this chapter, important points were noticed that can be extrapolated to more complex cases. In addition, the theory should work regardless of the complexity of the structures involved and using a simple test case was considered enough for their experimental validation.

The main objective of this chapter is to verify the FRF coupling and CMS formulations when using real **experimentally-derived models.** As discussed previously, such models are required either because of natural frequencies' inconsistencies and noise effects (FRF coupling) or due to the type of formulation (CMS). This requirement will be demonstrated during the development of the chapter. Considering this main objective, some additional objectives were set. These are as follows:

- to show the importance of properly choosing the measurement points; and
- to show the importance of properly positioning the transducers exactly at the chosen measurement points;
- to show the need for residual compensation and RDOFs. Therefore:
  - to compare the different residual compensation techniques (mainly those developed by the author) when using real data and according to the coupling formulation used;
  - to validate the finite-difference RDOFs derivation;
- to compare the results from the coupling formulations and to give some guidelines into that;
- to show the usefulness of the FL and IF1 (or FIF) curves in comparing FRFs collectively.

Some of these objectives are interrelated. For example, the importance of properly choosing the measurement points is related to the derivation of the RDOFs. The positioning of the

transducers is linked with the residual problem and so on. More about these and the other points will be explained in the following sections. First, the test structures and experimental set-up used in the studies are described.

6.2. TEST STRUCTURES

As briefly mentioned in chapter 5, two beams were used for the validation of the techniques presented in this thesis. First, they were tested separately so as to use their data in the experimental coupling formulations. Then, they were welded together and tested again in order to compare the results obtained in the previous step with the ones obtained for the whole structure. Here, the individual beams are referred to as ***long*** and ***short*** beams, whereas the whole beam is referred to as the ***coupled*** beam.

Instead of having the additional worry about mass loading effects of the "transducers", the individual structures were considered collectively. This means that, actually, each structure consisted of the beam itself, plus one accelerometer and 2 dummy masses. These masses were used to avoid reciprocity problems when measuring the translational FRFs required for the rotational derivations (as explained in chapter 5 and addressed again later). Such an assumption does not invalidate the study reported here. The long beam was described in section 5.5 of chapter 5 (see Figure 5.3) and will not be repeated here. Its weight is 2.22 Kg and is stated in order to be compared with the weight of the accelerometer chosen.

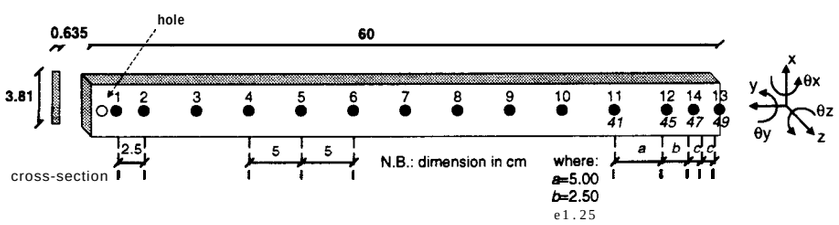

Figure 6.1 - Short beam used for the experimental validations

The short beam is shown in Figure 6.1. It was also made of mild steel, and had dimensions 60 x 3.81 x 0.635 cm. Its weight is 1.14 Kg. Although 6 directions are shown in this figure, only one plane of symmetry was again considered (z and θx), ignoring, therefore, motion in and about the axial direction. Since the lengths of the beams are not that different, the same mesh spacing used for the long beam was assumed for both (that is, 5 cm and 1.25 cm for the experimental and the FE meshes, respectively). This spacing resulted in 13 experimental nodes (with one extra node used for the rotational derivation - node 14) and 49 FE nodes. This beam was also tested in a "free-free" configuration, suspended by soft elastic bands close to experimental node

number 1 (located 2.5 cm from the tip because of the suspension used). The coupling node considered for this structure is at the other end of the beam (i.e. experimental node 13 or FE node 49)' and it is, therefore, the node where the RDOF derivations[2] are required. The correspondence between the FE and experimental nodes needed for the rotational derivation studies is also shown in this figure, since some comparisons of results were performed between them. The beam was excited at the neutral axis such that no torsional modes were excited.

Figure 6.2 shows the assembly of the two individual beams to yield the coupled beam. However, only the experimental nodes are sketched this time. Moreover, to keep the same numbers as for the individual beams and to avoid confusion by doing that, S and L were added to each node number to represent short and long beam nodes, respectively. Only the coupling coordinate was re-numbered and is called 1C now (which corresponds to either 13S or 15L, as shown in this figure). It should be noticed that the original axis system for the long beam was changed (although the axes are not drawn there), since the coupled beam was tested suspended at the hole located on the short beam (close to node 1S). This observation is very important when performing the coupling calculations, since the off-diagonal FRFs in the FRF coupling formulation, as well as the RDOF for the CMS formulation, have their signs changed by that. This point will be demonstrated in the respective sections.

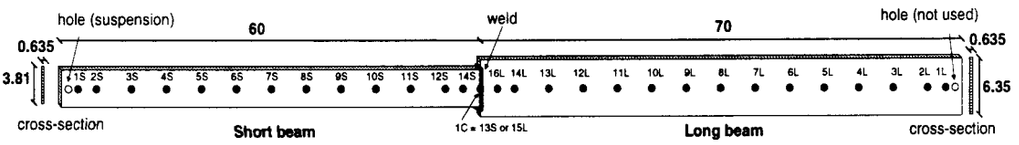

Figure 6.2 - Coupled beam used for the experimental validations

6.3. EXPERIMENTAL SET-UP AND FURTHER CONSIDERATIONS

In order to keep the tests simple and to avoid shaker-structure interaction problems, hammer excitation was used. This type of test, although one of the simplest to set the structure into vibration, is not without its own problems and these will be addressed towards the end in this section. The excitation is provided by an impact hammer, usually with a set of different tips and heads which are used to extend the frequency and force level ranges for testing. The softer the tip, the lower the frequencies one can excite and the harder the tip, the higher the frequencies

[1] Node references in the subsequent figures will always be related to theexperimental mesh.
[2] By RDOF derivations one means both the rotational amplitude derivations and the rotational FRF derivations.

one can excite. It is very important in this type of test to make the correct choice of the hammer tip in order to ensure the desired level of the response measured. Attached with the impactor there is a force transducer to detect the force felt by the impactor which is equal and opposite in sign to that felt by the structure. In a hammer test, the accelerometer is kept at a fixed point and the force transducer (which is attached to the hammer) is moved around all the points on the mesh. By doing this, one row of the full FRF matrix is obtained. Following Maxwell's reciprocity rule, this row would be equivalent to its corresponding column. If rotational derivations are required, extra measurements have to be made (as will be explained in more detail in section 6.5). Figure 6.3 shows the set-up of the equipment for a hammer test.

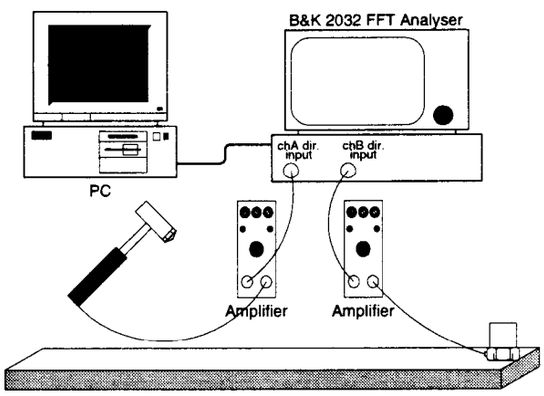

Figure 6.3 - Experimental set-up for hammer testing

Before each test is carried out, it is important to perform a calibration of the instruments used to make sure that the sensitivity has been set up properly [41]. The same procedure is followed at the end of each test to guarantee that nothing has been changed during the tests. A relatively simple technique provides a convenient solution to this task. As the concern is with the ratio of acceleration to force, and not with the absolute value of either individual parameter, it would suffice to calibrate the ratio of the sensitivities of the two channels, resulting in a calibration factor of the form: xxx volts/volts of acceleration/force. A suitable procedure for the simultaneous calibration of a response channel together with the force channel is thus to measure the accelerance of a rigid mass whose mass is accurately know. This ratio will have the units of l/mass. For example, when using a 10 Kg mass in the calibration, one should obtain a flat line at the accelerance value of -20 dB (re 1 ms^{-2}/N). This was the calibration procedure used.

For all tests reported here (i.e. on the short, long and coupled beams), the excitation was applied by a PCB hammer and the responses were measured by a B&K type 4367 accelerometer (with cross-axis sensitivity of 1.3% and 13.3 grams weight). The accelerometer was fixed at each measurement point using beeswax. Exceptions to this procedure were those

measurement points related to the rotational derivation, where the accelerometer was fixed using mounting pads glued to the structure. Such a procedure was adopted to guarantee that the responses were always measured at the same positions, since the analyser used could only measure two channels at a time. As a result, the accelerometer had to be moved for each translational measurement used in the RDOF derivations. The dummy masses were also moved to avoid reciprocity problems in this case. The FRFs were acquired using a B&K 2032 FFT analyser with the H_1 option chosen (i.e. cross spectrum between the response and force signals over the auto-spectra of the force [41]). A typical set-up of the analyser for a hammer test is shown in Table 6.1. Values between brackets are those changed from one structure to the other.

Table 6.1 - Set-up on the B&K analyser for a hammer test:

MEASUREMENT	Dual Spectrum Averaging		
TRIGGER	Ch. A +Slope LEVEL: +0.10 MAX. INPUT		
DELAY	TRIG. A: -5.12 ms Ch A→B: 0.00 ms		
AVERAGING	Linear 3 Auto accent		
FREQ. SPAN	1.6 kHz	ΔF: 2 Hz T: 500 ms	ΔT: 244μs
CENTRE FREQ.	Baseband		
WEIGHT CH. A	Transient	SHIFT:(3.90) ms	LENGTH:(9.03) ms
WEIGHT CH. B	Exponential	SHIFT:(2.19) ms	LENGTH:(133.78) ms
GENERATOR	disabled		

Some observations need to be made related to this table. The measured frequency range of interest for the structures tested was set from 0 Hz to 1600 Hz. This includes 5 flexural modes for the short beam, 6 flexural modes for the long beam and 13 flexural modes for the coupled beam. When one sets up the frequency span to the value above into the analyser, the analyser reads 2048 data points from the A/D converter and stores them into the time record. A frequency resolution of 2 Hz, a record length of 500 ms and a sampling interval of 244 μs are automatically set up as a result of being directly related with this frequency span. These 2048 real numbers can be converted into a spectrum of 1024 complex lines. However, as the anti aliasing filter has no sharp cut-off-frequency, only 801 lines are displayed. Since there was no need for zoom measurements (which could be required as a result of poor frequency resolution, for example), baseband option was used throughout the tests.

Channel A is the force transducer signal and Channel B is the acceleration response signal. Due to the instantaneous nature of the force, transient window should be used with the former. On the other hand, exponential window should be used with the latter since: (1) most of the important information is concentrated in the initial part of the time record and (2) to guarantee that the signal has been processed before the other one starts. The correct selection of the

exponential window length is important, since the shorter it is, the higher the value of damping artificially imposed to the measured system. This imposed damping cannot easily be separated from the true damping.

The format of display chosen in these tests was the magnitude of the frequency response H_1, together with the coherence. DUAL SPECTRUM AVERAGING was used to obtain the coherence value. Normally for a hammer test, an average of 5 impacts is used. However, the more one increases the number of impacts, the more difficult it is to get a coherence near unity (which means, good coherence). For this reason, the number of impacts chosen in the present tests was only 3, which turned out to be the best value for the average. Using only one average, although giving a good coherence, may not give a good FRF curve (since noise problems are not average out) and does not guarantee the correct location of the anti-resonances. This latter comment results from the difficulty of assuring where the structure is hit. Averaging the hits may indicate some problems in that respect, although it does not necessary say that the location of the hit is correct. Nevertheless, is very unlikely that a mistake is going to be repeated in every hit. If the structure is hit in different positions, low coherence around the anti-resonances is obtained as a result and this is one of the known sources of low coherence in impact tests.

When using a hammer test, apart from coherence problems, an additional and most serious problem can happen: the occurrence of double hits. This problem is common when the structure under test is not very heavy and is tested under free-free condition, since the structure can bounce back into the hammer. Both these problems were carefully monitored and avoided in the results reported here, although at the expense of a lengthier test. Double hits create difficulties in the signal processing stage and the way they were avoided was by using a lighter hammer (PCB hammer) and hitting the structure cautiously.

6.4. MEASUREMENT OF TRANSLATIONAL FRFS

6.4.1. INTRODUCTION

Only translational FRFs were measured for all structures of interest, with the necessary rotational FRFs or modal parameters derived from that. The procedure used for the latter was described in chapter 5 and will be addressed again in section 6.5. Returning to the translational FRFs, the first thing done was to choose the measurement mesh. In fact, this was decided considering the total length of the beams and an FE pre-analysis. As quoted in section 6.2, the same mesh spacing was used (i.e. 5 cm) for all beams.

The translational FRFs and their respective modal parameters were obtained by measuring the response at the coupling node and moving the excitation around the other nodes so as to obtain the bottom row of the FRF matrix. This meant that node13S was used for the short beam, node 15L for the long beam and node1C for the coupled beam. Additional measurements were made for the RDOF derivation, but this will be addressed later. After measuring the entire row of FRFs, these curves were compared with the FE pre-analysis curves and some discrepancies were found around the anti-resonances. Studies were performed to try to establish why this had happened and it was discovered that the accelerometer was not properly placed at the tip of the beams. This problem is discussed further in the following section.

6.4.2. IMPORTANCE OF THE TRANSDUCER'S POSITIONS

One of the problems with small structures is the correct placement of the transducers, mainly when the measurement is related to coupling coordinates and further use is to be made of the data. As will be demonstrated here, small shifts in the correct location of the transducers cause the anti-resonances to be shifted from their correct positions as well. Such an effect is the same as that caused by the lack of residual terms, although it may occur in a different extent. So, if just the FRF curves are available to the analyst to perform an FRF coupling analysis, wrong predictions will be obtained as a result and that will be difficult to trace from either reason.

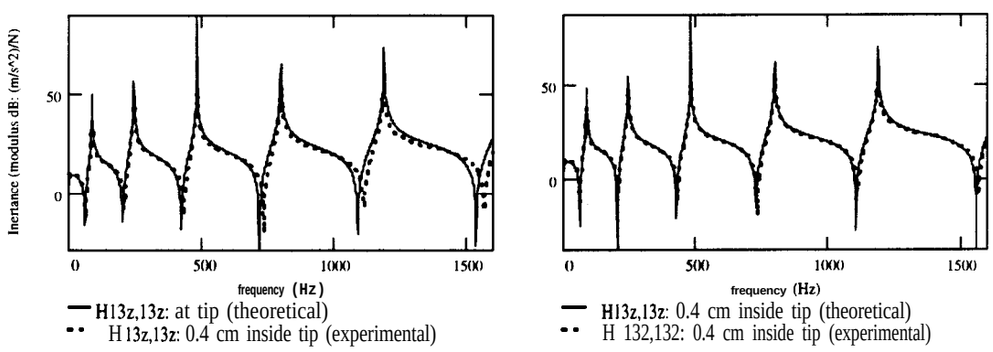

Figure 6.4 - Short beam experimental versus theoretical FRF curves for different accelerometer position ($H_{13z,13z}$)

In order to make sure that the differences observed between the experimental FRFs and those obtained from FE solution were caused by the shift in the accelerometer position, the beams were re-analysed. The FE mesh this time accounted for the position where the accelerometer was fixed experimentally (i.e. 0.4 cm from the tip of beam). The FE curves still did not include any damping effects. Figure 6.4 shows two comparison plots between the experimental and FE obtained FRF curves. On the left-hand plot, the FE assumed the accelerometer at the very tip of

the beam, while the experimental FRF had the transducer actually located 0.4 cm to the inside. On the right-hand plot, the FE was corrected to allow the accelerometer to be located as it was experimentally. The results now agreed much better.

In fact, only two experimental FRFs close to the suspension point did not agree with the new FE-obtained curves and this disagreement occurred around their strong anti-resonances. Figure 6.5 shows the referred FRFs, together with their coherence plots. As seen, the coherence plots have a lot of noise around the region where the mismatch occurred, and that may explain the reason for the discrepancies. Just for the sake of comparison, Figure 6.6 shows two different sets of FRF curves (using the same format as before), where a much cleaner coherence plot is observed. Drops around the anti-resonances still occurred, although they are much narrower and, virtually, noise-free.

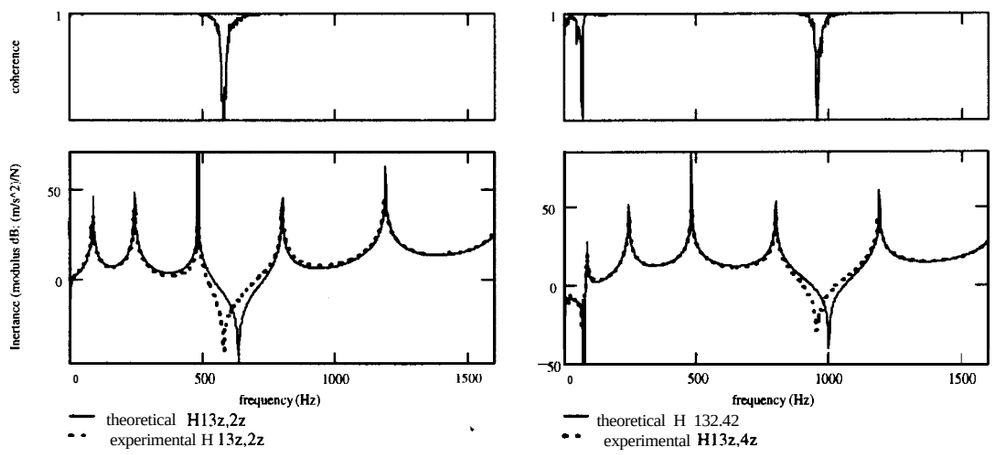

Figure 6.5 - Problems at experimental FRFs for short beam against theoretical result (accelerometer at 0.4 cm from tip)

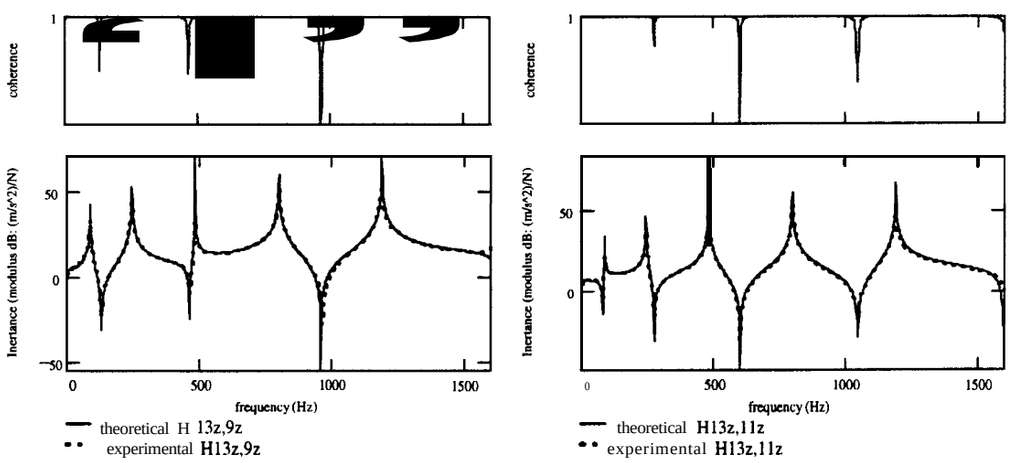

Figure 6.6 - Example of correlated experimental and theoretical FRFs for short beam (accelerometer at 0.4 cm from tip)

The above-mentioned discrepancies could have been detected through the FL and IFI comparison curves, although these curves do not identify in which FRFs the problem happened. Their advantage, as mentioned in the chapter 2, is to quickly check if there is a problem. Then, a better comparison is needed. To show that, these curves were calculated for the new FE and the measured FRF vectors. The results presented in Figure 6.7 included all measured FRF curves in the vector calculation, while the results in Figure 6.8 excluded the two badly discrepant ones (i.e. $H_{13z,2z}$ and $H_{13z,4z}$). In each figure, the FL curves are plotted on the left, with the IFI curves plotted on the right. Analysing Figure 6.7 first, it is seen that both comparison curves show that there are some discrepancies between the FE and experimental curves. However, while the IFI shows some extra spikes at the positions where the mismatch in the anti-resonances happened for $H_{13z,2z}$ and $H_{13z,4z}$ curves, the FL curves are very insensitive to that. These extra spikes are highlighted by two vertical lines in the plots. When the discrepant FRFs were eliminated from the calculations, the comparison curves agreed quite well to each other (Figure 6.8). It is important to stress again that, in order to use these curves as comparison parameters, they have to include the same number of terms. Therefore, for Figure 6.8, the theoretical results also had the mentioned FRFs eliminated.

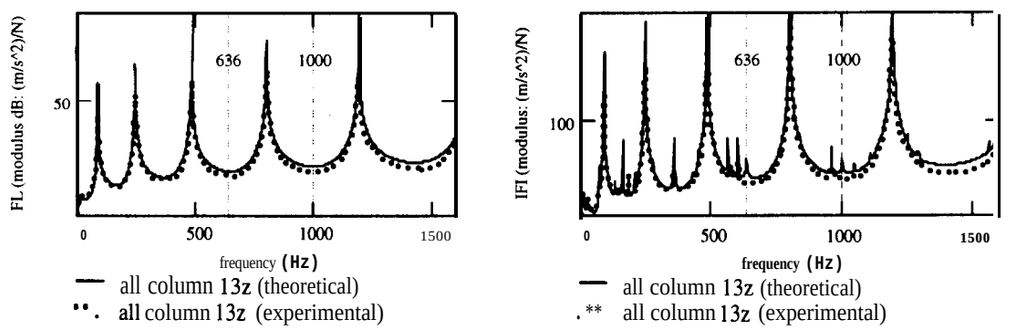

Figure 6.7 - Short beam FL and IFI curves for the experimental and FE-obtained FRFs (all curves; accelerometer at 0.4 cm from tip)

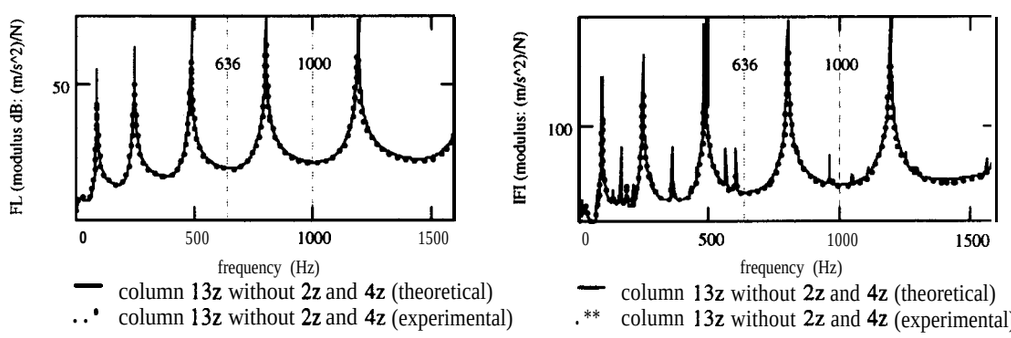

Figure 6.8 - Short beam FL and IFI curves for the experimental and FE-obtained FRFs (without $H_{13z,2z}$ and $H_{13z,4z}$; accelerometer at 0.4 cm from tip)

Although only the short beam results were presented above, the same observations are valid for the long beam results.

To show the consequences this wrong accelerometer position would have in the coupling predictions, the FE-derived FRF curves were used in the FRF coupling calculations. The results are shown in Figure 6.9. As seen, the anti-resonance shifts in the sub-structures FRFs caused poor FRF predictions, both in terms of natural frequencies, as well as anti-resonances. The higher modes are the most affected, despite the last one (at 1554.2 Hz) being difficult to see due to its level. Residual modes also tend to cause this behaviour, since the lower modes are normally better represented. This coupling prediction would have been obtained using this initial set of measurements.

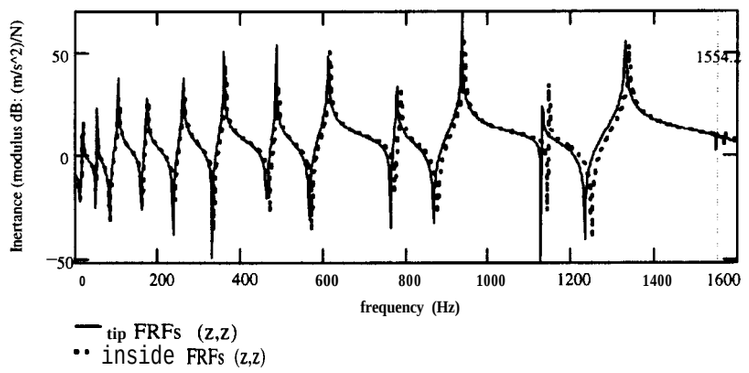

Figure 6.9 - $H_{1Cz,1Cz}$ coupling predictions (theoretical) with accelerometer at tip and 0.4 cm from tip for each sub-system

So, having confirmed that the accelerometer was wrongly placed and knowing the consequences this would have in the coupling predictions, it was moved to the correct position and the translational measurements were performed again. One of the problems of testing extremities is that, for the accelerometer to be correctly fixed at the extremity, not all its base can be mounted into the structure. This was the reason why the accelerometer was wrongly sited at the first place. Correct measurements can be obtained if its centre coincides as close as possible to the extremity and this was the procedure adopted. Nevertheless, a small shift of about 0.1 cm was still required for a proper mounting.

Then, after repeating the measurements, the new experimental FRFs were compared again with the original FE-derived curves (i.e. the ones at the tip). The curves agreed with each other much better now, although very small discrepancies are still visible due to the accelerometer's shift mentioned. Those comparisons are shown in the FL and IFI curves given in Figure 6.10 and Figure 6.11 (for the long beam) and Figure 6.12 (for the short beams), where the strongest

discrepancies are highlighted by vertical lines. The reason why two different sets of results are presented for the long beam is explained in the following paragraph. Before that however, it is worth mentioning the reason why $H_{15z,2z}$ and $H_{15z,4z}$ were eliminated from these results. They had the same sort of problem as that reported for the short beam in Figure 6.5 around the anti-resonances and since these coordinates were not of interest for the coupling process, little effort was put into trying to improve their measurements. Besides, these anti-resonance problems do not affect the modal parameters of these curves. They could only influence their residual values, depending on the formulation adopted to calculate that.

The two sets of results for the long beam are presented in order to stress the extra advantage of the FL and IFI parameters: that is, the possibility of detecting calibration errors. Although the calibration was checked during the tests, a small error of 0.5 dB passed undetected. Only when the FL and IFI curves were calculated could this error be seen clearly (Figure 6.10). Then, the experimental FRF levels were corrected and the comparison curves were calculated again, with the results presented in Figure 6.11 and Figure 6.12. They agree reasonably well taking into consideration the still remaining accelerometer's shift.

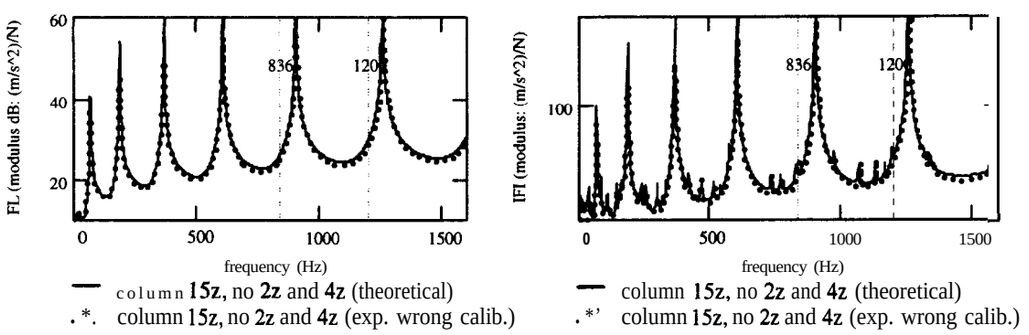

Figure 6.10 - Long beam FL and IFI curves for the experimental and FE-obtained FRFs (accelerometer at "tip"; wrong experimental calibration)

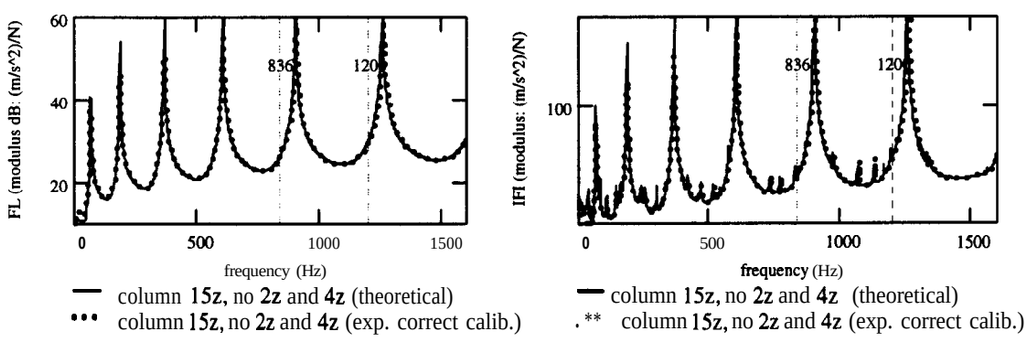

Figure 6.11 - Long beam FL and IFI curves for the experimental and FE-obtained FRFs (accelerometer at "tip"; correct experimental calibration)

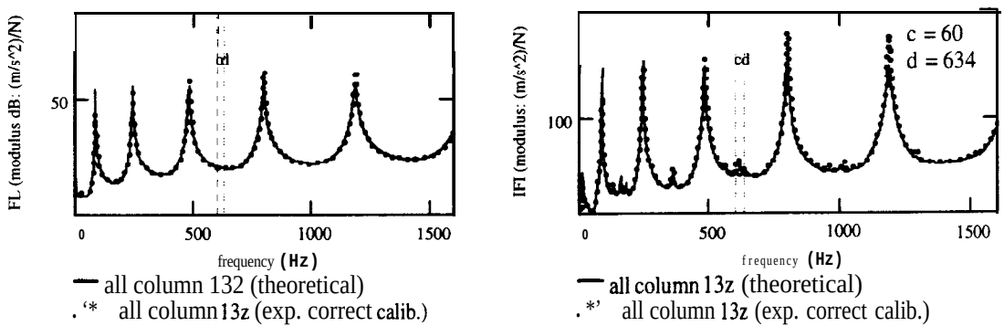

Figure 6.12 - Short beam FL and IFI curves for the experimental and FE-obtained FRFs (accelerometer at "tip")

The same calibration error was present in both short and long beams' measurements. Therefore, this error could have been corrected only at the coupling FRF predictions, what can be understood by recalling equation (2.10) and adding the calibration errors, as follows:

$$\left(\left[e\cdot H_A\right]^{-1}\oplus\left[e\cdot H_B\right]^{-1}\right)^{-1}=e\cdot\left(\left[H_A\right]^{-1}\oplus\left[H_B\right]^{-1}\right)^{-1} \tag{6.1}$$

The same argument applies for the modal coupling, where the error factor can be assumed to be constant for all eigenvectors and equal to the square root of the error. Such comments are only valid though if the error is constant for all FRF curves involved for each sub-system in the coupling process. The error in the eigenvectors can be interpreted by the modal summation formula below:

$$H_{ij}(\omega)=\sum_{r=1}^{N}\frac{\phi_{ir}\phi_{jr}}{\lambda_r^2-\omega^2}\quad\therefore\quad e\cdot H_{ij}(\omega)=\sum_{r=1}^{N}\frac{\left(\sqrt{e}\cdot\phi_{ir}\right)\left(\sqrt{e}\cdot\phi_{jr}\right)}{\lambda_r^2-\omega^2} \tag{6.2}$$

6.4.3. MODAL PARAMETERS AND RESIDUAL TERMS

After measuring a row of the FRF matrix for each sub-structure, all the modal parameters within the measured frequency range of interest can be obtained, as well as the residual terms for that particular row. These parameters are needed for two reasons: (1) to perform the correct CMS coupling and (2) to obtain a consistent modal data set which can be subsequently used to obtain the "correct" smoothed FRFs. These smoothed FRFs are used to eliminate the noise incorporated in the measurements and are required in the FRF coupling calculations.

The line-fit method of modal analysis [86] was employed to provide the experimental modal parameters of each structure. These modal parameters were augmented by the analytical rigid-body modes (based on the geometry), as the structures were tested under "free-free" conditions. Therefore, when regenerating the FRF curves, only the high-frequency residual terms had to be

compensated for in order to obtain the "correct" smoothed FRF curves. This topic is addressed next. However, before going to that, the augmented natural frequencies and mode-shapes obtained using this method are compared to the FE values. This is performed using the frequency and MAC plots presented in Figure 6.13 and Figure 6.14 for the short and long beams, respectively. Moreover, since the MAC plot is only a visual means of interpreting the modes' correlation, to have a better idea about the values themselves, the MAC matrix is written alongside the MAC plot. It is clearly seen that the correlation between FE and experiments for both structures is very good. The rigid-body modes for the long beam have their position interchanged, although the correlation was not affected by that.

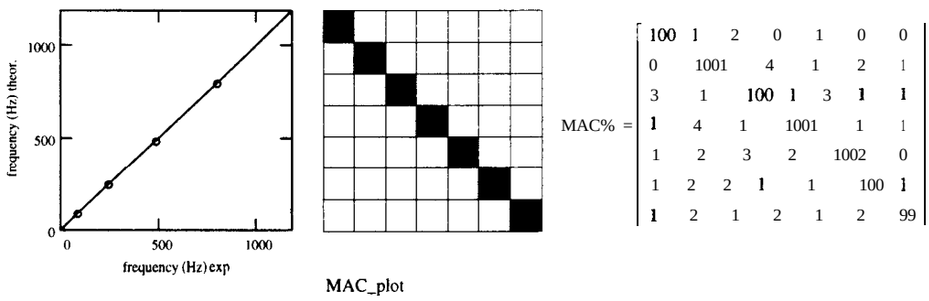

Figure 6.13 - Frequency and MAC plots between experimental and FE solutions, with MA6 values (short beam)

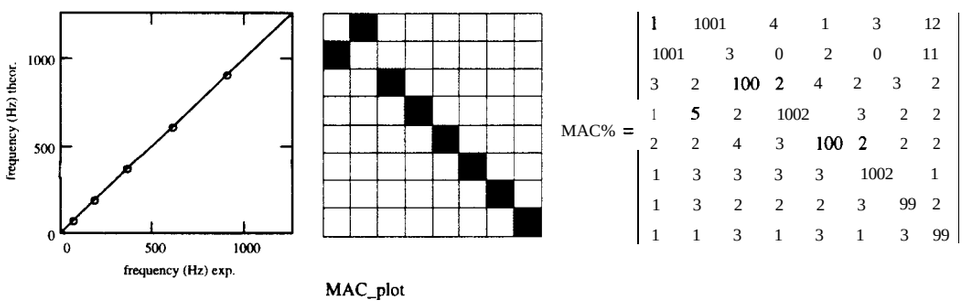

Figure 6.14 - Frequency and MAC plots between experimental and FE solutions (long beam)

As mentioned in chapter 2, having the modes correlated to each other does not necessarily guarantee that the FRF curves calculated using such modal parameters are correct (or in better terms, complete). This explains why the comparison has to go beyond that, and why FRF comparison parameters where sought. The consequences of the insufficiency in terms of number of modes (i.e. the residual effect) can be seen in Figure 6.15. This figure shows the regenerated (without residual compensation) FRF curves at the coupling coordinate for the short and long beams, respectively. Since all lower modes are included in the regeneration, only

the high-frequency residual modes are missing from these curves. So, the experimentally-based residual compensation techniques presented in chapter 4 were used to improve the quality of the regeneration. Emphasis was given to the techniques developed by the author, that is, the high-frequency pseudo-mode compensation and the residual terms in series form. The experimental validation of the techniques is performed here only for the short beam, since some indication about that was given for the long beam in chapter 5.

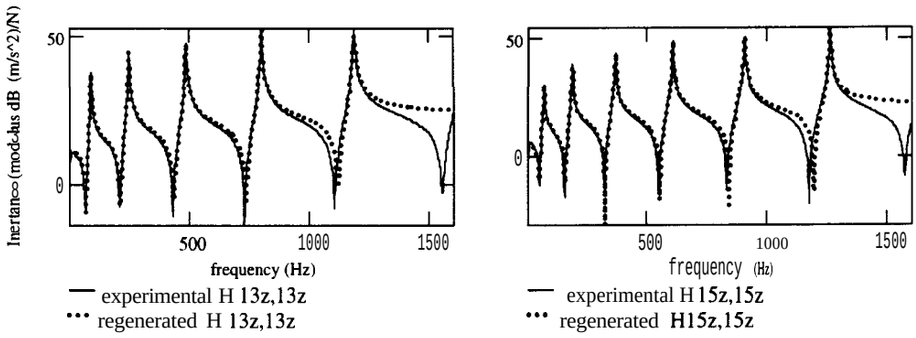

Figure 6.15 - Measured and regenerated FRF curves at the coupling coordinate for the short and long beam, respectively

Table 6.2 - Modal parameters of short beam plus the 3 pseudo-mode test case's predictions

	m1	m2	m3	m4	m5	m6	m7	case 1	case 2	case 3
freq.	0	0	87.71	244.96	482.8	796.97	1184.69	1669.06	1097.99	800.55
η	0	0	3.09E-2	1.04E-2	7.53-3	4.45E-3	4.97E-3	1.02E-2	3.11E-2	1.10E-2
	0.93679	-1.4603	1.60859	-1.39527	1.1976	-0.97006	0.7436	-0.50434	-0.66090	0.00931
	0.93679	-1.35213	1.17507	-0.67901	0.20852	0.22535	-0.6002	0.72726	-0.08870	-0.02199
	0.93679	-1.08171	0.48135	0.39554	-1.04459	1.21879	-1.18243	0.57510	0.47443	-0.08773
	0.93679	-0.81128	-0.13309	1.08365	-1.2215	0.53292	0.46087	-0.99416	0.01022	-0.00541
	0.93679	-0.54085	-0.67942	1.24084	-0.35487	-0.91556	1.35128	-0.45188	-0.34513	0.03814
Re	0.93679	-0.27043	-1.0226	0.84085	0.78888	-1.24196	-0.06688	1.13118	-0.36700	0.07013
ϕ	0.93679	0	-1.16654	0.098	1.353	-0.14374	-1.35018	0.40089	0.02745	0.02908
	0.93679	0.27043	-1.09305	-0.71896	0.91305	1.17399	-0.38599	-1.22257	-0.28704	0.06025
	0.93679	0.54085	-0.79758	-1.2248	-0.2268	1.06557	1.23673	-0.11513	-0.04200	0.11767
	0.93679	0.81128	-0.33043	-1.19031	-1.1459	-0.33935	0.7544	1.43239	0.45038	0.11350
	0.93679	1.08171	0.23986	-0.60568	-1.1435	-1.25771	-0.90075	0.06749	0.83283	0.15922
	0.93679	1.35213	0.93847	0.44141	-0.00716	-0.41079	-0.73984	-1.14522	0.32003	0.12807
	0.93679	1.48735	1.2695	0.96124	0.70695	0.45694	0.19406	-0.14670	-0.01411	0.08788
	0.93679	1.62256	1.5436	1.48002	1.42876	1.41965	1.37758	1.70480	0.52917	0.07404
	0	0	-0.05989	0.02043	-0.00314	-0.00202	-0.01495	-0.01065	-0.26918	-0.20546
	0	0	-0.01345	0.00978	0.00248	j-0.00006	I-0.04197	I-0.01855	0.08325	0.12821
	0	0	-0.0117	-0.00244	j-0.00447	0.02615	j-0.05695	-0.03455	0.17753	0.06100
	0	0	0.00345	-0.01284	-0.0021	0.00645	0.04263	0.03005	-0.04966	-0.14408
	0	0	0.01468	-0.01408	j-0.00471	I-0.02564	0.08919	0.03464	-0.23321	0.10633
Im	0	0	0.02799	-0.01075	0.00657	I-0.03076	-0.0077	j-0.00909	0.30101	0.22112
ϕ	0	0	0.02726	-0.00024	I-0.01851	0.00771	0.01511	0.00864	I-0.451771	-0.03409
	0	0	0.03273	0.01052	I-0.01202	I-0.00234	0.0097	0.00545	0.34626	j-0.06370
	0	0	0.01387	0.01639	I-0.00784	-0.0256	0.00031	0.01168	0.34728	0.12819
	0	0	0.00919	0.0189	0.00778	-0.01184	-0.00976	0.03242	-0.03564	0.02163
	0	0	0.00157	0.00994	0.01075	0.00032	-0.01785	-0.00986	0.45056	-0.24477
	0	0	0.00725	-0.00585	0.01115	0.01253	0.01157	0.00124	0.10824	0.36601

The first residual compensation technique used was the high-frequency pseudo-mode formulation. Table 6.2 above shows the mentioned modal parameters for the short beam, where the second and third columns represent the rigid-body modes and the next 5 columns show the elastic modes. The last 3 columns of this table are the pseudo-mode predictions calculated using different choices of frequency points. Case 1 used frequency points evenly spread from 1400 to 1600 Hz, every 20 Hz (i.e. towards the end of the frequency range, as recommended in chapter 4). Case 2, on the other hand, used frequency points from 800 to 1200 Hz, every 20 Hz, while case 3 used frequency points from 600 to 1000 Hz, every 20 Hz. These cases were selected to show the importance of the frequency point choice.

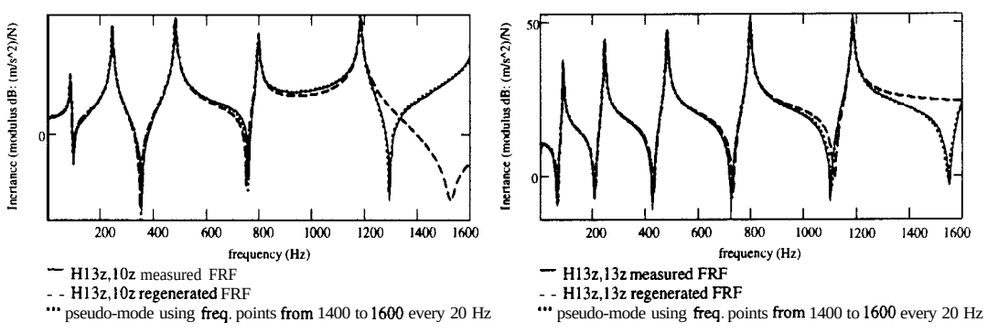

Figure 6.16 - $H_{13z,10z}$ and $H_{13z,13z}$ respectively: measured, regenerated (without residual) and pseudo-mode smoothed FRF curves (case 1 of Table 6.2)

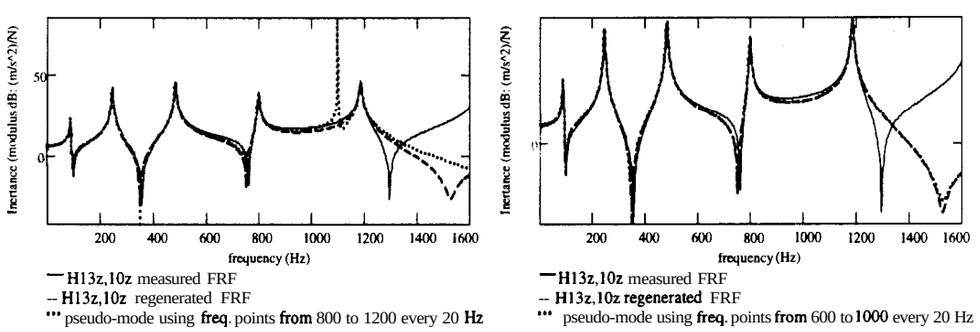

Figure 6.17 - $H_{13z,10z}$: measured, regenerated (without residual) and pseudo-mode smoothed FRF curves (cases 2 and 3 of Table 6.2)

Figures 6.16 and 6.17 show the measured, the regenerated (without residuals) and the pseudo-mode smoothed FRF curves (for each case of Table 6.2) for transfer FRF $H_{13z,10z}$. This FRF was chosen because it is not the point FRF used to calculate the pseudo-mode frequency. Due to the development of the technique, the pseudo-modes for point FRFs normally tend to be much more accurate than for transfer FRFs. Besides, this curve has a strong high-frequency residual term influence. Nevertheless, $H_{13z,13z}$ for case 1 of Table 6.2 is also shown in Figure 6.16, since

this is the FRF of interest for the coupling process and this case provided the correct solution, as explained below.

Analysing these figures, it is observed that the approach worked very well when using the first selection of frequency points (case 1), despite the residual effect on the plotted curves (Figure 6.16). When the points were chosen more towards the middle of the frequency range (case 2), a fictitious mode "appeared" which, as mentioned in chapter 4, is not correct (left side of Figure 6.17). The last choice of frequency points (case 3) also produced a fictitious mode, although this is not seen in Figure 6.17 (right side). Comparing this latter prediction with the regenerated FRF, it can be seen that virtually no improvement was made over the regenerated FRF. This can be explained by the fact that the estimated pseudo-mode frequency for this case is almost coincident with the 6th mode of the structure (see Table 6.2). Close to resonances, the residual effect is almost non-existent.

The other residual compensation techniques tried were the static residual compensation and the residual compensation in series form. The latter was truncated after the second term, though, and that corresponded to a dynamic residual compensation. The main reason for that is related to the maximum residual compensation order that can be used in the CMS formulation without increasing its complexity. The results are presented in Figure 6.18 for both $H_{13z,10z}$ and $H_{13z,13z}$. Although the dynamic residual compensation did not manage to give the correct residual compensation yet, the series term was not considered further for the reason mentioned above. Nevertheless, an improvement over the static residual compensation was achieved (even being small for the coupling coordinate $H_{13z,13z}$).

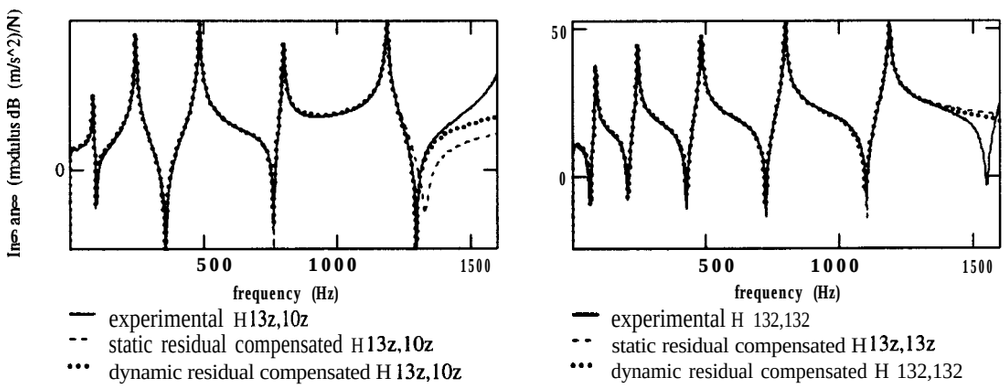

Figure 6.18 - Static and dynamic residual compensations for $H_{13z,10z}$ and $H_{13z,13z}$

However, some additional data are needed for the coupling process and these are related to the rotational DOFs. As seen in Figure 6.19, performing the coupling using only translational FRF

yields to completely wrong predictions. Rotations need to be obtained as well, either in FRF or modal parameter format and this topic is addressed next.

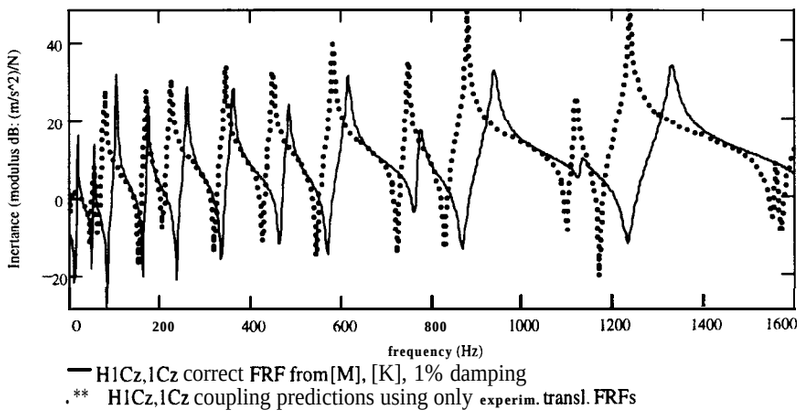

Figure 6.19 - Experimental $H_{1Cz,1Cz}$ coupling predictions using only translational data

6.5. DERIVATION OF ROTATIONAL FRFS

6.5.1. INTRODUCTION

This subject was first treated in chapter 5. As stressed there, the RDOF derivation was not the main concern of this work and the simplest technique to derive such coordinates or FRFs was chosen, that is, the finite-difference technique. Both modal parameters (plus residual terms) and FRF curves derivations were thoroughly investigated there. Several results for the long beam were presented, where a mixture between first- and second-order finite-difference approximations was used whenever necessary to obtain a better rotational FRF prediction. In this section, the RDOF derivation is treated again, now for the short beam. However, only experimental derivation results are shown this time. Moreover, as the conclusions for the short beam are the same as those drawn for the long beam in chapter 5, only some of the short beam results will be presented. Those are confined to the FRF curves derivation. The modal parameters plus residual terms derivation will be addressed only in the CMS application (section 6.6.3).

In order to derive the rotational parameters using either first- or second-order finite-difference approximations, extra measurements from the ones mentioned in the section 6.4 are necessary. Actually, these measurements are required only by the rotation/moment FRF curves or residual terms derivation, since rotation/force quantities or rotational coordinates can be derived using just the set of translational FRFs already measured. As the lengths of the short and long beams are not very different, the same spacing between accelerometers was used for the rotational

derivations of both structures. That corresponds to 2.5 cm between accelerometers and was decided on the basis of an FE pre-analysis test, as mentioned previously. It is already known from the long beam results that this is the best spacing to obtain the necessary quantities. Nevertheless, wherever possible, some other spacings are used to show the consequences this parameter has on the predictions. Next, the results for the short beam are presented.

6.5.2. RESULTS

Before starting to calculate the rotational quantities, the first thing to do is to check the quality of the translational measurements. To ensure that the measurements were correct, reciprocity checks were performed and their quality investigated. The dummy masses were used exactly to guarantee that. Figure 6.20 shows this set of results for the actual accelerometer's spacing adopted. Small discrepancies are seen for the reciprocal $H_{12z,13z}$ and $H_{13z,12z}$ measurements, but, in general, the quality is quite good and the reciprocity can be considered satisfactory.

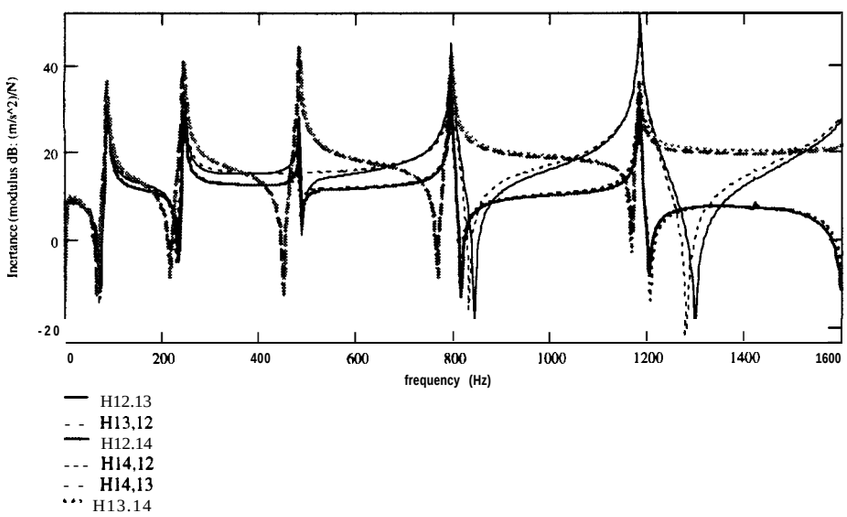

Figure 6.20 - Reciprocity checks for the experimental translational FRFs needed for the rotational derivations, s=0.025 m (z direction)

The format of the results presented here follows that for the long beam presented in chapter 5. As it happened there, two different spacings can be used for the first-order approximation (s = 0.025 m and s = 0.050 m). On the other hand, only one spacing can be used for the second-order approximation (s = 0.025 m), unless considering rotation/force derivation that allows s = 0.050 m to be used as well. Hereafter, the experimental rotational derivations are always going to be compared to the correct FE-derived curves.

Figure 6.21 shows the results obtained for the first case (i.e. first-order approximation). As seen, the quality of the derivations starts deteriorating towards the higher end of the frequency range. None of the spacing assumed produced good results, and the larger the spacing, the worse the predictions. Moreover, the quality of the rotation/force derivations is generally much better than those for the rotation/moment. To highlight the noise effects present in the derivations (not evident in the previous figure), the individual curves are plotted in Figure 6.22. As noticed, this effect is confined to the lower frequency range and is much stronger for the rotation/moment predictions than for the rotation/force ones. Increasing the spacing reduces the effects of noise in that region, although jeopardises the quality of the anti-resonances at the higher frequency range, as mentioned above.

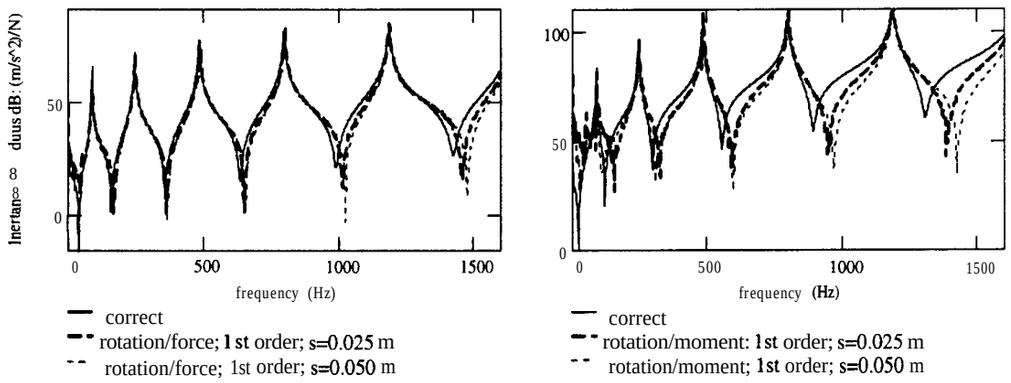

Figure 6.21 - $H_{13\theta x,13z}$ and $H_{13\theta x,13\theta x}$ derived from experimental translations (first-order approximation and different spacings) to show shift in anti-resonances

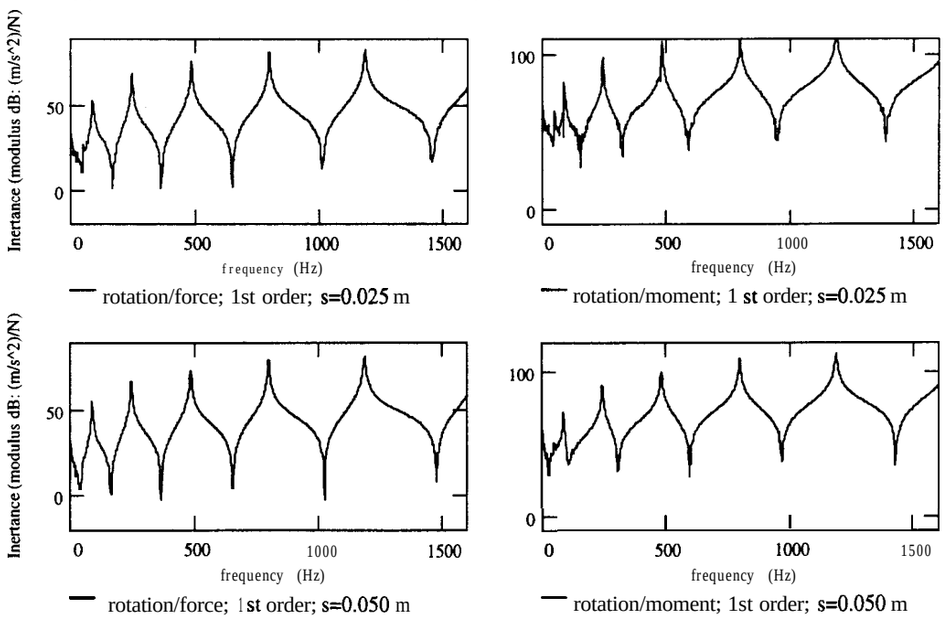

Figure 6.22 - Individual $H_{13\theta x,13z}$ and $H_{13\theta x,13\theta x}$ derived from experimental translations (first-order approximation and different spacings) to highlight noise effects

So, the second-order approximation was used and that produced a much better prediction (Figure 6.23). The spacing adopted for the coupling analysis later on (that is, s = 0.025 m) managed to reproduce the required FRFs with quite good accuracy. The problem is the noise effects once again. Actually, it is much stronger now than it was for the first-order approximation (Figure 6.22). As observed in the individual curves (Figure 6.24), the noise effect in the lower frequency range is minimised if the spacing adopted is increased. Nevertheless, this has the side effect of shifting the anti-resonances position, as happened for the previous case. In Figure 6.24, the translational FRF is compared with the FE-derived one, to show the agreement between them and to justify the comparisons made so far.

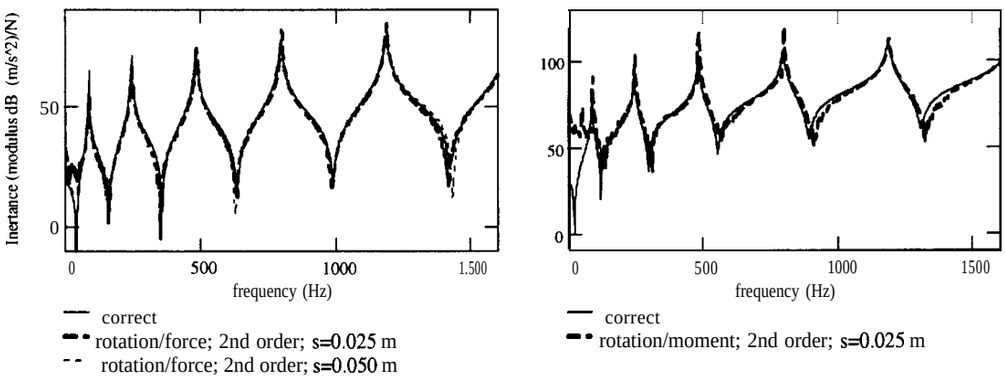

Figure 6.23 - $H_{13\theta x,13z}$ and $H_{13\theta x,13\theta x}$ derived from experimental translations (second-order; different spacings) to show shift in anti-resonances

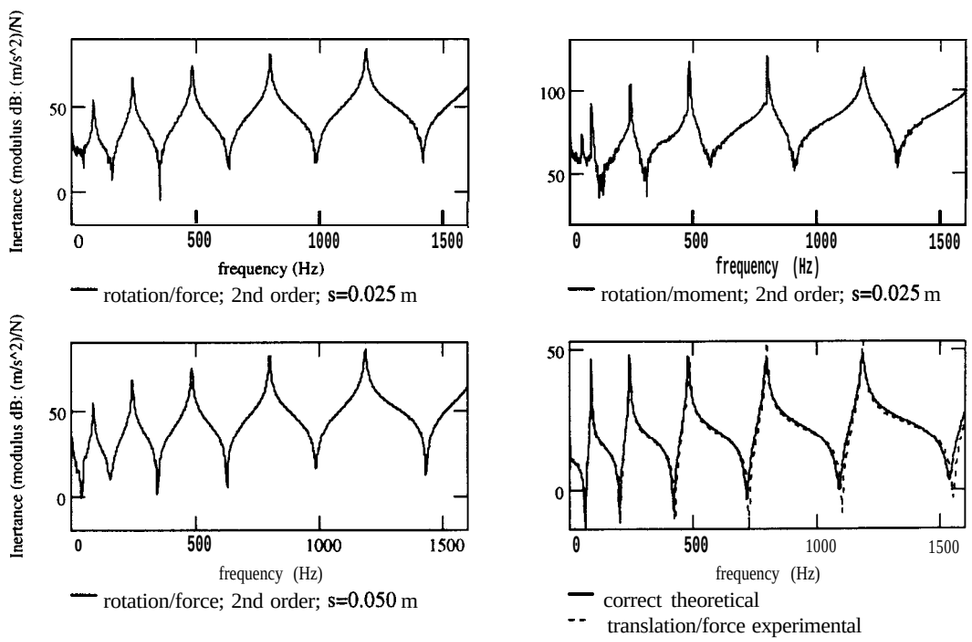

Figure 6.24 - Individual $H_{13\theta x,13z}$ and $H_{13\theta x,13\theta x}$ derived from experimental translations (second-order; different spacings) and theoretical against experimental $H_{13z,13z}$

As stressed in chapter 5, the noise effects appear as a direct consequence of the mathematical manipulation of the data. Small noise effects, which are not visible in the individual translational measurements (Figure 6.20), are heavily amplified during the calculations. Therefore, the use of the directly-derived rotational related FRF curves is not recommended for further applications, as will be demonstrated in section 6.6.1. The solution is to smooth the FRF curves prior the calculations and this is the series of results shown next. Only the second-order finite-difference approximation is considered from now on, since it proved to be the most correct solution for the FRF curves derivation. The smoothing of the FRFs has to guarantee that the residual effects are also taken into consideration, otherwise the derived curves are not going to be correct either. So, the experimentally-based residual compensation techniques presented in chapter 4 (and employed here in section 6.4.3) are used again to do that.

Figure 6.25 shows the derivations obtained when using the regenerated translational FRF curves to highlight what would happen if no residual compensation is used in the smoothing process. Although the predictions are correct at the very low frequency range, that agreement deteriorates as the frequency increases. Moreover, the rotation/moment FRF is much more affected by the residual effects than the rotation/force curve and that trend follows the conclusions drawn in chapter 4. This is also confirmed in the following residual compensations. When the regenerated FRF curves include the static residual compensation (Figure 6.26), the results are improved considerably towards the higher end of the frequency range. However, some mismatch is still present at the higher range. So, the dynamic residual compensation is used to improve that even further (Figure 6.27). Despite the fact that the predictions using the dynamic residual compensation are not correct yet, no further terms in the residual compensation in series form are considered. This procedure is adopted because these results could not be used in the CMS formulation later on, as mentioned several times. Figure 6.28 and Figure 6.29 present the derivations when the residual compensation is made using the high-frequency pseudo-mode approach. The difference between these figures is in the eigensolution used to regenerate the FRF curves used in the high-frequency pseudo-mode formulation. In the former figure, the regenerated curves were obtained using the eigensolution calculated for each one of the 3 columns involved. In the latter figure, on the other hand, the regenerated curves were obtained using a consistent eigensolution based on the coupling node (13). In Figure 6.28, anti-resonance problems in the lower frequency range happen as a result of the small frequency discrepancies caused by the inconsistent eigensolution. Such problems were solved when using the consistent pseudo-mode compensation (Figure 6.29), although the rotation/moment

prediction has some anti-resonance problems in the higher frequency range. Nevertheless, this mismatch is much less serious for further applications than that present in Figure 6.28.

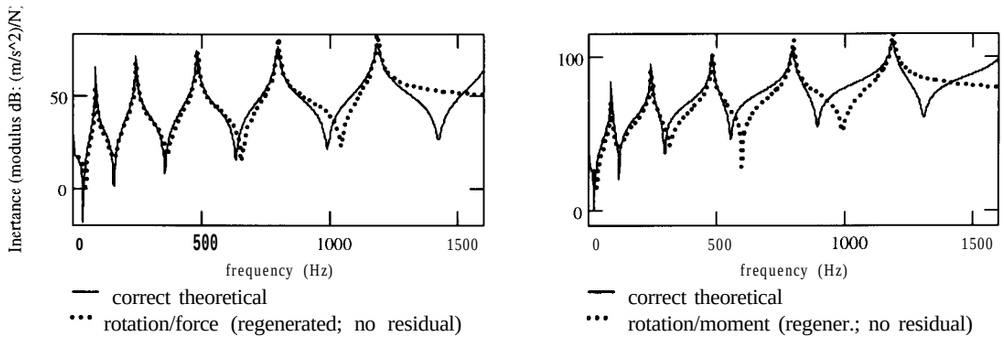

Figure 6.25 - Rotational derived FRFs using regenerated translational FRFs (second-order approximation; s = 0.025 m)

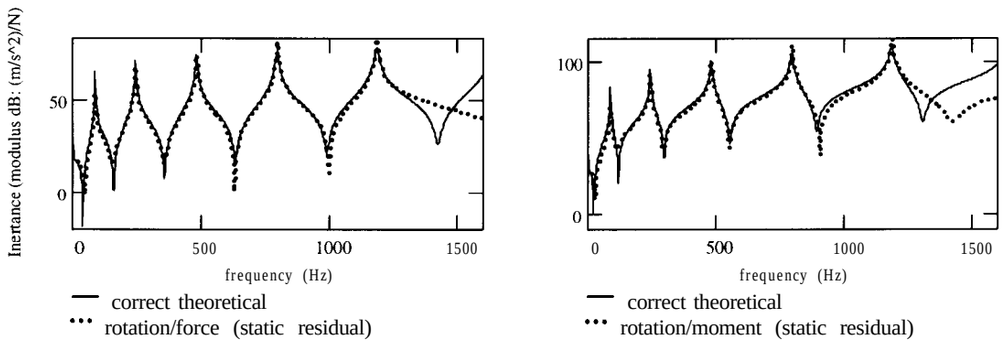

Figure 6.26 - Rotational derived FRFs using static-residual compensated translational FRFs (second-order approximation; s = 0.025 m)

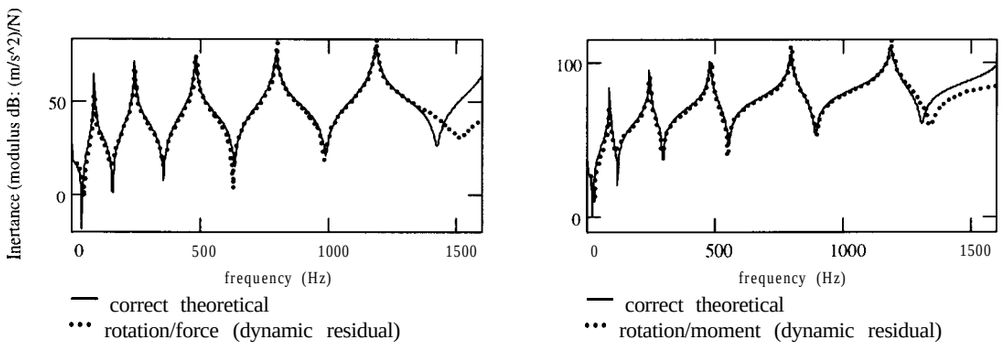

Figure 6.27 - Rotational derived FRFs using dynamic-residual compensated translational FRFs (second-order approximation; s = 0.025 m)

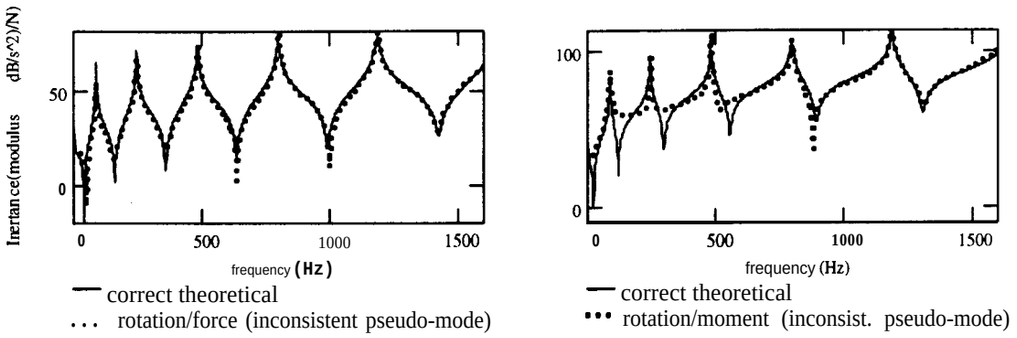

Figure 6.28 - Rotational derived FRFs using inconsistent pseudo-mode compensated translational FRFs (second-order approximation; s = 0.025 m)

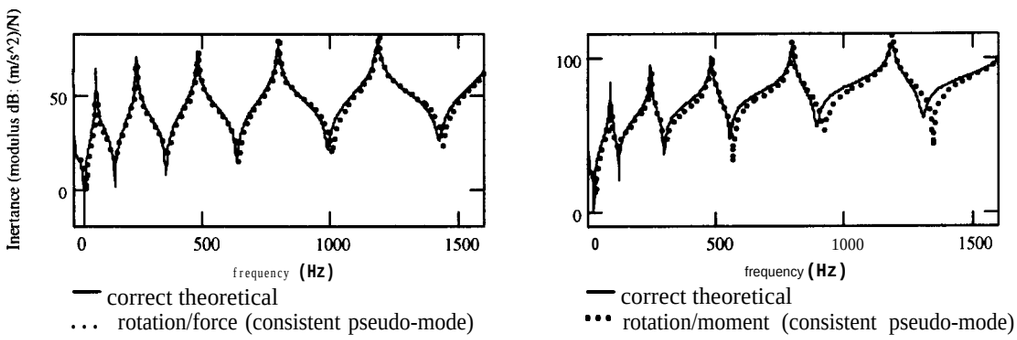

Figure 6.29 - Rotational derived FRFs using consistent pseudo-mode compensated translational FRFs (second-order approximation; s = 0.025 m)

In the following section, the rotational derivations obtained above and the modal ones not shown here are used in further applications. Both CMS and FRF coupling formulations are considered, where a mixture between rotational derivation approximation and residual compensation employed is investigated.

6.6. STRUCTURAL COUPLING ANALYSIS USING MEASURED DATA

6.6.1. INTRODUCTION

The coupling analysis of interest in this study was confined to the coupling coordinates. For that, depending on the technique used, all necessary FRFs or modal parameters plus residual terms had to be obtained, including those related to RDOFs. As mentioned at the beginning of this chapter, to guarantee that the results obtained from the coupling analysis are correct, the actual coupling of the physical structures was performed. Then, the coupled structure was tested and the results compared. The coupling predictions could also have been compared with the FE solution of the coupled structure and this was the procedure adopted here (as explained

next). Nevertheless, it was important to have the experimental results to confirm the FE solution as well.

Figure 6.30 shows the comparison between the measured and the FE-obtained FRFs. The two curves agree almost perfectly with each other. Even the anti-resonances agree very well. The only problem is an extra resonance showing around (1200 Hz) for the measured curve. A further inspection into this problem demonstrated that the extra peak was, in fact, a torsional mode that should not have been excited, since the measurements were performed at the neutral axis. To confirm that, Figure 6.31 shows the same FRF curve as before compared now with another FRF measurement made such that the torsional modes were excited. The extra peak is shown to coincide with one of the torsional modes, although this was the only one present. Despite the care taken to eliminate it, this was not possible. It is believed that there was a slight misalignment in the welding of the two structures, what resulted in that effect. Nevertheless, since the theoretical FRF produced the same measured FRF (apart from this torsional mode), the former will be used for the subsequent comparison of results.

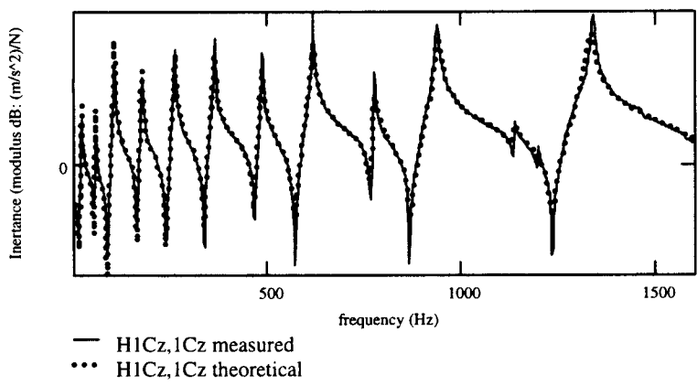

Figure 6.30 - Measured against theoretical FRF at the coupling coordinate ($H_{1Cz,1Cz}$)

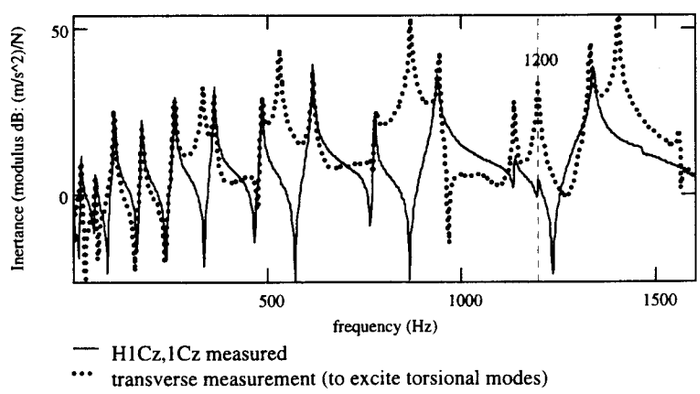

Figure 6.31 - Comparison of measurements with/without exciting torsional modes

6.6.2. FRF COUPLING

The first coupling technique to be employed here is the FRF coupling method presented in chapter 2. One of the problems that may happen when calculating coupling predictions using experimental data is that related to the correct direction of the sub-structures. Both of them have to assume the same global axis system. This requirement may not be met when the structures are tested under free-free condition. Then, the sign of one of the sub-structures has to be correct during the calculation. The off-diagonal FRFs are the only terms affected by this change, since the diagonal terms (when changed) have this change made twice; thereby cancelling it.

This problem was present for the current coupling studies. Then, the sign of the appropriate long beam FRFs were changed, since the global axis assumed was that for the short beam (due to the suspension adopted for the measurements of the coupled beam, as mentioned in section 6.2). To stress the importance of complying with the global axis system, the first coupling prediction shown will not assume such correction. The prediction obtained is presented in Figure 6.32. In order to avoid noise, inconsistencies or rotational related FRFs problems (which could make one misinterpret the errors), theoretical FRFs were used in this example. As noticed, the prediction is completely wrong.

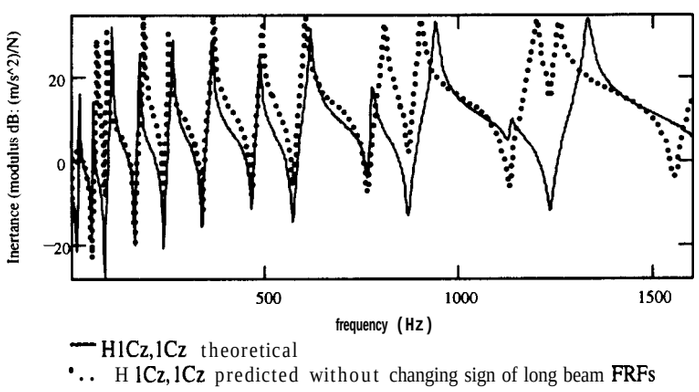

Figure 6.32 - $H_{1Cz,1Cz}$ coupling predictions without correcting the direction of the long beam FRFs (using theoretical input data)

There are two paths which could have been followed for obtaining the FRFs required for the FRF coupling calculations. The first one involves the regeneration of the translational curves (including residual compensation) and posterior derivation of the rotational-related FRFs. The second one involves the derivation of the rotational parameters from the translational modal parameters and residual matrices in separate, and posterior regeneration of the FRF curves using such derived data. These paths are better understood looking at Figure 6.33. The residual

matrix represented there is a generic residual matrix and can be obtained using any one of the residual matrix formulations given in chapter 4. However, the rotational-related derivation of frequency-dependent residual matrices is not as effective as that of frequency-independent ones. Therefore, the first path is more suitable when using frequency-dependent residual matrices. Consequently, the results presented in this section follow the first path, whereas the second path will be used in the following section on CMS coupling. Nevertheless, the second path could have been used here with the static residual or residual in series form, although these were considered only for the first path.

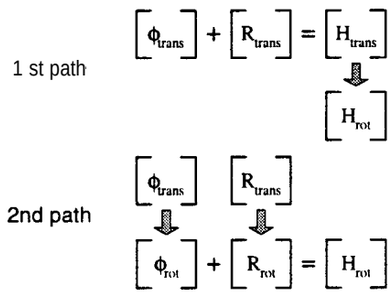

Figure 6.33 - Paths for obtaining the FRFs for the FRF coupling formulation with rotational related coordinates

Several different FRF coupling test cases were tried and these are presented in Table 6.3. They use the FRF derivations presented in the previous section and in chapter 5. Following the results presented there, second-order finite-difference approximation (with s = 0.025 m) was used for all the FRF coupling predictions shown hereafter. There is no need to show the coupling predictions using the first order approximation, since it did not produce accurate rotational FRF derivations. The first column of Table 6.3 is the case number used for reference. The second column indicates the type of FRF curves used as input and it is directly related to the third and fourth columns. Those columns show the figures where the FRFs used for each sub-structure are found. They are further split into two, since the translation/force FRF is normally presented in a different figure to that for the rotation/force and rotation/moment FRFs. These figures are important in trying to interpret the coupling predictions, which are presented in the figures given in the last column of this table.

Table 6.3 - Figures related to the experimental FRF coupling test cases

case	type	Short beam FRFs		Long beam FRFs		Coupled predictions
		13z,13z	13θx,13z & 13θx,13θx	15z,15z	15θx,15z & 15θx,15θx	1Cz,1Cz
1	measured	Figure 6.24	Figure 6.24	Figure 5.9	Figure 5.9	Figure 6.34 (Left)
2	regenerated	Figure 6.15	Figure 6.25	Figure 6.15	Figure 5.10	Figure 6.34 (Right)
3	static residual	Figure 6.18	Figure 6.26	Figure 6.18	Figure 5.11	Figure 6.35 (Left)
4	dynamic residual	Figure 6.18	Figure 6.27	Figure 6.18	Figure 5.12	Figure 6.35 (Right)
5	inconsistent pseudo-mode	Figure 6.16	Figure 6.28	not shown	Figure 5.13	Figure 6.36 (Left)
6	consistent pseudo-mode	Figure 6.16	Figure 6.29	not shown	Figure 5.14	Figure 6.36 (Right)

The first test case tried (case 1) is to stress again why experimentally-derived models should be obtained for use in further applications. The measured FRF curves were used "directly" in the FRF coupling calculations. The reason why the word "directly" is used between inverted commas is because rotational-related FRF curves had to be obtained first and these were the measured curves used in the FRF coupling formulation (as shown in Table 6.3). The $H_{1Cz,1Cz}$ prediction for this case is presented on the left-hand plot of Figure 6.34. The last natural frequency is highlighted by a vertical line there, since the correct FRF curve does not show it due to the its damping value. Although the general shape of the FRF prediction matches the correct solution, problems are clear. In the lower frequency region, some of the anti-resonances have lost their sharpness. This is attributed to noise and inconsistency problems in that region at the experimentally-derived rotational FRFs. Some spurious peaks also appear as a result of these natural frequency inconsistencies. So, to get rid of these problems, the use of experimentally-derived models is recommended. Once more it is important to mention that these models have to be complete, and that requires residual term compensation.

To illustrate the effect of ignoring residual compensation in the FRFs used for the FRF coupling calculations, the second test case was tried (case 2). The coupling prediction is presented on the right-hand plot of Figure 6.34. Because of the anti-resonance problems towards the higher frequency range in the sub-structures FRFs, not even the natural frequency predictions are correct in that region. The last three modes are missed altogether (although the last one would not be visible anyway).

So, in order to improve the above results, the derived FRFs were compensated using the static and the dynamic residual compensation (cases 3 and 4 of Table 6.3). The new coupling predictions are presented in Figure 6.35. This time, all visible coupled natural frequencies are seen, although the one around 1330 Hz has still some error associated with it. However, the error decreases as the residual compensation approximation increases: that is, the dynamically-compensated FRFs produced better results than the statically-compensated curves. This was expected, since the input data were already much better. Actually, the predictions for the dynamic case are "almost" correct.

As the last FRF coupling test cases tried, the derived FRFs compensated using high-frequency pseudo-mode approximation were used. The predictions obtained when using the inconsistent and consistent pseudo-mode compensated FRFs are given in Figure 6.36. The former prediction (case 5) is as bad as that obtained for case 1, although no noise effect is present this time. The loss of anti-resonance shapes and the extra peaks are caused by the inconsistencies in the

natural frequency predictions (already seen in the rotation/moment FRFs used), as it happened for case 1. The latter prediction (case 6), on the other hand, does not have such problems, although it did not manage to produce the correct predictions yet. The reason can be traced back to anti-resonance problems around the higher frequency region for the rotation/moment FRF curves derived for the sub-structures (see Table 6.3 for reference figures).

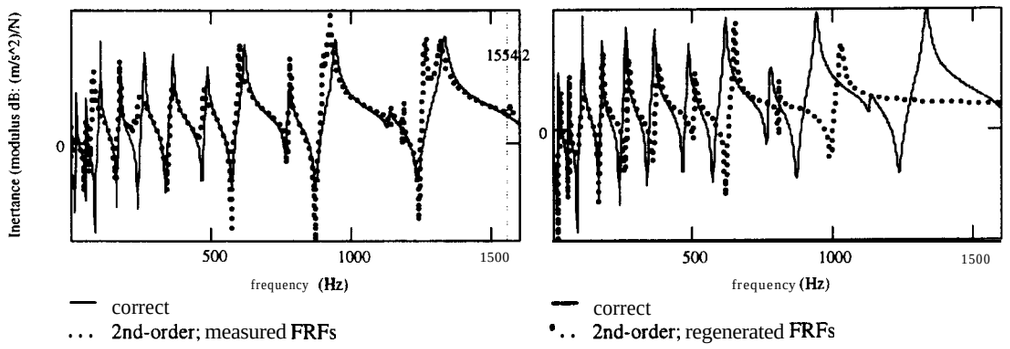

Figure 6.34 - $H_{1Cz,1Cz}$ coupling predictions using measured and regenerated FRF curves (with 2nd-order RDOFs derivation)

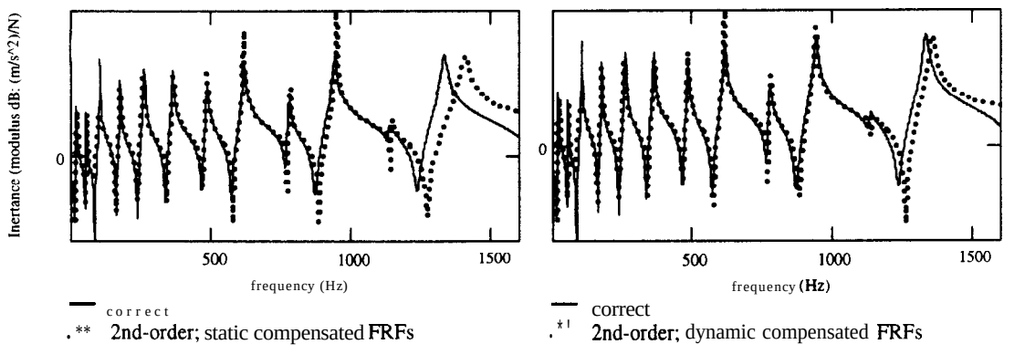

Figure 6.35 - $H_{1Cz,1Cz}$ coupling predictions using static and dynamic compensated FRF curves (with 2nd-order RDOFs derivation)

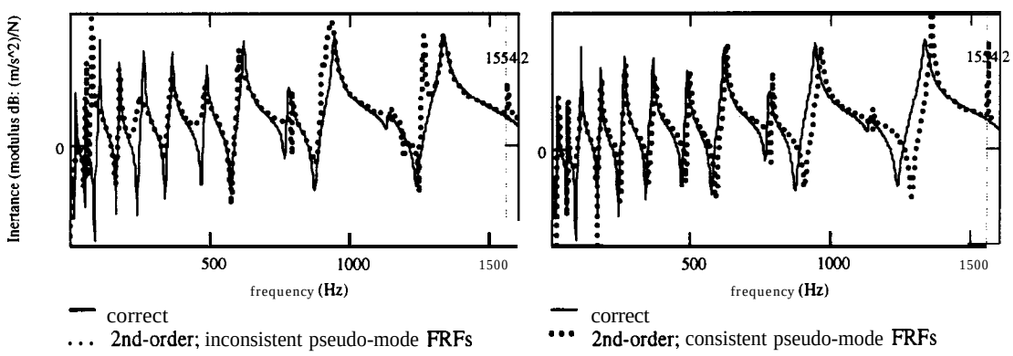

Figure 6.36 - $H_{\cdot\cdot}$ coupling predictions using inconsistent and consistent pseudo-

From the series of results presented in this section, one can conclude that the best option is to use the experimentally-derived models with dynamic residual compensation. If necessary, though, the compensation can go even further in the series. The only reason why it was stopped here is to allow a comparison with the CMS predictions presented next.

6.6.3. CMS COUPLING

The CMS technique is the second type of coupling to be discussed in this chapter. As quoted in chapter 3, this technique does not suffer from noise or inconsistencies problems, since the CMS input data is already in modal format. Therefore, in that sense, it is much better than the FRF coupling technique. Actually, the data required are the same as those recommended above for the smoothing of the FRF curves needed for the FRF coupling formulations. One extra advantage of the CMS over the FRF coupling method is related to the inclusion of rotational-related quantities. It is much easier for the former method to employ a mixture of finite-difference approximations to obtain such quantities, since the second path shown in Figure 6.33 is used. In this case, much better prediction can be obtained, as shown next. This could be anticipated by looking at the results presented for the derivation of the modal parameters and residual terms given in chapter 5.

It is already known from all previous results that residual compensation has to be included in the sub-structures' input data for a correct coupled structure prediction. Therefore, there is no point in showing again the predictions which would have been obtained when it is not included (i.e. Hurty's formulation; presented in section 3.4 of chapter 3). Moreover, this would result in the same prediction as that shown on the right-hand side of Figure 6.34. Only the formulations which allow experimental residual compensation are investigated in this section: that is, MacNeal's and the IECMS formulations. Different finite-difference approximations were used for the rotational coordinates and residual terms derivations. However, only some of the possible combinations between these derivations are shown here (following the conclusions from chapter 5).

Figure 6.37 shows the frequency comparison plots for the test cases tried. The vertical axis has the correct natural frequency values for the coupled system, while the horizontal axis has these same values plotted again to obtain the 45" correlation line. This is followed by the natural frequency values obtained from MacNeal's formulation and, finally, from the IECMS formulation. One vertical and one horizontal line are included at the frequency value of 1600 Hz to mark the upper frequency of interest. Despite the error in the last mode being large from

both formulations, clearly the IECMS produced much better results. The difference between the plot on the left from the one on the right is in the finite-difference approximation used to derive the rotational coordinate. Only the second-order finite-difference approximation was used in this section for the derivation of residual terms, since it produces much better results than using the first-order approximation, as mentioned before.

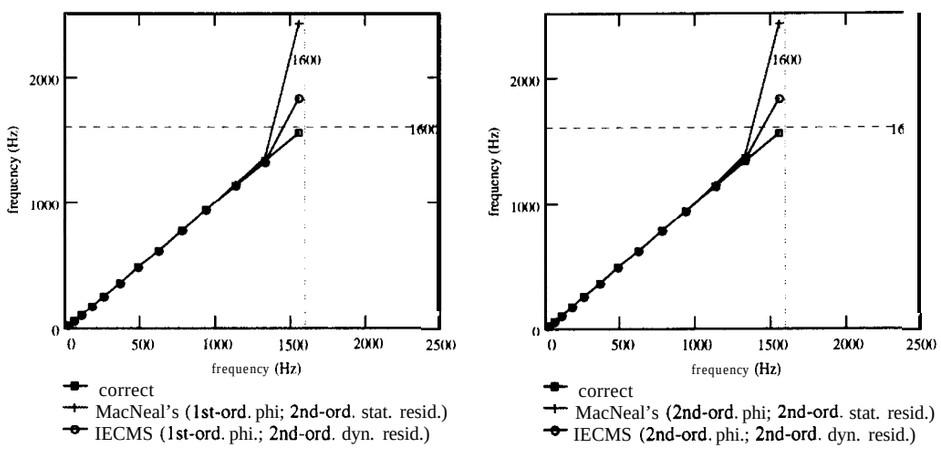

Figure 6.37 - Frequency comparison plot for the different CMS formulations using different rotational approximations and different residual compensations

The $H_{1Cz,1Cz}$ plots obtained using the above solutions are presented in Figures 6.38 and 6.39 for the first- and second-order rotational coordinate derivations, respectively. MacNeal's solution is plotted on the left-hand side of these figures, and has only static residual compensation. On the right-hand side is plotted the IECMS solution, which has both static and dynamic residual compensations. Not surprisingly, the IECMS FRFs are much better than MacNeal's FRFs. When comparing the same formulation, however, using different approximations for the rotational coordinate, it is noticed that the first-order approximation led to a much better result. Even the anti-resonances around the lower frequency range have a better definition. Apart from the fact that the last natural frequency that has a larger error associated with it (only seen in Figure 6.37), one can regard the solution obtained from the IECMS with first-order approximation for the rotational coordinates and second-order approximation for the residual matrices to be virtually correct.

Comparing Figure 6.39 with Figure 6.35 (since they used the same input data but different coupling techniques), it is seen that these display approximately the same results. The CMS predictions are slightly more heavily damped than the FRF coupling ones, due to the type of calculations involved.

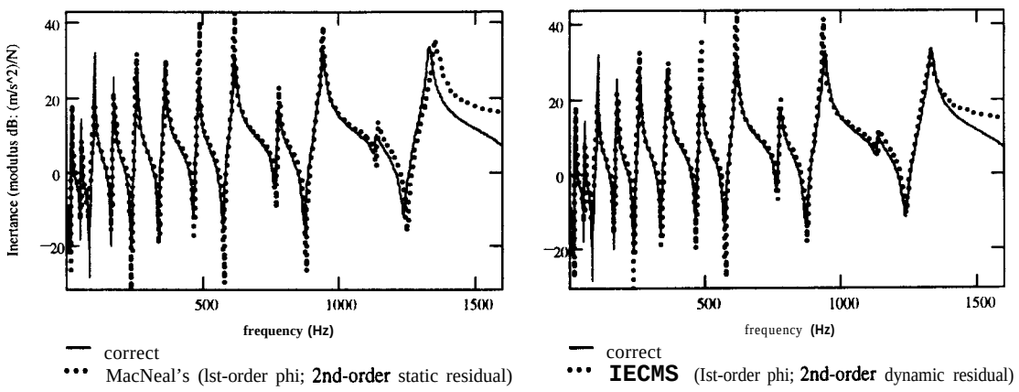

Figure 6.38 - $H_{1Cz,1Cz}$ MacNeal's and IECMS coupling predictions using lst-order approximation for rotational coordinates and Pnd-order approximation for residual compensation

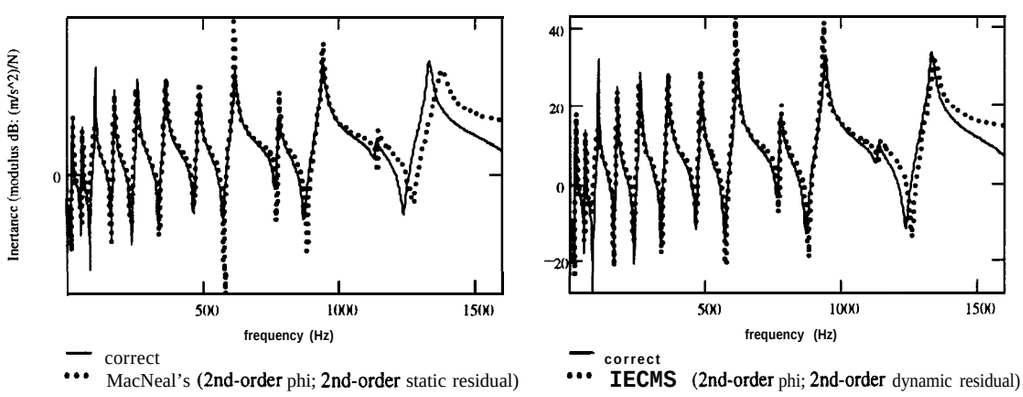

Figure 6.39 - $H_{1Cz,1Cz}$ MacNeal's and IECMS coupling predictions using Pnd-order approximation for rotational coordinates and Pnd-order approximation for residual compensation

The last point to show here is the problem mentioned in the FRF coupling section about the correct sign of the sub-structures input data. In the CMS formulation, the residual compensation matrices have their signs changed in exactly the same way as that explained for the FRFs in the FRF coupling formulations. The eigenvectors, on the other hand, will have this change directly related to the coordinate axes. In the example here, this means that the rotational coordinates and the off-diagonal residual terms will have their signs changed, while the translational coordinates and the diagonal residual terms remain the same. The FRF obtained without considering the referred change for the long beam parameters is shown in Figure 6.40 for the IECMS solution using second-order rotational coordinate and residual terms approximation. The prediction is equivalent to that obtained from the same FRF coupling case and shown in Figure 6.32, the difference now being related to the use of experimental data, instead of theoretical values.

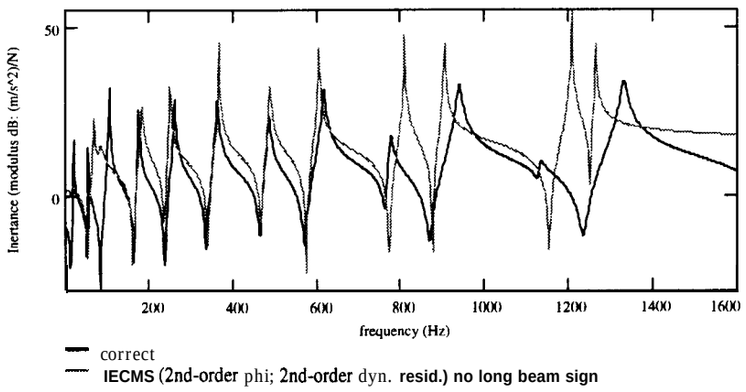

Figure 6.40 - $H_{1Cz,1Cz}$ IECMS coupling predictions without correcting the direction of the long beam rotational coordinates and residual terms

6.7. CONCLUSIONS OF THE CHAPTER

In this chapter, the FRF coupling and CMS formulations for coupled structure dynamic analysis have been validated using real experimental data. Hammer tests were used here to obtain the necessary measured FRFs and although this type of test is one of the simplest to set the structure into vibration, it is not without its own problems. The coherence has to be checked to ensure that the structure is excited always at the same position and double hits should be avoided. For the latter, a lighter hammer is recommended. As illustrated here, another very important point is the need for the correct placement of the transducers. This is of particular significance when the measurement is related to a coupling coordinate and further use is to be made of the data. Small shifts in the actual positions of the transducers may cause the same anti-resonance shift effects as that caused by the lack of residual modes. Such shifts jeopardise the quality of the coupled predictions. The choice of measurement points is also important, but now related to the rotational-related derivation (which is generally necessary). The spacing between accelerometers required by the finite-difference approximation has to be such that the displacement of the modes of interest is properly described.

In order to evaluate the quality of the measured data, the FL and IFI (or FIF) comparison functions can be used. Any two sets of measured FRF data can be compared (repeatability check) or the measured data can be compared with a theoretical solution using these functions. The latter procedure was the one adopted here. As shown, these functions managed to detect even small calibration errors and anti-resonance problems (the latter being detected only by the IF1 parameter) and although they do not give any indication about which FRF curve is incorrect, they do give a quick check into the quality of the measurements. If problems are not seen in both curves, it is very likely that the measurements are correct.

The residual terms and RDOF derivation formulations had also to be validated. Analysing the residual compensation formulations separately, the high-frequency pseudo-mode approximation generally produced the best results. However, when this approximation is used in the derivation of RDOF quantities, only by using a consistent formulation are "good" results obtained. The word "good" is between inverted commas because some anti-resonance problems may still be present in such compensated curves and these problems can be spread equally over the frequency range of interest in the derived curves. The FRFs compensated using static or dynamic residual terms may not be as good as that achieved by the high-frequency pseudo-mode approach, although their quality gets better as one goes to the higher frequencies. This guarantees the frequency range where the predictions are more reliable. Although extra terms could be used to improve the regeneration even further, the dynamic residual compensation normally provides a good compensation. Moreover, this compensation corresponds to the maximum order that can be used in the CMS formulations without increasing the complexity of the formulation. As a result, dynamic residual compensation is recommended.

The first-order finite-difference approximation should be used to derive rotational coordinates, whereas the second-order approximation should be used to derive rotational FRFs or rotational-related residual *terms.* Thus, whenever possible, the rotational coordinates and residual terms should be derived separately and the results used in the regeneration of FRF curves. However, such a procedure is more suitable for frequency-independent residual formulations. When using a frequency-dependent residual formulation, the regenerated translational DOF FRFs have to be compensated first and the resulting curves used in the rotational DOF FRF derivation.

The IECMS formulation developed in this thesis produced much better coupling predictions than the existing MacNeal's formulation. Until the present work, the latter was the only CMS formulation available using experimental data only and a valuable improvement was, therefore, achieved here. The use of dynamic residual compensation yielded the best results for the FRF coupling formulation as well. Although the high-frequency pseudo-mode approximation produced the best residual compensations for the individual curves (as mentioned above), when using the derived rotational curves in the FRF coupling formulation, the results were not as good as those obtained by the dynamic residual compensation. This confirms once again the recommendation for the use of dynamic residual compensation.

CHAPTER 7: CONCLUSIONS

7.1. GENERAL CONCLUSIONS

7.1.1. REMARKS

The research described in this thesis investigated the use of experimentally-derived models for further dynamic analysis of structures. The so-called "experimental route" was followed since the data from tests provide a more realistic description of the behaviour of the structures under examination. The structural coupling analysis (SCA) technique was chosen as the application method of particular interest, so as to study the limitations present in this type of model (that is, numbers of modes and coordinates included in the description). Both FRF coupling and CMS techniques were employed, where ways of solving the models' limitations were investigated. Each one of these techniques works with a different format of input data: while the FRF coupling uses FRF data, the CMS uses modes (plus residual terms). Nevertheless, the requirements for a correct coupling prediction are more or less the same in both cases and these requirements are concluded next.

7.1.2. REQUIREMENTS FOR A CORRECT COUPLING PREDICTION

From what has been demonstrated during this work, one can summarise the following requirements for a correct coupling prediction: (1) noise-free data; (2) consistent modal data sets; (3) inclusion of all modes (or their effects) and (4) inclusion of all important coordinates (particularly those related to RDOFs). Violation of any of the above four requirements may cause the predictions to be in error. However, it is difficult to quantify the error resulting from each one or to rank their importance.

Therefore, the use of experimentally-derived models in structural coupling analysis is recommended. These models are needed either to minimise measurement noise and inconsistency problems (FRF coupling method) or due to a requirement of the formulation (CMS coupling method). Requirements (1) and (2) are automatically satisfied when using experimentally-derived models. Requirements (3) and (4) are not satisfied directly and are, in fact, the

limitations present in this type of models. The consequences of not complying with requirements (3) and (4) are concluded below.

7.1.3. CONSEQUENCES OF MODAL AND SPATIAL INCOMPLETENESS IN SCA

The consequence *of* leaving out modes in a coupling process is coordinate-dependent, both in the "coupling sense", as well as in the "predictions sense". The "coupling sense" means the location where the coupling is performed. Some coordinates have stronger residual effects than others. Then, if the coupling performed involves these coordinates, and no account is taken to compensate for that, the errors involved are going to be high. The "predictions sense" means the coordinates involved (i.e. slave or coupling). While it is essential to have all modes (or residual compensation) for the coupling coordinates, their inclusion in the slave coordinates is only necessary if response in such coordinates is of subsequent interest. Some techniques were developed in this work for solving the residual problem and the conclusions regarding which one is better than the other will be addressed in the following section.

The ***consequence of leaving out coordinates*** is also coordinate-dependent. All coupling coordinates have to be included, although only the slave coordinates which are of further interest are necessary. Among the coupling coordinates that should be included are the normally-ignored RDOFs. The finite-difference technique revisited in this thesis provides a means of solving such problems.

Modal incompleteness tends to overestimate the natural frequency predictions, while spatial incompleteness tends to underestimate them. The combination of the two does not have a clear pattern. All the above conclusions are equally valid for the FRF coupling and the CMS formulations.

7.1.4. RESIDUAL TERMS COMPENSATION

Several techniques were presented in this work to try to compensate for the effects of the high-frequency residual terms (and, thereby, to account for all modes of the structure). Special attention was paid to the formulations using experimental data only, although analytical and combined approaches were also investigated. So far, apart from curve-fitting approaches, only three techniques existed to obtain the high-frequency residual terms from experimental data and these are: (1) the standard frequency-dependent formulation; (2) the experimental static residual formulation and (3) the high-frequency pseudo-mode single-term formulation. Two other experimentally-based techniques were developed in this research to be added to this list: (4) an

experimental residual formulation in series form and (5) a high-frequency pseudo-mode formulation. Although all the experimental approaches can be used starting from analytical data, the contrary is not true. Another formulation developed was the mass-residual approach, although it is an analytical approach still. As will be quoted shortly, some benefits for its use are clear and this approach should be pursued further.

Looking at the various residual compensation formulations individually, the best ones would be the standard frequency-dependent formulation (1) or the high-frequency pseudo-mode formulation (5). Both of these are frequency-dependent and improve the regenerated FRFs over the entire frequency range. Another advantage of the high-frequency pseudo-mode formulation is it global nature, where all FRFs have their out-of-range modes compensated in one go. If more than one column of the FRF matrix needs to be compensated for the lack of residual terms using this formulation, this has to be done considering a consistent modal data set. Otherwise, when using these compensated curves in coupling predictions, the same problem that is present when using raw FRF data may occur again: that is, the incidence of spurious peaks. The high-frequency pseudo-mode formulation (5) is better than the high-frequency pseudo-mode single term formulation (3) because it is not so sensitive to the choice of frequency points used in the calculation as the latter is, although it is also sensitive.

The static residual formulation (2) generally provides better predictions around the lower frequency range (due to the nature of its approximation). When the modal density is high, the static residual compensation fails to provide a good approximation and extra terms in the residual series are required. This is a situation when the formulation proposed by the author (4) is of particular interest. Prior to this work, in order to get higher terms in the series, either the high-frequency out-of-range modes or the mass matrix of the system were needed. The formulation proposed in this thesis circumvents such a need, at the same time providing quite accurate compensation compared with the mentioned ones. The improvement is achieved from the lower modes upwards, increasing with the power of the approximation used. Two terms in the series generally provide quite accurate compensation, and that corresponds to a dynamic residual compensation. An important point about the experimental residual terms in the series form formulation is the choice of the frequency point where the dynamic residual term is evaluated. The quality of this choice has to be checked by calculating a high-frequency pseudo-eigenvalue based also on the static residual term.

One shortcoming of all the above residual formulations apart from the high-frequency pseudo-mode approach is that all necessary residual terms have to be calculated individually.

Moreover, none of them could be used to estimate residual terms in unmeasured FRFs. The mass-residual approach could be used to solve these shortcomings. Although it has not been demonstrated in this work how to obtain the mass matrix of a system experimentally, the author believes that this matrix is easier to derive and to confirm in such situations than is the stiffness matrix. The use of this formulation proved to be better than not using any residual compensation at all and generally provided quite accurate compensation for strongly-affected FRFs. It is based on the same idea as the residual term in the series form formulation, where a high-frequency pseudo-mass mode is calculated to control the quality of the formulation.

7.1 .5. RESIDUAL TERMS TRENDS

Trends in the residual terms were analysed in this work. Although the high-frequency residual terms are the stiffness-like effects of modes at frequencies much lower than their natural frequencies, a link was discovered between these terms and the mass of the system: the smaller the mass, the bigger the residual effects. Despite the fact that this conclusion can only be applied for point FRFs, it helps in choosing the FRF to be used in the mass-residual approach developed in this research or in the measurement of the most important FRFs. The other trends observed are related to their importance at resonances and anti-resonances, point and transfer FRFs or translational and rotational DOFs. It was observed that residual terms are mainly important around anti-resonances, and have relatively little significance around resonances. Also, their effect is much bigger for point than transfer FRFs, where one can say that the biggest residual term will be for a point FRF, while the smallest will be for a transfer FRF. Moreover, rotational-related FRFs have much stronger residual effects than do translational ones. The FRFs involving a mixture of the two are affected somewhere in between.

7.1.6. ESTIMATION OF RDOFS

As illustrated in this thesis, it is important to have RDOFs in the experimentally-derived models used in coupling predictions. The finite-difference approximation was employed to obtain such DOFs, since it proved to be one of the simplest techniques to use while at the same time providing quite accurate predictions. The important point about this technique is the choice of the spacing used between accelerometers which has to be such that the displacement of the modes of interest is properly described. This spacing is directly related to the order of the finite-difference approximation used. Increasing the order of the approximation for the rotation/force FRF estimation requires a smaller spacing between accelerometers. On the other hand, increasing the order for the rotation/moment FRF requires a larger spacing.

The rotational-related FRFs derived using raw FRF data were found to be very sensitive to noise effects present in the translational FRF used, with the rotation/moment FRF being the most affected by that. To minimise these noise problems, a larger spacing between accelerometers has to be adopted, with the side effect of shifting the position of the higher anti-resonances. Therefore, another solution should be adopted and that is to smooth the translational FRFs first by using a consistent modal data set plus residual compensation and later to derive the necessary rotational parameters (lst-path). Also, the rotational FRF quantities can be derived from the modal data and residual matrices in separate and the smoothed rotational curves obtained from that (2nd-path). The first two derivation matrices for the 2nd-path are the ones required by the CMS formulation, while the final curves in both paths are the ones required by the FRF coupling formulations.

It was concluded in this research that the first-order approximation produces better results for the rotation/force FRFs, while the second-order approximation produces better results for the rotation/moment FRFs. Moreover, the first-order finite-difference approximation should be used to derive rotational coordinates, while second-order finite-difference approximation should be used to derive either rotational-related residual terms or rotational FRF matrices.

7.1.7. RESIDUAL COMPENSATION AND RDOFS IN COUPLING FORMULATIONS

The experimental residual terms formulation in series form developed in this work allowed the improvement of the experimental CMS formulation used so-far and proposed by MacNeal (i.e. first-order CMS approximation). The residual matrices obtained in that case are no longer frequency-dependent and this is the only requirement for the CMS formulations. The frequency dependency comes only at the regeneration stage, when the dynamic residual matrix (and higher terms) is multiplied by the frequency value at each point of interest. Therefore, this compensation approach is also good with FRF coupling formulations. Although higher residual compensation matrices could be used, increasing that would increase also the complexity of the CMS formulations. This is not true, however, for the FRF coupling formulation. The second-order CMS approximation generally provides good accuracy and this was the approximation used here, where a new second-order formulation called IECMS was developed. Although it uses the same approach as was proposed by Craig and Chang, it has the extra advantage of being applicable for the case when only experimental data are available. The Craig-Chang formulation requires either the mass matrix of the system or the high-frequency out-of-range modes. The results obtained from the new IECMS formulation are much better than the ones

obtained from the first-order approximation formulation (MacNeal's). Until the present work, the latter was the only CMS formulation available using experimental data only.

It was observed that although the high-frequency pseudo-mode formulation produced accurate compensations for the individual translational FRFs, its use in RDOF derivations did not yield the expected results. Therefore, the FRF coupling predictions using those data were also not as good as desired. The recommendation in this thesis is to use the dynamic residual compensation and follows the conclusion quoted in the previous section. Besides, this type of residual compensation can be applied for both FRF coupling and CMS formulations, as just mentioned.

7.1.8. PARAMETERS TO COMPARE FRF CURVES

Two comparison curves were developed in this research to compare the quality of FRFs collectively: the FL (frequency level) and the FIF (frequency indicator function) or its inverse, the IF1 (inverse frequency indicator). The difference between the FIF and the IF1 is only the direction of the resonance peaks and this is the reason why they are not considered as two different formulations. The FL and FIF (or IFI) curves should be used in conjunction with each other. While the former gives a clearer indication about the natural frequencies of the FRFs used, the latter gives an indication about the anti-resonances. When two sets of FL and FIF (or IFI) curves are plotted against each other, an assessment of the predictions is obtained. These curves are also good at detecting calibration problems, even when the errors involved are small. Although these comparison curves do not indicate in which FRFs the discrepancies occur, they are a quick way of checking the predictions.

7.1.9. EXPERIMENTAL CONSIDERATIONS

Some special considerations should be taken when performing the measurements of the FRFs necessary for the coupling process. The most important of all is the proper placement of the transducers, mainly when making measurements at coupling coordinates. The effect of slightly shifting the transducer positions causes the measured anti-resonances to be shifted as well, and that can be misinterpreted by the lack of residual compensation when just the FRF curves are available for the analyst. When using these measured curves (i.e. the ones obtained with the transducers wrongly placed) in the FRF coupling predictions, the same consequence as leaving out residual compensation is obtained. The other important points are related to the hammer testing. The position of hitting the structure should be monitored using the coherence check and double hits should be avoided. The latter point may be circumvented by using a lighter hammer.

7.2. SUGGESTION FOR FUTURE WORK

The residual terms' formulations proposed in this research, as well as the ones available so far, are not capable of compensating completely for the residual influence at coordinates other than the ones measured. Although this was a primary aim of the research, this question remained still unanswered. The closest one could get to solving that problem was the mass-residual approach developed here, although the need for the mass matrix of the system remains a shortcoming of the approach from an experimental point of view. Therefore, one of the suggestions for a continuation of this work is to try to construct a mass matrix for the system from experimental data only. The few formulations available for this do not yield a good mass matrix estimation, mainly because the input data used are truncated. The mass matrix has the advantage over the stiffness matrix in that its estimation can be checked (e.g., by weighing the structure). Nevertheless, as well as trying to estimate the mass matrix from experiments, effort can be put into the experimental estimation of the stiffness matrix of the system. In such a case, the standard static residual formulation or the residual formulation in series form could be used to compensate for the lack of high-frequency residual modes.

Rotational-related parameters proved to be very important for the coupling formulations used in this thesis. Although the problem was tackled here by using the finite-difference formulations, the author believes that efforts should be made in trying to measure these quantities directly. Therefore, research into rotational transducers should be more seriously investigated. Also, the use of lasers to obtain such parameters should be made easier to the users, and more accurate, since they are still a bit cumbersome to use and prone to experimental set-up errors.

APPENDIX A: MATRIX MANIPULATION FOR THE REFINED MOBILITY COUPLING METHOD

In this appendix, a step-by-step derivation of the refined mobility coupling formulation introduced in chapter 2 is presented. Although the starting point should be equation (2.14) repeated below:

$$[H_C]^{-1} = \begin{bmatrix} H_A^{ss} & H_A^{sc} & 0 \\ H_A^{cs} & H_A^{cc} & 0 \\ 0 & 0 & I \end{bmatrix}^{-1} + \begin{bmatrix} I & 0 & 0 \\ 0 & H_B^{cc} & H_B^{cs} \\ 0 & H_B^{sc} & H_B^{ss} \end{bmatrix}^{-1} - \begin{bmatrix} I & 0 & 0 \\ 0 & 0 & I \\ 0 & I & 0 \end{bmatrix} \tag{2.14}$$

its simplified notation defined by equation (2.14a) is assumed first, i.e.:

$$[H_C]^{-1} = [H'_A]^{-1} + [H'_B]^{-1} - [I'] \tag{2.14a}$$

The referred pre- and post-multiplication mentioned in chapter 2 is performed as follows:

$$[H_C]^{-1}[H'_B] = [H'_A]^{-1}[H'_B] + [H'_B]^{-1}[H'_B] - [I'][H'_B] \tag{A.1}$$

$$[H'_A][H_C]^{-1}[H'_B] = [H'_A][H'_A]^{-1}[H'_B] + [H'_A][H'_B]^{-1}[H'_B] - [H'_A][I'][H'_B] \tag{A.2}$$

$$[H'_A][H_C]^{-1}[H'_B] = [H'_B] + [H'_A] - [H'_A][I'][H'_B] \tag{A.3}$$

$$[H'_A]^{-1}[H'_A][H_C]^{-1}[H'_B][H'_B]^{-1} = [H'_A]^{-1}([H'_B] + [H'_A] - [H'_A][I'][H'_B])[H'_B]^{-1} \tag{A.4}$$

so that the following equation can be obtained:

$$[H_C]^{-1} = [H'_A]^{-1}([H'_B] + [H'_A] - [H'_A][I'][H'_B])[H'_B]^{-1} \tag{2.15}$$

Finally, the coupled system FRF predictions can be calculated by inverting equation (2.15) as shown by the following equation:

$$[H_C] = [H'_B]([H'_B] + [H'_A] - [H'_A][I'][H'_B])^{-1}[H'_A] \tag{2.16}$$

To get the refined FRF coupling formulation sought after, the partitioned matrices expressed in equation (2.14) have to be used in the above equation. The first step is to evaluate the multiplication inside the brackets, which results in:

$$[H'_A][I][H'_B] = \begin{bmatrix} H_A^{ss} & H_A^{sc} & 0 \\ H_A^{cs} & H_A^{cc} & 0 \\ 0 & 0 & I \end{bmatrix} \begin{bmatrix} I & 0 & 0 \\ 0 & 0 & I \\ 0 & I & 0 \end{bmatrix} \begin{bmatrix} I & 0 & 0 \\ 0 & H_B^{cc} & H_B^{cs} \\ 0 & H_B^{sc} & H_B^{ss} \end{bmatrix} = \begin{bmatrix} H_A^{ss} & 0 & 0 \\ H_A^{cs} & 0 & 0 \\ 0 & H_B^{sc} & H_B^{ss} \end{bmatrix} \tag{A.5}$$

Then, the whole bracket is evaluated as follows:

$$[H'_B]+[H'_A]-[H'_A][I][H'_B]=$$
$$=\begin{bmatrix} I & 0 & 0 \\ 0 & H_B^{cc} & H_B^{cs} \\ 0 & H_B^{sc} & H_B^{ss} \end{bmatrix}+\begin{bmatrix} H_A^{ss} & H_A^{sc} & 0 \\ H_A^{cs} & H_A^{cc} & 0 \\ 0 & 0 & I \end{bmatrix}-\begin{bmatrix} H_A^{ss} & 0 & 0 \\ H_A^{cs} & 0 & 0 \\ 0 & H_B^{sc} & H_B^{ss} \end{bmatrix}=\begin{bmatrix} I & H_A^{sc} & 0 \\ 0 & H_A^{cc}+H_B^{cc} & H_B^{cs} \\ 0 & 0 & I \end{bmatrix} \quad \text{(A.6)}$$

Taking the inverse of the above result, yields:

$$\begin{bmatrix} I & H_A^{sc} & 0 \\ 0 & H_A^{cc}+H_B^{cc} & H_B^{cs} \\ 0 & 0 & I \end{bmatrix}^{-1}=\begin{bmatrix} I & -H_A^{sc}\left(H_A^{cc}+H_B^{cc}\right)^{-1} & H_A^{sc}\left(H_A^{cc}+H_B^{cc}\right)^{-1}H_B^{cs} \\ 0 & \left(H_A^{cc}+H_B^{cc}\right)^{-1} & -\left(H_A^{cc}+H_B^{cc}\right)^{-1}H_B^{cs} \\ 0 & 0 & I \end{bmatrix} \quad \text{(A.7)}$$

Pre-muitiplying the above result by the augmented FRF matrix of sub-system B, and post-multiplying by the augmented FRF matrix of sub-system A (as defined by equation (2.16)), the above equation results in:

$$[H_C]=\begin{bmatrix} I & 0 & 0 \\ 0 & H_B^{cc} & H_B^{cs} \\ 0 & H_B^{sc} & H_B^{ss} \end{bmatrix}\begin{bmatrix} I-H_A^{sc}\left(H_A^{cc}+H_B^{cc}\right)^{-1} & H_A^{sc}\left(H_A^{cc}+H_B^{cc}\right)^{-1}H_B^{cs} \\ 0 & \left(H_A^{cc}+H_B^{cc}\right)^{-1} & -\left(H_A^{cc}+H_B^{cc}\right)^{-1}H_B^{cs} \\ 0 & 0 & I \end{bmatrix}\begin{bmatrix} H_A^{ss} & H_A^{sc} & 0 \\ H_A^{cs} & H_A^{cc} & 0 \\ 0 & 0 & I \end{bmatrix}=$$
$$=\begin{bmatrix} H_A^{ss}-H_A^{sc}\left(H_A^{cc}+H_B^{cc}\right)^{-1}H_A^{cs} & H_A^{sc}-H_A^{sc}\left(H_A^{cc}+H_B^{cc}\right)^{-1}H_A^{cc} & H_A^{sc}\left(H_A^{cc}+H_B^{cc}\right)^{-1}H_B^{cs} \\ H_B^{cc}\left(H_A^{cc}+H_B^{cc}\right)^{-1}H_A^{cs} & H_B^{cc}\left(H_A^{cc}+H_B^{cc}\right)^{-1}H_A^{cc} & -H_B^{cc}\left(H_A^{cc}+H_B^{cc}\right)^{-1}H_B^{cs}+H_B^{cs} \\ H_B^{sc}\left(H_A^{cc}+H_B^{cc}\right)^{-1}H_A^{cs} & H_B^{sc}\left(H_A^{cc}+H_B^{cc}\right)^{-1}H_A^{cc} & -H_B^{sc}\left(H_A^{cc}+H_B^{cc}\right)^{-1}H_B^{cs}+H_B^{ss} \end{bmatrix} \quad \text{(A.8)}$$

A further simplification can be made by splitting up the above $[H_C]$ matrix into two, such that the first matrix contains the information about the unmodified components alone:

$$[H_C]=\begin{bmatrix} H_A^{ss} & H_A^{sc} & 0 \\ H_A^{cs} & H_A^{cc} & 0 \\ 0 & 0 & H_B^{ss} \end{bmatrix}-\cdots$$
$$\cdots\begin{bmatrix} H_A^{sc}\left(H_A^{cc}+H_B^{cc}\right)^{-1}H_A^{cs} & H_A^{sc}\left(H_A^{cc}+H_B^{cc}\right)^{-1}H_A^{cc} & -H_A^{sc}\left(H_A^{cc}+H_B^{cc}\right)^{-1}H_B^{cs} \\ H_A^{cs}-H_B^{cc}\left(H_A^{cc}+H_B^{cc}\right)^{-1}H_A^{cs} & H_A^{cc}-H_B^{cc}\left(H_A^{cc}+H_B^{cc}\right)^{-1}H_A^{cc} & H_B^{cc}\left(H_A^{cc}+H_B^{cc}\right)^{-1}H_B^{cs}+H_B^{cs} \\ -H_B^{sc}\left(H_A^{cc}+H_B^{cc}\right)^{-1}H_A^{cs} & -H_B^{sc}\left(H_A^{cc}+H_B^{cc}\right)^{-1}H_A^{cc} & H_B^{sc}\left(H_A^{cc}+H_B^{cc}\right)^{-1}H_B^{cs} \end{bmatrix} \quad \text{(A.9)}$$

Furthermore, the terms of the middle row of the second matrix in the above equation can be re-written as:

$$H_A^{cs}-H_B^{cc}\left(H_A^{cc}+H_B^{cc}\right)^{-1}H_A^{cs}=\left(I-H_B^{cc}\left(H_A^{cc}+H_B^{cc}\right)^{-1}\right)H_A^{cs}=$$
$$=\left(\left(H_A^{cc}+H_B^{cc}\right)-H_B^{cc}\right)\left(H_A^{cc}+H_B^{cc}\right)^{-1}H_A^{cs}=H_A^{cc}\left(H_A^{cc}+H_B^{cc}\right)^{-1}H_A^{cs} \quad \text{(A.10a)}$$

$$H_A^{cc} - H_B^{cc}\left(H_A^{cc} + H_B^{cc}\right)^{-1} H_A^{cc} = \left(I - H_B^{cc}\left(H_A^{cc} + H_B^{cc}\right)^{-1}\right)H_A^{cc} =$$
$$= \left(\left(H_A^{cc} + H_B^{cc}\right) - H_B^{cc}\right)\left(H_A^{cc} + H_B^{cc}\right)^{-1} H_A^{cc} = H_A^{cc}\left(H_A^{cc} + H_B^{cc}\right)^{-1} H_A^{cc} \quad \text{(A.lOb)}$$

$$H_B^{cc}\left(H_A^{cc} + H_B^{cc}\right)^{-1} H_B^{cs} - H_B^{cs} = \left(H_B^{cc}\left(H_A^{cc} + H_B^{cc}\right)^{-1} - I\right)H_B^{cs} =$$
$$= \left(H_B^{cc} - \left(H_A^{cc} + H_B^{cc}\right)\right)\left(H_A^{cc} + H_B^{cc}\right)^{-1} H_B^{cs} = -H_A^{cc}\left(H_A^{cc} + H_B^{cc}\right)^{-1} H_B^{cs} \quad \text{(A.10c)}$$

So, equation (A.9) becomes:

$$[H_C] = \begin{bmatrix} H_A^{ss} & H_A^{sc} & 0 \\ H_A^{cs} & H_A^{cc} & 0 \\ 0 & 0 & H_B^{ss} \end{bmatrix} - \cdots$$
$$\cdots \begin{bmatrix} H_A^{sc}\left(H_A^{cc} + H_B^{cc}\right)^{-1} H_A^{cs} & H_A^{sc}\left(H_A^{cc} + H_B^{cc}\right)^{-1} H_A^{cc} & -H_A^{sc}\left(H_A^{cc} + H_B^{cc}\right)^{-1} H_B^{cs} \\ H_A^{cc}\left(H_A^{cc} + H_B^{cc}\right)^{-1} H_A^{cs} & H_A^{cc}\left(H_A^{cc} + H_B^{cc}\right)^{-1} H_A^{cc} & -H_A^{cc}\left(H_A^{cc} + H_B^{cc}\right)^{-1} H_B^{cs} \\ -H_B^{sc}\left(H_A^{cc} + H_B^{cc}\right)^{-1} H_A^{cs} & -H_B^{sc}\left(H_A^{cc} + H_B^{cc}\right)^{-1} H_A^{cc} & H_B^{sc}\left(H_A^{cc} + H_B^{cc}\right)^{-1} H_B^{cs} \end{bmatrix} \quad \text{(A.11)}$$

By simplifying the above equation even further one gets to the final refined FRF coupling formulation presented in chapter 2 and used throughout the thesis:

$$[H_C] = \begin{bmatrix} H_A^{ss} & H_A^{sc} & 0 \\ H_A^{cs} & H_A^{cc} & 0 \\ 0 & 0 & H_B^{ss} \end{bmatrix} - \begin{bmatrix} H_A^{sc} \\ H_A^{cc} \\ -H_B^{sc} \end{bmatrix} \left[H_A^{cc} + H_B^{cc}\right]^{-1} \begin{bmatrix} H_A^{cs} & H_A^{cc} & -H_B^{cs} \end{bmatrix} \quad \text{(2.17)}$$

APPENDIX B: DERIVATION OF THE CONSTRAINED MODE-SHAPE MATRIX IN PHYSICAL SPACE

In this appendix, the constrained mode-shape matrix of the sub-systems in physical space for the CMS formulation without residual compensation is developed. This concept was introduced in chapter 3, section 3.4. So, coming back to equation (3.16) there, i.e.:

$$[\phi_{xC}] = \begin{bmatrix} \phi_A & 0 \\ 0 & \phi_B \end{bmatrix} [\beta] [\phi_{qC}] \tag{3.16}$$

and remembering that the following notation was introduced:

$$[\phi_{x\beta}] = \begin{bmatrix} \phi_A & 0 \\ 0 & \phi_B \end{bmatrix} [\beta] \tag{B.1}$$

one can achieve the desired objective. The above matrices can be expanded using equations (3.7) and (3.12) as follows:

$$[\phi_{x\beta}] = \begin{bmatrix} \phi_A^{cc} & \phi_A^{cr} & 0 & 0 \\ \phi_A^{sc} & \phi_A^{sr} & 0 & 0 \\ 0 & 0 & \phi_B^{cc} & \phi_B^{cr} \\ 0 & 0 & \phi_B^{sc} & \phi_B^{sr} \end{bmatrix} \begin{bmatrix} 0 & I & 0 \\ I & 0 & 0 \\ Am & Bm & -Cm \\ 0 & 0 & I \end{bmatrix} \tag{B.2}$$

Then, performing this multiplication results in:

$$[\phi_{x\beta}] = \begin{bmatrix} \phi_A^{cr} & \phi_A^{cc} & 0 \\ \phi_A^{sr} & \phi_A^{sc} & 0 \\ \phi_B^{cc} Am & \phi_B^{cc} Bm & -\phi_B^{cc} Cm + \phi_B^{cr} \\ \phi_B^{sc} Am & \phi_B^{sc} Bm & -\phi_B^{sc} Cm + \phi_B^{sr} \end{bmatrix} \tag{B.3}$$

However, the third row in equation (B.3) can be simplified further, by recalling the formulas for matrices *[Am]*, *[Bm]* and [Cm] in equation (3.12). Using these values yields to the required constraint matrix below:

$$[\phi_{x\beta}] = \begin{bmatrix} \phi_A^{cr} & \phi_A^{cc} & 0 \\ \phi_A^{sr} & \phi_A^{sc} & 0 \\ \phi_A^{cr} & \phi_A^{cc} & 0 \\ \phi_B^{sc} Am & \phi_B^{sc} Bm & -\phi_B^{sc} Cm + \phi_B^{sr} \end{bmatrix} \tag{3.17a}$$

APPENDIX C: THE INVALIDITY OF [β] CONSTRAINT IN THE RESIDUAL COMPENSATED CMS

As mentioned in chapter 3, section 35.2, if the final number of modes is greater than the final number of coordinates for the coupled system, the set of equations to be solved is redundant. As the CMS formulation without residual compensation (equation (3.15)) is able to constrain this set of equations using matrix [β] (equation (3.12)), the author thought that the natural way of constraining the redundant set of equations for the case of CMS formulation with residual compensation (equation (3.29)) would be to use the same constraint matrix. However, performing the partial multiplication in the partitioned matrices used in equation (3.29) and (3.12) the final results obtained were exactly the same partitioned matrices showed in equations (3.15). This is shown here in details.

For the case of a truncated modal set, the only values known in the mode-shape matrix expressed by equation (3.18) are the ones related to the low-frequency modes $[\phi^l]$. For the derivation here, this matrix will then be partitioned according to the partition necessary for the constraint matrix [β], i.e.:

$$[\phi^l] = \begin{bmatrix} \phi^{cc} & \phi^{cr} \\ \phi^{sc} & \phi^{rr} \end{bmatrix} \tag{C.1}$$

Basically, what we are trying to prove here is that if one pre-multiplies equation (3.29) by $[\beta]^T$ and post-multiplies it by [β], this equation is converted back to equation (3.15). Performing this multiplication, one can write:

$$[\beta]^T \begin{bmatrix} I_A & 0 \\ 0 & I_B \end{bmatrix} [\beta] \begin{Bmatrix} \ddot{q}_A \\ \ddot{q}_B \end{Bmatrix} + [\beta]^T \begin{bmatrix} \lambda_A^2 + \phi_A^{clT} Kc\, \phi_A^{cl} & -\phi_A^{clT} Kc\, \phi_B^{cl} \\ -\phi_B^{clT} Kc\, \phi_A^{cl} & \lambda_B^2 + \phi_B^{clT} Kc\, \phi_B^{cl} \end{bmatrix} [\beta] \begin{Bmatrix} q_A \\ q_B \end{Bmatrix} = \begin{Bmatrix} 0 \\ 0 \end{Bmatrix} \tag{C.2}$$

or using the format in equation (3.14):

$$[\beta]^T [\beta] \{\ddot{q}\} + [\beta]^T [K_{rc}] [\beta] \{q\} = \{0\} \tag{C.3}$$

It is straightforward to see that the first part of equation (C.3) gives the same result as matrix [Mm] showed in equation (3.15a). The second part of this equation that has to be elaborated to show that, at the end, it is equal to equation (3.15b).

Before starting showing that, matrix $[K_{rc}]$ will be partitioned in more detailed as below:

$$[K_{rc}]=\begin{bmatrix} \begin{bmatrix}\lambda_{Ac}^2 & 0\\ 0 & \lambda_{As}^2\end{bmatrix}+\begin{bmatrix}\phi_A^{cc\,T}\\ \phi_A^{cs\,T}\end{bmatrix}[Kc]\begin{bmatrix}\phi_A^{cc} & \phi_A^{cs}\end{bmatrix} & -\begin{bmatrix}\phi_A^{cc\,T}\\ \phi_A^{cs\,T}\end{bmatrix}[Kc]\begin{bmatrix}\phi_B^{cc} & \phi_B^{cs}\end{bmatrix} \\ -\begin{bmatrix}\phi_B^{cc\,T}\\ \phi_B^{cs\,T}\end{bmatrix}[Kc]\begin{bmatrix}\phi_A^{cc} & \phi_A^{cs}\end{bmatrix} & \begin{bmatrix}\lambda_{Bc}^2 & 0\\ 0 & \lambda_{Bs}^2\end{bmatrix}+\begin{bmatrix}\phi_B^{cc\,T}\\ \phi_B^{cs\,T}\end{bmatrix}[Kc]\begin{bmatrix}\phi_B^{cc} & \phi_B^{cs}\end{bmatrix} \end{bmatrix} \quad (C.4)$$

Developing equation (C.4), yields:

$$[K_{rc}]=\begin{bmatrix} \lambda_{Ac}^2+\phi_A^{cc\,T}Kc\phi_A^{cc} & \phi_A^{cc\,T}Kc\phi_A^{cs} & -\phi_A^{cc\,T}Kc\phi_B^{cc} & -\phi_A^{cc\,T}Kc\phi_B^{cs} \\ \phi_A^{cs\,T}Kc\phi_A^{cc} & \lambda_{As}^2+\phi_A^{cs\,T}Kc\phi_A^{cs} & -\phi_A^{cs\,T}Kc\phi_B^{cc} & -\phi_A^{cs\,T}Kc\phi_B^{cs} \\ -\phi_B^{cc\,T}Kc\phi_A^{cc} & -\phi_B^{cc\,T}Kc\phi_A^{cs} & \lambda_{Bc}^2+\phi_B^{cc\,T}Kc\phi_B^{cc} & \phi_B^{cc\,T}Kc\phi_B^{cs} \\ -\phi_B^{cs\,T}Kc\phi_A^{cc} & -\phi_B^{cs\,T}Kc\phi_A^{cs} & \phi_B^{cs\,T}Kc\phi_B^{cc} & \lambda_{Bs}^2+\phi_B^{cs\,T}Kc\phi_B^{cs} \end{bmatrix} \quad (C.5)$$

Recalling matrix [β]:

$$[\beta]=\begin{bmatrix} 0 & I & 0\\ I & 0 & 0\\ Am & Bm & -Cm\\ 0 & 0 & I \end{bmatrix} \quad (C.6)$$

Its full transpose form can be written as:

$$[\beta]^T=\begin{bmatrix} 0 & I & \phi_A^{cs\,T}\phi_B^{cc-T} & 0\\ I & 0 & \phi_A^{cc\,T}\phi_B^{cc-T} & 0\\ 0 & 0 & -\phi_B^{cs\,T}\phi_B^{cc-T} & I \end{bmatrix} \quad (C.7)$$

Performing the first multiplication for the second part of equation (C.3), yields:

$$[\beta]^T[K_{rc}]=\begin{bmatrix} 0 & \lambda_{As}^2 & Am^T\lambda_{Bc}^2 & 0\\ \lambda_{Ac}^2 & 0 & Bm^T\lambda_{Bc}^2 & 0\\ 0 & 0 & -Cm^T\lambda_{Bc}^2 & \lambda_{Bs}^2 \end{bmatrix} \quad (C.8)$$

It can be seen that this first multiplication already destroyed the residual compensation given by [Kc]. Carry on the multiplication at the second part of equation (C.3), yields the final result:

$$[\beta]^T[K_{rc}][\beta]=\begin{bmatrix} \lambda_{As}^2+Am^T\lambda_{Bc}^2 Am & Am^T\lambda_{Bc}^2 Bm & -Am^T\lambda_{Bc}^2 Cm\\ Bm^T\lambda_{Bc}^2 Am & \lambda_{Ac}^2+Bm^T\lambda_{Bc}^2 Bm & -Bm^T\lambda_{Bc}^2 Cm\\ -Cm^T\lambda_{Bc}^2 Am & -Cm^T\lambda_{Bc}^2 Bm & \lambda_{Br}^2+Cm^T\lambda_{Bc}^2 Cm \end{bmatrix} \quad (C.9)$$

which is identical to *[Km]* matrix showed in equation (3.15b), as we wanted to prove.

APPENDIX D: CORRECT PHYSICAL MODE-SHAPE MATRIX FOR THE UNCOUPLED SUB-SYSTEMS

In this appendix, the uncoupled mode-shape matrix in physical space is going to be derived taking into consideration the residual compensation related to the out-of-range modes. This concept was given in chapter 3, section 3.5.2. The first step is to recall the transformation equation (3.18) i.e.:

$$\{x\} = \begin{bmatrix} \phi^l & \phi^h \end{bmatrix} \begin{Bmatrix} p^l \\ p^h \end{Bmatrix} \tag{3.18}$$

The expanded form of the above equation for the case when a first-order approximation to the residual compensation is used to represent the high-frequency residual terms is expressed by equation (3.23), repeated below:

$$\{x\} = [\phi^l]\{p_l\} + [\phi^h][\lambda_h^2]^{-1}[\phi^h]^T\{f\} \tag{3.23}$$

It is important to remember that forces are assumed to be applied only at coupling coordinates. Therefore, considering that and partitioning the above equation in terms of coupling (c) and slave (s) coordinates, the following equation can be written:

$$\begin{Bmatrix} x^c \\ x^s \end{Bmatrix} = \begin{bmatrix} \phi^{cl} \\ \phi^{sl} \end{bmatrix} \{p^l\} + \begin{bmatrix} \phi^{ch} \\ \phi^{sh} \end{bmatrix} [\lambda_h^2]^{-1} \begin{bmatrix} \phi^{ch} \\ \phi^{sh} \end{bmatrix}^T \begin{Bmatrix} f^c \\ 0 \end{Bmatrix} \tag{D.1}$$

Performing the necessary multiplication and using the notation for the residual terms compensation matrix (equation (3.24)) in partitioned form, yields to:

$$\begin{Bmatrix} x^c \\ x^s \end{Bmatrix} = \begin{bmatrix} \phi^{cl} \\ \phi^{sl} \end{bmatrix} \{p^l\} + \begin{bmatrix} R^{cc} \\ R^{sc} \end{bmatrix} \{f^c\} \tag{D.2}$$

The top part of equation (D.2), when written for each sub-system, represents actually equations (3.25a) and (3.25b) used to derive the CMS formulation. Re-assembling equation (D.2), results in:

$$\begin{Bmatrix} x^c \\ x^s \end{Bmatrix} = \begin{bmatrix} \phi^{cl} & R^{cc} \\ \phi^{sl} & R^{sc} \end{bmatrix} \begin{Bmatrix} p^l \\ f^c \end{Bmatrix} \tag{D.3}$$

To arrive to the derivation wanted, one has to substitute the force vector on the RHS of equation (D.3) by equations (3.28a) and (3.28b). Equation (3.28a) is repeated here for clarity, that is:

$$\{f_A^c\} = [Kc]\left([\phi_B^{cl}]\{p_B^l\} - [\phi_A^{cl}]\{p_A^l\}\right) \tag{3.28a}$$

So, following the just specified steps, equation (D.3) can be developed considering both sub-systems as:

$$\begin{Bmatrix} x_A^s \\ x_A^c \\ x_B^c \\ x_B^s \end{Bmatrix} = \begin{bmatrix} \phi_A^{sl} & R_A^{sc} & 0 & 0 \\ \phi_A^{cl} & R_A^{cc} & 0 & 0 \\ 0 & 0 & \phi_B^{cl} & R_B^{cc} \\ 0 & 0 & \phi_B^{sl} & R_B^{sc} \end{bmatrix} \begin{bmatrix} I & 0 \\ -Kc\phi_A^{cl} & Kc\phi_B^{cl} \\ 0 & I \\ Kc\phi_A^{cl} & -Kc\phi_B^{cl} \end{bmatrix} \begin{Bmatrix} p_A^l \\ p_B^l \end{Bmatrix} \tag{D.4}$$

Now, an analogy can be made between equation (D.4) and equation (3.31) below:

$$[\phi_{xC}] = \begin{bmatrix} \phi_A & 0 \\ 0 & \phi_B \end{bmatrix} [T] [\phi_{pC}] \tag{3.3 1}$$

The first two matrices on the RHS of both equations are equivalent. Thus, the required matrix derivation is represented by the multiplication of these matrices in equation (D.4), i.e.:

$$[\phi_{xAB}] = \begin{vmatrix} \phi_A^{sl} - R_A^{sc} Kc\phi_A^{cl} & R_A^{sc} Kc\phi_B^{cl} \\ \phi_A^{cl} - R_A^{cc} Kc\phi_A^{cl} & R_A^{cc} Kc\phi_B^{cl} \\ R_B^{cc} Kc\phi_A^{cl} & \phi_B^{cl} - R_B^{cc} Kc\phi_B^{cl} \\ R_B^{sc} Kc\phi_A^{cl} & \phi_B^{sl} - R_B^{sc} Kc\phi_B^{cl} \end{vmatrix} \tag{3.32}$$

APPENDIX E: DERIVATION OF MODAL CONSTANTS AND FRFS

As mentioned in chapter 4, section 4.4, having only one row or column of the full FRF matrix [H(o)] does not mean that one can reconstruct the full matrix. Although the following relationship is valid for each mode:

$$_r A_{ij} = {}_r A_{ii}\, {}_r A_{jj} \tag{4.4}$$

one cannot say the same for:

$$H_{ij}^2 = H_{ii}\, H_{jj} \tag{4.5}$$

since the value of H is made up of a summation of several modes, as shown in equation (4.1)

To prove this, a 2 DOF system is going to be considered. Calling the denominator of equation (4.1) as C 1, for the first mode, and C2, for the second mode, leads:

$$H_{ij} = \frac{{}_1 A_{ij}}{C_1} + \frac{{}_2 A_{ij}}{C_2} \tag{E.1a}$$

$$H_{ii} = \frac{{}_1 A_{ii}}{C_1} + \frac{{}_2 A_{ii}}{C_2} \tag{E.2b}$$

$$H_{jj} \quad \frac{{}_1 A_{jj}}{C_1} + \frac{{}_2 A_{jj}}{C_2} \tag{E.3c}$$

Using the above equations yields the following expression for the LHS of equation (4.5):

$$H_{ij}^2 = \left(\frac{{}_1 A_{ij}}{C_1} + \frac{{}_2 A_{ij}}{C_2} \right)^2 = \frac{{}_1 A_{ij}^2}{C_1^2} + 2\frac{{}_1 A_{ij}\, {}_2 A_{ij}}{C_1 C_2} + \frac{{}_2 A_{ij}^2}{C_2} \tag{E.4}$$

The RHS of this same equation becomes:

$$H_{ii} H_{jj} = \left(\frac{{}_1 A_{ii}}{C_1} + \frac{{}_2 A_{ii}}{C_2} \right)\left(\frac{{}_1 A_{jj}}{C_1} + \frac{{}_2 A_{jj}}{C_2} \right) = \frac{{}_1 A_{ii}\, {}_1 A_{jj}}{C_1^2} + \frac{{}_1 A_{ii}\, {}_2 A_{jj}}{C_1 C_2} + \frac{{}_2 A_{ii}\, {}_1 A_{jj}}{C_1 C_2} + \frac{{}_2 A_{ii}\, {}_2 A_{jj}}{C_2^2} \tag{E.5}$$

Since the first and the last terms of the RHS of equations (E.4) and (E.5) are identical, according to equation (4.4), the only way equation (4.5) would be true is when:

$$2\left({}_1 A_{ij}\, {}_2 A_{ij} \right) = \left({}_1 A_{ii}\, {}_2 A_{jj} \right) + \left({}_2 A_{ii}\, {}_1 A_{jj} \right) \tag{E.6}$$

This is clearly not the case. Only when one individual mode at a time is considered is equation (4.5) valid. For example, if just the first mode is examined, only the first terms of the RHS of equations (E.4) and (E.5) are present, and that follows the relationship expressed by equation (4.5). The same argument would be valid if instead of using *H, R* would be used. The non-

observance of equation (4.5) is due to the presence of more than one mode in the system, as demonstrated above.

REFERENCES (IN ALPHABETIC ORDER)

ABREVIATIONSUSED :

- AIAA "American Institute of Aeronautics and Astronautics"
- AMD "Applied Mechanics Division, ASME"
- ASA "Acoustical Society of America"
- ASCE "American Society of Civil Engineers"
- ASME "American Society of Mechanical Engineers"
- IMAC "International Modal Analysis Conference"
- ISMA "International Seminar on Modal Analysis"
- IJAEMA "International Journal of Analytical and Experimental Modal Analysis"
- JSV "Journal of Sound and Vibration"

1. Ahmed, I.
Reducing the Effects of Residual Modes in Measured Frequency-Response Data
IJAEMA, 2(3), pp. 113-120 (1987)

2. Allemang, R.J. and Brown, D.L
A Correlation Coefficient for Modal Testing
Proc. IMAC I, pp. 110-l 16 (1983)

3. Allemang, R.J.and Brown, D.L.
A Review of Modal Parameter Estimation Concepts
Proc.of 11 th ISMA - KULeuven, Al-3 (1986)

4. ASA Standards
American National Standard: Guide to the Experimental Determination of Rotational Mobility Properties and the Complete Mobility Matrix
ASA 34-1984, ANSI S2.34-1984 (1984)

5. Avitabile, P., O'Callahan, J., Chou, C-M.and Kalkunte, V.
Expansion of Rotational Degrees-of--freedom for Structural Dynamic Modification
Proc. IMAC V, pp. 950-955 (1987)

6. Avitable, P.and O'Callahan, J.C.
Understanding Structural Dynamic Modification and the Effect of Truncation
IJAEMA, 6(4), pp. 215-235 (1991)

7. Benfield, W.A.and Hruda R.F.
Vibration Analysis of Structures by Component Mode Substitution
AIAA Journal, 9(7), pp. 1255-1261 (1971)

8. Bertran, A.
Using Modal Substructuring Techniques in Modelling Large Flexible Spacecraft
Joint ASCE/ASME Mechanics Conference, AMD - Vo1.67, pp. 205-220 (1985)

9. Bill, B. and Wicks, A.L.
Measuring Simultaneously Translational and Angular Acceleration with the New Translational Angular Piezobeam (TAP) System
Sensors and Actuators, A21-A23, pp. *282-284 (1990)*

10. Bishop, R.E.D.and Johnson, D.C.
The Mechanics of Vibration
Cambridge University Press (1960)

11. Bokelberg, E. H., Sommer, H, J., Trethewey, M. W. and Chu, C-H.
Simultaneous Measurement of Six Coordinate vibration: Three Translations and Three Rotations
Proc. IMAC XI, pp. 522-526 (1993)

12. Brassard, J.and Massoud, M.
Identification of a Complete Mobility Matrix of a Synthesied System from Component Mobility Measurements
Proc. IMAC V, pp. 319-323 (1987)

13. Braun, S.G.
On the Incompleteness of Modal Representation: Some Problems and Solutions
Proc.of the Structural Dynamics: Recent Advances, pp. 38-53 (1994)

14. Braun, S.G.and Ram, Y.M.
Predicting the Effect of Structural Modification: Upper and Lower Bounds due to Modal Truncation
IJAEMA, 6(3), pp. 201-213 (1991)

15. Brillhart, R.D., Hunt, D.L., Flanigan, C.C., Guinn, Rand Hull, R.
Transfer Orbit Stage Modal Survey, Part I: Measurement of Free-Free Modes and Residual Flexibility
Proc. IMAC VII, pp. 1150-l 156 (1989)

16. Brinkman, B.A.
Generating Modal Parameters that Compensate for Residual Energy
Proc. IMAC IV, pp. 119-122 (1986)

17. Brinkman, B.A.
A Quantitative Study Using Residual Modes to Improve Dynamic Models
Proc. IMAC V, pp. 671-678 (1987)

18. Cafeo, J.A., Trethewey, M.W., Rieker, J.R.and Sommer III, H.J.
Application of a Three Degree of Freedom Laser Vibrometer for Experimental Modal Analysis
Proc. IMAC IX, pp. 1161-1167 (1991)

19. Cafeo, J.A.; Trethewey, M.W.and Sommer, H.J.
Measurement and Application of Experimental Rotational Degrees of Freedom for Mode Shape Refinement
IJAEMA, 7(4), pp. 255-269 (1992)

20. Cafeo, J. A., Trethewey, M. W. and Sommer III, H. J.
On the Use of Measured Rotational Degrees-of-Freedom in Structural Dynamic Modification
Proc. IMAC XI, pp. 96-101 (1993)

21. Camarda, C.J.; Haftka, R.T.and Riley, M.F.
An Evaluation of Higher-Order Modal Methods for Calculating Transient Structural Response
Computers & Structure, 27(1), pp. 89-101 (1987)

22. Chang, K-J., Jung, J-H., Jee, T-H. and Park, Y-P.
Modal Synthesis Method Using Interpolated Rotational Degrees-of-Freedom
Proc. IMAC XIV, pp. 1621-1627 (1996)

23. Chen, H.C.; Yee, E.K.; Wang, I.C.and Tsuei, Y.G.
A Direct Modal Synthesis Technique for Dynamic Analysis
Proc. IMAC XII, pp. 1537-1544 (1994)

24. Chen, W-H.and Chemg, J-S.
Modal Synthesis Via Combined Experimental and Finite Element Technique Considering Rotational Effects
JSV, Vol.103(1), pp. l-l 1 (1985)

25. Chung, K.R.and Lee, C.W.
An Efficient Method for Compensating Truncated Higher Modes in Structural Dynamics Modification
Proc. Instn. Mech. Engrs., Vol.200, No Cl, pp. 41-48 (1986)

26. Coppolino, R.N.
Hybrib Experimental/Analytical Dynamic Models of Aerospace Structures
Joint ASCE/ASME Mechanics Conference, AMD - Vo1.67, pp. 79- 107 (1985)

27. Craig Jr., R.R.and Bampton, M.C.C.
Coupling of Substructures for Dynamic Analyses
AIAA Journal, 6(7), pp. 1313-1319 (1968)

28. Craig Jr., R.R.and Chang, C-J.
A Review of Substructure Coupling Methods for Dynamic Analysis
13th Annual Meeting (Society of Engineering Science), Advances in Engineering Science, Vol.2, NASA CP-2001, pp. 393-408 (1976)

29. Craig Jr., R.R.and Chang, C-J.
Substructure Coupling for Dynamic Analysis and Testing
NASA Contractor Report, NASA CR-278 1 (1977)

30. Craig Jr., R.R.
Structural Dynamics: An Introduction to Computer Methods
John Wiley & Sons (198 1)

31. Craig Jr., R.R.
A Review of Time-Domain and Frequency Domain Component Mode Synthesis Methods
IJAEMA, 2(2), pp. 59-72 (1987)

32. Craig Jr., R.R.
Substructure Methods in Vibration
Transation of the ASME: Journal of Vibration and Acoustics, Vo1.117, pp. 207-213 (1995)

33. Deel, J.C and Luk, Y.W.
Modal Testing Considerations for Structural Modification Applications
Proc. IMAC III, pp. 46-52 (1985)

34. Doebling, S.W.
Measurement of Structural Flexibility Matrices for Experiments with Incomplete Reciprocity
Ph.D.Thesis - College of Engineering, University of Colorado (1995)

35. Duncan, W.J.
Mechanical Admittances and Their Applications to Oscillation Problems
HMSO Report and Memoranda No. 2000 (1946)

36. Elliot, K.B.and Mitchell, L.D.
The Effect of Modal Truncation on Modal Modification
Proc. IMAC V, pp. 72-78 (1987)

37. Ewins, D.J.and Sainsbury, M.G.
Mobility Measurements for the Vibration Analysis of Connected Structures
Shock and Vibration Bulletin, 42(1), pp. 105-122 (1972)

38. Ewins, D.J.and Gleeson, P.T.
Experimental Determination of Multidirectional Mobility Data for Beams
Shock and Vibration Bulletin, 45(5), (1975)

39. Ewins, D.J.; Silva, J.M.M.and Maleci, G.
Vibration Analysis of a Helicopter Plus an Externally-Attached Structure
Shock and Vibration Bulletin, 50(2), pp. 155- 17 1 (1980)

40. Ewins, D.J.
On Prediction Point Mobility Plots From Measurements of Other Mobility Parameter
JSV, 70 (1), pp. 69-75 (1980)

41. Ewins, D.J.
Modal Testing: Theory and Practice
Research Study Press (1984)

42. Ewins, D.J.
Modal Test Requirements for Coupled Structure Analysis Using Experimentally-Derived Component Models
Joint ASCE/ASME Mechanics Conference, AMD - Vo1.67, pp. 31-47 (1985)

43. Ewins, D.J.
Analysis of Modified or Coupled Structures Using FRF properties
Internal report, No. 86002 (1986)

44. Friswell, M.I.; Garvey, S.D. and Penny, J.E.T.
Model Reduction Using Dynamic and Iterative IRS Techniques
JSV, 186(2), pp. 311-323 (1995)

45. Furusawa, M.and Tominaga T.
Rigid-Body Mody Enhancement and Rotational Dof Estimation for Experimental Modal Analysis
Proc. IMAC IV, pp. 1149-I 155 (1986)

46. Gialamas, T., Tsahalis, D., Bregant, L., Otte, D. and Van der Auweraer, H.
Substructuring by Means of FRFs: Some Investigations on the Significance of Rotational DOFs
Proc. IMAC XIV, pp. 619-625 (1996)

47. Gladwell, G.M.L.
Branch Mode Analysis of Vibrating Systems
JSV, 1, pp. 41-59 (1964)

48. Gleeson, P.T.
Identification of Spatial Models
Ph.D.Thesis - Imperial College, University of London (1979)

49. Goldenberg, Sand Shapiro, M.
A Study of Modal Coupling Procedures
NASA Contract No. NAS- 10635-8, NASA CR- 112252 (1972)

50. Goldman, R.L.
Vibration Analysis by Dynamic Partitioning
AIAA Journal, 7(6), pp. 1152-1154 (1969)

51. Goyder, H.G.D.
Methods and Application of Structural Modelling from Measured Structural Frequency Response Data
JSV, 68(2), pp. 209-230 (1980)

52. Grafe, H.
On the Significance of Various Design Parameters of Vibrating Structures in High-Frequency Regions
Private communication (1995)

53. Guyan, R.J.
Reduction of Stiffness and Mass Matrices
AIAA Journal, 3(2), pp. 380 (1965)

54. Gwinn, K.W.; Lauffer, J.P.and Miller, A.K.
Component Mode Synthesis Using Experimental Modes Ehanced by Mass Loading
Proc. IMAC VI, pp 1088-1093 (1988)

55. Haisty, B.S.and Springer, W.T.
A Simplified Method for Extracting Rotational Degrees-of-Freedom Information From Modal-Test Data
IJAEMA, 1(3), pp. 35-39 (1986)

56. Heer, E.and Lutes, L.D.
Application of the Mechanical Receptance Coupling Principle to Spacecraft Systems
Shock and Vibration Bulletin, 38(2), (1968)

57. Hintz, R.M.
Analytical Methods in Component Mode Synthesis
AIAA Journal, 13 (8), pp. 1007-1015 (1975)

58. Hitchings, D.
NAFEMS: A Finite Element Dynamics Primer
NAFEMS publication (1992)

59. Hou, S.N.
Review of Modal Synthesis Techniques and a New Approach
Shock and Vibration Bulletin, 40, (1969)

60. Hruda, R.F.
A Recommendation on the Use of Free-Free/Residual Flexibility Versus Fixed-Interface Dynamic Models for Shuttle Loads Analyses
Joint ASCE/ASME Mechanics Conference, AMD - Vo1.67, pp. 221-228 (1985)

61. Hu, H.M.; Ju, M.S.and Tsuei, Y.G.
Comparison Study of Modal Synthesis Methods
Proc. IMAC XI, pp. 877-882 (1993)

62. Hurty, W.C.
Vibrations of Structural Systems by Component Mode Synthesis
Proc. ASCE, Journal Eng. Mech. Div., 86, pp. 51-69 (1960)

63. Hurty, W.C.
Dynamic Analysis of Structural Systems Using Component Modes
AIAA Journal, 3(4), pp. 678-685 (1965)

64. Imamovic, N.
FOREST Technique
To be published

65. Imregun, M., Robb, D.A.and Ewins, D.J.

66. Imregun, M.and Visser, W.J.
A Review of Model Updating Techniques
Shock and Vibration Digest, 23(1), pp. 9-20 (1991)

67. Jetmundsen, B., Bielawa, R.L.and Flannelly, W.G.
Generalized Frequency Domain Substructure Synthesis
Journal of the American Helicopter Society, pp. 55-64 (1988)

68. Kanda, H., Wei, M.L., Allemang, R.J.and Brown, D.L.
Structural Dynamic Modifications Using Mass Additive Technique
Proc. IMAC IV, pp. 691-699 (1986)

69. Klosterman, A.L.
On the Experimental Determination and Use of Modal Representation of Dynamic Characteristics
Ph.D.Thesis - University of Cincinatti (1972)

70. Kochersberger, K.and Mitchell, L.D.
The use of an Improved Residual Model and Sine Excitation to Iteratively Determine Mode Vectors
Proc. IMAC XII, pp. 356-362 (1994)

71. Lamontia, M.A.
On the Determination and Use of Residual Flexibilities, Inertia Restraints and Rigid-Body Modes
Proc. IMAC I, pp. 153-159 (1982)

72. Larsson, P.O.
Dynamic Analysis of Assembled Structures Using Frequency-Response Functions: Improved Formulation of Constraints
IJAEMA, 5(1), pp. 1-12 (1989)

73. Laughlin, D.R., Andaman, A.A. and Sebesta, H.R.
Inertial Angular Rate Sensors: Theory and Applications
Sensors, pp. 20-24 (Oct. 1992)

74. Leung, Y .T.
Accelerated Convergence of Dynamic Flexibility in Series Form
Eng.Struct., Vol. 1, pp. 203-206 (1979)

75. Leuridan, J., Otte, D., Grangier, H.and Aquilina, R.
Coupling of Structures Using Measured FRFS by Means of SVD-Based Data Reduction Techniques
Proc. IMAC VIII, pp. 213-220 (1990)

76. Lin, A.C.Y, Yee, E.K.L., Gu, Y.S.and Tsuei Y.G.
Case Study of the Comparison of Modal Force Method and Modal Modeling in Modal Synthesis
Proc. IMAC VIII, pp. 248-254 (1990)

77. Licht, T.R.
Angular Vibration Measurments Transducers and Their Configuration
Proc. IMAC III, pp. 503-506 (1985)

78. Llorca, F; Gerard, A.and Brenot, D.
Improving Interface Conditions in Modal Synthesis Methods.Application to a Bolted Assembly of Rectangular Plates
Proc. IMAC XII, pp. 411-417 (1994)

79. Lutes, L.D.and Heer, E.
Receptance Coupling of Structural Components Near a Component Resonance Frequency
Jet Propulsion Laboratory Technical Memorandum 33-4 11, October (1968)

80. MacNeal, R.H.
A Hybrid Method Of Component Mode Representation For Structural Dynamic Analysis
Computer and Structures, v.1, pp. 581-601 (1971)

81. Maldonado, G.O.and Singh, M.P.
Random Response of Structures by a Force Derivative Approach
JSV, 155(1), pp. 13-29 (1991)

82. Maleci, G.and Young, J.W.
The Effect of Rotational Degrees of Freedom in System Analysis (SA) via Building Block Approach (BBA)
Proc. IMAC III, pp. 1040- 1045 (1985)

83. Martinez, D.R.and Miller, A.K.
Combined Experimental/Analytical Modelling of Dynamic Structural Systems: Introduction
Joint ASCE/ASME Mechanics Conference, AMD - Vo1.67, pp. iii-iv (1985)

84. Martinez, D.R.; Miller, A.K.and Came, T.G.
Combined Experimental/Analytical Modeling of Shell/Payload Structures
Joint ASCE/ASME Mechanics Conference, AMD - Vo1.67, pp. 167-194 (1985)

85. Meirovitch, L.
Computational Methods in Structural Dynamics
Sijthoff & Noordhoff (1980)

86. MODENT
Users Guide
ICATS - Imperial College, Analysis, Testing and Software (1992)

87. Ng'andu, A.N., Fox, C.H.J.and Williams, E.J.
Estimation of Rotational Degrees-of--freedom Using Curve and Surface Fitting
Proc. IMAC XI, pp. 620-626 (1993)

88. Ng'andu, A.N.; Fox, C.H.J.and Williams, E.J.
On the Estimation of Rotational Degrees-of-Freedom Using Spline Functions
Proc. IMAC XIII, pp. 791-797 (1995)

89. Noble, B.and Daniel, J.W.
Applied Linear Algebra - Second Edition
Prentice-Hall Inc.(1977)

90. O'Callahan, J.C.; Lieu, I-W.and Chou, C-M.
Determination of Rotational Degrees-of-freedom for Moment Transfers in Structural Modification
Proc. IMAC III, pp. 465-470 (1985)

91. O'Callahan, J.C., Avitabile, R., Lieu, I-W., Madden, R.
An Efficient Method of Determining Rotational Degrees-of-freedom from Analytical and Experimental Modal Data
Proc. IMAC IV - pp. 50-58 (1986)

92. Okubo, N.And Matsuzaki, T.
Determination of Residual Flexibilty and its Effective Use in Structural Modification
Proc. IMAC VII, pp. 578-583 (1989)

93. Oliver, D.
Non-Contact Vibration Imager for Wide Range of Component Sizes and Displacement Amplitudes
Proc. IMAC VI, pp 629-638 (1988)

94. Ram, Y.M.and Braun, S.G.
Structural Dynamic Modifications Using Truncated Data: Bounds for the Eigenvalues
Mechanical System and Signal Processing, 4(1), pp. 39-52 (1990)

95. Randall, R.B .; Gao, Y .and Sestiery, A.
Phantom Zeros in Curve-Fitted Frequency Response Functions
Mechanical System and Signal Processing, 8(6), pp. 607-622 (1994)

96. Ratcliffe, M.J. and Lieven, N.A.J.
Measuring Rotations Using a Easer Doppler Vibrometer
Proc. IMAC XIV, pp. 1002-1008 (1996)

97. Ren, Y .and Beards, C.F.
On Substructure Synthesis with FRF data
JSV, 185(5), pp. 845-866 (1995)

98. Rorrer, R.A.L.; Wicks, A.L.and Williams, J.
Angular Acceleration Measurements of a Free-Free Beam
Proc. IMAC VII, pp. 1300-1304 (1989)

99. Rubin, S.
Improved Component-Mode Representation for Structural Dynamic Analysis
AIAA Journal, 13(8), pp. 995-1006 (1975)

100. Sainsbury, M.G.
Vibration Analysis of Damped Complex Structures
Ph.D.Thesis - Imperial College, University of London (1976)

101. Salvini, P. and Sestieri, A.
Predicting the Frequency Response Function of a Structure When Adding Constraints
IJAEMA, 8(1), pp. 55-62 (1993)

102. Sanderson, M.A.
Direct Measurement of Moment Mobility
Report F93-02, ISSN 0283-832X, Chalmers University of Technology, Department of Applied Acoustics (1993)

103. Sattinger, S.S.
A Method for Experimentally Determining Rotational Mobilities of Structures
Shock and Vibration Bulletin, 50(2), pp. 17-27 (1980)

104. Silva, J.M.M.
Measurement and Applications of Structural Mobility Data for the Vibration Analysis of Complex Structures
Ph.D.Thesis - Imperial College, University of London (1978)

105. Silva, J.M.M. and Femandes, M.M.R.
Dynamic Analysis and Modeling of the Blades of a Wind Energy Converter
Proc. IMAC V, pp. 1129-1135 (1987)

106. Skingle, G.W.
A Review of the Procedure for Structural Modification Using Frequency Response Functions
Internal report, No. 87 10 (1987)

107. Skingle, G.W.
Structural Dynamic Modification Using Experimental Data
Ph.D.Thesis - Imperial College, University of London (1989)

108. Smiley, R.G.and Brinkman, B.A
Rotational Degrees-of-Freedom in Structural Modification
Proc. IMAC II, pp. *937-939 (1984)*

109. Smith, J.E.
Measurement of the Total Structural Mobility Matrix
Shock and Vibration Bulletin, 40(7), pp. 51-84 (1969)

110. Smith, M.J.
An Evaluation of Component Mode Synthesis for Modal Analysis of Finite Element Models
Ph.D.Thesis, University of British Columbia (1993)

111. Smith, M.J.and Hutton, S.G.
Estimating Residual Terms for Frequency Response Function Matrix
To be published

112. Smith, K.S.and Peng, C-Y.
SIR-C Modal Survey: A Case Study in Free-Free Testing
Proc. IMAC XII, pp. 176-183 (1994)

113. Snyder, V.W.
Structural Modification and Modal Analysis - A Survey
IJAEMA, 1(1), pp. 45-52 (1986)

114. Sohaney, R.C.and Bonnecase, D.
Residual Mobilities and Structural Dynamic Modifications
F'roc. IMAC VII, pp. 568-574 (1989)

115. Sriram, P.; Craig, J.I. and Hanagud, S.
A Scanning Laser Doppler Vibrometerfor Modal Testing
IJAEMA, 5(3), pp. 155-167 (1990)

116. Stanbridge, A.B.and Ewins, D.J.
Measurement of Translational and Angular Vibration Using a Scanning Laser Doppler Vibrometer
Proc.of 1st Int.Conf.on Vibration Measurements by Laser Techniques: Advances and Applications, pp. 37-47 (1994)

117. Stassis, A.C.and Whittaker, A.R.
Structural Modifications Using Raw Frequency Response Functions: Some Practical Observations
Proc.of 1 lth ISMA - KULeuven, El-3 (1986)

118. Stebbins, M.A; Blough, J.R.; Shelley; S.J. and Brown, D.L
Measuring and Including the Effects of Moments and Rotations for the Accurate Modeling of Transmitted Forces
Proc. IMAC XIV, pp. 429-436 (1996)

119. Suarez, L.E.and Matheu, E.E.
A Modal Synthesis Technique Based on the Force Derivative Method
Transation of the ASME: Journal of Vibration and Acoustics, Vol.1 14, pp. 209-216 (1992)

120. Suarez, L.E.and Singh, M.P.
Modal Synthesis Method for General Dynamic Systems
ASCE, Journal of Engineering Mechanics, 187(7), pp. 1488-1503 (1992)

121. Tolani, S.K.and Rocke, R.D.
Modal Truncation of Substructures Used in Free Vibration Analysis
Transation of the ASME: Journal of Engineering for Industry, Paper No. 75-DET-82, pp. l-8 (1975)

122. Trethewey, M.W.; Sommer, H.J.and Cafeo, J.A.
A Dual Beam Easer Vibrometer for Measurement of Dynamic Structural Rotations and Displacements
JSV, 164(1), pp. 67-84 (1993)

123. Tsuei, Y.G.and Yee, E.K.L.
An Investigation to the Solution of Component Modal Synthesis
Proc. IMAC VI, pp 383-388 (1988)

124. Tsuei, Y.G., Yee, E.K.L.and Lin, A.C.Y.
Physical Interpretation and Application of a Component Modal Synthesis Technique (Modal Force Method)
Proc. IMAC VIII, pp. 35-42 (1990)

125. Ulm, ST.
Investigation into the Effective Use of Structural Modification
Proc. IMAC IV, pp. 1279-1286 (1986)

126. Urgueira, A.P.V.and Ewins, D.J.
A Refined Modal Coupling Technique for Including Residual Effects of Out-of-Range Modes
Proc. IMAC VII, pp. 299-306 (1989)

127. Urgueira, A.P.V.
Dynamic Analysis of Coupled Structures Using Experimental Data
Ph.D.Thesis - Imperial College, University of London (1989)

128. Wang, Wand Kirkhope, J.
Complex Component Mode Synthesis for Damped Systems
JSV, 181(5), pp. 781-800 (1995)

129. Whang, B.; Gilbert, W.E. and Zilliacus, S.
Two Visually Meaninful Correlation Measures for Comparing Calculated and Measured Response Histories
Shock and Vibration, 1(4), pp. 303-316 (1994)

130. William. R.; Crowley, J. and Vold, H.
The Multivariate Mode Indicator Function in Modal Analysis
Proc. IMAC III, pp. 65-71 (1985)

131. Williams, E.J. and Green, J.S.
A Spatial Curve Fitting Technique for Estimation of Rotational Degrees of Freedom
Proc. IMAC VIII, pp. 376-381 (1990)

132. Yasuda, C., Riehle, P.J., Brown, D.L.and Allemang, R.J.
An Estimation Method for Rotational Degrees-of-freedom Using a Mass Additive Technique
Proc. IMAC II, pp. 877-886 (1984)

RELATED WORK BY THE AUTHOR

PUBLICATIONS

1. Duarte, M.L.M. and Ewins, D.J.
   The Importance of Rotational Degrees-Of-Freedom and Residual Terms in Coupled Structure Analysis
   Proc. DINAME 95, pp. l-5 (1995)

2. Duarte, M.L.M. and Ewins, D.J.
   Some Insights Into the Importance of Rotational Degrees-of-Freedom and Residual Terms in Coupled Structure Analysis
   Proc. IMAC XIII, pp. 164-170 (1995)

3. Duarte, M.L.M. and Ewins, D.J.
   High-Frequency Pseudo-Mode Approximation for High-Frequency Residual Terms
   Proc. IMAC XIV, pp. 261-266 (1996)

4. Duarte, M.L.M. and Ewins, D.J.
   lmproved Experimental Component Mode Synthesis (IECMS) with Residual Compensation Based Purely on Experimental Results
   Proc. IMAC XIV, pp. *641-647 (1996)*

5. Duarte, M.L.M. and Ewins, D.J.
   On the Comparison of FRF Predictions Calculated by Mobility Coupling Formulation
   Proc. IMAC XIV, pp. 1472-1477 (1996)

6. Duarte, M.L.M. and Ewins, D.J.
   Experimental Estimation of the High-Frequency Residual Term Based on Two Extra Parameters
   Accepted to ISMA 2 1, KULeuven (1996)

7. Duarte, M.L.M. and Ewins, D.J.
   Modal Versus Response Coupling: Comparison of Predictions when Using the Same Input Data
   Accepted to ISMA 21, KULeuven (1996)

DYNAMIC SECTION INTERNAL REPORTS

1. Duarte, M.L.M.
   Experiences with the Modal Testing Facilities in the Dynamic Section
   Internal Report, No. 92001 (1992)

2. Duarte, M.L.M.
   High-Frequency Residual Terms - Observing and Understanding Their Behaviour
   Internal Report, No. 92002 (1992)

3. Duarte, M.L.M.
Residual Terms - A Literature Survey
Internal Report, No. 92003 (1992)

4. Duarte, M.L.M.
The Influence of Residual Terms when Performing a Structural Modification - Part 1
Internal Report, No. 92004 (1992)

5. Duarte, M.L.M.
The Influence of Residual Terms when Performing a Structural Modification - Part 2
Internal Report, No. 93004 (1993)

6. Duarte, M.L.M.
Component Mode Synthesis Techniques from Experimental Data
Internal Report, No. 94002 (1994)

7. Duarte, M.L.M.
An Innovative Approach for the High-Frequency Residual Terms (with Review)
Internal Report, No. 95001 (1995)

CLARIFICATION (CHAPTER 2, PAGE 41):

[4] This fact comes as a result of using dB scale in the above formulation, where no sign is taken into consideration and the correct position of the peaks is consequently lost. The reason why the maxima should correspond to the resonances and the minima should correspond to the anti-resonances effects is mainly for visualisation purposes (as the FIF curve has the same format of an FRF curve). The correct resonance position can be found using the FL curve presented in section 2.4.1. When the position of the resonance is shown as minima, the IFI given in equation (2.4) is used (again, just for visualisation purposes).

CLARIFICATION (CHAPTER 4, PAGE 104):

[8] Equation (4.39) may fail at 0 Hz mainly for "free-free" structures. The reason why this may happen is purely numerical since, in this case, it is difficult to calculate residual terms at 0 Hz. Therefore, the frequency obtained from the high-frequency pseudo-mass mode may be inside the frequency range of interest and this should be avoided. By choosing a different frequency point, no numerical problem is likely to occur and the mentioned shortcoming is solved.